B-physics in the Standard Model and Beyond

Dissertation

zur

Erlangung der naturwissenschaftlichen Doktorwürde
(Dr. sc. nat.)

vorgelegt der

Mathematisch-naturwissenschaftlichen Fakultät

der

Universität Zürich

von

Marzia Bordone

aus

Italien

Promotionskommission

Prof. Dr. Gino Isidori
Prof. Dr. Massimiliano Grazzini
Prof. Dr. Nicola Serra

Zürich, 2018

"Be not afraid of greatness.
Some are born great,
some achieve greatness,
and some have greatness
thrust upon 'em."

William Shakespeare,
Twelfth Night

Zusammenfassung

In der jüngeren Vergangenheit liessen sich vermehrt Hinweise auf die Verletzung der Flavor-Universalität von Leptonen in semileptonischen Zerfällen von B-Mesonen feststellen. In den gemessenen Observablen zeigt sich ein interessantes Muster von Anomalien im Vergleich zum Standardmodell, was zu verschiedenen Versuchen führte, die zugrundeliegende Physik von B-Zerfällen besser zu verstehen oder die Anomalien mit Modellen neuer Physik zu erklären. Diese Arbeit befasst sich mit beiden Ansätzen.
Nach einem kurzen Überblick über den Flavoursektor des Standardmodells und die gängigen Werkzeuge der B-Physik wird die Struktur der B-Zerfälle detaillierter studiert, mit einem besonderen Schwerpunkt auf die Vorhersage der entsprechenden Zerfallsraten. Es wird gezeigt, dass präzise Vorhersagen dabei helfen können, das Muster der gemessenen Anomalien besser zu verstehen. Wir befassen uns zuerst mit Flavourübergängen des Typs $b \to c$ und stellen verschiedene neue Ansätze vor: Zum Einen diskutieren wir eine Methode zum Abzug des Hintergrunds, die auf analytischen Vorhersagen für R_D basiert. Zum Anderen demonstrieren wir die Extraktion von R_D aus Messdaten auf eine Art, die unabhängig von der bisher gebräuchlichen ist. Ausserdem studieren wir einen neuen Zerfallskanal um Lepton-Flavouruniversalität in Zerfällen vom Typ $b \to c$ zu untersuchen. Danach diskutieren wir die neutralen Flavourübergänge vom Typ $b \to s$ and stellen die momentan aktuellste Vorhersage der Observablen $R_{K^{(*)}}$ vor.
Der darauffolgende Abschnitt der Arbeit befasst sich mit der Konzeption von Modellen neuer Physik. Zuerst konzentrieren wir uns dabei auf eine Konstruktion einer effektiven Feldtheorie basierend auf einer $U(2)^n$ Flavoursymmetrie, mit der sich die Möglichkeit ergibt, die beobachteten Anomalien auf eine konsistente Weise zu beschreiben. Wir studieren die Anwendung auf Kaon-Physik und die sich dadurch ergebenen Implikationen. Schliesslich stellen wir einen ersten konkreten Ansatz vor, die Anomalien in einem UV-vollständigen Modell mit einem Eich-Leptoquark zu erklären.

Abstract

In the recent years, a few hints of lepton flavour universality violation have been observed in semileptonic decays of B mesons. The measurements show a pattern of anomalies with respect to the Standard Model predictions: this triggered interest and attempts either to better understand the underlying physics which governs B decays or to address the problem within a New Physics scenario. Both approaches are attempted in this thesis.
After a brief review of the flavour sector of the Standard Model and the main tools used in B-physics, we study in details the anatomy of B decays, focusing on deriving predictions for channels of interest. We show how precision physics can be important to help disentangle the pattern of anomalies measured. We deal first with $b \to c$ transitions, proposing different new ideas. We present a method for background subtraction based on analytical calculations for R_D and its extraction from data in an independent way with respect to the ones adopted so far; furthermore we investigate a new channel for testing lepton flavour universality in $b \to c$ decays. We then discuss the neutral transition $b \to s$ and we present the most up to date prediction for the observables $R_{K^{(*)}}$.
Then we move to the model building part, where we first concentrate on an effective field theory approach based on $U(2)^n$ flavour symmetry, showing the possibility to consistently explain the pattern of anomalies. We analyse the possibility to link this description to kaon physics and the implications. Finally, we propose one of the first attempt to address the anomalies in a UV complete model for a gauge leptoquark.

Contents

Contents vii

Introduction 1

I Flavour physics in the Standard Model 3

1 The flavour structure in the Standard Model and the flavour problem 5
1.1 From the Higgs mechanism to the CKM matrix . . . 5
1.2 The CKM matrix . . . 7
1.3 The SM as an EFT: the flavour problem . . . 9
1.4 Flavour Symmetries beyond the SM . . . 12
1.4.1 Minimal Flavour Violation . . . 12
1.4.2 $U(2)^5$ . . . 13

2 B-physics: tools and phenomenology 17
2.1 General remarks on Effective Field Theories . . . 17
2.1.1 The path integral formulation . . . 17
2.1.2 The matching procedure . . . 19
2.2 EFTs for B-physics . . . 21
2.2.1 The weak Lagrangian . . . 22
2.2.2 HQET . . . 23
2.3 Hadronic matrix elements . . . 26
2.4 The present status: data vs SM predictions . . . 28

II Precise predictions within the Standard Model: charged current processes 33

3 Impact of leptonic τ decays on the distribution of $B \to P\mu\overline{\nu}$ decays 35
3.1 Introduction . . . 35
3.2 Setup . . . 36
3.2.1 Kinematics . . . 36
3.2.2 Decay Rate . . . 38
3.3 Numerical results . . . 40
3.3.1 $\overline{B} \to D\mu X_{\overline{\nu}}$ . . . 40
3.3.2 $\overline{B} \to \pi\mu X_{\overline{\nu}}$ . . . 42
3.3.3 Implications for the extraction of $|V_{cb}|$ and $|V_{ub}|$ . . . 43
3.4 Summary . . . 43

4 Testing lepton flavour universality in semileptonic $\Lambda_b \to \Lambda_c^*$ decays **45**
4.1 Introduction . . . 45
4.2 Form factors for $\Lambda_b \to \Lambda_c^*$ transitions . . . 46
4.2.1 Helicity form factors . . . 46
4.2.2 Heavy-quark expansion . . . 47
4.3 Phenomenology . . . 52
4.3.1 Parametrisation of the Isgur-Wise functions . . . 52
4.3.2 Benchmarking the form factors' parameters from Zero Recoil Sum Rules . 52
4.3.3 Observables . . . 55
4.4 Prospects for the determination of the $\Lambda_b^0 \to \Lambda_c^{*+}$ form factors using LHCb data . 56
4.4.1 Experimental situation . . . 56
4.4.2 Fits to the differential decay rate . . . 58
4.4.3 Projected precision on the $R_{\Lambda_c^*}$ predictions . . . 58
4.5 Conclusion . . . 60

III Precise predictions within the Standard Model: neutral current processes **61**

5 On the Standard Model predictions for R_K and R_{K^*} **63**
5.1 Introduction . . . 63
5.2 QED corrections in R_M . . . 63
5.2.1 Universal radiation function . . . 64
5.2.2 Parameterization of the non-radiative spectrum . . . 66
5.3 Numerical results . . . 67
5.4 SM predictions for R_{K^*} in the low q^2 region. . . . 69
5.5 Conclusions . . . 70

IV Model building for the anomalies **73**

6 Semi-leptonic B-physics anomalies: a general EFT analysis within $U(2)^n$ flavour symmetry **75**
6.1 Introduction . . . 75
6.2 Setup . . . 76
6.3 Observables . . . 78
6.3.1 Semi-leptonic $b \to c$ transitions . . . 79
6.3.2 Semi-leptonic $s \to u$ transitions . . . 82
6.3.3 $\Delta F = 2$ processes . . . 83
6.3.4 FCNC $b \to s$ transitions . . . 83
6.3.5 Leptonic τ decays . . . 85
6.3.6 Semi-leptonic LFV transitions . . . 86
6.4 Consistency of the EFT construction . . . 87
6.4.1 Power-counting scheme . . . 87
6.4.2 Constraints from direct searches . . . 89
6.4.3 Processes starting at $O(|V_L|^2)$ . . . 90
6.4.4 Upper bound on $|V_{L_1}/V_{L_2}|$ . . . 90
6.5 Conclusions . . . 91

7 Probing Lepton Flavour Universality with $K \to \pi\nu\bar{\nu}$ decays **93**
7.1 Introduction . . . 93
7.2 The $K \to \pi\nu\bar{\nu}$ decays . . . 94

7.3 The EFT approach to LFU violations based on $U(2)_q \times U(2)_\ell$ . . . 95
7.4 Physical observables . . . 96
7.4.1 The $R_{D^{(*)}}$ anomaly . . . 96
7.4.2 LFU violating contributions to $K \to \pi\nu\overline{\nu}$ . . . 97
7.4.3 Correlations between $B \to K^{(*)}\nu\overline{\nu}$ and $K \to \pi\nu\overline{\nu}$ . . . 98
7.4.4 Constraints and connections to other observables . . . 100
7.5 Conclusions . . . 101

8 A three-site gauge model for flavour hierarchies and flavour anomalies 103
8.1 Introduction . . . 103
8.2 The model . . . 104
8.2.1 Yukawa structure . . . 106
8.2.2 Origin of the effective Yukawa operators . . . 107
8.2.3 Gauge boson spectrum at the TeV scale . . . 109
8.3 Phenomenological analysis . . . 111
8.4 Summary and conclusions . . . 113

Conclusions 115

A Appendix to Chapter 2 117
A.1 $\overline{B} \to P$ form factors . . . 117
A.2 Scalar Products . . . 118
A.3 Results for the Legendre Ansatz in $P_3(y)$ . . . 119

B Appendix to Chapter 4 123
B.1 Details on the Rarita-Schwinger object . . . 123
B.2 Details on the form factor definitions . . . 124
B.3 Helicity Amplitudes . . . 126
B.3.1 $1/2^+ \to 1/2^-$ . . . 126
B.3.2 $1/2^+ \to 3/2^-$ . . . 129
B.4 Details on the Kinematics . . . 134
B.5 Explicit Spinor Representations . . . 135
B.6 Formulae . . . 135
B.7 Additional material on the sensitivity study . . . 135

C Appendix to Chapter 6 137
C.1 Hadronic Form Factors for $B \to V$ or $B \to P$ transitions . . . 137
C.2 Differential decay width for $B \to K\ell\bar{\ell}$ . . . 138

Scientific publications 139

Acknowledgements 141

Ringraziamenti 143

Bibliography 145

Introduction

The Standard Model (SM) of fundamental interactions provides the most stunning theory of the last sixty years. It describes the interactions of elementary particles with gauge bosons which mediate strong, weak and electromagnetic interaction; the framework which allows such description is provided by quantum field theory. Evidences that this theory accurately describes what is seen in nature came slowly but unquestionably, starting from the observation of $W^{\pm}$ and Z^0 bosons to the most recent discovery of the Higgs boson.
A rich physics program tested the SM at high accuracy for many years. As a result, it has been verified that the SM succeeds in describing accurately many phenomena which happen at the electroweak scale. However, it is also undeniable that sectors of the SM need further investigation and understanding and they may leave open an interesting question: is there any dynamics not yet observed beyond the SM?
The answer is rather intriguing. We know that phenomena like neutrino masses or dark matter cannot be addressed by any sector of the SM: this points unequivocally to the need of enlarging the SM adding some New Physics (NP) at some (higher) scale. On the other hand, knowing that the SM is not the definitive theory to describe elementary particles makes us wonder whether also some sectors of the SM itself can still leave space for NP effects.
One of the natural place where NP can be hidden is the flavour sector. With flavour sector we mean the study of transitions between quarks belonging to different families. Since many of them are suppressed in the SM or not well measured yet, it could be possible find some NP effects in them.
Recently, hints of deviations between the SM predictions and experimental measurements have been observed in semileptonic decay of b quarks. Even though the experimental sensitivity is not yet enough to have a clean proof of the presence of NP in such decays, they represent a coherent pattern of anomalies which require further investigations. This is the focus of this thesis.
The approach we follow is twofold: on one hand, we pursue a systematic study of a selected set of flavour-changing observables, with the goal of reducing their theoretical error within the SM. On the other hand, employing a model building approach, we identify correlations among different low-energy observables that could shed light on the nature of the hypothetic NP responsible for the anomalies.
The thesis is organised as follows. In Part I we introduce the basic tools exploited throughout the thesis: in chapter 1 we review the flavour sector of the SM, with emphasis on the bounds on NP obtained through flavour observable and two possible motivated extensions beyond the SM of this sector; in chapter 2 we summarise the main tool utilised in B physics and we give some details on both the experimental and the theory status on a few observables which play an important role in the following chapters. Part II is dedicated to the study of semileptonic charged-current b decays. In chapter 3 we study possible background sources to the decay $B \to D\mu\overline{\nu}_{\mu}$, while in chapter 4 we propose to exploit a new decay to expand our knowledge on the anomalies, namely the baryonic $\Lambda_b \to \Lambda_c^*\tau\overline{\nu}_{\tau}$ decay. Part III is dedicated to the study

of flavour changing neutral currents: in particular in chapter 5 we present the most up to date SM prediction of the observables $R_{K^{(*)}}$. Part IV is dedicated to model building. In chapter 6 we propose an analysis of current data within an EFT framework based on the $U(2)^5$ flavour symmetry, with special emphasis on the correlation between the anomalies and further flavour constraints. In chapter 7 we analyse the correlation between the anomalies and kaon physics, highlighting which scenarios could provide non negligible effects also in kaon decays. In chapter 8 we present one of the first attempts of building a UV complete model for a vector leptoquark to address the anomalies. We summarise our results and achievements in the Conclusions.

Part I

Flavour physics in the Standard Model

Chapter 1

The flavour structure in the Standard Model and the flavour problem

The SM succeeds in describing the interactions of the basic constituents of matter in terms of very simple objects: a set of fermion fields and a set of vector gauge fields which mediate weak, electromagnetic and strong interactions. In addition, a single scalar field (the Higgs field) is introduced to describe the effective masses of both the weak gauge fields (W and Z) and the fermions, resulting from the spontaneous breaking of the electroweak gauge symmetry.

The fermions, both leptons and quarks, are grouped into three families characterised by the same gauge quantum numbers. The difference among the three families are only the mass terms, or better the interactions of the different fermions with the Higgs field (denoted Yukawa interaction). This structure implies that weak, strong and electromagnetic interactions of the SM fermions are "universal" (i.e. the same among the three families), and that any different behaviour among the different families originates from the Yukawa interaction. This peculiar structure is a key built-in property of the SM: testing it provides powerful tool to investigate the validity of the model. Testing the universality of fermion interactions is one of the key goal of what we generically denote as "flavour physics", namely the investigation of the transitions between fermions belonging to different families.

In this chapter we review the flavour structure of the SM: in sections 1.1-1.2 we revise the link between the mass terms and the flavour structure in the SM itself; in sections section 1.3 we explore the possibility of New Physics (NP) and how to constrain it through flavour observables; in section 1.4 we propose two possible extensions of the flavour sector beyond the SM.

1.1 From the Higgs mechanism to the CKM matrix

The SM Lagrangian consists mainly of two separate parts: the gauge and the Higgs sector. The gauge sector describes the gauge vector bosons' interactions among themselves and the fermions. It is completely specified by the local symmetry of the SM: $G_{\rm SM} = SU(3)_c \times SU(2)_L \times U(1)_Y$ and the assignment of the fermion's quantum numbers under $G_{\rm SM}$. In a very compact way, we can express the Lagrangian of the gauge sector as in the following:

$$\mathcal{L}_{\rm gauge} = \sum_{i=1}^{3} \sum_{\psi=Q_L^i,\cdots,e_R^i} \overline{\psi} i \not{D} \psi - \sum_{i=1}^{3} \frac{1}{4} W^a_{\mu\nu} W^{a,\mu\nu} - \frac{1}{4} B_{\mu\nu} B^{\mu\nu} - \sum_{i=1}^{8} \frac{1}{4} G^a_{\mu\nu} G^{a,\mu\nu} \,. \tag{1.1}$$

For completeness, we recall the transformation properties of the fermion fields under $G_{\rm SM}$:

$$\begin{aligned} Q_L^i &\sim \left(3, 2, \frac{1}{6}\right) \quad L_L^i \sim \left(1, 2, -\frac{1}{2}\right) \\ u_R^i &\sim \left(3, 1, \frac{2}{3}\right) \quad d_R^i \sim \left(3, 1, -\frac{1}{3}\right) \quad e_R^i \sim (1, 1, -1)\ , \end{aligned} \tag{1.2}$$

where the index i denotes the three flavours (i.e. $i = 1, 2, 3$).
The structure of eq. (1.1) implies that the gauge sector respects a global *flavour symmetry*. With flavour symmetry we mean a symmetry of the Lagrangian in the flavour space, which corresponds to the freedom to rotate in flavour space the five fields defined in eq. (1.2). It is easy to see that in the case of eq. (1.1), the global flavour symmetry is the following one:

$$\mathcal{G}_{\rm flavour}^{\rm SM} = U(3)^5 = U(1)^5 \times \mathcal{G}_q \times \mathcal{G}_\ell\,, \tag{1.3}$$

where

$$\mathcal{G}_q = SU(3)_{Q_L} \times SU(3)_{u_R} \times SU(3)_{d_R}\,, \qquad \mathcal{G}_\ell = SU(3)_{L_L} \times SU(3)_{e_R}\,. \tag{1.4}$$

Out of $\mathcal{G}_{\rm flavour}^{\rm SM}$, the subgroups $\mathcal{G}_q$ and $\mathcal{G}_\ell$ control flavour changing dynamics. They allow to rotatex the SM matter fields in flavour space through unitary matrices V_i, as

$$Q_L^i \to V_Q^{ij} Q_L^j\,, \quad L_L^i \to V_L^{ij} L_L^j\,, \quad u_R^i \to V_u^{ij} u_R^j\,, \quad d_R^i \to V_d^{ij} d_R^j\,, \quad e_R^i \to V_e^{ij} e_R^j\,. \tag{1.5}$$

Three out of the five $U(1)$ subgroups of $\mathcal{G}_{\rm flavour}^{\rm SM}$ can be identified with the total baryon and lepton number and the weak hypercharge; these subgroups are not broken by the Yukawa interactions of the SM. The remaining two $U(1)$ subgroups can be identified with the Peccei-Quinn symmetry and a global rotation of the right-handed leptons. They are broken in the SM by the Yukawa interactions: note that this charateristic is not general; in fact, a different specification of the Higgs sector (e.g. introducing more than one Higgs boson) may preserve them.

Both the local $G_{\rm SM}$ and the global $\mathcal{G}_{\rm flavour}^{\rm SM}$ symmetries are broken by the introduction of a scalar field, namely the Higgs field, which transforms as a doublet of $SU(2)_L$. The local symmetry is spontaneously broken when the Higgs field acquires a vacuum expectation value (vev):

$$\langle H \rangle = \frac{1}{\sqrt{2}} \begin{pmatrix} 0 \\ v \end{pmatrix}\,, \tag{1.6}$$

where $v = (\sqrt{2} G_F)^{-1/2} \approx 246$ GeV.
The global flavour symmetry is explicitly broken by the Yukawa interaction which involves the Higgs field and the SM fermion fields:

$$-\mathcal{L}_{\rm SM} = Y_d^{ij} \overline{Q}_L^i H d_R^j + Y_u^{ij} \overline{Q}_L^i \tilde{H} u_R^j + Y_e^{ij} \overline{L}_L^i H e_R^j + \text{h.c.}\,. \tag{1.7}$$

Since the Yukawa matrices Y_a are in principle arbitrary and not proportional to the identity, both $\mathcal{G}_q$ and $\mathcal{G}_\ell$ are badly broken up to some residual $U(1)$ in the lepton sector.
In principle, each Yukawa matrix requires two independent unitary rotations to be diagonalised, i.e. $Y_a^{\rm diag} = V_L^a Y_a V_R^{a\dagger}$; this means that in the quark sector, four independent matrices are needed. Due to the flavour symmetry $\mathcal{G}_q$, we have the freedom to perform rotations in flavour space. This allows us to choose three out of four matrices needed to diagonalise the Yukawa matrices. Starting from the basis in which Y_d is diagonal, known also as the down-quark basis, we can eliminate the right-handed rotation in the up sector, obtaining

$$Y_d = \lambda_d\,, \qquad Y_u = V^\dagger \lambda_u\,, \tag{1.8}$$

where

$$\lambda_d = \text{diag}(y_d, y_s, y_b)\,, \qquad \lambda_u = \text{diag}(y_u, y_c, y_t)\,. \tag{1.9}$$

The choice of starting from the down-quark basis is not unique. However, starting from arbitrary Y_d and Y_u, it is not possible to diagonalise both of them at the same time with a single rotation. In other words, it is not possible to construct a basis in which both the interaction terms and the Yukawa interactions are diagonal in flavour space. This means that in any case we are left with an a priori unknown unitary mixing matrix V, known as the Cabibbo-Kobayashi-Maskawa (CKM) [1–3] mixing matrix, which corresponds to the misalignment of the Yukawa couplings on the left-handed site.
In the leptonic sector, assuming the absence of neutrino masses[1], it is possible to diagonalise Y_e without any observable consequence.

In full generality, a 3×3 unitary matrix is described by three real angles and six complex phases. In the case of the CKM matrix, further five complex phases can be reabsorbed in the definition of the quark fields, leaving four physical parameters: three real angles and one complex CP-violating phase.
The mixing between quark families introduced by the CKM matrix affects also the gauge sector. The Lagrangian in eq. (1.1) is written in the *interaction basis*, namely in the basis where the interaction between gauge bosons and quarks are diagonal in flavour space. Introducing the CKM matrix to diagonalise the Yukawa and hence the mass terms, means to change the basis from the interaction one to the so-called *mass basis*. In this basis, the gauge interactions with quarks are not diagonal anymore; in particular, the charged current terms are modified as in the following:

$$J^{\mu}_{W}|_{\text{quark}} = \overline{u}^{i}_{L}\gamma^{\mu}d^{i}_{L} \rightarrow V^{ij}\overline{u}^{i}_{L}\gamma^{\mu}d^{j}_{L}\,, \tag{1.10}$$

while the neutral current remains unchanged.

1.2 The CKM matrix

The CKM matrix can be parametrised in different ways; the standard one is in terms of three rotation angles θ_{ij} and a complex phase δ, as

$$\begin{aligned} V &= \begin{pmatrix} V_{ud} & V_{us} & V_{ub} \\ V_{cd} & V_{cs} & V_{cb} \\ V_{td} & V_{ts} & V_{tb} \end{pmatrix} \\ &= \begin{pmatrix} c_{12}c_{13} & s_{12}c_{13} & s_{13}e^{-\delta} \\ -s_{12}c_{23} - c_{12}s_{23}s_{12}e^{i\delta} & c_{12}c_{23} - s_{12}s_{23}s_{13}e^{i\delta} & s_{23}c_{13} \\ s_{12}s_{23} - c_{12}c_{23}s_{13}e^{i\delta} & -s_{23}c_{12} - s_{12}c_{23}s_{13}e^{i\delta} & c_{23}c_{13} \end{pmatrix}, \end{aligned} \tag{1.11}$$

where $c_{ij} = \cos\theta_{ij}$ and $s_{ij} = \sin\theta_{ij}$, with $i, j = 1, 2, 3$.
At this point, for a better understanding, it is quite interesting to look at the numerical structure of the CKM matrix. If we refer in particular to the magnitude of each element, we have [8]:

$$|V| = \begin{pmatrix} 0.97434^{+0.00011}_{-0.00012} & 0.22506 \pm 0.00050 & 0.00357 \pm 0.00015 \\ 0.22492 \pm 0.00050 & 0.97351 \pm 0.00013 & 0.0411 \pm 0.0013 \\ 0.00875^{+0.00032}_{-0.00033} & 0.0403 \pm 0.0013 & 0.99915 \pm 0.00005 \end{pmatrix}. \tag{1.12}$$

From eq. (1.12) we see a strong hierarchy between the elements of the CKM matrix, according to which the off-diagonal terms are rather small, while the diagonal ones approach the unity. This allows us to write down a new parametrisation of the CKM matrix, where the hierarchy just described is manifest. We can choose to expand the elements of the CKM in powers of a small

[1] In many extensions of the SM, neutrino mass terms appear. It is then possible to apply the very same procedure just described for the quark sector and define the analogous of the CKM matrix for the lepton sector, namely the Pontecorvo-Maki-Nakagawa-Sakata (PMNS) [4–7] mixing matrix.

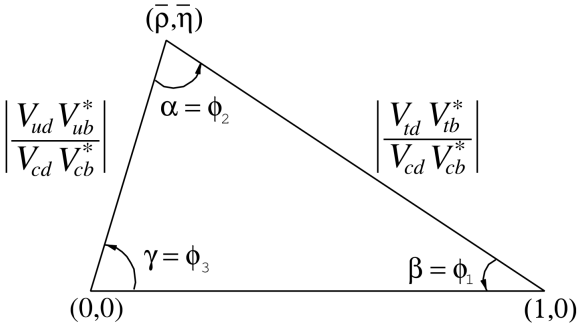

Figure 1.1: The CKM unitary triangle.

parameter λ, defined as $\lambda \equiv |V_{us}| \approx 0.22$. This procedure give rise to the so-called Wolfenstein parametrisation, through which the CKM matrix acquires the form:

$$V = \begin{pmatrix} 1 - \frac{\lambda^2}{2} & \lambda & A\lambda^3(\varrho - i\eta) \\ -\lambda & 1 - \frac{\lambda^2}{2} & A\lambda^2 \\ A\lambda^3(1 - \varrho - i\eta) & -A\lambda^2 & 1 \end{pmatrix} + \mathcal{O}(\lambda^4)\,, \tag{1.13}$$

where A, ϱ and η are free parameters.
At a high level of accuracy, the expansion up to $\mathcal{O}(\lambda^4)$ is not sufficient, and further terms must be included. The standard procedure is to define the set of parameters $\{\lambda, A, \varrho, \eta\}$ in terms of the angles c_{ij} and s_{ij}, as

$$\lambda \equiv s_{12}\,, \quad A\lambda^2 \equiv s_{23}\,, \quad A\lambda^3(\varrho - i\eta) \equiv s_{13}e^{-i\delta}\,. \tag{1.14}$$

Up to order $\mathcal{O}(\lambda^5)$, the CKM matrix is parametrised as

$$V = \begin{pmatrix} 1 - \frac{\lambda^2}{2} - \frac{1}{8}\lambda^4 & \lambda + \mathcal{O}(\lambda^7) & A\lambda^3(\varrho - i\eta) \\ -\lambda + \frac{1}{2}A\lambda^5[1 - 2(\varrho + i\eta)] & 1 - \frac{\lambda^2}{2} - \frac{1}{8}\lambda^4(1 + 4A^2) & A\lambda^2 + \mathcal{O}(\lambda^8) \\ A\lambda^3(1 - \overline{\varrho} - i\overline{\eta}) & -A\lambda^2 + \frac{1}{2}A\lambda^4[1 - 2(\varrho + i\eta)] & 1 - \frac{1}{2}A^2\lambda^4 \end{pmatrix}, \tag{1.15}$$

where

$$\overline{\varrho} = \varrho\left(1 - \frac{\lambda^2}{2}\right) + \mathcal{O}(\lambda^4)\,, \qquad \overline{\eta} = \eta\left(1 - \frac{\lambda^2}{2}\right) + \mathcal{O}(\lambda^4)\,. \tag{1.16}$$

In order to test the CKM structure, it is useful to exploit its properties, namely that the CKM matrix must be unitary. This property is translated in the following two relations

$$i)\ \sum_{k=1,\cdots 3} V^*_{jk}V_{kj} = 1\,, \qquad ii)\ \sum_{k=1\cdots 3} V^*_{ik}V_{kj\neq i} = 0\,. \tag{1.17}$$

These relations can be used as a strong test of the validity of SM, since they are typical of the SM construction according to which the CKM matrix is the only source of mixing between quarks. Through an experimental test of the validity of eq. (1.17), bounds on new sources of flavour mixing can be set.
An example can be seen if we take $l = 1$ and $j = 3$ among the relations of type $ii)$ in eq. (1.17), namely

$$\begin{gathered} V_{ud}V^*_{ub} + V_{cd}V^*_{cb} + V_{td}V^*_{tb} = 0 \\ \frac{V_{ud}V^*_{ub}}{V_{cd}V^*_{cb}} + \frac{V_{td}V^*_{tb}}{V_{cd}V^*_{cb}} + 1 = 0 \qquad \leftrightarrow \qquad [\overline{\varrho} + i\overline{\eta}] + [(1 - \overline{\varrho}) - i\overline{\eta}] + 1 = 0\,. \end{gathered} \tag{1.18}$$

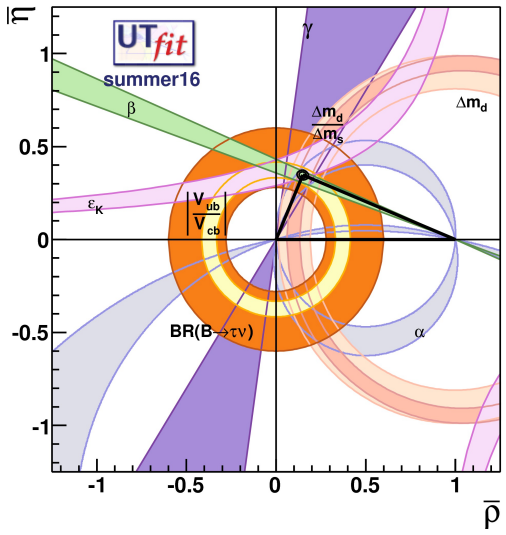

Figure 1.2: Allowed region in the $\overline{\varrho}$ and $\overline{\eta}$ plane [9].

Expressing eq. (1.18) in terms of $\overline{\varrho}$ and $\overline{\eta}$ is particularly convenient since we obtain a relation where all the terms are of the very same order in λ. Usually eq. (1.18) is represented as a unitary triangle in the complex plane, as in figure 1.1. We stress that the triangle described by eq. (1.18) or alternatively figure 1.1 is invariant under phase transformations of the quark fields. In fact such transformations will rotate the triangle in figure 1.1 in the complex plane but the angle and length of the sides will not vary. This implies that the angles and sides of the unitary triangles are indeed observable quantities and hence suitable to be measured.

Besides the magnitude of the CKM elements presented in eq. (1.12), the set of parameters $\{\lambda, A, \varrho, \eta\}$ can be fitted using various decay channels. In the specific, $|V_{us}|$ and $|V_{cb}|$ or equivalently λ and A, can be determined with high accuracy from $K \to \pi\ell\nu$ and $B \to X_c\ell\nu$ decays respectively. According to [9], they are:

$$\lambda = 0.22497 \pm 0.00069\,, \qquad A = 0.833 \pm 0.012\,. \tag{1.19}$$

The results in eq. (1.19) are used as inputs to constrain $\overline{\varrho}$ and $\overline{\eta}$ through appropriate and sensitive observables. Usually, the constraint on $\overline{\varrho}$ and $\overline{\eta}$ are translated in the constraints on the CKM unitarity triangles. The result is shown in figure 1.2, where all the constraints are consistent with the following values for $\overline{\varrho}$ and $\overline{\eta}$:

$$\overline{\varrho} = 0.153 \pm 0.013\,, \qquad \overline{\eta} = 0.343 \pm 0.011 \tag{1.20}$$

1.3 The SM as an EFT: the flavour problem

Even though the SM succeeds in providing an excellent theory for the fundamental interactions, it still fails in explaining various phenomena. A clear example is the need to add to the ordinary matter what is called dark matter, a yet unidentified type of matter which is needed to describe several cosmological and astrophysical observations. Another example is the unexplained imbalance between baryons and anti-baryons observed in the universe: both matter and antimatter should have been produced in equal amounts in the Big Bang, but nowadays the universe is made up only of baryonic matter. A third example is the nature of neutrino masses: given the evidence of neutrino oscillations, the fact that the SM must be completed with mass terms for the neutrinos is undeniable. However, if this mass could come from a Dirac type mass term or from a Majorana type is yet unknown.

The three examples just mentioned are only a few phenomena which cannot be addressed in the SM. This points to a direction in which the SM must be completed in order to include the explanation to many effects such the ones mentioned above. Since at the the electroweak scale m_W the SM predictions for many phenomena agree with the measurements, we can think of it as a low energy realisation of a more complete theory which is characterised by a scale $\Lambda \gg m_W$. The nature of the heavy degrees of freedom at scale Λ is not known. However, due to the large energy separation between Λ and m_W we can integrate them out to obtain a description of their effect at the m_W-scale through effective operators. More details on this procedure are discussed in section 2.1. The full Lagrangian is made of two parts: the SM Lagrangian and an infinite tower of effective operators with dimension $d > 4$, constructed from the SM fields and suppressed by powers of the heavy scale Λ.
This procedure is analogous to obtaining the Fermi Lagrangian for leptons by integrating out the W from the full SM. The main difference between the SM case and the beyond standard model case is that we don't know the exact nature of the high scale dynamics. This implies that the values of the effective couplings of the higher dimensional operators cannot be determined a priori or linked to any fundamental constant. However, we know they must respect the low-energy symmetries of the system, in particular the SM gauge symmetry.
From these assumptions, the Lagrangian of the SM seen as an EFT, can be written as

$$\mathcal{L}_{\text{eff}} = \mathcal{L}_{\text{gauge}} + \mathcal{L}_{\text{higgs}} + \mathcal{L}_{\text{Yukawa}} + \Delta\mathcal{L}_{d>4}\,, \tag{1.21}$$

where $\Delta\mathcal{L}_{d>4}$ encodes the higher-dimensional operators:

$$\Delta\mathcal{L}_{d>4} = \sum_{d>4}\sum_{n=1}^{N_d} \frac{c_n^{(d)}}{\Lambda^{d-4}}\mathcal{O}_n^{(d)}\,. \tag{1.22}$$

Even though we don't have any prior on the effective coefficients $c_n^{(d)}$ and the scale Λ, we can expect them to fulfil the following properties:

- The scale Λ is expected to be $\mathcal{O}(1\text{ TeV})$. In fact, if the scale Λ would be too high, it could generate a big contribution to the corrections to the Higgs mass. This issue is generally addressed as *hierarchy "problem"*.
- Without introducing any fine-tuning in the coupling constants, the effective couplings are expected to be $\mathcal{O}(1)$ parameters if they are not suppressed due to symmetry reasons.

The fact that several dimension six operators contributing to flavour changing processes do not respect these expectations goes under the so-called *flavour problem*.
The easiest way of quantifying the flavour problem is to perform tests of flavour-changing processes. As a first approximation we can neglect the effect of NP for processes that arise in the SM already at tree level. As a consequence, the values of $|V_{us}|$, $|V_{cb}|$ and $|V_{ub}|$ are NP free in this limit. We can then use the measurements of the SM loop mediated observables to set bounds on NP operators. Specifically, we need to address the mixing of neutral mesons, such as B_d, B_s and K^0, which are generically denoted as $\Delta F = 2$ processes. In full generality, the SM contribution to $\Delta F = 2$ amplitudes are dominated by box-diagrams mediated by a top quark exchange, with an effect of the form:

$$\mathcal{M}^{\text{SM}}_{\Delta F=2} \approx \frac{G_F^2 m_t^2}{16\pi^2}\left(V_{3i}^* V_{3j}\right)^2 \langle\overline{M}|(\overline{d}_L^i\gamma^\mu d_L^j)^2|M\rangle\; F\left(\frac{m_t^2}{m_W^2}\right)\,, \tag{1.23}$$

where $M = B_d, B_s, K^0$, F is a loop function which gives an order one contribution and i, j denotes the flavour indices of the valence quarks accordingly to the choice of the state M.
The magnitude and phase of all the mixing processes just mentioned have been measured with great accuracy. As we can see from figure 1.2, every time the experimental informations are

Operator	Bounds on Λ in TeV ($c_{\rm NP}=1$)		Bounds on $c_{\rm NP}$ ($\Lambda=1$ TeV)		Observables
	Re	Im	Re	Im	
$(\bar{s}_L\gamma^\mu d_L)^2$	1.1×10^3	2.0×10^4	4.5×10^{-9}	0.6×10^{-9}	$\Delta m_K;\epsilon_K$
$(\bar{s}_R d_L)(\bar{s}_L d_R)$	2.4×10^4	4.3×10^5	0.5×10^{-10}	1.3×10^{-12}	$\Delta m_K;\epsilon_K$
$(\bar{c}_L\gamma^\mu u_L)^2$	1.8×10^3	1.0×10^4	0.3×10^{-7}	0.3×10^{-9}	$\Delta m_D;\lvert q/p\rvert,\Phi_D$
$(\bar{c}_R u_L)(\bar{c}_L u_R)$	8.0×10^3	4.5×10^4	0.2×10^{-8}	0.2×10^{-10}	$\Delta m_D;\lvert q/p\rvert,\Phi_D$
$(\bar{b}_L\gamma^\mu d_L)^2$	1.0×10^3	1.0×10^3	6.3×10^{-7}	7.1×10^{-7}	$\Delta m_{B_d};S_{\psi K_S}$
$(\bar{b}_R d_L)(\bar{b}_L d_R)$	3.5×10^3	3.5×10^3	6.2×10^{-8}	5.4×10^{-8}	$\Delta m_{B_d};S_{\psi K_S}$
$(\bar{b}_L\gamma^\mu s_L)^2$	2.3×10^2	2.3×10^2	1.3×10^{-5}	1.4×10^{-5}	$\Delta m_{B_s};S_{\psi\phi}$
$(\bar{b}_R s_L)(\bar{b}_L s_R)$	4.8×10^2	4.8×10^2	1.1×10^{-6}	1.2×10^{-6}	$\Delta m_{B_s};S_{\psi\phi}$

Table 1.1: Bounds on dimension six operators which contributes to $\Delta F=2$ processes, assuming a generic coupling $c_{\rm NP}/\Lambda^2$. The bounds in the second column are on Λ when setting $c_{\rm NP}=1$, in the third column on $c_{\rm NP}$ when setting $\Lambda=1$ TeV. The last column contains the observables used to derive the bounds.

precise, the NP contribution cannot exceed the size of the SM contribution. The translation of this fact into bounds on the scale of NP follows rather smoothly: let's consider the following set of $\Delta F=2$ dimension six operators

$$\mathcal{O}^{ij}_{\Delta F=2}=(\overline{Q}^i_L\gamma^\mu Q^j_L)\,, \tag{1.24}$$

where again i,j are the flavour indices in the mass basis. The operators in eq. (1.24) give a tree level contribution to $\Delta F=2$ amplitudes, which would be proportional to the effective coupling c_{ij}. Imposing that $\mathcal{M}^{\rm NP}_{\Delta F=2}<\mathcal{M}^{\rm SM}_{\Delta F=2}$ implies the following bound on the NP scale:

$$\Lambda<\frac{3.4\text{TeV}}{|V^*_{3i}V_{3j}|/|c_{ij}|^{1/2}}<\begin{cases}9\times10^3\ \text{TeV}\times|c_{21}|^{1/2} & \text{from}\quad K^0-\overline{K}^0\,,\\ 4\times10^2\ \text{TeV}\times|c_{31}|^{1/2} & \text{from}\quad B_d-\overline{B}_d\,,\\ 7\times10\ \ \text{TeV}\times|c_{32}|^{1/2} & \text{from}\quad B_s-\overline{B}_s\,.\end{cases} \tag{1.25}$$

It is of course possible to refine this analysis, putting separate bounds on real and imaginary part of the coefficients c_{ij}, and including operators with different Lorentz structures. The result are summarised in table 1.1. The conclusions we can draw are mainly two:

- In the case of a NP model with an arbitrary flavour structure (i.e. $c_{ij}=1$), the expected NP scale Λ is way higher than the $\mathcal{O}$(TeV), hence the model needs fine tuning.
- If we aim to have a NP scale $\Lambda\sim1$ TeV, we need a strong argument such that $c_{ij}\leq|V^*_{3i}V_{3j}|^2$.

Note that the strong constraints extracted from $\Delta F=2$ observables are a consequence of their strong suppression in the SM itself. In fact, they are loop suppressed and GIM and CKM suppressed.
Nevertheless, we stress that despite the very good agreement between SM prediction and experimental measurements of B_d and K^0 mixing, further studies and measurements are very important. In fact, any improvement on the present bounds will help constraining the NP scale and the possible different structures that can arise.

1.4 Flavour Symmetries beyond the SM

As shown in the previous sections, the peculiarity of SM flavour structure due to the CKM rotation in flavour space renders very complicated to evade experimental bounds. In order to do so, it is convenient to introduce a *flavour symmetry* and a set of specific breaking terms. The specification of the flavour symmetry and the associated (small) breaking terms allows to determine a pattern for the various flavour-violating couplings. In such way, the strong hierarchy of the NP coupling, as expected from table 1.1, can be justified. We briefly review two possible and well motivated choices: Minimal Flavour Violation (MFV) [10] and $U(2)^5$ [11].

1.4.1 Minimal Flavour Violation

The main point of MFV consists in the fact that the flavour-violating interactions of the NP sector are linked to the structure of Yukawa couplings in the SM itself. From an operative point of view, this means to impose on the NP the very same flavour symmetry and the symmetry-breaking term that we find in the SM.
In order to construct a model which respects the MFV hypothesis we need to specify two feature. The first one is the flavour symmetry, which will be nothing but the flavour symmetry of the SM in absence of Yukawa terms, described in eq. (1.3). Since the global symmetry of eq. (1.3) is already broken in the SM, we need to introduce breaking terms also in the NP model. The specification of the breaking terms is the second ingredient of our construction. The minimal choice of MFV consists in introducing terms which break the flavour symmetry in the very same way as they do in the SM. This means that the Yukawa terms are the only breaking source of the flavour symmetry.
In order to actively introduce this fact, we can promote Y_d and Y_u to be non-dynamical fields named *spurions*, which have non-trivial transformation property under $\mathcal{G}_q$:

$$Y_u \sim (3, \overline{3}, 1)\,, \qquad Y_d \sim (3, 1, \overline{3})\,. \tag{1.26}$$

In the effective theory approach presented in section 1.3, we can affirm that the effective theory satisfies the MFV hypothesis in the quark sector if all the higher dimensional operators constructed through the SM fields and Y_i fields are invariant under CP and under the flavour group $\mathcal{G}_q$.
According to this rule, we can construct operators via an arbitrary number of Yukawa fields, since they are dimensionless. In practice, this means to have terms of the type $\left[Y_a(Y_a)^\dagger\right]^n$, with $a = u, d$. However, we can notice that the eigenvalues of the Yukawa matrices are small apart for the top one, and the off-diagonal terms of the CKM matrix are small. This allows us to completely neglect all the terms proportional to $\left[Y_d(Y_d)^\dagger\right]^n$ in the basis in which Y_d is diagonal. Instead, for the up-type quark Yukawa matrix, the leading and non negligible contributions are proportional to the top Yukawa and read

$$\left[Y_u(Y_u)^\dagger\right]^n_{ij}\Big|_{i\neq j} \approx y_t^n V_{ti}^* V_{tj}\,. \tag{1.27}$$

As a consequence, the leading effects in $\Delta F = 1$ and $\Delta F = 2$ amplitudes will be CKM suppressed as in the SM:

$$\begin{aligned}
\mathcal{A}(d^i \to d^j)_{\rm MFV} &= (V_{ti}^* V_{tj})\mathcal{A}_{\rm SM}^{(\Delta F=1)}\left[1 + a_1 \frac{16\pi^2 m_W^2}{\Lambda^2}\right]\,, \\
\mathcal{A}(M_{ij} \to \overline{M}_{ij})_{\rm MFV} &= (V_{ti}^* V_{tj})^2\mathcal{A}_{\rm SM}^{(\Delta F=2)}\left[1 + a_2 \frac{16\pi^2 m_W^2}{\Lambda^2}\right]\,,
\end{aligned} \tag{1.28}$$

where $\mathcal{A}_{\rm SM}^{(i)}$ are the SM top-mediated loop amplitudes and a_i are $\mathcal{O}(1)$ real parameters. Note that the parameters a_i depend on the specific choice of operator but they are flavour independent.

This implies that for any quark transition $s \to d$, $b \to d$ and $b \to s$, once the CKM dependence is taken out, the relative correction for transition of the same type will be the same. If this behaviour would be detected in experiment, it could provide a strong proof on the validity of MFV hypothesis.
Another interesting feature of MFV pointed out in [12] is that several contraints used to determine the CKM elements are not affected by NP. As we can see from figure 1.2, only ϵ_K and Δm_{B_d} are sensitive to NP effects in the MFV framework.

1.4.2 $U(2)^5$

The MFV construction is very interesting and provides a framework in which many constraints are fulfilled. However it doesn't provide any prescription to address the fermion mass problem, namely the hierarchy between the Yukawa couplings in the SM.
A step in this direction can be made introducing a $U(2)^n$ flavour symmetry, where the first two generations are governed by a $U(2)$ symmetry weakly broken. As a consequence, only Yukawa terms for the third generation are allowed, while the ones for the light families are forbidden by the symmetry and are allowed only if (small) breaking terms are introduced. This goes in the direction of motivating the strong hierarchy between the Yukawa couplings of the different families.
In details, the flavour symmetry that we want to introduce reads

$$\mathcal{G}_{\text{flavour}} = U(2)_q \times U(2)_\ell \times \mathcal{G}_R \ . \tag{1.29}$$

For either the third generation of quarks and leptons, the left-handed fields are a singlet under the complete flavour group $\mathcal{G}_{\text{flavour}}$ Under $U(2)_q \times U(2)_\ell$ the light generations of left-handed fields combine into doublets and possess non trivial transformation properties. In practice we have:

$$\begin{aligned} Q \equiv (q_L^1, q_L^2) \sim (2,1) \ , \qquad q_{3L} \equiv q_L^3 \sim (1,1) \ , \\ L \equiv (\ell_L^1, \ell_L^2) \sim (1,2) \ , \qquad \ell_{3L} \equiv \ell_L^3 \sim (1,1) \ . \end{aligned} \tag{1.30}$$

As regards $\mathcal{G}_R$, we chose it to have the form

$$\mathcal{G}_R = U(2)_{u_R} \times U(2)_{d_R} \times U(2)_{e_R} \, , \tag{1.31}$$

such that $E = (\mu_R, e_R)$ transforms as a doublet under $U(2)_{e_R}$ and similarly for the right-handed up and down type quarks.
We now want to describe Yukawa couplings in this framework. As a first step we notice that in absence of any breaking terms of $\mathcal{G}_{\text{flavour}}$ the Yukawa matrices contain a non-zero entry only for the top and the bottom. They assume the form

$$Y_{u(d)} = y_{t(b)} \begin{pmatrix} 0 & 0 \\ 0 & 1 \end{pmatrix} \tag{1.32}$$

where the first top left element represents a null 2×2 matrix, the top right a null 1×2 matrix and the bottom left a null 2×1 matrix. Already at this stage, without the introduction of any breaking terms, we have a big Yukawa coupling for the third generation, while the ones for the light generations are zero. Although we know that the in reality the Yukawa for the light generations are not exactly zero, this step goes in the direction of introducing an hierarchy for the Yukawa.
The second step consists in identifying a minimal set of spurions which allow to recover the full SM Yukawa couplings and, at the same time, to maintain a CKM-like structure for possible FCNC transitions. This is achieved through the following

1. We introduce a leading spurion V, which transforms under $U(2)_q \times U(2)_\ell$ as $V_Q \sim (2,1)$. The Yukawa matrices are modified as follows:

$$Y_u = y_t \begin{pmatrix} 0 & x_t V_Q \\ 0 & 1 \end{pmatrix} \qquad \text{and} \qquad Y_d = y_b \begin{pmatrix} 0 & x_b V_Q \\ 0 & 1 \end{pmatrix}, \tag{1.33}$$

   where x_t and x_b are free parameters. What we achieved so far is giving mass to the third generations and construct the mixing terms between light and heavy generations. Since our final goal is to obtain a CKM-like structure, we expect that $|V_Q| \sim |V_{ts}| \sim 0.04$.

2. We introduce the mass and mixing terms for light generations by introducing the two further subleading spurions ΔY_u and ΔY_d, which transform under $U(2)_q \times U(2)_{u_R}$ and $U(2)_q \times U(2)_{d_R}$ respectively as bidoublets :

$$Y_u = y_t \begin{pmatrix} \Delta Y_u & x_t V_Q \\ 0 & 1 \end{pmatrix} \qquad \text{and} \qquad Y_d = y_b \begin{pmatrix} \Delta Y_d & x_b V_Q \\ 0 & 1 \end{pmatrix}. \tag{1.34}$$

Regarding the lepton sector, a very similar construction can be achieved.

It is niw interesting to see how the spurions are connected with the CKM matrix. First we choose a basis where we can parametrise the leading spurion V as

$$V_Q = \epsilon \, U_V \hat{s}_2 \,, \qquad s_2 = \begin{pmatrix} 0 \\ 1 \end{pmatrix}, \tag{1.35}$$

where U_V is a 2×2 unitary matrix and ϵ is a real parameter expected to be of order $|V_{cb}|$. The spurion ΔY_u and ΔY_d can be decomposed as

$$\begin{aligned} \Delta Y_u &= U^\dagger_{Q_u} \Delta Y^d_u U_U \,, \\ \Delta Y_d &= U^\dagger_{Q_d} \Delta Y^d_d U_D \,, \end{aligned} \tag{1.36}$$

where $\Delta Y^d_u = \mathrm{diag}(\lambda_{d_1}, \lambda_{d_2})$ and $\Delta Y^d_d = \mathrm{diag}(\lambda_{u_1}, \lambda_{u_2})$ and U_i are 2×2 unitary matrices. If we perform a suitable rotation in the subspace $U(2)^3$ of the quarks, the matrices U_V, U_U and U_D can be eliminated. In this basis we can express the Yukawa matrices as

$$Y_u = y_t \begin{pmatrix} U^\dagger_{Q_u} \Delta Y^d_u & \epsilon x_t \hat{s}_2 \\ 0 & 1 \end{pmatrix}, \tag{1.37}$$

$$Y_d = y_b \begin{pmatrix} U^\dagger_{Q_d} \Delta Y^d_d & \epsilon x_b \hat{s}_2 \\ 0 & 1 \end{pmatrix}. \tag{1.38}$$

At this point we need to address the relevant CP phases. First we note that the phase in y_t and y_b can be reabsorbed into a rotation of t^c and b^c and through a rephasing of u^c and d^c we can set the diagonal entries of $\Delta Y^d_{u,d}$ to be real. For symmetry reason we keep both phases in $x_{b,t}$ and we parametrise as $x_f \to x_f e^{i\phi_f}$, where x_f is real and positive. The last components to discuss are the matrices $U_{Q_{u,d}}$ which assume the general form

$$U_{Q_f} = \begin{pmatrix} c_f & s_f e^{i\alpha_f} \\ -s_f e^{-i\alpha_f} & c_f \end{pmatrix}. \tag{1.39}$$

In the following we set $s_f \ll 1$, as naturally implied by the alignment of the spurions $\Delta Y_{u,d}$ in the $U(2)_Q$ with respect to the leading breaking spurions.

We can now look at the diagonalisation of the Yukawa matrices and hence at the CKM structure. The Yukawa are diagonalised by

$$U_{u_L} Y_u U^\dagger_{u_R} = \mathrm{diag}(y_u, y_c, y_t) \,, \qquad U_{d_L} Y_d U^\dagger_{d_R} = \mathrm{diag}(y_d, y_s, y_b) \,. \tag{1.40}$$

The left-handed up-type diagonalisation matrix can be expressed to a good approximation as

$$U_{u_L} = \begin{pmatrix} U_{Q_u} & 0 \\ 0 & 1 \end{pmatrix} \times R_{23}(s_t, \phi_t) = \begin{pmatrix} c_u & s_u e^{i\alpha_u} & -s_u s_t e^{i(\alpha_u+\phi_t)} \\ -s_u e^{-i\alpha_u} & c_u c_t & -c_u c_t e^{i\phi_t} \\ 0 & s_t e^{-i\phi_t} & c_t \end{pmatrix} , \tag{1.41}$$

where $s_t/c_t = \epsilon x_t$ and R_{23} encodes the mixing between second and third generation. For the down quarks sector the expansion is the same. These expression are valid up to corrections of order $\lambda_{u_2(d_2)}$ to the $1-2$ and $2-3$ elements of $U_{u_L(d_L)}$ and even smaller corrections to the $1-3$ elements.
As regards the right-handed diagonalisation matrices, they become the identity if the light-quark masses vanish. Neglecting the first generation eigenvalue and working at first order in $\epsilon\lambda_{u_2(d_2)}$ we get

$$U_{u_R} = \begin{pmatrix} 1 & 0 & 0 \\ 0 & 1 & -\lambda_{u_2} s_t e^{i\phi_t} \\ 0 & \lambda_{u_2} s_t e^{-i\phi_t} & 1 \end{pmatrix} . \tag{1.42}$$

A similar expansion holds for U_{d_R} with the substitutions $\lambda_{u_2} \to \lambda_{d_2}$, $s_t \to s_b$ and $\phi_t \to \phi_b$.
We can now look at the CKM matrix, defined as $V = \left(U_{u_L} U_{d_L}^\dagger\right)^*$. Using the above parametrisation we obtain

$$V \approx \begin{pmatrix} c_u c_d + s_u s_d e^{i(\alpha_d-\alpha_u)} & -c_u s_d e^{-i\alpha_d} + s_u c_d e^{-\alpha_u} & s_u s e^{-i(\alpha_u-\xi)} \\ c_u s_d e^{i\alpha_d} - s_u c_d e^{i\alpha_u} & c_u c_d + s_u s_d e^{-i(\alpha_d-\alpha_u)} & c_u s e^{i\xi} \\ -s_d s e^{i(\alpha_d-\xi)} & -s c_d e^{-i\xi} & 1 \end{pmatrix} , \tag{1.43}$$

where $s = \epsilon(x_b e^{-i\phi_b} - x_t e^{-i\phi_t})$. At this stage, we want to match eq. (1.43) to the standard CKM parametrisation. To do so we rephase imposing that at the leading order we are working with V_{ud}, V_{us}, V_{cb}, V_{tb} and V_{cs} are real, getting

$$V = \begin{pmatrix} 1 - \frac{\lambda^2}{2} & \lambda & s_u s e^{-i\delta} \\ -\lambda & 1 - \frac{\lambda^2}{2} & c_u s \\ -s_d s e^{i(\phi+\delta)} & -s c_d & 1 \end{pmatrix} , \tag{1.44}$$

where $\phi = \alpha_d - \alpha_u$ and the phase δ and the real positive parameter λ are defined by

$$s_u c_d - c_u s_d e^{i\phi} = \lambda e^{i\delta} . \tag{1.45}$$

The parametrisation eq. (1.43) is equivalent to the Wolfenstein parametrisation up to $\mathcal{O}(\lambda^4)$ presented in eq. (1.13). Further powers in the expansion parameters can be considered and the quantities s_u, s_d, s and ϕ can be determined in terms of the CKM parameters. Using tree level inputs we get

$$s = |V_{cb}| = 0.0411 \pm 0.0005 , \qquad \frac{s_u}{c_u} = \frac{|V_{ub}|}{|V_{cb}|} = 0.095 \pm 0.008 , \qquad s_d = -0.22 \pm 0.01 . \tag{1.46}$$

As a consequence of $U(2)$ symmetry, the ratio $|V_{td}/V_{ts}|$ is of order λ and the smallness of s_u/s_d reflects into the the value of $|V_{ub}/V_{td}|$. This hypothesis agrees with the alignment of the spurions ΔY_u and V in the $U(2)_Q$ flavour space, as indicated by the ratio m_u/m_c.

Chapter 2

B-physics: tools and phenomenology

An important role in this thesis is played by decays of hadrons with a b quark. The description of such processes can be rather non trivial, since hadrons are described by non perturbative dynamics. Also, many of these decays involve a complex interplay of strong, weak and electromagnetic interactions beyond the lowest-order, rendering the calculation of their branching ratios quite challenging.
Fortunately, a powerful tool helps to simplify both problems, namely substituting the full SM with a suitable EFT. Through an EFT it is possible to reduce a non trivial interaction to a simplified form. As an example, the full SM is equivalent to considering the effective Fermi theory for leptons when we want to calculate the branching fraction for muon decay into leptons.
In this chapter we are going to exploit the powerfulness of EFT applied to B physics. First, in section 2.1, we briefly summarise the main general aspects of EFTs, in particular trying to highlight the hypothesis under which such prescription is valid. In section 2.2 we present two effective theories commonly used in B physics. In section 2.3 we discuss the problems arising when we consider hadronic transitions and finally in section 2.4 we summarise the state-of-the-art of the SM prediction for some chosen observables and the comparison with data.

2.1 General remarks on Effective Field Theories

2.1.1 The path integral formulation

An EFT approach is a very convenient tool to use in quantum field theory. In fact, it provides a formalism to apply every time we deal with a multi-scale problem. By means of it, we obtain a substantial simplification of the calculation on a given field theory.
The main idea behind EFT is very simple. Let us consider a quantum field theory with a large fundamental scale M, and suppose we are interested in investigating processes at a scale $E \ll \Lambda$. It is quite natural to ask if, given the gap between Λ and M, we can perform an expansion of quantities as decay rates or cross sections in powers of E/M. This can be achieved through the following steps:

1. We introduce a cut-off scale $\Lambda < M$ such that we divide the fields in our theory into low-frequency and high-frequency modes

$$\phi = \phi_L + \phi_H \,, \tag{2.1}$$

where ϕ_L contains the modes with frequency $\omega < \Lambda$ and ϕ_H the ones with $\omega > \Lambda$. We can think about Λ as a threshold scale, above which often we do not know anything about our theory. Due to the construction we are building, the low energy physics will be described by means of ϕ_L only.

All the quantities we would like to calculate in our theory, are expressed in terms of correlation functions. They can be expressed in the path integral formalism as:

$$\langle 0|T\{\phi_L(x_1)\dots\phi_L(x_n)\}|0\rangle = \frac{1}{Z[0]}\left(-i\frac{\delta}{\delta J_L(x_1)}\right)\dots\left(-i\frac{\delta}{\delta J_L(x_n)}\right)Z[J_L]\Big|_{J_L=0}, \quad (2.2)$$

where

$$Z[J_L] = \int \mathcal{D}\phi_L\mathcal{D}\phi_H e^{iS(\phi_L,\phi_H)+i\int \mathrm{d}^d x\ J_L(x)\phi_L(x)} \quad (2.3)$$

is the generating functional of the theory. The action is defined as $S(\phi_L,\phi_H)=\int \mathrm{d}^d x\mathcal{L}(x)$, where d is the dimension of space-time and the Lagrangian $\mathcal{L}(x)$ depends on both ϕ_L and ϕ_H. Note that since we are interested in a correlation function like eq. (2.2) where only the low-frequency modes appear, also in the interaction term in eq. (2.3) it suffices to specify the sources for the light degrees of freedom.

2. The second step is performing the path integral over the high-frequency fields. This gives

$$Z[J_L] \equiv \int \mathcal{D}\phi_L e^{iS_\Lambda(\phi_L)+i\int \mathrm{d}^d x J_L(x)\phi_L(x)}\,, \quad (2.4)$$

where

$$e^{iS_\Lambda(\phi_L)} = \int \mathcal{D}\phi_H\ e^{iS(\phi_L,\phi_H)} \quad (2.5)$$

is called the *Wilsonian action* and depends on the choice for the cut-off Λ that we applied. The procedure through which we removed the heavy degrees of freedom is also referred to as *integrating out* the high-frequency modes from the generating integral.

3. The final step consists in expanding the the action $S_\Lambda(\phi_L)$ in terms of local operators made up by the light fields. The expansion can be done because we assumed $E \ll \Lambda$ and it is often called the operator product expansion (OPE). The result of this procedure can be summarised as

$$S_\Lambda(\phi_L) = \int \mathrm{d}^d x\ \mathcal{L}^{\text{eff}}_\Lambda(x)\,, \quad (2.6)$$

where

$$\mathcal{L}^{\text{eff}}_\Lambda(x) = \sum_i g_i Q_i(\phi_L(x))\,, \quad (2.7)$$

is called *effective Lagrangian*. Theoretically, it is an infinite sum over the local operators Q_i, which are made up from the light fields only, weighted over the different Wilson coefficients g_i. The selection of the operators appearing in eq. (2.7) depends on the symmetry of theory we are working with.

The only point which still remains unclear is about the predictive power of the effective low energy theory just constructed. In fact, the sum in eq. (2.7) contains in principle an infinite number of operators, and apparently there is no motivation to restrict it to a few. In order to have a better understanding, we can work out the dimensional analysis for the Wilson coefficients g_i. In fact, if we denote the mass dimension of the effective coupling as $[g_i] = -\gamma_i$, we can perform the following expansion:

$$g_i = C_i M^{-\gamma_i} \quad (2.8)$$

where the coefficients C_i are dimensionless and are expected to be $\mathcal{O}(1)$ parameters.
At the low scale $E \ll \Lambda < M$ the contribution of each operator Q_i to any observable will scale as

$$C_i\left(\frac{E}{M}\right)^{\gamma_i} = \begin{cases} \mathcal{O}(1) & \text{if } \gamma_i = 0\,, \\ \ll 1 & \text{if } \gamma_i > 0\,, \\ \gg 1 & \text{if } \gamma_i < 0\,. \end{cases} \quad (2.9)$$

From this it is immediate to see that only operators with $\gamma_i \leq 0$ give an important contribution at low energy. This means that we are able to truncate the series in eq. (2.7) at some order in E/M depending on the precision goal we aim to; once this is set, only a finite number of effective operators will contribute at low energy.

2.1.2 The matching procedure

The path integral formulation just presented consists in a very interesting and precise method to derive an effective Lagrangian from a complete theory. However, when we want to get rid of high energy modes associated with quark and gluons, the path integral cannot be used. In fact, the following two problems arise: first the path integral is not gaussian if QCD effects are taken into account; second, at low energy strong interactions are not perturbative.
These difficulties are overcome using a *matching procedure*, made up of the following points:

1. We list all the possible gauge invariant operators at a fixed dimension in perturbation theory, allowed by the symmetries and the quantum numbers of the low energy fields for a given problem. Again, as in the path integral formulation, the accuracy we want to achieve determines at which order we truncate the series of possible operators.

2. We write down the effective Lagrangian, where the Wilson coefficients C_i are unknown quantities
$$\mathcal{L}^{\text{eff}} = \sum_{d>4} \sum_i \frac{C_i}{\Lambda^{d-4}} Q_i \,. \tag{2.10}$$

3. We extrapolate the values of the Wilson coefficients by comparing some amplitudes in the full theory and the effective theory, namely
$$\mathcal{A}_n = \langle f_n | \mathcal{L} | i_n \rangle = \sum_{d>4} \sum_i \frac{C_i}{\Lambda^{d-4}} \langle f_n | Q_i | i_n \rangle + \text{higher power corrections} \tag{2.11}$$
at a given order in perturbation theory.

With this procedure we can extract the values of the Wilson coefficients at the high scale where the full theory lives. However, typically the effective Lagrangian framework that we are building is used at a different energy scale. In order to evaluate the Wilson coefficients at any scale we have to solve the renormalisation group equations (RGE) for the Wilson Coefficients.
This task can be challenging, depending on the level of accuracy needed. Some technical comments on this procedure are in order.

Matching at one loop order. When matching an EFT to the full theory, two cases can arise. Either the structure of radiative corrections is the same for the full theory and the EFT, or they are different. As a result, in the latter case the expansion of the propagator of the heavy degrees of freedom and the loop integral do not commute:
$$\int \mathrm{d}^d p \frac{1}{M^2 - p^2} f(p) \neq \frac{1}{M^2} \int \mathrm{d}^d p \left(1 + \frac{p^2}{M^2} + \dots\right) f(p) \,. \tag{2.12}$$

The differences between the r.h.s. and the l.h.s. arise in the large loop momentum region $p^2 \sim M^2$, but for such large momenta QCD is weakly coupled. In such regime, perturbation theory is valid and can be used to calculate the differences between the matrix elements in the two theories: such effects are accounted for by the Wilson coefficients. Further comments are in order

- The IR regulators which appear in each intermediate step of the calculations, cancel into the result for the Wilson coefficients.

- Usually matrix elements in the effective theory are more singular than the ones in the complete theory, and require additional UV subtractions (as the operator renormalisation). This yields the renormalisation-scale and -scheme dependence of the Wilson coefficients.

Renormalization-Group Improved Perturbation Theory The renormalization-group (RG) improved perturbation theory must be used every time in which, when calculating the Wilson coefficients, the high scale M and the low scale μ where we would like to calculate our matrix elements in the EFT are widely separated. As a consequence, the expansion parameter will not be simply α_s but rather $\alpha_s \log \frac{M^2}{\mu^2}$, and the latter can assume rather large values. Such logarithms must be resummed at all orders in perturbation theory. Such resummation is achieved by solving the RG equations. The procedure works as follows: at leading order (LO) all terms of the form $\left(\alpha_s \log \frac{M^2}{\mu^2}\right)^n$ with $n = 0, \ldots, \infty$ are resummed. The result of this process is an $\mathcal{O}(1)$ contribution to the Wilson coefficents. At next-to-leading order (NLO), also terms of the type $\alpha_s \left(\alpha_s \log \frac{M^2}{\mu^2}\right)^n$ are resummed, giving an overall $\mathcal{O}(\alpha_s)$ contribution.

Anomalous dimensions In order to perform the resummations just discussed, it is useful to take a look at the renormalisation of the operators involved in the effective Lagrangian. Suppose to have a complete basis of operators $\{Q_i(\mu)\}$ with $i = 1, \ldots n$ at a fixed dimension. Once we fix the scale μ, we can imagine to vary it by an infinitesimal quantity $\delta\mu$. What happens is that due to this variation, some terms from the operator will migrate to the Wilson coefficients and vice versa, but the observables must remain unchanged. In practice this means:

$$\mathcal{A} = \sum_{i=1}^{n} C_i(\mu)\langle Q_i(\mu)\rangle = \sum_{i=1}^{n} C_i(\mu - \delta\mu)\langle Q_i(\mu - \delta\mu)\rangle \tag{2.13}$$

where $\mathcal{A}$ denotes any observable. In other words we are saying that the observables must be scale independent:

$$\frac{d\mathcal{A}}{d\log\mu} = 0 \qquad \Rightarrow \qquad \frac{d}{d\log\mu}\sum_{i=1}^{n} C_i(\mu)\langle Q_i(\mu)\rangle = 0\,. \tag{2.14}$$

From eq. (2.14) we need to perform the derivative of both $C_i(\mu)$ and $\langle Q_i(\mu)\rangle$. In order to do so, we recall that the operators form a complete basis: this means that its derivative can be expressed as a linear combination of the operators in the basis with suitable weights, namely

$$\frac{d}{d\log\mu}\langle Q_i(\mu)\rangle \equiv -\sum_{j=1}^{n} \gamma_{ij}(\mu)\langle Q_j(\mu)\rangle\,. \tag{2.15}$$

The coefficients γ_{ij} are dimensionless and they measure the change of the operators under scale variation. Note that they are free of any large logarithms. Commonly they are addressed as *anomalous dimensions*. We can now plug in eq. (2.15) into eq. (2.14) to get an equation for the Wilson coeffcients:

$$\sum_{j=1}^{n}\left[\frac{d}{d\log\mu}C_j(\mu) - \sum_{i=1}^{n} C_i(\mu)\gamma_{ij}(\mu)\right]\langle Q_j(\mu)\rangle = 0\,. \tag{2.16}$$

Using again the fact that the operators form a basis and hence they are linearly independent, we obtain:

$$\frac{d}{d\log\mu}C_j(\mu) - \sum_{i=1}^{n} C_i(\mu)\gamma_{ij}(\mu) = 0\,. \tag{2.17}$$

This is the RG running for the Wilson coefficients. It is convenient to express it in matrix form as

$$\frac{d}{d\log\mu}\vec{C}(\mu) = \hat{\gamma}^T(\mu)\vec{C}(\mu)\,. \tag{2.18}$$

We can perform a further manipulation. In fact we note that the anomalous dimension matrix $\hat{\gamma}$ depends on the scale μ only through its dependence on the strong coupling $\alpha_s(\mu)$. We can then perform a change of variable from $\log\mu$ to $\alpha_s(\mu)$ introducing the QCD β-function defined as $\beta = d\alpha_s(\mu)/d\log\mu$. We obtain

$$\frac{d}{d\alpha_s(\mu)}\vec{C}(\mu) = \frac{\gamma^T(\alpha_s(\mu))}{\beta(\alpha_s(\mu))}\vec{C}(\mu)\,. \tag{2.19}$$

In order to solve the RG equations for the Wilson coefficients we need to determine some initial conditions. This would be nothing but the sets of Wilson coefficients evaluated at some scale M. The unique solution to eq. (2.19) is

$$\vec{C}(\mu) = T_\alpha \exp\left[\int_{\alpha_s(M)}^{\alpha_s(\mu)} \mathrm{d}\alpha_s \frac{\hat{\gamma}(\alpha_s)}{\beta(\alpha_s)}\right]\vec{C}(M)\,, \tag{2.20}$$

where T_α is an ordering operator.
The integration in eq. (2.20) depends in the anomalous dimension for each process and it can be rather involved to carry out. Nevertheless we can perform a controlled expansion of the quantities involved in, such as $\gamma(\alpha_s)$, $\beta(\alpha_s)$ and $\vec{C}(M)$. For simplicity, we also discuss only the case in which we have one single Wilson coefficient: the generalisation can be found in [13]. In our framework we have

$$\gamma(\alpha_s) = \gamma_0\frac{\alpha_s}{4\pi} + \mathcal{O}(\alpha_s^2)\,, \qquad \beta(\alpha_s) = -2\alpha_s\left[\beta_0\frac{\alpha_s}{4\pi} + \mathcal{O}(\alpha_s^2)\right]\,, \qquad C(M) = 1 + \mathcal{O}(\alpha_s)\,, \tag{2.21}$$

which brings us to the leading order solution

$$C(\mu) = \left(\frac{\alpha_s(\mu)}{\alpha_s(M)}\right)^{-\frac{\gamma_0}{2\beta_0}}\left[1 + \mathcal{O}(\alpha_s)\right]\,. \tag{2.22}$$

The LO approximation we just used is meant for illustration purposes only, since it does not provide the required accuracy. At NLO the accuracy we get is comparable with the one of a one-loop calculation for a single scale problem. At this stage we need the two loop calculation for the anomalous dimensions. The state of art of many calculations is nowadays the next-to-next to leading order (NNLO) approximation.

2.2 EFTs for B-physics

The study of B-physics is extremely well suited for an EFT approach. In fact in this field we have a typical multi-scale problem. Starting from the scale of the electroweak interactions m_W, we can construct an EFT independent of the vector bosons and the top quark, valid up to the scale $\mu = m_b$. This allows to substitute the full SM Lagrangian with an effective one made up by four fermions operators weighted by some Wilson coefficients. In this field usually the Wilson coefficients are addressed to as *short distance* effects. The result for cases of interest is discussed in section 2.2.1.
On the other hand, another class of interesting phenomena is the description of the non-perturbative dynamics which characterise hadrons. Also in this case, two different scale appear: the high one is the mass of the heavy quark m_b and the low one is the confinement scale Λ_{QCD}. This scale separation gives rise to an effective theory description of a non perturbative dynamics when the decaying hadron has an heavy quark (b or c). This theory goes under the name

of *heavy quark effective theory* (HQET) and can be used to calculate the form factors for a hadronic process, which are also addressed to as *long distance* effects. Their definitions and uses are discussed in section 2.3. The basic concepts from which HQET is build are summarised in section 2.2.2.

2.2.1 The weak Lagrangian

The weak Lagrangian at low energies is constructed starting from the complete SM and integrating out the heavy degrees of freedom such as the top quark, the W and the Z gauge bosons. The complete basis we obtain is rather large. However, since the focus of this thesis is on b quark decays, we can restrict the discussion only to the relevant operators for this type of processes. On top of that, given the focus of this thesis, we will consider two classes of processes: semileptonic b-hadron decays and flavour changing neutral current processes.

Semileptonic charged-current Lagrangian

Our task here is very easy: let us consider the charged-current semileptonic Lagrangian

$$\mathcal{L}_W^{\rm SM} = \frac{g}{\sqrt{2}} J_W^\mu(x) W_\mu^+(x) + \text{h.c.}\,, \tag{2.23}$$

where

$$J_W^\mu(x) = V_{ij}\overline{u}_L^i \gamma^\mu d_L^j + \overline{e}_L^j \gamma^\mu \nu_L^j \tag{2.24}$$

is the weak charged current for quarks and leptons in the mass basis. We can now integrate out the W field at tree level. The leading effective Lagrangian acquires the following form

$$\mathcal{L}_{\rm eff}^{\rm leading} = -\frac{4G_F}{\sqrt{2}} g_{\mu\nu} J_W^\mu(x) J_W^{\nu\dagger}(x)\,, \tag{2.25}$$

where we obtain the following relation between the Fermi constant and the W mass: $G_F/\sqrt{2} = g^2/8m_W^2$. Since our interest is in semileptonic decays, we may extract from eq. (2.25) the relevant terms, obtaining

$$\mathcal{L}_{\rm eff}^{\rm semilept.} = -\frac{4G_F}{\sqrt{2}} V_{ij}\overline{u}_L^i(x)\gamma^\mu d_L^j(x)\overline{\nu}_L(x)\gamma_\mu e_L(x) + \text{h.c.}\,, \tag{2.26}$$

where the lepton and consequently the neutrino can belong to each of the three families. Already at this order, eq. (2.26) gives an extremely accurate description of semileptonic weak decays. In fact, adding further terms will include corrections of the order $\mathcal{O}(m_B^2/m_W^2)$ to the decay amplitudes, which arise when we take into account operators with dimension eight in the effective Lagrangian. However, in most of the cases, such terms are negligible.
As we saw in section 2.1, QCD corrections are very important and must be taken into account properly. However, the case of charged semileptonic decays is very simple because the operator eq. (2.26) is not renormalised by QCD. QED effects have been calculated in [14, 15] and found to be small.

Flavour changing neutral-current transitions

The case of flavour changing neutral currents (FCNC) transitions is more complicated. In fact, in the SM, such transitions are forbidden at tree level and arise at least at one loop order. Also, contrary to what we saw for the semileptonic transitions, for FCNC the QCD corrections are extremely important and a careful treatment of the RG must be taken into account.
For sake of simplicity we will now present the basis of operators referring to a specific choice

of quarks, namely for transition of the type $b \to s$. At dimension six, the effective Hamiltonian can be expressed as

$$\begin{aligned}\mathcal{H}_{\text{eff}}^{\Delta B=1} = -\frac{4G_F}{\sqrt{2}}\Bigg[V_{ub}V_{us}^*\left(C_1(\mathcal{O}_{1c}-\mathcal{O}_{1u})+C_2(\mathcal{O}_{2c}-\mathcal{O}_{2u})\right)\\ + V_{tb}V_{ts}^*\sum_{i\neq 1u,2u} C_i(\mu)\mathcal{O}_i(\mu)\Bigg] + \text{h.c.}\,,\end{aligned} \tag{2.27}$$

where we used CKM unitarity to eliminate the structure $V_{cb}V_{cs}^*$.
The operators in eq. (2.27) are defined as follows

$$\begin{aligned}
\mathcal{O}_{1c} &= (\bar{s}_L\gamma_\mu T^a c_L)(\bar{c}_L\gamma^\mu T^a b_L)\,, & \mathcal{O}_{2c} &= (\bar{s}_L\gamma_\mu c_L)(\bar{c}_L\gamma^\mu b_L)\,,\\
\mathcal{O}_{1u} &= (\bar{s}_L\gamma_\mu T^a u_L)(\bar{u}_L\gamma^\mu T^a b_L)\,, & \mathcal{O}_{2u} &= (\bar{s}_L\gamma_\mu u_L)(\bar{u}_L\gamma^\mu b_L)\,,\\
\mathcal{O}_3 &= (\bar{s}_L\gamma_\mu b_L)\sum_q(\bar{q}_L\gamma^\mu q_L)\,, & \mathcal{O}_5 &= (\bar{s}_L\gamma_\mu\gamma_\nu\gamma_\rho b_L)\sum_q(\bar{q}_L\gamma^\mu\gamma^\nu\gamma^\rho q_L)\,,\\
\mathcal{O}_4 &= (\bar{s}_L\gamma_\mu T^a b_L)\sum_q(\bar{q}_L\gamma^\mu T^a q_L)\,, & \mathcal{O}_6 &= (\bar{s}_L\gamma_\mu\gamma_\nu\gamma_\rho T^a b_L)\sum_q(\bar{q}_L\gamma^\mu\gamma^\nu\gamma^\rho T^a q_L)\,,\\
\mathcal{O}_7 &= \frac{e}{(4\pi)^2}m_b(\bar{s}_R\sigma^{\mu\nu}b_L)F_{\mu\nu}\,, & \mathcal{O}_9 &= \frac{e^2}{(4\pi)^2}(\bar{s}_L\gamma_\mu b_L)(\bar{\ell}\gamma^\mu\ell)\,,\\
\mathcal{O}_8 &= \frac{g_s}{(4\pi)^2}m_b(\bar{s}_R\sigma^{\mu\nu}T^a b_L)G_{\mu\nu}\,, & \mathcal{O}_{10} &= \frac{e^2}{(4\pi)^2}(\bar{s}_L\gamma_\mu b_L)(\bar{\ell}\gamma^\mu\gamma_5\ell)\,.
\end{aligned} \tag{2.28}$$

Here $F_{\mu\nu}$ and $G^a_{\mu\nu}$ are the field strength tensor of the photon and the gluon respectively.
The Wilson coefficients of the operators in eq. (2.28) must be evaluated at an arbitrary renormalisation scale below the electroweak scale. At this purpose, the RG-improved perturbation theory techniques are helpful and allow the resummation of large logarithms. The state of the art of the calculation in the SM can be found in [16–19], where both the anomalous dimensions and the Wilson coefficients are evaluated at NNLO.
The interest that we have is to use the effective Hamiltonian in eq. (2.27) to evaluate transitions of the type $b \to s\ell\ell$, which are mediated by the operators $\mathcal{O}_7$, $\mathcal{O}_9$ and $\mathcal{O}_{10}$. We stress that the complete basis of operators in eq. (2.28) is required even for these transitions. In fact, looking at the form of the anomalous dimension matrix presented in [16–19], we can immediately see that it is not diagonal. This means that the Wilson coefficients mix due to the running. In particular the Wilson coefficient C_9 at a scale $\mu \approx m_b$ receives contributions also from the four quark operators. We note also that C_{10} is not renormalised by QCD corrections.

In the case of NP scenarios, the basis in eq. (2.28) is not sufficient. In fact, depending from the structure of the high energy degrees of freedom we want to probe, more operators can arise. The NP may not respect the chirality of the SM and interactions of the type $V+A$ can arise. On this purpose, we can introduce the chirality flipped operators $\mathcal{O}'_i$, where $i = 7, 9, 10$, obtained from the operators $\mathcal{O}_i$ by the exchange $L(R) \leftrightarrow R(L)$. Moreover, NP may provide (pseudo-)scalar operators. The list of further operators needed to take into account any NP effect is as follows

$$\mathcal{O}_S^{(\prime)} = \frac{e^2}{(4\pi)^2}(\bar{s}_{R(L)}b_{L(R)})(\bar{\ell}\ell)\,, \quad \mathcal{O}_P = \frac{e^2}{(4\pi)^2}(\bar{s}_{R(L)}b_{L(R)})(\bar{\ell}\gamma_5\ell)\,. \tag{2.29}$$

2.2.2 HQET

HQET is an effective theory constructed on the following hypothesis: if we only consider hadrons with a heavy quark (i.e. a b or a c quark), the mass of the heavy quark is much higher than the confinement scale Λ_{QCD}. Such gap between the two energy scales provides the perfect scenario for an effective theory approach. Inside the hadron, the energy of the heavy quark $E \sim m_{b,c}$

can be seen as a short distance effect with respect to the light degrees of freedom with energy $E \sim \Lambda_{\rm QCD}$. Basically, HQET aims to describe soft interactions of a single heavy quark into a single hadron.
The heavy quark is surrounded by a strongly interacting cloud of light quarks, antiquarks and gluon. This cloud is often referred to as *brown muck*.

The first step of the construction is to observe that inside the hadron the heavy quark moves almost at the same velocity of the hadron v and it is almost on-shell. This allows to parametrise the heavy quark momentum as

$$p_Q^\mu = m_Q v^\mu + k^\mu \,, \tag{2.30}$$

where k^μ is the residual momentum and the magnitude of its components is much smaller than m_Q. Any interaction of the heavy quark with the brown muck will induce a shift in the residual momentum of order $\Delta k^\mu \sim \Lambda_{\rm QCD}$, but as $m_Q/\Lambda_{\rm QCD} \to \infty$ the variation of the heavy quark velocity vanishes.
At this stage, we notice that we can rewrite the heavy field as a superposition of large and small component, defined as

$$\begin{aligned} h_v(x) &= e^{i m_Q v\cdot x} P_+ Q(x) \,, \\ H_v(x) &= e^{i m_Q v\cdot x} P_- Q(x) \,, \end{aligned} \tag{2.31}$$

where $P_\pm$ are projector operators defined as

$$P_\pm = \frac{1 \pm \not{v}}{2} \,. \tag{2.32}$$

From the definitions above, it follows that

$$Q(x) = \; e^{-i m_Q v\cdot x} \left[h_v(x) + H_v(x) \right] \,. \tag{2.33}$$

It is straight forward to verify that $\not{v} h_v(x) = h_v(x)$ and $\not{v} H_v(x) = -H_v(x)$. In the rest frame, h_v corresponds to the two upper components of Q, while H_v to the lower ones. Furthermore, we can see that h_v annihilates a heavy quark with velocity v, while H_v creates a heavy anit-quark with velocity v.
We can now rewrite the QCD Lagrangian in terms of the projection h_v and H_v just described. We obtain

$$\mathcal{L}_Q = \overline{h}_v i v\cdot D h_v - \overline{H}_v (i v\cdot D + 2m_Q) H_v + \overline{h}_v i \not{D}_\perp H_v + \overline{H}_v i \not{D}_\perp h_v \,, \tag{2.34}$$

where $D_\perp^\mu = D^\mu - v^\mu v\cdot D$ satisfies the condition of being orthogonal to the heavy quark velocity: $v\cdot D_\perp = 0$.
Some comments on eq. (2.34) are in order. It is manifest that h_v describes massless degrees of freedom, while H_v corresponds to fluctuations with twice the heavy quark mass. These are the heavy degrees of freedom which will be eliminated in the construction of the effective theory. The last two terms in eq. (2.34) mix the h_v and H_v components, and will give rise to non-local terms in the effective Lagrangian, as we will see shortly.
The heavy degrees of freedom can be eliminated using the equations of motion in QCD. Recalling that the equations of motion for the field Q read $(i\not{D} - m_Q)Q = 0$, and using the decomposition of the field Q in eq. (2.33), we obtain:

$$i\not{D} h_v + (i\not{D} - 2m_Q) H_v = 0 \,. \tag{2.35}$$

By means of multiplication by $P_\pm$, eq. (2.35) can be turned into the following set of independent equations:

$$-i v\cdot D h_v = i\not{D}_\perp H_v \,, \tag{2.36}$$

$$(i v\cdot D + 2m_Q) H_v = i\not{D}_\perp h_v \,. \tag{2.37}$$

In particular, eq. (2.37) can be solved with respect to H_v

$$H_v = \frac{1}{2m_Q + iv\cdot D - i\eta} i\not{D}_\perp h_v \,. \tag{2.38}$$

The equation of motion for h_v can be found substituting eq. (2.38) into eq. (2.36). The effective Lagrangian looks like

$$\mathcal{L}_{\text{eff}} = \overline{h}_v iv\cdot D h_v + \overline{h}_v i\not{D}_\perp \frac{1}{2m_Q + iv\cdot D - i\eta} i\not{D}_\perp h_v \,. \tag{2.39}$$

Given the exponential factor in eq. (2.33), the dependence of the heavy quark field h_v on x is very mild, and in momentum space derivatives of h_v give terms proportional to the residual momentum. This means that the effective Lagrangian eq. (2.39) can be expanded in powers of iD/m_Q. It useful to use the following identity to readjust the second term in eq. (2.39)

$$P_+ i\not{D}_\perp i\not{D}_\perp P_+ = P_+ \left[(iD_\perp)^2 + \frac{g_s}{2}\sigma_{\alpha\beta}G^{\alpha\beta}\right] P_+ \,, \tag{2.40}$$

where $[iD_\alpha, iD_\beta] = ig_s G_{\alpha\beta}$ is the definition of the gluon strength tensor. At order $1/m_Q$, the effective Lagrangian can be rewritten as

$$\mathcal{L}_{\text{eff}} = \overline{h}_v iv\cdot D h_v + \frac{1}{2m_Q}\overline{h}_v (iD_\perp)^2 h_v + \frac{g_s}{4m_Q}\overline{h}_v \sigma_{\alpha\beta}G^{\alpha\beta} h_v + \mathcal{O}\left(\frac{1}{m_Q^2}\right) . \tag{2.41}$$

In the limit $m_Q \to \infty$ we are left with only one term

$$\mathcal{L}_\infty = \overline{h}_v iv\cdot D h_v \,. \tag{2.42}$$

The Lagrangian in eq. (2.42) is the HQET Lagrangian.
We can now study the symmetries of HQET Lagrangian. Since there are no Dirac matrices in eq. (2.42), the interaction of the heavy quark with a gluon leaves its spin unchanged. This ensures that $\mathcal{L}_\infty$ is invariant under the $SU(2)$ symmetry group. We can study the action of such group on the heavy quark fields. For simplicity, we can do so in the rest frame, where the generators of spin $SU(2)$ look like

$$S^i = \frac{1}{2}\begin{pmatrix} \sigma^i & 0 \\ 0 & \sigma^i \end{pmatrix} = \frac{1}{2}\gamma_5\gamma^0\gamma^i \,, \tag{2.43}$$

where σ^i are the Pauli matrices. In a general frame, we can fix a set of three orthonormal vectors such that $v\cdot e = 0$ and define the generator of spin symmetry as $S^i = \frac{1}{2}\gamma_5 \not{v}\not{e}^i$. It can be verified explicitly that the matrices S^i follow a $SU(2)$ algebra and they commute with $\not{v}$:

$$[S^i, S^j] = i\epsilon^{ijk}S^k \,, \qquad [\not{v}, S^i] = 0 \,. \tag{2.44}$$

We can now study the effect of an infinitesimal transformation of $SU(2)$ spin symmetry applied on $\mathcal{L}_\infty$. The heavy quark field transforms as $h_v \to (1 + \vec{\epsilon}\cdot\vec{S})h_v$, which leaves the HQET Lagrangian invariant

$$\delta\mathcal{L}_\infty = \overline{h}_v [iv\cdot D, i\vec{\epsilon}\cdot\vec{S}] h_v = 0 \,, \tag{2.45}$$

preserving also the on-shell condition $\not{v} h_v = h_v$.
There is another symmetry arising, linked to the fact that the heavy quark mass do not appear in $\mathcal{L}_\infty$. Supposing to have N_h heavy quarks moving at the same velocity v, the Lagrangian $\mathcal{L}_\infty$ can be easily extended as

$$\mathcal{L}_\infty = \sum_{i=1}^{N_h} \overline{h}_v^i \; iv\cdot D h_v^i \,. \tag{2.46}$$

This Lagrangian is clearly invariant under rotations in flavour space. If we combine this result with the spin symmetry, the symmetry group under which the Lagrangian is invariant becomes $SU(2N_h)$ and it's called the *heavy quark spin-flavour symmetry*. Physically it means that in the limit $m_Q \to \infty$ the strong interactions of a heavy quark are independent of its spin and mass.

2.3 Hadronic matrix elements

In the next chapter of this thesis great emphasis will be given to decays of hadrons with a b quark. In light of this, it is important to have a look at these processes in more details.
Generically speaking, the hadronic transitions we are interested in are of the type $H_b \to H_q$, where H_b is a generic hadron with a b quark and H_q a generic hadronic final state. In the following we will specialise in the case $q = u, c, s$.
When we calculate any observable we need to evaluate the following matrix element

$$\mathcal{A} \propto \langle f|\mathcal{O}|i\rangle\,, \tag{2.47}$$

where i and f are a generic initial and final state and $\mathcal{O}$ any operator.
In the case we want to address we can further decompose

$$|i\rangle = H_b\,, \qquad |f\rangle = H_q F_\ell\,, \qquad \mathcal{O} = \overline{q}\,\Gamma^\mu b\,\tilde{\mathcal{O}}_\mu\,. \tag{2.48}$$

where F_ℓ is a generic final state made up of leptons, $\tilde{\mathcal{O}}_\mu$ is an operator which may contain quarks or leptons and Γ^μ is any Lorentz structure that may arise in our theory.
The parametrisation of such amplitudes is rather challenging: in fact, since in both initial and final states we deal with hadrons, we somehow need to estimate non-perturbative effects. However, a relevant distinction arises, namely concerning the form of $\tilde{\mathcal{O}}_\mu$. If $\tilde{\mathcal{O}}_\mu$ contains only leptons, the amplitude $\mathcal{A}$ factorises in a hadronic $\mathcal{A}^\mu_{\text{had}}$ and leptonic $\mathcal{A}^{\text{lept}}_\mu$ defined as

$$\begin{aligned} \mathcal{A}^\mu_{\text{had}} &= \langle H_q|\overline{q}\,\Gamma^\mu b\,|H_b\rangle\,, \\ \mathcal{A}^{\text{lept}}_\mu &= \langle F_\ell|\tilde{\mathcal{O}}_\mu|0\rangle\,. \end{aligned} \tag{2.49}$$

The leptonic part encoded by $\mathcal{A}^{\text{lept}}_\mu$ is trivial to evaluate. The hadronic amplitude $\mathcal{A}^\mu_{\text{had}}$ can be parametrised in terms of *form factors*, namely distributions which parametrise the fact that the interaction driven by the operator $\overline{q}\,\Gamma^\mu b$ happens inside the hadrons and not between free quarks.
The strategy to evaluate the form factors reads as follows:

1. We identify the number of Lorentz independent structures needed to describe the specific hadronic transition we are interested in. This depends on the quantum numbers of the hadrons in the initial and final states and on the Lorentz structures Γ^μ.

2. We assign to each structure a form factor. This means that the number of independent Lorentz structures is the same as the independent form factors.

The only ingredient we are still missing is the structure of the form factors. Unfortunately there are very few first principles that can help us in parametrising the form factors.
One powerful instrument is Lattice QCD (LQCD), which allows us to calculate the non-perturbative effects encoded in the form factors. However, LQCD calculations of the form factors are not available for all hadronic final state and in their whole kinematical spectrum. One of the controversial cases involves excited mesons: for them, only partial calculations are known and usually more theory inputs are needed to complete LQCD predictions.
In the case in which $\tilde{\mathcal{O}}_\mu$ is made up by only quarks, the factorisation in eq. (2.49) is not possible, and the amplitude must be evaluated all together. There are non-perturbative techniques able to evaluate such contributions, but their description goes beyond the scope of this thesis. However, we will point out the most up to date literature on such attempts when needed.

From now on, we will concentrate on the parametrisation of form factors in some specific case: $B \to P$ decay, where P is a generical pseudoscalar and $B \to V$, where V is a vector particle.

The decomposition for the hadronic matrix element for the $B \to P$ transitions is as follow

$$\langle P(k) \,|\, \overline{q} b \,|\, B(p) \rangle = \frac{m_B^2 - m_P^2}{m_b(\mu) + m_q(\mu)} f_0(q^2)\,, \tag{2.50}$$

$$\langle P(k) \,\big|\, \overline{q} \gamma_\mu b \,\big|\, B(p) \rangle = \left[(p+k)_\mu - \frac{m_B^2 - m_P^2}{q^2} q_\mu \right] f_+(q^2) + \frac{m_B^2 - m_P^2}{q^2} q_\mu f_0(q^2)\,, \tag{2.51}$$

$$\langle P(k) \,\big|\, \overline{q} \sigma_{\mu\nu} b \,\big|\, B(p) \rangle = \frac{i}{m_B + m_P} \left[(p+k)_\mu q_\nu - q_\mu (p+k)_\nu \right] f_T(q^2)\,, \tag{2.52}$$

where the momentum transfer is defined as $q^\mu = p^\mu - k^\mu$. The functions $f_+(q^2)$, $f_0(q^2)$ and $f_T(q^2)$ are known as vector, scalar and tensor form factor respectively. Note that eq. (2.50) and eq. (2.51) are related via the QCD equations of motion for quark fields. The decay channel we will use in the following are $P = \pi, D, K$. In all these decay channels, accurate LQCD results are available. They are presented in Refs. [20–22].

Regarding the transition $B \to V$, the structures needed are more involved. The general parametrisation looks like

$$\langle V(k) \,|\, \overline{q} \gamma_5 b \,|\, B(p) \rangle = -2i \frac{m_V}{m_b(\mu) - m_q(\mu)} (\eta^* \cdot q) A_0(q^2)\,, \tag{2.53}$$

$$\langle V(k) \,\big|\, \overline{q} \gamma_\mu b \,\big|\, B(p) \rangle = 2 \frac{V_0(q^2)}{m_B + m_V} \epsilon_{\mu\nu\rho\sigma} \eta^{*\nu} p^\rho k^\sigma\,, \tag{2.54}$$

$$\begin{aligned} \langle V(k) \,\big|\, \overline{q} \gamma_\mu \gamma_5 b \,\big|\, B(p) \rangle = i\eta^{*\nu} \Bigg[& 2m_V A_0(q^2) \frac{q_\mu q_\nu}{q^2} + (m_B + m_V) A_1(q^2) \left(g_{\mu\nu} - \frac{q_\mu q_\nu}{q^2} \right) \\ & - A_2(q^2) \frac{q_\nu}{m_B + m_V} \left((p+k)_\mu - \frac{m_B^2 - m_V^2}{q^2} (p-k)_\mu \right) \Bigg]\,, \end{aligned} \tag{2.55}$$

$$\langle V(k) \,\big|\, \overline{q} i\sigma_{\mu\nu} q^\nu b \,\big|\, B(p) \rangle = -2T_1(q^2) \epsilon_{\mu\nu\rho\sigma} \eta^{*\nu} p^\rho k^\sigma\,, \tag{2.56}$$

$$\begin{aligned} \langle V(k) \,\big|\, \overline{q} i\sigma_{\mu\nu} \gamma_5 q^\nu b \,\big|\, B(p) \rangle = {} & iT_2(q^2) \left[\eta_\mu^* (m_B^2 - m_V^2) - (\eta^* \cdot q)(p+k)_\mu \right] \\ & + T_3(q^2)(\eta^* \cdot q) \left[q_\mu - \frac{q^2}{m_B^2 - m_V^2} (p+k)_\mu \right]\,, \end{aligned} \tag{2.57}$$

where η_μ denotes the polarisation vectors of V.
The state of the art of the form factors is more involved in the vector case. For $V = K^*$ LQCD results have been produced at high q^2 [23, 24], while at low q^2 light cone sum rules apply. A combined fit of the two results to a z-expansion parametrisation of the form factor is presented in [25]. On top of this, non-perturbative contributions non proportional to the form factors may arise from four quarks operators. Addressing this effects is rather complex; nevertheless, they may generate sizeable effects in the amplitude for $B \to K^* \ell\ell$ decays. Many attempts to parametrise such contributions have been carried out and the details are in [26, 27].
In the $V = D^*$ case LQCD inputs are available only in the zero-recoil point. This is a good example where HQET plays an important role. In fact, through the techniques of HQET, it is possible to relate at leading order all the form factors for a $B \to D^*$ transition to a universal form factor known as *Isgur-Wise function* $\xi(w)$, where $w = v \cdot v'$ and v, v' are the velocity of the b and c quarks respectively. In this framework, the hadronic matrix elements for a $B \to D^*$ transitions are expressed as

$$\frac{1}{\sqrt{m_B m_D}} \langle D^*(v', \eta) \left| \overline{c}_{v'} \gamma^\mu b_v \right| B(v) \rangle = i\epsilon^{\mu\nu\rho\sigma} \eta_\nu^* v'_\rho v_\sigma \xi(w)\,, \tag{2.58}$$

$$\frac{1}{\sqrt{m_B m_D}} \langle D^*(v', \eta) \left| \overline{c}_{v'} \gamma^\mu \gamma_5 b_v \right| B(v) \rangle = \left[\eta^{*\mu} (v \cdot v' + 1) - v'^\mu \eta^* \cdot v \right] \xi(w)\,. \tag{2.59}$$

The remarkable consequence comes from the fact that comparing eq. (2.53) and eq. (2.54) to eq. (2.58) and eq. (2.59) respectively, we can express the form factors $V(q^2)$ and $A_{0,1,2}(q^2)$ at leading order in the heavy quark expansion in term of a unique Isgur-Wise functions $\xi(w)$.
This comparison works only at leading power in $1/m_{b,c}$ and do not address QCD corrections proportional to powers of α_s. Such corrections are calculated in [28].
Even using this description, some inputs are needed to have a numerical expression for the form factors. Such inputs are obtained using data. In [29] we find a collection of all the inputs and expression needed to parametrise the form factors. A more updated analysis can be found in [30].

2.4 The present status: data vs SM predictions

The techniques presented in the previous sections of this chapter are very useful to build up the SM prediction for many observables in semileptonic and rare B decays. What turns out to happen is that when we compare the SM predictions for such quantities to the experimental measurements, some tension is observed, making these processes very interesting to be further investigated.
In the following, we list and discuss the most relevant observables for the channel $b \to c\ell\overline{\nu}_\ell$ and $b \to s\ell^+\ell^-$.

Semileptonic $b \to c\ell\nu$

In the $b \to c\ell\nu$ channel, the key observables are the universality ratios $R_{D^{(*)}}$, defined as:

$$R_{D^{(*)}} = \frac{\mathcal{B}(B \to D^{(*)}\tau\overline{\nu}_\tau)}{\mathcal{B}(B \to D^{(*)}\mu\overline{\nu}_\mu)}\,. \tag{2.60}$$

The choice of introducing a ratio instead of looking at the single branching ratios comes from the fact that the uncertainties on a single branching ratio can be big. This comes from the fact that the uncertainties on the form factors are rather big. As a consequence, we need to find observables in which the dependence on the form factors is rather small and hence the error is also reduced. The ratios $R_{D^{(*)}}$ are the first example of observable built following this principle. Before showing the SM prediction for $R_{D^{(*)}}$, it is worth discussing the anatomy of such ratios. The decay width of the process $B \to D^{(*)}\tau\overline{\nu}_\tau$ can be expressed as a sum of two terms:

$$\begin{aligned}
\frac{\mathrm{d}\Gamma_\tau}{\mathrm{d}q^2} &= \frac{\mathrm{d}\Gamma_{\tau,1}}{\mathrm{d}q^2} + \frac{\mathrm{d}\Gamma_{\tau,2}}{\mathrm{d}q^2}\,,\\
\frac{\mathrm{d}\Gamma_{\tau,1}}{\mathrm{d}q^2} &= \frac{\mathrm{d}\Gamma}{\mathrm{d}q^2}\left(1-\frac{m_\tau^2}{q^2}\right)^2\left(1+\frac{m_\tau^2}{2q^2}\right)\,,\\
\frac{\mathrm{d}\Gamma_{\tau,2}}{\mathrm{d}q^2} &= \Gamma_0\,\frac{m_\tau^2}{q^2}c_0\,,
\end{aligned} \tag{2.61}$$

where $\frac{\mathrm{d}\Gamma}{\mathrm{d}q^2}$ represents the decay width in the case of massless charged lepton in the final state and Γ_0 is a normalisation factor. The coefficient c_0 encodes a sum of modulus square of form factors, weighted on some kinematical functions which depend on the hadronic final state we are taking into account, namely the D or the D^* case. As a general comment so far we note that since $\frac{\mathrm{d}\Gamma_{\tau,2}}{\mathrm{d}q^2}$ is proportional to the mass of the charged lepton in the final state, it is non negligible in the semitauonic mode only. This means that the in the semimuonic mode, we can consider the muon to be massless and approximate the decay width with $\frac{\mathrm{d}\Gamma}{\mathrm{d}q^2}$. This approximation is well justified also numerically.

The decomposition eq. (2.61) reflects also onto the ratios $R_{D^{(*)}}$ which can also be written as a sum of terms as

$$R_{D^{(*)}} = R^{\tau,1}_{D^{(*)}} + R^{\tau,2}_{D^{(*)}}\,, \tag{2.62}$$

where

$$R^{\tau,1}_{D^{(*)}} = \frac{\int_{m_\tau^2}^{q^2_{\rm max}} \mathrm{d}q^2\, \frac{\mathrm{d}\Gamma_{\tau,1}}{\mathrm{d}q^2}}{\int_0^{q^2_{\rm max}} \mathrm{d}q^2\, \frac{\mathrm{d}\Gamma}{\mathrm{d}q^2}}\,, \qquad \text{and} \qquad R^{\tau,2}_{D^{(*)}} = \frac{\int_{m_\tau^2}^{q^2_{\rm max}} \mathrm{d}q^2\, \frac{\mathrm{d}\Gamma_{\tau,2}}{\mathrm{d}q^2}}{\int_0^{q^2_{\rm max}} \mathrm{d}q^2\, \frac{\mathrm{d}\Gamma}{\mathrm{d}q^2}}\,, \tag{2.63}$$

and $q^2_{\rm max} = (m_B - m_{D^{(*)}})^2$.
For the $B \to D$ case, both $R^{\tau,1}_{D^{(*)}}$ and $R^{\tau,2}_{D^{(*)}}$ can be precisely determined due to LQCD determinations of the form factors. Recently, in [31], the two lattice results in [21, 32] have been combined leading to

$$\begin{aligned} R^{\tau,1}_D = 0.176 \qquad R^{\tau,2}_D = 0.123\,, \\ R^{\rm SM}_D = 0.299 \pm 0.003\,, \end{aligned} \tag{2.64}$$

where we can see that the mass dependent terms encoded in $R^{\tau,2}_D$ are large.
In the $B \to D^*$ channel the situation is more complicated since, as already mentioned, the LQCD determination of the form factors is rather poor, and many inputs are extracted from data. The decomposition in eq. (2.61) shows why this point is rather delicate. The data driven inputs for the form factors for the $B \to D^*$ mode must be extracted in the semimuonic channel since the experimental spectrum in the semitauonic case is not reliable enough. This implies that all the information needed to determine the form factors encoded in the coefficient c_0 of eq. (2.61) can't be extracted from data and hence we must rely on theory inputs as the ones from HQET. As it is shown in [30], as a consequence of this fact the uncertainty on $R^{\tau,2}_{D^{(*)}}$ is large. However, when we look at the numerical value of $R^{\tau,1}_{D^*}$, $R^{\tau,2}_{D^*}$ and eventually R_{D^*} we find [30]:

$$\begin{aligned} R^{\tau,1}_{D^*} = 0.232 \qquad R^{\tau,2}_{D^*} = 0.028\,, \\ R^{\rm SM}_{D^*} = 0.260 \pm 0.008\,. \end{aligned} \tag{2.65}$$

Therefore, even if potentially the uncertainty on $R^{\tau,2}_{D^{(*)}}$ might contribute heavily to the error budget of R_{D^*}, the magnitude of $R^{\tau,2}_{D^{(*)}}$ is so small with respect to the one of $R^{\tau,1}_{D^{(*)}}$ that the overall contribution to the error budget does not exceed a few per cent.
On the experimental side, BaBar, Belle and LHCb collaboration provided several measurements of both $R_{D^{(*)}}$ universality ratios. The results are summarised in table 2.1. The difference between the three Belle determinations [33–35] is the method applied to reconstruct the τ in the final state, namely through its leptonic or hadronic decays. The same argument holds for the LHCb determinations in [36, 37].
If we average the experimental results for R_D and R_{D^*} [38] and we compare them to the SM predictions, we obtain 2.4σ and 2.6σ deviations respectively for the two observables. It is quite interesting to look also at the combined deviation, which turns out to be of $\sim 3.7\sigma$ with respect to the SM. From a phenomenological point of view, this is very interesting. In fact, the $B \to D^{(*)}\ell\nu$ decays happen in the SM at tree level, and such big deviation needs a big tree level contribution in a NP scenario to be explained. As a consequence, as we will see in Part IV, the the effective scale of NP must be rather low.

FCNC $b \to s\ell\ell$

The FCNC $b \to s\ell\ell$ offer a variety of channels to be probed. In the following we refer to the most sensitive up to now.

	R_D	R_{D^*}
BaBar	$0.440 \pm 0.058 \pm 0.042$ [39]	$0.440 \pm 0.058 \pm 0.042$ [39]
Belle	$0.375 \pm 0.064 \pm 0.026$ [33]	$0.293 \pm 0.038 \pm 0.015$ [33] $0.302 \pm 0.030 \pm 0.011$ [34] $0.270 \pm 0.035^{+0.028}_{-0.025}$ [35]
LHCb	-	$0.336 \pm 0.027 \pm 0.030$ [36] $0.285 \pm 0.019 \pm 0.029$ [37]

Table 2.1: Experimental measurements of R_D and R_{D^*}.

$R_K[1\ \text{GeV}^2, 6\ \text{GeV}^2]$	$R_{K^*}[1.1\ \text{GeV}^2, 6.0\ \text{GeV}^2]$	$R_{K^*}[0.045\ \text{GeV}^2, 1.1\ \text{GeV}^2]$
$0.745^{+0.090}_{-0.074} \pm 0.036$ [42]	$0.69^{+0.11}_{-0.07} \pm 0.05$ [43]	$0.66^{+0.11}_{-0.07} \pm 0.03$ [43]

Table 2.2: Experimental measurements of the universality ratios $R_{K^{(*)}}$ performed by LHCb.

As shown for the semileptonic decays, also in this case it is possible to construct quantities with low uncertainties. Following this principle, we can construct the following observable

$$\mathcal{R}_M[q^2_{\text{min}}, q^2_{\text{max}}] \equiv \frac{\int_{q^2_{\text{min}}}^{q^2_{\text{max}}} \frac{\mathrm{d}\mathcal{B}(B\to M\mu^+\mu^-)}{\mathrm{d}q^2}\mathrm{d}q^2}{\int_{q^2_{\text{min}}}^{q^2_{\text{max}}} \frac{\mathrm{d}\mathcal{B}(B\to Me^+e^-)}{\mathrm{d}q^2}\mathrm{d}q^2}\,, \tag{2.66}$$

where M can be any hadron with an s quark with allowed quantum numbers and q^2 is the invariant mass of the lepton pair in the final state. Given the measurements available so far, we will discuss the case $M = K, K^*$. An interesting and important point is the binning choice for such observables. In fact, looking at the $B \to K$ or $B \to K^*$ spectrum, many resonances arise. The most important ones are the J/Ψ and the $\psi(2S)$, which are bound states of $c\bar{c}$ quarks. The choice of binning must be done in such a way that in the region of choice the pollution due to the resonances is under control. Moreover, for the mode $M = K^*$, we need also to disentangle the low q^2 region from the rest of the spectrum: in fact, due to the contribution of the operator $\mathcal{O}_7$ in eq. (2.28), at very high recoil the process is dominated by an almost on-shell photon.
The experimental measurements for the universality ratios performed by LHCb are summarised in table 2.2. The most up to date SM predictions for the ratios $R_{K^{(*)}}$ are presented in [40] and are discussed in details in chapter 5. For completeness, we report the results postponing the discussion of their derivations to chapter 5:

$$R^{\text{SM}}_K[1\ \text{GeV}^2, 6\ \text{GeV}^2] = 1.00 \pm 0.01\,, \tag{2.67}$$

$$R^{\text{SM}}_{K^*}[1.1\ \text{GeV}^2, 6.0\ \text{GeV}^2] = 1.00 \pm 0.01\,, \tag{2.68}$$

$$R^{\text{SM}}_{K^*}[0.045\ \text{GeV}^2, 1.1\ \text{GeV}^2] = 0.91 \pm 0.03\,. \tag{2.69}$$

The comparison of eq. (2.67) with the measurements in table 2.2 shows a deviation from 2.1σ to 2.6σ for the different bins.
Before commenting further on the relevance of such results and on further observables, it is worth to discuss more the bin $q^2 \in [0.045\ \text{GeV}^2, 1.1\ \text{GeV}^2]$ for R_{K^*}. The fact that the operator $\mathcal{O}_7$ dominates the SM prediction at very low q^2 makes the interpretation of the deviation in this bin rather intriguing. As shown in [41] even in the presence of new physics scenarios able to explain the tension in the region $q^2 \in [1\ \text{GeV}^2, 6\ \text{GeV}^2]$, the low q^2 bin remains controversial.

Apart from the universality ratios, other observables have been measured. In particular, great effort has been made to study the decay $B \to K^*(\to K\pi)\mu^+\mu^-$. The study of this decay

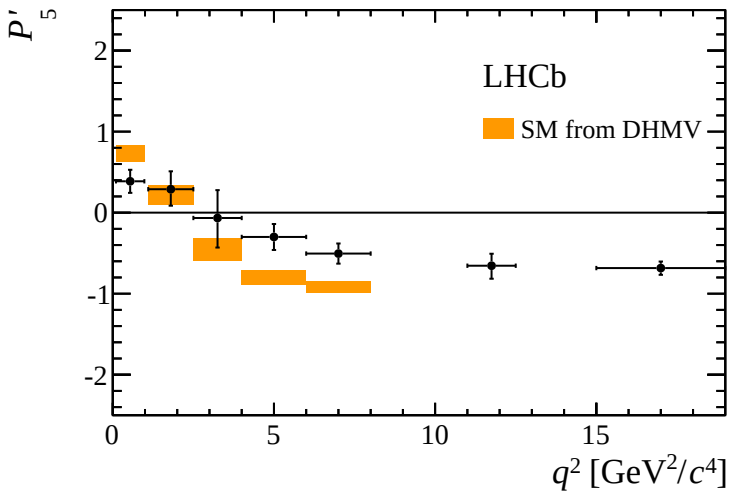

Figure 2.1: Experimental measurement of the observable P_5' in comparison with the SM predictions.

mode offers a rich variety of angular observables to be tested. For completeness and better understanding, we report the decay width for the decay $B \to K^*(\to K\pi)\mu^+\mu^-$ avareged on the CP conjugate state

$$\begin{aligned}\frac{1}{\mathrm{d}(\Gamma+\overline{\Gamma})/\mathrm{d}q^2}\frac{\mathrm{d}^4(\Gamma+\overline{\Gamma})}{\mathrm{d}q^2\mathrm{d}\Omega} = \frac{9}{32\pi}\Big[&\frac{3}{4}(1-F_L)\sin^2\theta_K + F_L\cos^2\theta_K + \frac{1}{4}(1-F_L)\sin^2\theta_K\cos 2\theta_\ell \\ &- F_L\cos^2\theta_K\cos 2\theta_\ell + S_3\sin^2\theta_K\sin 2\theta_\ell\cos 2\phi \\ &+ S_4\sin 2\theta_K\sin 2\theta_\ell\cos\phi + S_5\sin 2\theta_K\sin\theta_\ell\cos\phi \\ &+ \frac{4}{3}A_{\mathrm{FB}}\sin^2\theta_K\cos\theta_\ell + S_7\sin 2\theta_K\sin\theta_\ell\sin\phi \\ &+ S_8\sin^2\theta_K\sin 2\theta_\ell\sin\phi + S_9\sin 2\theta_K\sin 2\theta_\ell\sin 2\phi\Big],\end{aligned} \tag{2.70}$$

where the angle definition follows from [44]. From the base of observables F_L, A_{FB} and S_i, we can define optimised observables, where the hadronic uncertainties are reduced. In particular, we highlight the following one

$$P_5' = \frac{S_5}{\sqrt{F_L(1-F_L)}}\,. \tag{2.71}$$

In figure 2.1 we see the measurements of P_5' in different bins of q^2 as shown in [44]. We can see that in the central bins, a deviation with the SM is observed at the level of 3.4σ. Some effort in the measure of P_5' has been made also by Belle. They perform the analysis not only in the muon mode but also in the electron mode. This is very interesting, because it could clarify if the deviations observed in the $b \to s\ell\ell$ channel are due to the muon or the electron modes or both. However, as shown in [45], the sensitivity is not enough to draw any conclusion. It's also worth to mention that ATLAS and CMS presented a measurement of P_5' in [46] and [47], but their measurements are affected by quite big errors. As a conclusion, so far no experiments have been able to confirm or reject the LHCb measurement.

The observables $R_{K^{(*)}}$ and P_5' here presented are the most significant one in the channel $b \to s\ell\ell$. Their significance is not high but it points to a coherent pattern of deviations with respect to the SM. Many analysis including all the data in the $b \to s\ell\ell$ channel have been performed

in [41, 48–54]. It is shown that the combined significance for this channel can be rather high, but a clear explanation of which physics lies underneath it is still far away.

Part II

Precise predictions within the Standard Model: charged current processes

Chapter 3

Impact of leptonic τ decays on the distribution of $B \to P\mu\overline{\nu}$ decays

3.1 Introduction

In this chapter we concentrate on the simplest of LFU ratios for the charged current hadronic transition $b \to c$, namely

$$R_P = \frac{\mathcal{B}(\overline{B} \to P\tau\overline{\nu})}{\mathcal{B}(\overline{B} \to P\mu\overline{\nu})}\,, \tag{3.1}$$

where $P = D, \pi$.

The theoretical estimate of R_P within the SM relies dominantly on the hadronic form factors f_+ (the vector form factor) and f_0 (the scalar form factor), see appendix A.1 for their definitions. For both final states, precise lattice QCD result of these form factors have recently been published [20,21]. In addition, Light-Cone Sum Rules (LCSRs) results for the $B \to \pi$ vector form factor and two of its derivatives have been obtained, which complement the lattice QCD results. According to these studies the SM prediction for R_D [21] is

$$R_D^{\rm SM} = 0.299 \pm 0.003\,. \tag{3.2}$$

On the experimental side, measurements of the ratio R_D have been published by both BaBar [39] and, more recently, by Belle [33],

$$R_D^{\rm BaBar} = 0.440 \pm 0.058 \pm 0.042\,, \quad R_D^{\rm Belle} = 0.375 \pm 0.064 \pm 0.026\,, \tag{3.3}$$

while only upper experimental bounds on R_π are available [55]. Combining Babar and Belle results, and normalizing them to the SM, leads to

$$\Delta R_D = \frac{R_D^{\rm exp}}{R_D^{\rm SM}} - 1 = 0.36 \pm 0.15\,. \tag{3.4}$$

This deviation from the SM is not particularly significant; however, a similar effect has been observed also in the R_{D^*} ratios [33,36,39]. Combining the two deviations, which are compatible with a universal enhancement of semileptonic $b \to c\tau\nu$ transitions over $b \to c\mu\nu$ ones, the discrepancy with respect to the SM raises to about $\sim 4\sigma$. This fact has stimulated several studies on possible New Physics (NP) explanations (see e.g. Ref. [56–59]). As pointed out in Ref. [58], because of $\tau \to \ell\overline{\nu}\nu$ decays, a possible enhancement of semileptonic $b \to c\tau\nu$ transitions may have a non-trivial impact in the extraction of $|V_{cb}|$ from the corresponding $b \to c\ell\nu$ modes, and this impact is likely to be different for exclusive and inclusive modes.

Our main goal is to analyze how leptonic $\tau \to \mu\overline{\nu}\nu$ decays affect the determination of R_P and, more generally, the kinematical distribution of $\overline{B} \to P\mu\overline{\nu}$ decays via the decay chain

$\overline{B} \to P\tau(\to \mu\overline{\nu}\nu)\overline{\nu}$ As we will discuss, our results provide a first attempt toward new strategies to improve the determination of R_P from data and, possibly, also the determination of $|V_{cb}|$ and $|V_{ub}|$. At first glance, leptonic τ decay modes might seem unimportant, since they occur at the expense of an additional power of the Fermi coupling G_F at the amplitude level. However, this process occurs on-shell and the suppression of the τ decay amplitude is compensated by the inverse of the τ lifetime appearing in the τ propagator. This becomes already apparent in the $\tau \to \mu\overline{\nu}_\mu\nu_\tau$ branching fraction: $\mathcal{B}(\tau \to \mu\overline{\nu}_\mu\nu_\tau) = (17.41 \pm 0.04)\%$ [60]. It is therefore interesting to calculate the rate for the decay chain $\overline{B} \to P\tau(\to \mu\overline{\nu}\nu)\overline{\nu}$, and compute numerically its impact on the observable rate of $\overline{B} \to P\mu X_{\overline{\nu}}$, $X_{\overline{\nu}} = \{\overline{\nu}, \overline{\nu}\nu\overline{\nu}\}$, to which we will henceforth refer as the "neutrino-inclusive" decay.

The layout of this chapter is as follows. We continue in section 3.2 with definitions and the bulk of our analytical results. Numerical results and their implications are presented in section 3.3, and we summarise in section 3.4. The appendices contain details on the form factors in appendix A.1, details on the kinematic variables in appendix A.2, and the numeric results of the 3ν PDFs in appendix A.3.

3.2 Setup

3.2.1 Kinematics

As anticipated in the introduction, in this analysis we assume that experiments cannot distinguish between the semileptonic decay $\overline{B} \to P\mu\overline{\nu}$ and $\overline{B} \to P\tau(\to \mu\overline{\nu}\nu)\overline{\nu}$ using the missing-mass information. This assumption certainly holds for analyses performed at hadron colliders (e.g., by the LHCb experiment[1]). On the other hand, it does not hold for analyses performed at e^+e^- colliders with flavour tagging based on the full reconstruction of the opposite B decay, where $\overline{B} \to P\mu\overline{\nu}$ and $\overline{B} \to P\tau(\to \mu\overline{\nu}\nu)\overline{\nu}$ will be clearly distinguished using the missing-mass information. The latter type of analyses will certainly provide precise results in the future; however, they cannot be performed at present and will require high statistics. It is therefore useful to discuss the case where there is no (or poor) missing-mass information.

We write for the neutrino-inclusive differential decay width to one muon:

$$\begin{aligned}\frac{\mathrm{d}\Gamma\left(\overline{B} \to P\mu X_{\overline{\nu}}\right)}{\mathrm{d}q^2\,\mathrm{d}\cos\theta_{[\mu]}} &\equiv \frac{\mathrm{d}\Gamma\left(\overline{B} \to P\mu\overline{\nu}_\mu\right)}{\mathrm{d}q^2\,\mathrm{d}\cos\theta_{[\mu]}} + \frac{\mathrm{d}\Gamma\left(\overline{B} \to P\tau(\to \mu\overline{\nu}_\mu\nu_\tau)\overline{\nu}_\tau\right)}{\mathrm{d}q^2\,\mathrm{d}\cos\theta_{[\mu]}} \\ &\equiv \frac{\mathrm{d}\Gamma_1}{\mathrm{d}q^2\,\mathrm{d}\cos\theta_{[\mu]}} + \frac{\mathrm{d}\Gamma_3}{\mathrm{d}q^2\,\mathrm{d}\cos\theta_{[\mu]}}\,.\end{aligned} \tag{3.5}$$

In the above, we introduce the shorthand Γ_n for the specific decay width with $n = 1$ or $n = 3$ neutrinos in the final state.[2] The kinematic variable are defined as follows.

- We define q^μ as the momentum transfer away from the $\overline{B}$-P system, *i.e.*: $q^\mu \equiv p^\mu - k^\mu$, where p and k are the momenta of the $\overline{B}$ and $P = D, \pi$ mesons, respectively. For Γ_1 this implies that q^μ coincides with the momentum of the lepton pair $\mu\overline{\nu}_\mu$. We stress that this does not hold for Γ_3.
- We define the angle $\theta_{[\mu]}$ via

$$\cos\theta_{[\mu]} \equiv 2\frac{\left(q - 2q_{[\mu]}\right)\cdot k}{\sqrt{\lambda}}\,. \tag{3.6}$$

[1] See the supplementary material to ref. [36], figure 9.

[2] We also drop the subscript for the neutrino flavour where possible. Note that effects of neutrino mixing and/or oscillation are not relevant to our study.

We abbreviate the Källén function $\lambda \equiv \lambda(M_B^2, M_P^2, q^2)$ here and throughout the current chapter. For Γ_1, the above formula coincides with

$$\cos\theta_{[\mu]} = 2\frac{\left(q_{[\overline{\nu}_\mu]} - q_{[\mu]}\right)\cdot k}{\sqrt{\lambda}}\,, \tag{3.7}$$

and the physical meaning of $\theta_{[\mu]}$ is the helicity angle of the muon in the $\mu\overline{\nu}_\mu$ rest frame, with $-1 \leq \cos\theta_\mu \leq +1$. We stress that for Γ_3 this physical interpretation is *no longer valid*. Yet, we find it convenient to keep using $\cos\theta_{[\mu]}$ for the description of the neutrino-inclusive rate $\Gamma(\overline{B} \to P\mu X_{\overline{\nu}})$. We emphasize also that the phase space boundaries for $\cos\theta_{[\mu]}$ in Γ_3 differ from those in Γ_1, and implicitly depend on the full kinematics of the 3ν decays.

For the description of Γ_3, we need to define further kinematic variables, which will be integrated over at a later point. We choose $q^2_{[\tau]}$, the mass square of the τ lepton; $q^2_{[\nu_\tau\overline{\nu}_\mu]} \equiv (q_{[\nu_\tau]} + q_{[\overline{\nu}_\mu]})^2$, the mass square of the two neutrinos produced in the τ decay; as well as five angles:

1. $\theta_{[\tau]}$, the helicity angle of the τ in the $\tau\overline{\nu}_\tau$ rest frame:

$$\cos\theta_{[\tau]} = \frac{(q - 2q_{[\tau]})\cdot k}{\beta_\tau\sqrt{\lambda}} + \frac{(1-2\beta_\tau)}{\beta_\tau}\frac{(M_B^2 - M_P^2 - q^2)}{2\sqrt{\lambda}}\,, \tag{3.8}$$

   where $2\beta_\tau \equiv 1 - q^2_{[\tau]}/q^2$,

2. ϕ, the azimuthal angle between the μ-$\nu_\tau\overline{\nu}_\mu$ plane and the $\overline{B}$-$\tau\overline{\nu}_\tau$ plane,

$$\varepsilon(p, q, q_{[\mu]}, q_{[\nu_\tau\overline{\nu}_\mu]}) = -\frac{1}{2}\beta_{\nu\overline{\nu}}\sqrt{1-2\beta_\tau}\beta_\tau q^2\sqrt{\lambda}\sin\phi\sin\theta^*_{[\mu]}\sin\theta_{[\tau]}\,, \tag{3.9}$$

3. $\theta^*_{[\mu]}$, the polar angle of the μ momentum in the τ rest frame with respect to $q_{[\nu_\tau\overline{\nu}_\mu]}$ in the τ rest frame:

$$\cos\theta^*_{[\mu]} = \frac{1}{2\beta_{\nu\overline{\nu}}\beta_\tau}\left[(1-2\beta_{\nu\overline{\nu}})(1-\beta_\tau) + \frac{(q_{[\mu]} - q_{[\nu_\tau\overline{\nu}_\mu]})\cdot q}{q^2}\right]\,, \tag{3.10}$$

   where $2\beta_{\nu\overline{\nu}} \equiv 1 - q^2_{[\nu_\tau\overline{\nu}_\mu]}/q^2_{[\tau]}$,

4. $\theta^{**}_{[\overline{\nu}_\mu]}$, the polar angle of the $\overline{\nu}_\mu$ momentum in the $\nu_\tau\overline{\nu}_\mu$ rest frame with respect to the μ momentum in the $\nu_\tau\overline{\nu}_\mu$ rest frame:

$$\cos\theta^{**}_{[\overline{\nu}_\mu]} = \frac{(q_{[\nu_\tau\overline{\nu}_\mu]} - 2q_{[\overline{\nu}_\mu]})\cdot q_{[\mu]}}{\beta_{\nu\overline{\nu}}q^2_{[\tau]}}\,. \tag{3.11}$$

5. ϕ^{**}, the azimuthal angle between the τ-μ and $\overline{\nu}_\mu$-ν_τ decay planes in the τ rest frame,

$$\varepsilon(q_{[\tau]}, q_{[\overline{\nu}_\tau]}, q_{[\mu]}, q_{[\nu_\tau\overline{\nu}_\mu]}) = \frac{1}{2}\beta_{\nu\overline{\nu}}\beta_\tau\sqrt{1-2\beta_{\nu\overline{\nu}}}q^2q^2_{[\tau]}\sin\theta^*_{[\mu]}\sin\theta^{**}_{[\overline{\nu}_\mu]}\sin\phi^{**}\,. \tag{3.12}$$

In general, we denote the solid angle in the $\tau\overline{\nu}_\tau$ rest frame without any asterisks, the solid angle within the τ rest frame with one asterisk, and the solid angle in the $\overline{\nu}_\mu\nu_\tau$ rest frame with two asterisks.

With the above definitions of the kinematics in mind, we can now begin discussing phenomenological applications. We wish to first address the case, in which a 3ν event is misinterpreted as a 1-neutrino event. In such a case, the misreconstructed $\cos\theta_{[\mu]}$ reads

$$\cos\theta_{[\mu]}\Big|_{3\nu} = 2\beta_{\nu\overline{\nu}}\Bigg\{\left(\frac{(1-2\beta_{\nu\overline{\nu}})}{\beta_{\nu\overline{\nu}}}+2\beta_\tau\right)\frac{M_B^2-M_P^2-q^2}{2\sqrt{\lambda}}+\beta_\tau\cos\theta_{[\tau]}$$
$$-\left(2\beta_\tau\frac{M_B^2-M_P^2-q^2}{2\sqrt{\lambda}}-(1-\beta_\tau)\cos\theta_{[\tau]}\right)\cos\theta^*_{[\mu]}-\sqrt{1-2\beta_\tau}\sin\theta^*_{[\mu]}\sin\theta_{[\tau]}\cos\phi\Bigg\}. \quad (3.13)$$

As an alternative to $\cos\theta_{[\mu]}$ we also consider E_μ, the muon energy in the B rest frame. It is defined in terms of Lorentz invariants as

$$E_\mu \equiv \frac{p\cdot q_{[\mu]}}{M_B}\,. \quad (3.14)$$

In the 1ν decay, E_μ is not independent from our nominal choice of kinematic variables q^2 and $\cos\theta_\mu$. The expression for E_μ reads

$$E_\mu\Big|_{1\nu} = \frac{1}{4M_B}\left[(M_B^2-M_P^2+q^2)-\sqrt{\lambda}\cos\theta_\mu\right], \quad (3.15)$$

and it attains its maximal value at $q^2=0$ and $\cos\theta_\mu=-1$. Its full range reads

$$m_\mu \le E_\mu\Big|_{1\nu} \le \frac{M_B^2-M_P^2}{2M_B}\,. \quad (3.16)$$

However, for a misreconstructed 3ν event we obtain instead

$$E_\mu\Big|_{3\nu} = \frac{\beta_{\nu\overline{\nu}}}{2M_B}\Big[(M_B^2-M_P^2+q^2)((1-\beta_\tau)+\beta_\tau\cos\theta^*_{[\mu]})$$
$$-\sqrt{\lambda}(\beta_\tau+(1-\beta_\tau)\cos\theta^*_{[\mu]})\cos\theta_{[\tau]}+\sqrt{1-2\beta_\tau}\sqrt{\lambda}\sin\theta^*_{[\mu]}\sin\theta_{[\tau]}\cos\phi\Big], \quad (3.17)$$

which now exhibits an additional dependence on the kinematics variables $\cos\theta^*_{[\mu]}$ and ϕ, as well as $q^2_{[\nu_\tau\overline{\nu}_\mu]}$. We find for its range

$$m_\mu \le E_\mu\Big|_{3\nu} \le \frac{M_B^2-M_P^2+m_\tau^2+\sqrt{\lambda(M_B^2,M_P^2,m_\tau^2)}}{4M_B}\,. \quad (3.18)$$

3.2.2 Decay Rate

In order to proceed, we require an analytic expression for the neutrino-inclusive differential decay rate. The result for Γ_1 is known for some time in the literature (see e.g. [61, 62] for reviews in the presence of model-independent NP contributions). However, Γ_3 has not been calculated to the best of our knowledge. We begin the computation with the matrix element for the $\overline{B}(p)\to P(k)\tau(q_{[\tau]})\overline{\nu}(q_{[\overline{\nu}_\tau]})$ transition:

$$i\mathcal{M} = -i\frac{G_F V_{cb}}{\sqrt{2}}\left[f_+(q^2)\left\{(p+k)^\mu-\frac{M_B^2-M_P^2}{q^2}q^\mu\right\}+f_0(q^2)\frac{M_B^2-M_P^2}{q^2}q^\mu\right]L_\mu^{(V-A)}, \quad (3.19)$$

with $q\equiv p-k=q_{[\tau]}+q_{[\overline{\nu}_\tau]}$. In the above, we abreviate the leptonic currents as

$$L_\mu^{(V-A)} \equiv \left[\overline{u}(q_{[\tau]})\gamma_\mu(1-\gamma_5)v(q_{[\overline{\nu}_\tau]})\right]. \quad (3.20)$$

The contributions to Γ_3 then arise from the leptonic decay of the τ. The corresponding matrix elements can be readily obtained through the replacement where m_τ and Γ_τ denote the mass and the total width of the τ lepton, respectively.

The fully-differential rate for the 3-neutrino final state can then be expressed as:

$$\begin{aligned}\frac{\mathrm{d}^7\Gamma_3}{\mathrm{d}q^2\,\mathrm{d}q^2_{[\nu_\tau\overline{\nu}_\mu]}\,\mathrm{d}^2\Omega\,\mathrm{d}\Omega^*\,\mathrm{d}^2\Omega^{**}} &= -\frac{3G_F^2|V_{cb}|^2\sqrt{\lambda}(q^2-m_\tau^2)(m_\tau^2-q^2_{[\nu_\tau\overline{\nu}_\mu]})\mathcal{B}(\tau\to\mu\overline{\nu}\nu)}{2^{17}\pi^5 m_\tau^8 M_B^3 q^2} \\ &\times\Big[|f_+|^2\left(T_1-\frac{M_B^2-M_D^2}{q^2}T_2+\frac{(M_B^2-M_D^2)^2}{q^4}T_3\right) \\ &+\ \mathrm{Re}\,(f_+\,f_0)\left(\frac{M_B^2-M_D^2}{q^2}T_2-2\frac{(M_B^2-M_D^2)^2}{q^4}T_3\right)+|f_0|^2\frac{(M_B^2-M_D^2)^2}{q^4}T_3\Big]\,, \end{aligned} \tag{3.21}$$

with auxilliary quantities

$$\begin{aligned} T_1 &\equiv (p+k)^\mu(p+k)^\nu\sum_{\text{spins}}\tilde{L}_\mu^{(V-A)}\tilde{L}_\nu^{*,(V-A)}\,, \\ T_2 &\equiv ((p+k)^\mu q^\nu+(p+k)^\nu q^\mu)\sum_{\text{spins}}\tilde{L}_\mu^{(V-A)}\tilde{L}_\nu^{*,(V-A)}\,, \\ T_3 &\equiv q^\mu q^\nu\sum_{\text{spins}}\tilde{L}_\mu^{(V-A)}\tilde{L}_\nu^{*,(V-A)}\,. \end{aligned} \tag{3.22}$$

In the above we abbreviate $\mathrm{d}^2\Omega = \mathrm{d}\cos\theta_{[\tau]}\,\mathrm{d}\phi$, $\mathrm{d}\Omega^* = \mathrm{d}\cos\theta^*_{[\mu]}$, and $\mathrm{d}^2\Omega^{**} = \mathrm{d}\cos\theta^{**}_{[\overline{\nu}_\mu]}\,\mathrm{d}\phi^{**}$, and we emphasize that the integration range over $\mathrm{d}\cos\theta$ goes from -1 to $+1$. The full expressions for $T_{1,2,3}$ are quite cumbersome to typeset. They can be found as ancillary files in [63]. We also find that the integration of eq. (3.21) over Ω^{**}, Ω^*, ϕ and $q^2_{[\nu_\tau\overline{\nu}_\mu]}$ yields $\mathcal{B}(\tau\to\mu\overline{\nu}_\mu\nu_\tau)\times\mathrm{d}^2\Gamma(\overline{B}\to P\mu\overline{\nu})/\mathrm{d}q^2\,\mathrm{d}\cos\theta_{[\tau]}$ as required. This is a successful crosscheck of our calculation.

In order to carry out our phenomenological study of the quantities $\cos\theta_{[\mu]}$ in eq. (3.13) and E_μ in eq. (3.17) in the decay chain $\overline{B}\to P\tau(\to\mu\overline{\nu}\nu)\overline{\nu}$, we do not require any dependence on the $\nu\overline{\nu}$ solid angle $\Omega^{**}=(\cos\theta^{**}_{[\overline{\nu}_\mu]},\phi^{**})$. We therefore integrate over the latter, and thus obtain the five-differential rate

$$\frac{\mathrm{d}^5\Gamma_3}{\mathrm{d}q^2\,\mathrm{d}q^2_{[\nu_\tau\overline{\nu}_\mu]}\,\mathrm{d}^2\Omega\,\mathrm{d}\Omega^*}=\frac{\tilde{\Gamma}_3}{\pi m_\tau^8 q^6}\Big[A+B\cos\theta_{[\tau]}+C\cos^2\theta_{[\tau]}+\big(D\sin\theta_{[\tau]}+E\sin\theta_{[\tau]}\cos\theta_{[\tau]}\big)\cos\phi\Big]\,, \tag{3.23}$$

with normalisation

$$\tilde{\Gamma}_3=\frac{|V_{cb}|^2G_F^2\mathcal{B}(\tau\to\mu\nu\overline{\nu})}{2^9\pi^3M_B^3}\,. \tag{3.24}$$

The angular coefficients in eq. (3.23) read

$$\begin{aligned} A &= [(q^2-m_\tau^2)(m_\tau^2-q^2_{[\nu_\tau\overline{\nu}_\mu]})]^2\sqrt{\lambda}\Big[(m_\tau^2+2q^2_{[\nu_\tau\overline{\nu}_\mu]})(|f_0|^2(M_B^2-M_P^2)^2m_\tau^2+|f_+|^2q^2\lambda) \\ &\quad-(m_\tau^2-2q^2_{[\nu_\tau\overline{\nu}_\mu]})(|f_0|^2(M_B^2-M_P^2)^2m_\tau^2-|f_+|^2q^2\lambda)\cos\theta^*_{[\mu]}\Big]\,, \\ B &= 2|f_0||f_+|m_\tau^2(M_B^2-M_P^2)\lambda[(q^2-m_\tau^2)(m_\tau^2-q^2_{[\nu_\tau\overline{\nu}_\mu]})]^2\Big[(m_\tau^2+2q^2_{[\nu_\tau\overline{\nu}_\mu]})-(m_\tau^2-2q^2_{[\nu_\tau\overline{\nu}_\mu]})\cos\theta^*_{[\mu]}\Big]\,, \\ C &= -|f_+|^2\lambda^{3/2}[(q^2-m_\tau^2)(m_\tau^2-q^2_{[\nu_\tau\overline{\nu}_\mu]})]^2\Big[(q^2-m_\tau^2)(m_\tau^2+2q^2_{[\nu_\tau\overline{\nu}_\mu]})+(q^2+m_\tau^2)(m_\tau^2-2q^2_{[\nu_\tau\overline{\nu}_\mu]})\cos\theta^*_{[\mu]}\Big]\,, \\ D &= 2m_\tau\sqrt{q^2}|f_0||f_+|(M_B^2-M_P^2)[(q^2-m_\tau^2)(m_\tau^2-q^2_{[\nu_\tau\overline{\nu}_\mu]})]^2(m_\tau^2-2q^2_{[\nu_\tau\overline{\nu}_\mu]})\lambda\sin\theta^*_{[\mu]}\,, \\ E &= 2m_\tau\sqrt{q^2}|f_+|^2[(q^2-m_\tau^2)(m_\tau^2-q^2_{[\nu_\tau\overline{\nu}_\mu]})]^2(m_\tau^2-2q^2_{[\nu_\tau\overline{\nu}_\mu]})\lambda^{3/2}\sin\theta^*_{[\mu]}\,. \end{aligned} \tag{3.25}$$

We can now proceed to to produce the pseudo-events that are distributed as eq. (3.23), which is a necessary prerequisite for our phenomenological applications in the following section.

3.3 Numerical results

Our numerical results are based on a Monte Carlo (MC) study of the decays $\overline{B} \to P\mu\overline{\nu}$ and $\overline{B} \to P\tau(\to \mu\nu\overline{\nu})\overline{\nu}$. For this purpose, we added the signal PDFs for both decays to the EOS library of flavour observables [64]. The relevant form factors f_+ and f_0 are taken in the BCL parametrization [65]. The BCL parameters are fitted from a recent lattice QCD studies [20, 21], and additionally Light-Cone Sum Rules results in the case of $\overline{B} \to \pi$ [66]; see appendix A.1 for details.

In order to obtain pseudo events for the neutrino inclusive decay, we carry out the following steps:

1. We draw $4.8 \cdot 10^6$ samples $\{\vec{X}_i^{(1)}\} = \{(q^2, \cos\theta_{[\mu]})_i\}$, which are distributed as their signal PDF P_1,
$$P_1(q^2, \cos\theta_{[\mu]}) \equiv \frac{1}{\Gamma_1} \frac{\mathrm{d}^2\Gamma_1}{\mathrm{d}q^2\, \mathrm{d}\cos\theta_{[\mu]}} \,. \tag{3.26}$$

2. We draw $4.8 \cdot 10^6$ samples $\{\vec{X}_i^{(3)}\} = \{(q^2, q^2_{[\nu_\tau\overline{\nu}_\mu]}, \cos\theta_{[\tau]}, \phi, \cos\theta^*_{[\mu]})_i\}$, which are distributed as their signal PDF P_3,
$$P_3(q^2, q^2_{[\nu_\tau\overline{\nu}_\mu]}, \cos\theta_{[\tau]}, \phi, \cos\theta^*_{[\mu]}) \equiv \frac{1}{\Gamma_3} \frac{\mathrm{d}^5\Gamma_3}{\mathrm{d}q^2\, \mathrm{d}q^2_{[\nu_\tau\overline{\nu}_\mu]}\, \mathrm{d}\cos\theta_{[\tau]}\, \mathrm{d}\phi\, \mathrm{d}\cos\theta^*_{[\mu]}} \,. \tag{3.27}$$

3. We combine the two sets of samples with weights $\omega_1 = \Gamma_1/(\Gamma_1 + \Gamma_3)$ and $\omega_3 = 1 - \omega_1$, respectively. The weights can be expressed in terms of R_P and $\mathcal{B}(\tau \to \mu\nu\overline{\nu})$:
$$\omega_1 = \frac{1}{1 + R_P \mathcal{B}(\tau \to \mu\nu\overline{\nu})} \,. \tag{3.28}$$

All samples are obtained from a Markov Chain Monte Carlo setup, which implements the Metropolis-Hastings algorithm [67, 68]. The first $8 \cdot 10^5$ samples per set are discarded, in order to minimize the impact from the Markov Chains' starting values. In order to avoid correlations from rejection of proposals, we only take every tenth sample. The effective sample size is therefore $4 \cdot 10^5$. We provide the so-obtained pseudo events online [69] in the binary HDF5 format[3].

3.3.1 $\overline{B} \to D\mu X_{\overline{\nu}}$

Distribution in $\cos\theta_{[\mu]}$ In the neutrino inclusive decay, the misreconstructed observable $\cos\theta_{[\mu]}$ as given in eq. (3.13) is no longer bounded by +1. We find that it attains its maximal value

$$\max\cos\theta_{[\mu]}\big|_{3\nu} \simeq 56.7 \qquad \text{for } q^2 = (M_B - M_D)^2, \quad q^2_{[\nu_\tau\overline{\nu}_\mu]} = m_\tau^2, \quad \cos\theta_{[\tau]} = -\cos\theta^*_{[\mu]} = 1 \,. \tag{3.29}$$

The distribution of $\cos\theta_{[\mu]}$ in the neutrino-inclusive decay is shown in figure 3.1a, where we also disentangle the individual 1ν and 3ν contributions. We find that $\cos\theta_{[\mu]}$ exceeds 1 for $\sim 23\%$ of the 3ν events, and exceeds 2 for $\sim 1.3\%$ of 3ν events. As a consequence, we decide against a

[3] See https://www.hdfgroup.org/HDF5/ for its description.

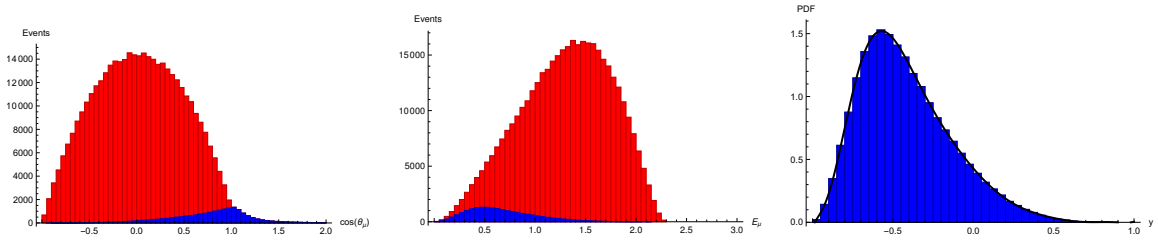

a b c

Figure 3.1: Histograms of $4 \cdot 10^5$ pseudo events for the neutrino inclusive decay $B \to D\mu X_{\overline{\nu}}$ [figures (a) and (b)], as well as for the decay $B \to D\tau(\to \mu\nu\overline{\nu})\overline{\nu}$ [figure (c)]. We show histograms of distributions in the (misreconstructed) angle $\cos\theta_\mu$ [figure (a)], and E_μ, the muon energy in the $\overline{B}$ rest frame [figure (b)]. The red areas correspond to the neutrino-inclusive decay, while the blue areas highlight the contributions stemming only from $B \to D\tau(\to \mu\nu\overline{\nu})\overline{\nu}$. We also show the histogram of $E_\mu\big|_{3\nu}$ and its compatibility with our ansatz eq. (3.34) [figure (c)].

parametrization of the neutrino-inclusive PDF $P(\cos\theta_\mu)$ in terms of Legendre polynomials (or any other orthonormal polynomial basis).

On the other hand, our findings imply that the $\cos\theta_{[\mu]}$ distribution can be used to extract the product $R_D\mathcal{B}(\tau \to \mu\overline{\nu}\nu)$ from data. We can indeed write

$$R_D\mathcal{B}(\tau \to \mu\overline{\nu}\nu) = \frac{\rho_D^{\text{exp}}}{\rho_D^0 - \rho_D^{\text{exp}}} \tag{3.30}$$

where

$$\rho_D^0 \equiv \frac{\#\text{of } 3\nu \text{ events with } \cos\theta_\mu > 1}{\text{total } \#\text{ of } 3\nu \text{ events}}\,, \qquad \rho_D^{\text{exp}} \equiv \frac{\#\text{of } X_\nu \text{ events with } \cos\theta_\mu > 1}{\text{total } \#\text{ of } X_\nu \text{ events}} \tag{3.31}$$

Based on our MC pseudo events, we find

$$\rho_D^0 = 0.234 \pm 0.001\,, \tag{3.32}$$

where the error is dominantly statistical, and arises from our limited number of MC samples. We explicitly cross check our uncertainty estimate by re-running the simulations with modified inputs on the $B \to D$ form factors. We find that shifting any single individual constraint in table A.1 by 1σ yields results that are compatible with the interval given in eq. (3.32).

The distribution in E_μ The distribution of E_μ in the neutrino-inclusive decay is shown in figure 3.1b. We find that a lower cut $E_\mu > 1.0\,\text{GeV}$ can reduce the rate of of misidentified 3ν events by a factor of ~ 4, while $\sim 76\%$ of the 1ν events (the signal) remain. This corresponds to a reduction of the rate of background events in the neutrino-inclusive decay from its maximum value of $R_D\mathcal{B}(\tau \to \mu\nu\overline{\nu}) \approx 5.2\%$ down to 1.3%.

Alternatively, one can subtract the 3ν background from the neutrino-inclusive rate. For this purpose we proceed to obtain the relevant PDF of 3ν events. Since the ranges of $E_\mu\Big|_{1\nu}$ and $E_\mu\Big|_{3\nu}$ are very similar, we can remap their union to a new kinematic variable y,

$$y \equiv \frac{2E_\mu}{E_\mu^{\text{max}}} - 1\,, \qquad \text{with } E_\mu^{\text{max}} = \max\left(E_\mu\Big|_{1\nu}, E_\mu\Big|_{3\nu}\right) \simeq 2.31\,\text{GeV}\,, \qquad \text{so that } -1 \le y \le +1\,. \tag{3.33}$$

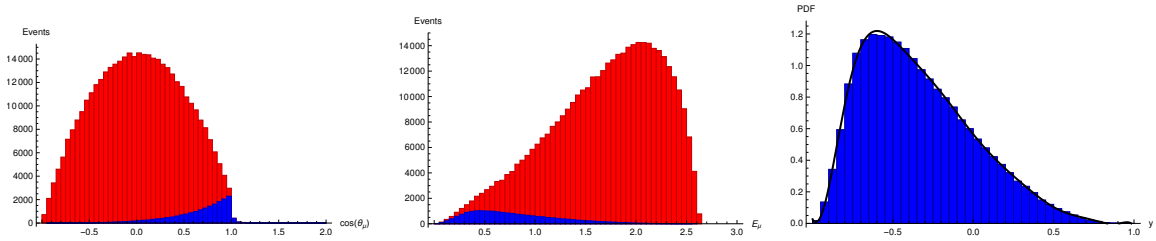

a b c

Figure 3.2: Histograms of $4 \cdot 10^5$ pseudo events for the neutrino inclusive decay $B \to \pi\mu X_{\overline{\nu}}$ [figures (a) and (b)], as well as for the decay $B \to \pi\tau(\to \mu\nu\overline{\nu})\overline{\nu}$ [figure (c)]. We show histograms of distributions in the (misreconstructed) angle $\cos\theta_\mu$ [figure (a)], and E_μ, the muon energy in the $\overline{B}$ rest frame [figure (b)]. The red areas correspond to the neutrino-inclusive decay, while the blue areas highlight the contributions stemming only from $B \to \pi\tau(\to \mu\nu\overline{\nu})\overline{\nu}$. We also show the histogram of $E_\mu\big|_{3\nu}$ and its compatibility with our ansatz eq. (3.34) [figure (c)].

We then make an ansatz for the PDF $P_3(y) \equiv \mathrm{d}\Gamma_3/\mathrm{d}y$ by expanding in Legendre polynomials $p_k(y)$:

$$P_3(y) = \frac{1}{2} + \sum_{k=1}^{12} c_k^{(3)} p_k(y)\,. \tag{3.34}$$

Since the Legendre polynomials form an orthogonal basis of function on the support $[-1,+1]$, the coefficients $c_k^{(3)}$ are independent of the degree of $P_3(y)$. Their mean values and covariance are obtained using the method of moments; see [70] for a recent review. We find that our ansatz eq. (3.34) describes the PDF exceptionally well, and refer to figure 3.1c for the visualization. Our results for the mean values and covariance matrix of the moments are compiled in table A.3. They can be used in upcoming experimental studies in order to cross check the signal/background discrimination.

3.3.2 $\overline{B} \to \pi\mu X_{\overline{\nu}}$

Based on the $\overline{B} \to \pi$ form factors parameters as described in appendix A.1, we obtain

$$R_\pi^{\mathrm{SM}} = 0.70 \pm 0.01\,, \tag{3.35}$$

which is in good visual agreement with the plot of R_π in figure 8 of Ref. [71]. This result implies a potentially larger impact of the 3ν decays as a background in the extraction of both R_π and $|V_{ub}|$.

Distribution in $\cos\theta_{[\mu]}$ As in the case of $\overline{B} \to D\mu X_{\overline{\nu}}$, the misreconstructed observable $\cos\theta_{[\mu]}$ is no longer bounded from above by $+1$. However, we find that its maximal value is much smaller for $\overline{B} \to \pi$ transitions than it is for $\overline{B} \to D$ transitions:

$$\max\cos\theta_{[\mu]}\big|_{3\nu} \simeq 3.75 \qquad \text{for } q^2 = (M_B - M_\pi)^2, \quad q^2_{[\nu_\tau\overline{\nu}_\mu]} = m_\tau^2, \quad \cos\theta_{[\tau]} = -\cos\theta^*_{[\mu]} = 1\,. \tag{3.36}$$

A consequence of this smaller upper bound in $\overline{B} \to \pi$ transitions, the tail of 3ν events is much lighter; see figure 3.2a. This is also reflected in our numerical result for the ratio ρ_π^0,

$$\rho_\pi^0 = (2.89 \pm 0.03) \cdot 10^{-2}\,. \tag{3.37}$$

We can therefore not recommend to extract the ratio R_π through a lower cut on $\cos\theta_{[\mu]}$. Our result also shows that more than 97% of 3ν events fall in the physical region of 1ν events.

Distribution in E_μ We find that a lower cut can reduce the rate of of misidentified 3ν events by a factor of ~ 10, while $\sim 69\%$ of the 1ν events (the signal) remain. This corresponds to a reduction of the rate of background events in the neutrino-inclusive decay from its maximum value of $R_\pi \mathcal{B}(\tau \to \mu\nu\overline{\nu}) \simeq 12.1\%$ down to $\sim 1.2\%$.

For the range of E_μ we find

$$\max\left(E_\mu\Big|_{1\nu}, E_\mu\Big|_{3\nu}\right) \simeq 2.64\,\text{GeV}\,, \tag{3.38}$$

and the energy ranges are overlapping given our numerical precision. Thus, the description of the neutrino-inclusive rate though E_μ, or equivalently y, should work even better for $\overline{B} \to \pi$ transitions than for $\overline{B} \to D$ transitions. Our results for the mean values and covariance matrix of the Legendre moments $c_k^{(3)}$ are compiled in table A.4. We refer to figure 3.2c for a comparison of $P_3(y)$ with our MC pseudo events.

3.3.3 Implications for the extraction of $|V_{cb}|$ and $|V_{ub}|$

Using the above results we can finally draw some semi-quantitative conclusions about the error in the extraction $|V_{cb}|$ and $|V_{ub}|$ from $b \to c(u)\ell\nu$ decays. The presence of the $\tau \to \mu\overline{\nu}\nu$ background in those processes can be dealt with, experimentally, in different ways. The two extreme cases we can envisage are the following: i) reduction of the background via explicit cuts; ii) fully inclusive subtraction. The first method can be applied to exclusive decays such as those discussed in the present chapter. As shown above, combining cuts in E_μ and $\cos\theta_{[\mu]}$ leads to a significant reduction of the $\tau \to \mu\overline{\nu}\nu$ contamination in $\overline{B} \to D\mu X_{\overline{\nu}}$, with negligible implications for the extraction of $|V_{cb}|$. However, this procedure cannot be applied to fully inclusive modes. In the latter case, the $\tau \to \mu\overline{\nu}\nu$ contamination is more likely to be simply subtracted from the total number of events. If this subtraction is made assuming the SM expectation of R_D (and R_{D*}), it leads to systematic error if $\Delta R_D \neq 0$, i.e. in presence of New Physics [58]. The maximal value of this error is

$$\frac{\Delta|V_{cb}|^{(\text{ incl.})}}{|V_{cb}|} = \frac{1}{2}\Delta R_D \mathcal{B}(\tau \to \mu\overline{\nu}\nu) \approx 0.9\%\,, \tag{3.39}$$

which is not far from the combined theory and experimental error presently quoted for $|V_{cb}|$ [60]. We thus conclude that the $\tau \to \mu\overline{\nu}\nu$ contamination must be carefully analyzed in the determination of $|V_{cb}|$.

The impact of the $\tau \to \mu\overline{\nu}\nu$ contamination is more difficult to be estimated in the $|V_{ub}|$ case. On the one hand, the large value of R_π leads to a potentially larger impact. On the other hand, even in inclusive analyses some cut on E_μ is unavoidable in order to reduce the $b \to c\ell\nu$ background: as shown above, this naturally leads to a significant reduction of the $\tau \to \mu\overline{\nu}\nu$ contamination. Given the present large experimental errors, the $\tau \to \mu\overline{\nu}\nu$ contamination is likely to be a subleading correction in the extraction of $|V_{ub}|$, but it is certainly an effect that has to be properly analyzed in view of future high-statistics data.

3.4 Summary

Lepton flavour Universality tests in charged-current semileptonic B decays provide a very interesting window on possible physics beyond the SM. In this chapter we have analyzed how the leptonic $\tau \to \mu\overline{\nu}\nu$ decays affect the determination of the LFU ratios R_P, where $P = D, \pi$. In particular, we have presented a complete analytical determination of the observable distributions (energy spectrum and helicity angle of the muon) of the $\overline{B} \to P\tau(\to \mu\overline{\nu}\nu)\overline{\nu}$ decay chain. This result has allowed us to identify clean strategies both to extract R_P from measurements of the $\overline{B} \to P\mu X_{\overline{\nu}}$ neutrino-inclusive rate, and also to minimize the impact of the $\tau \to \mu\overline{\nu}\nu$ decay in

the three-body $\overline{B} \to P\mu\nu$ modes. Finally, this study has also allowed us to conclude that the $b \to c\tau(\to \ell\overline{\nu}\nu)\nu$ background in $b \to c\ell\nu$ decays represents a non-negligible source of uncertainty for the extraction of $|V_{cb}|$ in presence of NP modifying R_D: its impact could reach the $\sim 1\%$ level and has to be analyzed with care mode by mode.

Chapter 4

Testing lepton flavour universality in semileptonic $\Lambda_b \to \Lambda_c^*$ decays

4.1 Introduction

In this chapter we will concentrate on Lepton Flavour Universality (LFU) in $b \to c\tau\overline{\nu}$ versus $b \to c\mu\overline{\nu}$ decays, in particular for Λ_b^0 decays. At the LHC, Λ_b^0 baryons are copiously produced, at approximately half the rate of B^0 mesons [72,73]. The decay involving the ground state charmed baryon, $\Lambda_b^0 \to \Lambda_c^+ \ell^- \nu_\mu$ has been studied in lattice QCD in Ref. [74] and precise SM predictions for the LFU ratio R_{Λ_c} are provided. In addition, the LHCb collaboration has recently measured the slope of the leading order Isgur-Wise (IW) function or the decay $\Lambda_b^0 \to \Lambda_c^+ \mu^- \nu_\mu$ [75]. While studying backgrounds to this decay, large samples of $\Lambda_c(2593)^+$ and $\Lambda_c(2625)^+$ candidates were reconstructed as background, which demonstrates the potential of precise LFU tests in these decays. Therefore, we propose to investigate the LFU ratios

$$R_{\Lambda_c^*} \equiv \frac{\mathcal{B}(\Lambda_b \to \Lambda_c^{*+} \tau^- \overline{\nu})}{\mathcal{B}(\Lambda_b \to \Lambda_c^{*+} \mu^- \overline{\nu})} \tag{4.1}$$

where Λ_c^{*+} denotes either the $\Lambda_c(2595)^+$ (with $J^P = 1/2^-$) or the $\Lambda_c(2625)^+$ (with $J^P = 3/2^-$) charmed baryon.

The challenge in exploiting these modes for LFU tests is controlling uncertainties related to hadronic matrix elements, which are genuinely non-perturbative objects. As a consequence of both baryons forming a doublet under Heavy Quark Spin Symmetry (HQSS), the hadronic matrix elements for the $\Lambda_b \to \Lambda_c^*$ transitions can be expressed – in the infinite mass limit – through a single IW function ζ [76] at leading power in $1/m$. The power suppressed contributions at the $1/m$ level – where $m = m_b, m_c$ – have been previously calculated in [77].

The purpose of this work is to provide for the first time all the necessary ingredients to carry out a LFU study of these decays. In section 4.2, we first revisit the definition of the hadronic form factors, and provide a helicity decomposition that is convenient for the description of the decay observables. Subsequently, we provide formulae for these hadronic form factors in the Heavy Quark Expansion (HQE) up to order α_s and $1/m$, beyond what has been done in the literature so far. Continuing in section 8.3, we model the kinematic dependence of the leading and subleading IW functions, and then provide a set of benchmark points based on inputs from non-perturbative approaches. Afterwards, we calculate the differential decay width, including the finite lepton-mass contributions that are necessary for testing LFU. The following section 4.4 shows the impact of using LHCb data for constraining the relevant form factor parameters, and control the theory uncertainties for the prediction of the LFU ratios. We conclude in section 4.5.

4.2 Form factors for $\Lambda_b \to \Lambda_c^*$ transitions

In the following we investigate form factors for the transitions

$$\Lambda_b^0(p, s_b) \to \begin{cases} \Lambda_c(2595)^+(k, J_z \equiv s_c) & \text{with } J^P = 1/2^- \\ \Lambda_c(2625)^+(k, J_z \equiv s_c + \lambda_c) & \text{with } J^P = 3/2^- \end{cases}, \tag{4.2}$$

where p and k denote the four momenta of the initial and final state respectively, and J^P indicates both angular momentum and parity eigenvalues of the Λ_c^{*+} states. The states' rest-frame helicities are denoted as s_b and J_z. Note that, for the $J^P = 3/2^-$ state, J_z can be decomposed into the rest-frame helicity of a $1/2^+$ spinor (s_c), and the polarisation of a polarisation vector $\eta \equiv \eta(\lambda_c)$. For later use we also define the momentum transfer to the leptons $q^\mu \equiv p^\mu - k^\mu$.

4.2.1 Helicity form factors

We define the hadronic matrix elements for vector and axialvector transitions to the $\Lambda_c(2595)^+$ state as:

$$\begin{aligned} \langle \Lambda_c(2595)^+(k, \eta(\lambda_c), s_c) | \, \bar{c}\gamma^\mu b \, | \Lambda_b^0(p, s_b) \rangle &= +\overline{u}_\alpha^{(1/2)}(k, \eta(\lambda_c), s_c) \left[\sum_i f_i(q^2) \Gamma_{V,i}^{\alpha\mu} \right] u(p, s_b) \,, \\ \langle \Lambda_c(2595)^+(k, \eta(\lambda_c), s_c) | \, \bar{c}\gamma^\mu\gamma_5 b \, | \Lambda_b^0(p, s_b) \rangle &= -\overline{u}_\alpha^{(1/2)}(k, \eta(\lambda_c), s_c) \left[\sum_i g_i(q^2) \gamma_5 \Gamma_{A,i}^{\alpha\mu} \right] u(p, s_b) \,, \end{aligned} \tag{4.3}$$

where $\overline{u}_\alpha^{(1/2)}$ is the spin 1/2 projection of a Rarita-Schwinger object $u_\alpha^{\mathrm{RS}}(k, \eta, s) \equiv \eta_\alpha(k) u(k, s)$ (see appendix B.1). For the hadronic matrix element of the vector and axialvector transitions to the $\Lambda_c(2625)^+$ state we use:

$$\begin{aligned} \langle \Lambda_c(2625)^+(k, \eta(\lambda_c), s_c) | \, \bar{c}\gamma^\mu b \, | \Lambda_b^0(p, s_b) \rangle &= +\overline{u}_\alpha^{(3/2)}(k, \eta(\lambda_c), s_c) \left[\sum_i F_i(q^2) \Gamma_{V,i}^{\alpha\mu} \right] u(p, s_b) \,, \\ \langle \Lambda_c(2625)^+(k, \eta(\lambda_c), s_c) | \, \bar{c}\gamma^\mu\gamma_5 b \, | \Lambda_b^0(p, s_b) \rangle &= -\overline{u}_\alpha^{(3/2)}(k, \eta(\lambda_c), s_c) \left[\sum_i G_i(q^2) \gamma_5 \Gamma_{A,i}^{\alpha\mu} \right] u(p, s_b) \,, \end{aligned} \tag{4.4}$$

where $\overline{u}_\alpha^{(3/2)}$ is the spin 3/2 projection of a Rarita-Schwinger object; see also appendix B.1. A possible basis of Dirac structures for the vector current is given in [78]. We choose a different basis for both vector and axialvector currents. We compile the list of all Dirac structures $\Gamma_{V(A),i}^{\alpha\mu}$ in appendix B.2.

We define the helicity amplitudes for the two currents $\Gamma^\mu = \gamma^\mu, \gamma^\mu\gamma_5$ as

$$\mathcal{A}_\Gamma(s_b, s_c, \lambda_c, \lambda_q) \equiv \langle \Lambda_c^*(s_c, \eta(\lambda_c)) | \, \bar{c} \, \Gamma^\mu \varepsilon_\mu^*(\lambda_q) b \, | \Lambda_b(s_b) \rangle \,, \tag{4.5}$$

where the $\varepsilon_\mu^*(\lambda_q)$ are a basis of polarisation vectors for the virtual W exchange with the polarisation states $\lambda_q \in \{t, 0, +1, -1\}$; see appendix B.4. Due to the fact that the angular momentum configurations λ_c and s_c eq. (4.5) can be independently chosen, there are more possible combinations of λ_c and s_c than physically permitted. We identify the helicity amplitudes with total angular moment $J = 1/2$ as

$$\begin{aligned} \mathcal{A}_\Gamma^{(1/2)}(+1/2, +1/2, 0) &\equiv -\sqrt{\frac{1}{3}} \mathcal{A}_\Gamma(+1/2, +1/2, 0, 0) + \sqrt{\frac{2}{3}} \mathcal{A}_\Gamma(+1/2, -1/2, +1, 0) \,, \\ \mathcal{A}_\Gamma^{(1/2)}(+1/2, +1/2, t) &\equiv -\sqrt{\frac{1}{3}} \mathcal{A}_\Gamma(+1/2, +1/2, 0, t) + \sqrt{\frac{2}{3}} \mathcal{A}_\Gamma(+1/2, -1/2, +1, t) \,, \\ \mathcal{A}_\Gamma^{(1/2)}(+1/2, -1/2, -1) &\equiv \sqrt{\frac{1}{3}} \mathcal{A}_\Gamma(+1/2, -1/2, 0, -1) - \sqrt{\frac{2}{3}} \mathcal{A}_\Gamma(+1/2, +1/2, -1, -1) \,. \end{aligned} \tag{4.6}$$

The complementary set of $J = 3/2$ amplitudes reads

$$\begin{aligned}
\mathcal{A}_\Gamma^{(3/2)}(+1/2,+3/2,+1) &\equiv \mathcal{A}_\Gamma(+1/2,+1/2,+1,+1)\,,\\
\mathcal{A}_\Gamma^{(3/2)}(+1/2,+1/2,0) &\equiv \sqrt{\frac{2}{3}}\mathcal{A}_\Gamma(+1/2,+1/2,0,0) + \sqrt{\frac{1}{3}}\mathcal{A}_\Gamma^{(3/2)}(+1/2,-1/2,+1,0)\,,\\
\mathcal{A}_\Gamma^{(3/2)}(+1/2,+1/2,t) &\equiv \sqrt{\frac{2}{3}}\mathcal{A}_\Gamma(+1/2,+1/2,0,t) + \sqrt{\frac{1}{3}}\mathcal{A}_\Gamma^{(3/2)}(+1/2,-1/2,+1,t)\,,\\
\mathcal{A}_\Gamma^{(3/2)}(+1/2,-1/2,-1) &\equiv \sqrt{\frac{2}{3}}\mathcal{A}_\Gamma(+1/2,-1/2,0,-1) + \sqrt{\frac{1}{3}}\mathcal{A}_\Gamma^{(3/2)}(+1/2,+1/2,-1,-1)\,.
\end{aligned} \tag{4.7}$$

For transitions to $J = 1/2$ the set of amplitudes in eq. (4.7) is required to vanish identically, and similarly for transitions to $J = 3/2$ the set in eq. (4.6) needs to be zero. We explicitly verify this to be the case for the structures listed in appendix B.2.

Our Dirac structures $\Gamma^{\alpha\mu}_{V(A),i}$ have been chosen such that the form factors $F_{1/2,\lambda_q}$ and $G_{1/2,\lambda_q}$, $\lambda_q \in \{t, 0, \perp\}$, correspond to transitions into $\Lambda_c(2593)^+$ states with $|J_z| = 1/2$, while the $\Lambda_c(2625)^+$ states with $|J_z| = 3/2$ are only produced via the form factors $F_{3/2,\perp}$ and $G_{3/2,\perp}$. Note that all helicity amplitudes depend only on one single form factor; see eqs. (B.49) – (B.51), eqs. (B.52) – (B.54), eqs. (B.91) – (B.94), and eqs. (B.95) – (B.98). We have therefore achieved a decomposition of the (axial)vector hadronic matrix elements in terms of helicity form factors as inspired by [79]. We note that our definitions of the form factors differ from the one adopted in [77], where the decomposition of the vector and axial vector hadronic matrix elements do not yield form factors for transitions with well-defined angular momentum of the final states. In particular in the conventions of [77] the time-like polarisation, which is relevant for the LFU ratio $R_{\Lambda_c^*}$, depends on linear combinations of multiple form factors instead of one form factor per current.

4.2.2 Heavy-quark expansion

In Ref. [77], the usual basis of form factors has been studied in the HQE up to $1/m$ contributions. We cross-check their results, and adapt them to our choice of a helicity basis for the form factors. In particular, we study the hadronic matrix elements in and beyond the heavy quark limit $m_b \to \infty$, $m_c \to \infty$ with $m_c/m_b = \text{const}$. Following [76], we use that the transition matrix elements can be written at leading power in the expansion as

$$\langle \Lambda_c^*(k,\eta,s_c)|\,\bar{c}\,\Gamma^\mu b\,|\Lambda_b^0(p,s_b)\rangle = \sqrt{4}\overline{u}_\alpha(m_{\Lambda_c^*}v',\eta,s_c)\Gamma^\mu u(m_{\Lambda_b}v,s_b)\zeta^\alpha(w)\,, \tag{4.8}$$

where $w \equiv v\cdot v' = (m_{\Lambda_b}^2 + m_{\Lambda_c^*}^2 - q^2)/(2m_{\Lambda_b}m_{\Lambda_c^*})$, v and v' are the four-velocities of the initial and final states, respectively, and Γ denotes a Dirac structure. Here the most general decomposition of the light-state transition amplitude ζ reads

$$\zeta^\alpha(w) = \zeta(w)(v - v')^\alpha\,. \tag{4.9}$$

As a consequence, at leading power all form factors can be expressed in terms of the single amplitude $\zeta(w)$, which must vanish at the zero hadronic recoil $w = 1$, which corresponds to $q^2 = (m_{\Lambda_b} - m_{\Lambda_c^*})^2$. In order to include also $1/m$ and α_s corrections, we use for the vector current (and similarly for the axialvector current)

$$\gamma^\mu \mapsto J_V^\mu = C_1(\overline{w})\gamma^\mu + C_2(\overline{w})v^\mu + C_3(\overline{w})v'^\mu + \Delta J_V^\mu\big|_{\mathcal{O}_1} + \Delta J_V^\mu\big|_{\mathcal{O}_8} + \mathcal{O}(\alpha_s/m, 1/m^2)\,, \tag{4.10}$$

with perturbative coefficients C_i and power corrections ΔJ_V^μ.

The perturbative functions C_i are the Wilson coefficients arising in the matching of HQET onto QCD. Their argument $\overline{w}$ is the recoil parameter as experienced by the heavy quarks within the hadrons. Note that for a decay to orbitally excited hadrons $\overline{w}$ is not the same as defined for transitions among ground-state baryons. Instead, we use

$$\overline{w} \equiv w\left(1+\frac{\overline{\Lambda}}{m_b}+\frac{\overline{\Lambda}'}{m_c}\right)-\left(\frac{\overline{\Lambda}}{m_c}+\frac{\overline{\Lambda}'}{m_b}\right), \tag{4.11}$$

where $\overline{\Lambda}$ and $\overline{\Lambda}'$ are the usual HQET parameters in the infinite mass limit. The above yields the product of heavy-quark velocities as defined in [80] in the limit $\overline{\Lambda}' \to \overline{\Lambda}$. We use the matching coefficients C_i to order α_s, which are given in eq. (3.111) of [80]. At the precision that we aim for, we do not require the renormalization-group improved matching coefficients, which can be extracted from [80], eq. (3.121).

In **??** we use only power corrections $\Delta J_V^\mu\big|_{\mathcal{O}_1}$ and $\Delta J_V^\mu\big|_{\mathcal{O}_8}$, arising from the local operators $\mathcal{O}_1$ and $\mathcal{O}_8$ as defined in [80], respectively. The remaining local operators only contribute at the order α_s/m and are therefore beyond the precision we aim for. The hadronic matrix elements of $\mathcal{O}_1$ and $\mathcal{O}_8$ can be parametrised as:

$$\langle\Lambda_c^*(k,\eta,s_c)|\,\Delta J_{V\mu}\big|_{\mathcal{O}_{1(8)}}\,|\Lambda_b^0(p,s_b)\rangle = \sqrt{4}\overline{u}_\alpha(m_{\Lambda_c^*}v',\eta,s_c)\left[\mathcal{O}_{1(8)}\right]_{\mu\beta}u(m_{\Lambda_b}v,s_b)\zeta_{b(c)}^{\alpha\beta}(w)\,, \tag{4.12}$$

where

$$\zeta_{(q)}^{\alpha\beta}(w) = (v-v')^\alpha\left[\zeta_1^{(q)}(w)v^\beta+\zeta_2^{(q)}(w)v'^\beta\right]+g^{\alpha\beta}\zeta_3^{(q)}(w)\,. \tag{4.13}$$

and $[\mathcal{O}_1]_{\mu\beta}=\gamma_\mu\gamma_\beta$, $[\mathcal{O}_8]_{\mu\beta}=\gamma_\beta\gamma_\mu$.
After some algebra, we obtain the following for the contributions from $\Delta J_{V\mu}\big|_{\mathcal{O}_1}$ and $\Delta J_{V\mu}\big|_{\mathcal{O}_8}$:

$$\begin{aligned}
\langle\Lambda_c^*(k,\eta,s_c)|\,\Delta J_{V\mu}\big|_{\mathcal{O}_1}\,|\Lambda_b^0(p,s_b)\rangle = \frac{1}{2m_b}\Big[&2\overline{u}_\alpha(m_{\Lambda_c^*}v',\eta,s_c)\gamma_\mu u(m_{\Lambda_b}v,s_b)v^\alpha\left(\zeta_1^{(b)}(w)-\zeta_2^{(b)}(w)\right)\\
&+4\overline{u}_\alpha(m_{\Lambda_c^*}v',\eta,s_c)u(m_{\Lambda_b}v,s_b)v^\alpha v'^\mu\zeta_2^{(b)}(w)\\
&+2\overline{u}_\alpha(m_{\Lambda_c^*}v',\eta,s_c)\gamma_\mu\gamma_\alpha u(m_{\Lambda_b}v,s_b)\zeta_3^{(b)}(w)\Big]\,,\\
\langle\Lambda_c^*(k,\eta,s_c)|\,\Delta J_{V\mu}\big|_{\mathcal{O}_8}\,|\Lambda_b^0(p,s_b)\rangle = \frac{1}{2m_c}\Big[&2\overline{u}_\alpha(m_{\Lambda_c^*}v',\eta,s_c)\gamma_\mu u(m_{\Lambda_b}v,s_b)v^\alpha\left(\zeta_2^{(c)}(w)-\zeta_1^{(c)}(w)\right)\\
&+4\overline{u}_\alpha(m_{\Lambda_c^*}v',\eta,s_c)u(m_{\Lambda_b}v,s_b)v^\alpha v^\mu\zeta_1^{(c)}(w)\\
&+2\overline{u}_\alpha(m_{\Lambda_c^*}v',\eta,s_c)\gamma^\alpha\gamma_\mu u(m_{\Lambda_b}v,s_b)\zeta_3^{(c)}(w)\Big]\,.
\end{aligned} \tag{4.14}$$

We can follow the very same steps also with the axial vector current. In this case we have:

$$\gamma^\mu\gamma_5 \mapsto J_A^\mu = C_1^{(5)}(\overline{w})\gamma^\mu\gamma^5+C_2^{(5)}(\overline{w})v^\mu\gamma^5+C_3^{(5)}(\overline{w})v'^\mu\gamma^5+\Delta J_A^\mu\big|_{\mathcal{O}_1^A}+\Delta J_A^\mu\big|_{\mathcal{O}_8^A}+\mathcal{O}(\alpha_s/m,1/m^2)\,, \tag{4.15}$$

where the subleading contributions $\Delta J_A^\mu\big|_{\mathcal{O}_1^A}$ and $\Delta J_A^\mu\big|_{\mathcal{O}_8^A}$ can by computed from

$$\langle\Lambda_c^*(k,\eta,s_c)|\,\Delta J_{A\mu}\big|_{\mathcal{O}_{1(8)}^A}\,|\Lambda_b^0(p,s_b)\rangle = \sqrt{4}\overline{u}_\alpha(m_{\Lambda_c^*}v',\eta,s_c)[\mathcal{O}_{1(8)}^A]_{\mu\beta}u(m_{\Lambda_b}v,s_b)\zeta_{b(c)}^{\alpha\beta}(w)\,, \tag{4.16}$$

and $[\mathcal{O}_1^A]_{\mu\beta} = \gamma_\mu\gamma^5\gamma_\beta$, $[\mathcal{O}_8^A]_{\mu\beta} = \gamma_\beta\gamma_\mu\gamma^5$. From this we obtain:

$$\begin{aligned}
\langle\Lambda_c^*(k,\eta,s_c)|\,\Delta J_{A\mu}\big|_{\mathcal{O}_1^A}\,|\Lambda_b^0(p,s_b)\rangle &= \frac{1}{2m_b}\Big[2\overline{u}_\alpha(m_{\Lambda_c^*}v',\eta,s_c)\gamma_\mu u(m_{\Lambda_b}v,s_b)v^\alpha\left(\zeta_1^{(b)}(w)+\zeta_2^{(b)}(w)\right)\\
&\quad -4\overline{u}_\alpha(m_{\Lambda_c^*}v',\eta,s_c)u(m_{\Lambda_b}v,s_b)v^\alpha v'^\mu\zeta_2^{(b)}(w)\\
&\quad +2\overline{u}_\alpha(m_{\Lambda_c^*}v',\eta,s_c)\gamma^\mu\gamma^5\gamma^\alpha u(m_{\Lambda_b}v,s_b)\zeta_3^{(b)}(w)\Big]\,,\\
\langle\Lambda_c^*(k,\eta,s_c)|\,\Delta J_{A\mu}\big|_{\mathcal{O}_8^A}\,|\Lambda_b^0(p,s_b)\rangle &= \frac{1}{2m_c}\Big[2\overline{u}_\alpha(m_{\Lambda_c^*}v',\eta,s_c)\gamma_\mu u(m_{\Lambda_b}v,s_b)v^\alpha\left(\zeta_1^{(c)}(w)+\zeta_2^{(c)}(w)\right)\\
&\quad +4\overline{u}_\alpha(m_{\Lambda_c^*}v',\eta,s_c)u(m_{\Lambda_b}v,s_b)v^\alpha v^\mu\zeta_1^{(c)}(w)\Big]\,,\\
&\quad +2\overline{u}_\alpha(m_{\Lambda_c^*}v',\eta,s_c)\gamma^\alpha\gamma^\mu\gamma^5 u(m_{\Lambda_b}v,s_b)\zeta_3^{(b)}(w)\Big]\,.
\end{aligned} \tag{4.17}$$

The subleading IW functions are related by the equations of motion. In particular we have that $v_\beta\zeta_{(b)}^{\alpha\beta} = 0$, and $v'_\beta\zeta_{(c)}^{\alpha\beta} = 0$. This leads to the following relations:

$$\zeta_1^{(b)}(w) + w\zeta_2^{(b)}(w) + \zeta_3^{(b)}(w) = 0\,, \tag{4.18}$$

$$w\zeta_1^{(c)}(w) + \zeta_2^{(c)}(w) = 0\,. \tag{4.19}$$

Furthermore we know that $i\partial_\alpha[\overline{h}_c(v')\Gamma h_b(v)] = \overline{h}_c(v')i\overleftarrow{D}_\alpha\Gamma h_b(v) + \overline{h}_c(v')\Gamma iD_\alpha h_b(v)$, where we denote $h_{b(c)}$ as the usual HQET fields. This identity allows us to write the following relations:

$$\zeta_1^{(b)}(w) + \zeta_1^{(c)}(w) = \overline{\Lambda}\zeta(w)\,, \tag{4.20}$$

$$\zeta_2^{(b)}(w) + \zeta_2^{(c)}(w) = -\overline{\Lambda}'\zeta(w)\,, \tag{4.21}$$

$$\zeta_3^{(b)}(w) + \zeta_3^{(c)}(w) = 0\,. \tag{4.22}$$

With these 5 relations we can reduce the initial 6 subleading IW functions to one independent subleading IW function. We find it convenient to use $\zeta_3^{(b)}$:

$$\begin{aligned}
\zeta_1^{(b)} &= -\frac{\zeta_3^{(b)}}{1-w^2} + \frac{w\zeta}{1-w^2}\left(\overline{\Lambda}' - \overline{\Lambda}w\right)\,, \qquad \zeta_2^{(b)} = +\frac{w\zeta_3^{(b)}}{1-w^2} - \frac{\zeta}{1-w^2}\left(\overline{\Lambda}' - \overline{\Lambda}w\right)\,,\\
\zeta_1^{(c)} &= +\frac{\zeta_3^{(b)}}{1-w^2} - \frac{\zeta}{1-w^2}\left(w\overline{\Lambda}' - \overline{\Lambda}\right)\,, \qquad \zeta_2^{(c)} = -\frac{w\zeta_3^{(b)}}{1-w^2} + \frac{w\zeta}{1-w^2}\left(w\overline{\Lambda}' - \overline{\Lambda}\right)\,.
\end{aligned} \tag{4.23}$$

From this point on we identify $\zeta_{\rm SL} \equiv \zeta_3^{(b)} = -\zeta_3^{(c)}$.

Beside the effects on local operators, we also need to consider effects from non-local insertions of the HQET Lagrangian at power $1/m$. Following the discussion in [77,80], non-local insertions of the kinetic operator give rise to an w-dependent shift $\eta_{\rm kin}(w)$ to the leading-power IW function $\zeta(w)$. We can absorb this shift into the definition of ζ:

$$\zeta(w) + \frac{1}{2m_bm_c}\left[m_b+m_c\right]\eta_{\rm kin}(w) \mapsto \zeta(w)\,. \tag{4.24}$$

The w-dependent shift due to the chromomagnetic operator is more delicate. The two contributions are:

$$\eta_{\rm mag}^{(c)}(w) : \left[g_{\mu\alpha}v_\nu\right]\overline{u}_J^\alpha(m_{\Lambda_c^*}v',\eta,s_c)\; i\sigma^{\mu\nu}\frac{1+\not{v}'}{2}\Gamma u(m_{\Lambda_b}v,s_b) \tag{4.25}$$

$$\eta_{\rm mag}^{(b)}(w) : \left[g_{\mu\alpha}v'_\nu\right]\overline{u}_J^\alpha(m_{\Lambda_c^*}v',\eta,s_c)\;\Gamma\frac{1+\not{v}}{2}\;i\sigma^{\mu\nu}u(m_{\Lambda_b}v,s_b)\,. \tag{4.26}$$

In [77], it is argued that the two functions $\eta^{(q)}_{\rm mag}(w)$ must vanish at zero recoil, and are expected to be small compared to the size of $\Lambda_{\rm QCD}$. We follow this argument, and therefore choose to not consider contributions from either $\eta^{(q)}_{\rm mag}(w)$ from this point on.

If we want now to express the form factors in terms of the leading and subleading IW functions we need to match the HQE expansion of the helicity amplitudes onto the direct calculation presented in Sec. 4.2.1. Concerning the $\Lambda_c(2595)^+$ final state, the comparison between eqs. (B.55)–(B.57) and eqs. (B.49)–(B.51) leads to

$$\begin{aligned} f_{1/2,0} =& \frac{\sqrt{s_+}}{2(m_{\Lambda_b} m_{\Lambda_c^*})^{3/2}} \Bigg\{ \Bigg[s_- \left(C_1(\overline{w}) + \frac{s_+ (C_2(\overline{w}) m_{\Lambda_c^*} + C_3(\overline{w}) m_{\Lambda_b})}{2 m_{\Lambda_b} m_{\Lambda_c^*} (m_{\Lambda_b} + m_{\Lambda_c^*})} \right) \\ &+ \frac{(m_{\Lambda_b} - m_{\Lambda_c^*})}{m_{\Lambda_b} + m_{\Lambda_c^*}} \left(\frac{m_{\Lambda_b}^2 - m_{\Lambda_c^*}^2 + q^2}{2 m_{\Lambda_b}} \overline{\Lambda} - \frac{m_{\Lambda_b}^2 - m_{\Lambda_c^*}^2 - q^2}{2 m_{\Lambda_c^*}} \overline{\Lambda}' \right) \Bigg] \zeta - 2 (m_{\Lambda_b} - m_{\Lambda_c^*}) \zeta_{\rm SL} \Bigg\}, \end{aligned} \tag{4.27}$$

$$\begin{aligned} f_{1/2,t} =& \frac{\sqrt{s_-}}{2(m_{\Lambda_b} m_{\Lambda_c^*})^{3/2}} \Bigg\{ \Bigg[C_1(\overline{w}) s_+ + \frac{(m_{\Lambda_b} + m_{\Lambda_c^*})}{m_{\Lambda_b} - m_{\Lambda_c^*}} \Bigg(\frac{m_{\Lambda_b}^2 - m_{\Lambda_c^*}^2 + q^2}{2 m_{\Lambda_b}} \left(\overline{\Lambda} + \frac{C_2(\overline{w}) s_+}{m_{\Lambda_b} + m_{\Lambda_c^*}} \right) \\ &- \frac{m_{\Lambda_b}^2 - m_{\Lambda_c^*}^2 - q^2}{2 m_{\Lambda_c^*}} \left(\overline{\Lambda}' - \frac{C_3(\overline{w}) s_+}{m_{\Lambda_b} + m_{\Lambda_c^*}} \right) \Bigg) \Bigg] \zeta - 2 \frac{(m_{\Lambda_b} + m_{\Lambda_c^*})^2}{m_{\Lambda_b} - m_{\Lambda_c^*}} \zeta_{\rm SL} \Bigg\}, \end{aligned} \tag{4.28}$$

$$f_{1/2,\perp} = \frac{\sqrt{s_+}}{2(m_{\Lambda_b} m_{\Lambda_c^*})^{3/2}} \Bigg\{ \Bigg[C_1(\overline{w}) s_- + \frac{3 m_{\Lambda_b}^2 + m_{\Lambda_c^*}^2 - q^2}{2 m_{\Lambda_b}} \overline{\Lambda} - \frac{m_{\Lambda_b}^2 + 3 m_{\Lambda_c^*}^2 - q^2}{2 m_{\Lambda_c^*}} \overline{\Lambda}' \Bigg] \zeta - 2 m_{\Lambda_b} \zeta_{\rm SL} \Bigg\}, \tag{4.29}$$

for the vector form factors, while for the axial-vector form factors the matching of eqs. (B.58)–(B.60) onto eqs. (B.52)–(B.54) gives

$$\begin{aligned} g_{1/2,0} =& \frac{\sqrt{s_-}}{2(m_{\Lambda_b} m_{\Lambda_c^*})^{3/2}} \Bigg\{ \Bigg[s_+ \left(C_1(\overline{w}) - \frac{s_- (C_2(\overline{w}) m_{\Lambda_c^*} + C_3(\overline{w}) m_{\Lambda_b})}{2 m_{\Lambda_b} m_{\Lambda_c^*} (m_{\Lambda_b} - m_{\Lambda_c^*})} \right) \\ &+ \frac{m_{\Lambda_b} + m_{\Lambda_c^*}}{m_{\Lambda_b} - m_{\Lambda_c^*}} \left(\frac{m_{\Lambda_b}^2 - m_{\Lambda_c^*}^2 + q^2}{2 m_{\Lambda_b}} \overline{\Lambda} - \frac{m_{\Lambda_b}^2 - m_{\Lambda_c^*}^2 - q^2}{2 m_{\Lambda_c^*}} \overline{\Lambda}' \right) \Bigg] \zeta - 2 (m_{\Lambda_b} + m_{\Lambda_c^*}) \zeta_{\rm SL} \Bigg\}, \end{aligned} \tag{4.30}$$

$$\begin{aligned} g_{1/2,t} =& \frac{\sqrt{s_+}}{2(m_{\Lambda_b} m_{\Lambda_c^*})^{3/2}} \Bigg\{ \Bigg[C_1(\overline{w}) s_- + \frac{(m_{\Lambda_b} - m_{\Lambda_c^*})}{m_{\Lambda_b} + m_{\Lambda_c^*}} \Bigg(\frac{m_{\Lambda_b}^2 - m_{\Lambda_c^*}^2 + q^2}{2 m_{\Lambda_b}} \left(\overline{\Lambda} - \frac{C_2(\overline{w}) s_-}{m_{\Lambda_b} - m_{\Lambda_c^*}} \right) \\ &- \frac{m_{\Lambda_b}^2 - m_{\Lambda_c^*}^2 - q^2}{2 m_{\Lambda_c^*}} \left(\overline{\Lambda}' + \frac{C_3(\overline{w}) s_-}{m_{\Lambda_b} - m_{\Lambda_c^*}} \right) \Bigg) \Bigg] \zeta - 2 \frac{(m_{\Lambda_b} - m_{\Lambda_c^*})^2}{m_{\Lambda_b} + m_{\Lambda_c^*}} \zeta_{\rm SL} \Bigg\}, \end{aligned} \tag{4.31}$$

$$g_{1/2,\perp} = \frac{\sqrt{s_-}}{2(m_{\Lambda_b} m_{\Lambda_c^*})^{3/2}} \Bigg\{ \Bigg[C_1(\overline{w}) s_+ + \overline{\Lambda} \frac{3 m_{\Lambda_b}^2 + m_{\Lambda_c^*}^2 - q^2}{2 m_{\Lambda_b}} - \overline{\Lambda}' \frac{m_{\Lambda_b}^2 + 3 m_{\Lambda_c^*}^2 - q^2}{2 m_{\Lambda_c^*}} \Bigg] \zeta - 2 m_{\Lambda_b} \zeta_{\rm SL} \Bigg\}. \tag{4.32}$$

Here and in the following we denote $s_\pm \equiv (m_{\Lambda_b} \pm m_{\Lambda_c^*})^2 - q^2$. Concerning the $\Lambda_c(2625)^+$ final state, the vector form factors are obtained by matching eqs. (B.99)–(B.102) with eqs. (B.91)–

(B.94)

$$F_{1/2,\perp} = \frac{\sqrt{s_+}}{2(m_{\Lambda_b} m_{\Lambda_c^*})^{3/2}} \left\{ \left[C_1(\overline{w}) s_- + \frac{3m_{\Lambda_b}^2 + m_{\Lambda_c^*}^2 - q^2}{2m_{\Lambda_b}} \overline{\Lambda} - \frac{m_{\Lambda_b}^2 + 3m_{\Lambda_c^*}^2 - q^2}{2m_{\Lambda_c^*}} \overline{\Lambda}' \right] \zeta + m_{\Lambda_b} \zeta_{\rm SL} \right\} , \tag{4.33}$$

$$\begin{aligned} F_{1/2,t} = & \frac{\sqrt{s_-}}{2(m_{\Lambda_b} m_{\Lambda_c^*})^{3/2}} \left\{ \left[C_1(\overline{w}) s_+ + \frac{m_{\Lambda_b} + m_{\Lambda_c^*}}{m_{\Lambda_b} - m_{\Lambda_c^*}} \left(\frac{m_{\Lambda_b}^2 - m_{\Lambda_c^*}^2 + q^2}{2m_{\Lambda_b}} \left(\overline{\Lambda} + \frac{C_2(\overline{w}) s_+}{m_{\Lambda_b} + m_{\Lambda_c^*}} \right) \right. \right. \right. \\ & \left. \left. \left. - \frac{m_{\Lambda_b}^2 - m_{\Lambda_c^*}^2 - q^2}{2m_{\Lambda_c^*}} \left(\overline{\Lambda}' - \frac{C_3(\overline{w}) s_+}{m_{\Lambda_b} + m_{\Lambda_c^*}} \right) \right) \right] \zeta + \frac{(m_{\Lambda_b} + m_{\Lambda_c^*})^2}{m_{\Lambda_b} - m_{\Lambda_c^*}} \zeta_{\rm SL} \right\} , \end{aligned} \tag{4.34}$$

$$\begin{aligned} F_{1/2,0} = & \frac{\sqrt{s_+}}{2(m_{\Lambda_b} m_{\Lambda_c^*})^{3/2}} \left\{ \left[s_- \left(C_1(\overline{w}) + \frac{s_+ (C_2(\overline{w}) m_{\Lambda_c^*} + C_3(\overline{w}) m_{\Lambda_b})}{2m_{\Lambda_b} m_{\Lambda_c^*} (m_{\Lambda_b} + m_{\Lambda_c^*})} \right) \right. \right. \\ & \left. \left. + \frac{m_{\Lambda_b} - m_{\Lambda_c^*}}{m_{\Lambda_b} + m_{\Lambda_c^*}} \left(\frac{m_{\Lambda_b}^2 - m_{\Lambda_c^*}^2 + q^2}{2m_{\Lambda_b}} \overline{\Lambda} - \frac{m_{\Lambda_b}^2 - m_{\Lambda_c^*}^2 - q^2}{2m_{\Lambda_c^*}} \overline{\Lambda}' \right) \right] \zeta + (m_{\Lambda_b} - m_{\Lambda_c^*}) \zeta_{\rm SL} \right\} , \end{aligned} \tag{4.35}$$

$$F_{3/2,\perp} = - \frac{\sqrt{s_+}}{2m_{\Lambda_b}^{3/2} m_{\Lambda_c^*}^{1/2}} \zeta_{\rm SL} , \tag{4.36}$$

while for the axial-vector form factor the comparison of eqs. (B.103)–(B.106) and eqs. (B.95)–(B.98) yields

$$G_{1/2,\perp} = \frac{\sqrt{s_-}}{2(m_{\Lambda_b} m_{\Lambda_c^*})^{3/2}} \left\{ \left[C_1(\overline{w}) s_+ + \frac{3m_{\Lambda_b}^2 + m_{\Lambda_c^*}^2 - q^2}{2m_{\Lambda_b}} \overline{\Lambda} - \frac{m_{\Lambda_b}^2 + 3m_{\Lambda_c^*}^2 - q^2}{2m_{\Lambda_c^*}} \overline{\Lambda}' \right] \zeta + m_{\Lambda_b} \zeta_{\rm SL} \right\} , \tag{4.37}$$

$$\begin{aligned} G_{1/2,t} = & \frac{\sqrt{s_+}}{2(m_{\Lambda_b} m_{\Lambda_c^*})^{3/2}} \left\{ \left[C_1(\overline{w}) s_- + \frac{m_{\Lambda_b} - m_{\Lambda_c^*}}{m_{\Lambda_b} + m_{\Lambda_c^*}} \left(\frac{m_{\Lambda_b}^2 - m_{\Lambda_c^*}^2 + q^2}{2m_{\Lambda_b}} \left(\overline{\Lambda} - \frac{C_2(\overline{w}) s_-}{m_{\Lambda_b} - m_{\Lambda_c^*}} \right) \right. \right. \right. \\ & \left. \left. \left. - \frac{m_{\Lambda_b}^2 - m_{\Lambda_c^*}^2 - q^2}{2m_{\Lambda_c^*}} \left(\overline{\Lambda}' + \frac{C_3(\overline{w}) s_-}{m_{\Lambda_b} - m_{\Lambda_c^*}} \right) \right) \right] \zeta + \frac{(m_{\Lambda_b} - m_{\Lambda_c^*})^2}{m_{\Lambda_b} + m_{\Lambda_c^*}} \zeta_{\rm SL} \right\} , \end{aligned} \tag{4.38}$$

$$\begin{aligned} G_{1/2,0} = & \frac{\sqrt{s_-}}{2(m_{\Lambda_b} m_{\Lambda_c^*})^{3/2}} \left\{ \left[s_+ \left(C_1(\overline{w}) - \frac{s_- (C_2(\overline{w}) m_{\Lambda_c^*} + C_3(\overline{w}) m_{\Lambda_b})}{2m_{\Lambda_b} m_{\Lambda_c^*} (m_{\Lambda_b} - m_{\Lambda_c^*})} \right) \right. \right. \\ & \left. \left. + \frac{m_{\Lambda_b} + m_{\Lambda_c^*}}{m_{\Lambda_b} - m_{\Lambda_c^*}} \left(\frac{m_{\Lambda_b}^2 - m_{\Lambda_c^*}^2 + q^2}{2m_{\Lambda_b}} \overline{\Lambda} - \frac{m_{\Lambda_b}^2 - m_{\Lambda_c^*}^2 - q^2}{2m_{\Lambda_c^*}} \overline{\Lambda}' \right) \right] \zeta + (m_{\Lambda_b} + m_{\Lambda_c^*}) \zeta_{\rm SL} \right\} , \end{aligned} \tag{4.39}$$

$$G_{3/2,\perp} = - \frac{\sqrt{s_-}}{2m_{\Lambda_b}^{3/2} m_{\Lambda_c^*}^{1/2}} \zeta_{\rm SL} . \tag{4.40}$$

Thus, at leading power in $1/m$ only the $(J, J_z) = (3/2, \pm 1/2)$ form factors receive contributions from the leading-power IW function. As a consequence, the sum rule at zero recoil ($w = 1$ or $s_- = 0$) as discussed later will be less sensitive to the contributions from the $J = 3/2$ amplitudes.

We note in passing that our results for the HQE of the form factors fulfil the relations

$$\begin{aligned} \frac{f_{1/2,t}(0)}{f_{1/2,0}(0)} &\equiv \frac{m_{\Lambda_b} + m_{\Lambda_c^*}}{m_{\Lambda_b} - m_{\Lambda_c^*}} , \quad \frac{g_{1/2,t}(0)}{g_{1/2,0}(0)} \equiv \frac{m_{\Lambda_b} - m_{\Lambda_c^*}}{m_{\Lambda_b} + m_{\Lambda_c^*}} , \\ \frac{F_{1/2,t}(0)}{F_{1/2,0}(0)} &\equiv \frac{m_{\Lambda_b} + m_{\Lambda_c^*}}{m_{\Lambda_b} - m_{\Lambda_c^*}} , \quad \frac{G_{1/2,t}(0)}{G_{1/2,0}(0)} \equiv \frac{m_{\Lambda_b} - m_{\Lambda_c^*}}{m_{\Lambda_b} + m_{\Lambda_c^*}} , \end{aligned} \tag{4.41}$$

as required by analyticity; i.e., any spurious poles of the hadronic matrix elements in the limit $q^2 \to 0$ do not correspond to any physical states with quantum numbers $B = -C = 1$, and therefore must be cancelled due to the above relations.

4.3 Phenomenology

4.3.1 Parametrisation of the Isgur-Wise functions

Determining the parameters of the leading and subleading IW functions is a crucial point to determine the form factors. Unfortunately, there are no first principles in HQET which allow us to estimate the q^2 dependence of the IW functions. In light of this, we need to infer a functional form for $\zeta(q^2)$ and $\zeta_{\rm SL}(q^2)$ through some other means. For the ground-state transition $\Lambda_b \to \Lambda_c$ and in the large N_c limit, it has been motivated in [81] to express the IW functions as exponential functions. Inspired by this, one of the models we consider here for the parametrisation of the leading and subleading IW function $\zeta(q^2)$ and $\zeta_{\rm SL}(q^2)$ is

$$\begin{aligned} \zeta(q^2)\Big|_{\rm exp} &\equiv \zeta(q^2_{\rm max}) \exp\left[\rho\left(\frac{q^2}{q^2_{\rm max}} - 1\right)\right], \\ \zeta_{\rm SL}(q^2)\Big|_{\rm exp} &\equiv \zeta(q^2_{\rm max})\delta_{\rm SL} \exp\left[\frac{\rho_{\rm SL}}{\delta_{\rm SL}}\left(\frac{q^2}{q^2_{\rm max}} - 1\right)\right]. \end{aligned} \tag{4.42}$$

where the normalisation $\zeta(q^2_{\rm max})$, the relative normalisation $\delta_{\rm SL}$ and the two shape parameters ρ and $\rho_{\rm SL}$ are to be determined.

We can also use a Taylor expansion of $\zeta(q^2)$ and $\zeta_{\rm SL}(q^2)$ around $q^2 \simeq q^2_{\rm max}$. For our purposes we use an expansion up to the first order in q^2:

$$\begin{aligned} \zeta(q^2)\Big|_{\rm lin} &\equiv \zeta(q^2_{\rm max})\left[1 + \rho\left(\frac{q^2}{q^2_{\rm max}} - 1\right)\right], \\ \zeta_{\rm SL}(q^2)\Big|_{\rm lin} &\equiv \zeta(q^2_{\rm max})\left[\delta_{\rm SL} + \rho_{\rm SL}\left(\frac{q^2}{q^2_{\rm max}} - 1\right)\right]. \end{aligned} \tag{4.43}$$

In the following we will refer to eq. (4.43) as the nominal parametrisation.

Both parametrisations have been chosen such that they share their complete parameter set, and such that both the leading and the subleading IW functions have a common normalisation $\zeta(q^2_{\rm max})$.

4.3.2 Benchmarking the form factors' parameters from Zero Recoil Sum Rules

The kinematic point of zero hadronic recoil is a special for bottom-to-charm transitions. In this point the hadronic form factors for $\Lambda_b \to X_c$ transitions, where X_c denotes a singly-charmed baryonic state, are minimally sensitive to the dynamics of the light degrees of freedom within the respective hadrons; see e.g. [82]. As a consequence, the inclusive spectral density for the forward matrix elements of two bi-local insertions of the weak current can be expressed in terms of $\Lambda_b \to X_c$ form factors. Inference of weighted sum of squares for the form factor normalisations follows in what is known as a Zero Recoil Sum Rule (ZRSR) [83, 84]. This is only possible since the spectral density consists of a sum of positive-definite exclusive terms.

The ZRSR is well established for $B \to D$ and $B \to D^*$ transitions, with OPE contributions known up to order α_s^2 [85]. After the first lattice QCD results for the $\Lambda_b \to \Lambda_c$ form factors appeared [74], they were scrutinised in the ZRSR framework [86]. The conclusion of the latter analysis is as follows. Given our present knowledge of the Λ_b forward matrix elements, and given the lack of mixed α_s/m results for the ZRSR, the lattice results for $\Lambda_b \to \Lambda_c$ transition lead to a negative contribution from non-ground state transitions. As mentioned above, negative contributions to the spectral density are not possible by construction. Hence, either the inclusive calculation of the spectral density yields too small a value, or the lattice results are too large.

For the discussion at hand, we will assume that the inclusive calculation underestimates the magnitude of the spectral density. Specifically, we assume that $1/m^4$ and $1/m^5$ terms in the Heavy-Quark-Expansion, which have not been taken into account due to lack of information on the relevant hadronic matrix elements, will increase the magnitude. A priori it is not intuitive that terms at order $1/m^4$ or beyond can make a qualitative difference to the ZRSR. However, there is precedent for numerically relevant shifts in the case of $B \to D^*$ [87]. In the latter study, it was observed that – based on rather precise knowledge of the HQE parameters for B mesons – the sum of $1/m^4$ and $1/m^5$ terms yields roughly a third of the $1/m^2$ and $1/m^3$ terms.

In the absence of further information on the Λ_b forward matrix elements, we will therefore proceed as follows. We will rescale the estimate of the $1/m^2$ and $1/m^3$ terms by a factor of 1.33, thereby copying the situation in $B \to D^*$ decays[1]. The corresponding shift can now accommodate fully the lattice results for the $\Lambda_b \to \Lambda_c$ form factors, as well as form factors for Λ_b decays to excited charm baryons. The setup of the ZRSR involves an upper bound on the excitation energies $\varepsilon \equiv M_{X_c} - M_{\Lambda_c}$ of the contributing charm baryons. For the analysis at hand, $\varepsilon \leq 0.7\,\text{GeV}$. Based on the known spectrum of charmed baryons [8, Ch. 109 Charmed Baryons], the ZRSR covers – beside the ground state – form factors for Λ_b decays into $\Sigma_c(2455)$, $\Sigma_c(2520)$, $\Lambda_c(2595)$, $\Lambda_c(2625)$, and $\Sigma_c(2800)$[2]. The Σ_c states form an isospin triplet and therefore carry isospin $I = 1$. Consequently, the transitions $\Lambda_b \to \Sigma_c$ violate isospin conservation, and we will assume them to be further suppressed with respect to the $\Lambda_b \to \Lambda_c^*$ transitions. This supposition is corroborated by the non-observation of $\Lambda_b \to \Sigma_c \ell\nu$ decays in the recent LHCb study [75]. Under the above assumptions, the inelastic parts of the ZRSR can be recast as matrix elements involving only $\Lambda_b \to \Lambda_c^*$ transitions.

Following the definitions and analysis of Ref. [86], applying the assumptions above we arrive at the following constraints at zero recoil:

$$\begin{aligned} F_{\text{inel}} &= 0.011^{+0.061}_{-0.055} \approx F_{\text{inel},1/2} + F_{\text{inel},3/2}\,, \\ G_{\text{inel}} &= 0.040^{+0.049}_{-0.052} \approx G_{\text{inel},1/2} + G_{\text{inel},3/2}\,. \end{aligned} \tag{4.44}$$

The individual contributions from the orbitally-excited Λ_c^* states for the vector current read:

$$F_{\text{inel},1/2} \equiv \frac{1}{N_V} \sum_{\Lambda_c^* \text{ spin}} \langle \Lambda_b^0(v,s_b)|\, \bar{b}\gamma^\mu c\, |\Lambda_c(2595)^+(v)\rangle \langle \Lambda_c(2595)^+(v)|\, \bar{c}\gamma_\mu b\, |\Lambda_b^0(v,s_b)\rangle \tag{4.45}$$

[1] We stress that this rescaling, and the corresponding shift to the inclusive upper bound on the form factor normalisations, is based on a supposition rather than data, and will only be used for the purpose of benchmarking the experimental sensitivity. Ultimately, only improved knowledge of the hadronic matrix elements will settle the discrepancy between the ZRSR and lattice results.

[2] We do not consider here the states of roughly 2.8 GeV to 2.9 GeV for which there exists no definite assignment as either a Λ_c, or a Σ_c state, or as a kinematical artifact in the $\Lambda_c\pi\pi$ spectrum. A recent LHCb analysis of $\Lambda_b \to \Lambda_c \ell\nu$ [75] suggests that the yield of $\Lambda_c\pi\pi$ background stemming from this kinematic region corresponds to roughly 10% of the first orbitally excited Λ_c^* states. Given the overall accuracy of our analysis, this further supports our decision not to consider these states.

$$= \frac{1}{3}\left[|f_{t,1/2}|^2 + |f_{0,1/2}|^2 \frac{(m_{\Lambda_b}+m_{\Lambda_c})^2}{(m_{\Lambda_b}-m_{\Lambda_c})^2} + 2|f_{\perp,1/2}|^2\right]_{\text{zero recoil}}, \tag{4.46}$$

and

$$F_{\text{inel},3/2} \equiv \frac{1}{N_V}\sum_{\Lambda_c^* \text{ spin}} \langle\Lambda_b^0(v,s_b)|\,\bar{b}\gamma^\mu c\,|\Lambda_c(2625)^+(v)\rangle\,\langle\Lambda_c(2625)^+(v)|\,\bar{c}\gamma_\mu b\,|\Lambda_b^0(v,s_b)\rangle \tag{4.47}$$

$$= \frac{2}{3}\left[|F_{t,1/2}|^2 + |F_{0,1/2}|^2 \frac{(m_{\Lambda_b}+m_{\Lambda_c})^2}{(m_{\Lambda_b}-m_{\Lambda_c})^2} + 2|F_{\perp,1/2}|^2 + 6|F_{\perp,3/2}|^2\right], \tag{4.48}$$

where $N_V = 1$. For the axialvector current, including the normalisation factor $N_A = 3$, the individual contributions read:

$$G_{\text{inel},1/2} \equiv \frac{1}{N_A}\sum_{\Lambda_c^* \text{ spin}} \langle\Lambda_b^0(v,s_b)|\,\bar{b}\gamma^\mu\gamma_5 c\,|\Lambda_c(2595)^+(v)\rangle\,\langle\Lambda_c(2595)^+(v)|\,\bar{c}\gamma_\mu\gamma_5 b\,|\Lambda_b^0(v,s_b)\rangle \tag{4.49}$$

$$= \frac{1}{9}\left[|g_{0,1/2}|^2 + |g_{t,1/2}|^2 \frac{(m_{\Lambda_b}+m_{\Lambda_c})^2}{(m_{\Lambda_b}-m_{\Lambda_c})^2} + 2|g_{\perp,1/2}|^2\right]_{\text{zero recoil}}, \tag{4.50}$$

and

$$G_{\text{inel},1/2} \equiv \frac{1}{N_V}\sum_{\Lambda_c^* \text{ spin}} \langle\Lambda_b^0(v,s_b)|\,\bar{b}\gamma^\mu\gamma_5 c\,|\Lambda_c(2625)^+(v)\rangle\,\langle\Lambda_c(2625)^+(v)|\,\bar{c}\gamma_\mu\gamma_5 b\,|\Lambda_b^0(p,s_b)\rangle \tag{4.51}$$

$$= \frac{2}{9}\left[|G_{0,1/2}|^2 + |G_{t,1/2}|^2 \frac{(m_{\Lambda_b}+m_{\Lambda_c})^2}{(m_{\Lambda_b}-m_{\Lambda_c})^2} + 2|G_{\perp,1/2}|^2 + 6|G_{\perp,3/2}|^2\right]_{\text{zero recoil}}. \tag{4.52}$$

In the zero-recoil point, both parametrisation eq. (4.42) and eq. (4.43) yield the same expressions, involving only the parameters $\zeta(q^2_{\text{max}})$ and δ_{SL}.

Using two uncorrelated gaussian distributions for F_{inel} and G_{inel} and using symmetrised 68% intervals based on eq. (4.44) we obtain correlated distributions for $\zeta(q^2_{\text{max}})$ and δ_{SL}. The $\zeta(q^2_{\text{max}})$ distribution is highly non-gaussian, and due to the large set of assumptions on which our results are founded, both distributions are not instructive for physics analyses. However, they can be used to define a benchmark point for further phenomenological analyses, in particular for the sensitivity study later on in this chapter. For later applications, we define the normalisation parameters of our benchmark point to be compatible with these distributions:

$$\zeta(q^2_{\text{max}}) = 0.25\,, \quad \delta_{\text{SL}} = -0.14\,, \tag{4.53}$$

corresponding to a subleading contribution of 14% of the leading-power IW function. This is fully in line with naive power-counting expectations for the subleading-power IW function.

Since the ZRSR cannot provide us with any information on the slopes of either IW function, we have to draw inspiration from elsewhere. Given the lower bound on the slope of the leading-power IW function for $B \to D^{(*)}$ transitions, we assume $\rho, \rho_{\text{SL}} \gtrsim 0.25$. On the other hand, in order to avoid unphysical zero crossings of the IW functions in the semileptonic region in the nominal parametrisation, we need to impose $\rho, \rho_{\text{SL}} \lesssim 0.75$. We choose to use the boundaries to define the slope parameters of our benchmark points as:

$$\rho = 0.25 \qquad \rho_{\text{SL}} = 0.25\,, \tag{4.54}$$

$$\rho = 0.25 \qquad \rho_{\text{SL}} = 0.75\,, \tag{4.55}$$

$$\rho = 0.75 \qquad \rho_{\text{SL}} = 0.75\,, \tag{4.56}$$

$$\rho = 0.75 \qquad \rho_{\text{SL}} = 0.25\,. \tag{4.57}$$

We emphasise again that these values are not viable for any physics analysis, and are merely used when studying the sensitivity to the IW function parameters for upcoming LHCb analyses.

4.3.3 Observables

The fully differential decay rate of an unpolarised Λ_b to a Λ_c^* with total angular momentum J can be written as

$$\frac{1}{\Gamma_0^{(\ell)}}\frac{\mathrm{d}^2\Gamma_J^{(\ell)}}{\mathrm{d}q^2\,\mathrm{d}\cos\theta_\ell} = \left(a_\ell^{(J)} + b_\ell^{(J)}\cos\theta_\ell + c_\ell^{(J)}\cos^2\theta_\ell\right), \quad \frac{1}{\Gamma_0^{(\ell)}}\frac{\mathrm{d}\Gamma_J^{(\ell)}}{\mathrm{d}q^2} = 2\left(a_\ell^{(J)} + \frac{1}{3}c_\ell^{(J)}\right), \tag{4.58}$$

with coefficient functions $a_\ell^{(J)}(q^2)$, $b_\ell^{(J)}(q^2)$, $c_\ell^{(J)}(q^2)$ for the specific final-state lepton flavour $\ell \in \{e, \mu, \tau\}$. The momentum transfer q^2 is defined as the invariant mass of the leptons in the final state, and θ_ℓ is the helicity angle of the charged lepton with the ℓ-ν_ℓ momentum in the Λ_b rest frame. Our choice of normalisation reads

$$\Gamma_0^{(\ell)}(q^2) = \frac{G_F^2 V_{cb}^2 \sqrt{s_+ s_-}\, m_{\Lambda_c^*}}{96\pi^3 m_{\Lambda_b}^2}\left(1 - \frac{m_\ell^2}{q^2}\right)^2, \tag{4.59}$$

which should not be confused with the total decay width

$$\Gamma_J^{(\ell)} = 2\int_{m_\ell^2}^{\left(m_{\Lambda_b} - m_{\Lambda_c}\right)^2} \mathrm{d}q^2\, \Gamma_0^{(\ell)}(q^2)\left(a_\ell^{(J)}(q^2) + \frac{1}{3}c_\ell^{(J)}(q^2)\right). \tag{4.60}$$

From the double-differential rate, we can construct two angular observables in addition to the q^2-differential decay rate: first, the forward-backward asymmetry

$$\begin{aligned} A_{\mathrm{FB}}(q^2) &\equiv \frac{1}{\mathrm{d}\Gamma_J^{(\ell)}/\mathrm{d}q^2}\int_{-1}^{+1}\mathrm{d}\cos\theta_\ell\left[\omega_{A_{\mathrm{FB}}}(\cos\theta_\ell)\frac{\mathrm{d}^2\Gamma_J^{(\ell)}}{\mathrm{d}q^2\,\mathrm{d}\cos\theta_\ell}\right] \\ &= \frac{1}{\mathrm{d}\Gamma_J^{(\ell)}/\mathrm{d}q^2}\,\Gamma_0^{(\ell)}(q^2) b_\ell^{(J)}(q^2), \end{aligned} \tag{4.61}$$

which arises from the term linear in $\cos\theta_\ell$. And secondly, the flat term

$$\begin{aligned} F_{\mathrm{H}}(q^2) &\equiv \frac{1}{\mathrm{d}\Gamma_J^{(\ell)}/\mathrm{d}q^2}\int_{-1}^{+1}\mathrm{d}\cos\theta_\ell\left[\omega_{F_{\mathrm{H}}}(\cos\theta_\ell)\frac{\mathrm{d}^2\Gamma_J^{(\ell)}}{\mathrm{d}q^2, \mathrm{d}\cos\theta_\ell}\right] \\ \mathrm{d} &= \frac{1}{\mathrm{d}\Gamma_J^{(\ell)}/\mathrm{d}q^2}\,2\Gamma_0^{(\ell)}(q^2)\left[a_\ell^{(J)}(q^2) + c_\ell^{(J)}(q^2)\right], \end{aligned} \tag{4.62}$$

which arises from a linear combination of the coefficients $a_\ell^{(J)}$ and $c_\ell^{(J)}$ that differs from the one comprising the decay rate eq. (4.60). The weight functions for both observables read:

$$\omega_{A_{\mathrm{FB}}}(\cos\theta_\ell) = \frac{3}{2}P_1(\cos\theta_\ell), \quad \omega_{F_{\mathrm{H}}}(\cos\theta_\ell) = 5P_2(\cos\theta_\ell) + P_0(\cos\theta_\ell). \tag{4.63}$$

In the above, P_n denotes the nth Legendre polynomial.

Note that the definition of the flat term F_H in eq. (4.62) is similar to the one proposed for e.g. the decay $B \to K\ell^+\ell^-$; see Ref. [88]. However, contrary to what happens in the mesonic decays in the limit $m_\ell \to 0$, the baryonic F_H does not vanish in the SM. This is due to the fact that the $\Lambda_b \to \Lambda_c^*$ transitions are also mediated by perpendicular polarisation states of the virtual W, which is impossible in the mesonic transitions.

For the decay to the $J = 1/2$ final state the coefficients are

$$2a_\ell^{(1/2)} = \Big[|f_{1/2,t}|^2 \frac{m_\ell^2}{q^2}(m_{\Lambda_b} - m_{\Lambda_c^*})^2 + \Big(|f_{1/2,0}|^2 (m_{\Lambda_b} + m_{\Lambda_c^*})^2 + |f_{1/2,\perp}|^2 (m_\ell^2 + q^2) \Big) + |g_{1/2,t}|^2 \frac{m_\ell^2}{q^2}(m_{\Lambda_b} + m_{\Lambda_c^*})^2 + \Big(|g_{1/2,0}|^2 (m_{\Lambda_b} - m_{\Lambda_c^*})^2 + |g_{1/2,\perp}|^2 (m_\ell^2 + q^2) \Big) \Big] , \quad (4.64)$$

$$2b_\ell^{(1/2)} = 2 \left[(f_{1/2,t} f_{1/2,0}) + (g_{1/2,t} g_{1/2,0}) \right] \frac{m_\ell^2}{q^2}(m_{\Lambda_b}^2 - m_{\Lambda_c^*}^2) - 4\, q^2 \left(f_{1/2,\perp} g_{1/2,\perp} \right) , \quad (4.65)$$

$$2c_\ell^{(1/2)} = - \left(1 - \frac{m_\ell^2}{q^2} \right) \Big[|f_{1/2,0}|^2 (m_{\Lambda_b} + m_{\Lambda_c^*})^2 - q^2 (|f_{1/2,\perp}|^2) + |g_{1/2,0}|^2 (m_{\Lambda_b} - m_{\Lambda_c^*})^2 - q^2 (|g_{1/2,\perp}|^2) \Big] . \quad (4.66)$$

For the $J = 3/2$ we have

$$a_\ell^{(3/2)} = \Big[|F_{1/2,t}|^2 \frac{m_\ell^2}{q^2}(m_{\Lambda_b} - m_{\Lambda_c^*})^2 + \Big(|F_{1/2,0}|^2 (m_{\Lambda_b} + m_{\Lambda_c^*})^2 + (|F_{1/2,\perp}|^2 + 3|F_{3/2,\perp}|^2)(m_\ell^2 + q^2) \Big) + |G_{1/2,t}|^2 \frac{m_\ell^2}{q^2}(m_{\Lambda_b} + m_{\Lambda_c^*})^2 + \Big(|G_{1/2,0}|^2 (m_{\Lambda_b} - m_{\Lambda_c^*})^2 + (|G_{1/2,\perp}|^2 + 3|G_{3/2,\perp}|^2)(m_\ell^2 + q^2) \Big) \Big] , \quad (4.67)$$

$$b_\ell^{(3/2)} = 2 \left[(F_{1/2,t} F_{1/2,0}) + (G_{1/2,t} G_{1/2,0}) \right] \frac{m_\ell^2}{q^2}(m_{\Lambda_b}^2 - m_{\Lambda_c^*}^2) - 4\, q^2 \left[F_{1/2,\perp} G_{1/2,\perp} + 3 F_{3/2,\perp} G_{3/2,\perp} \right] , \quad (4.68)$$

$$c_\ell^{(3/2)} = - \left(1 - \frac{m_\ell^2}{q^2} \right) \Big[|F_{1/2,0}|^2 (m_{\Lambda_b} + m_{\Lambda_c^*})^2 - q^2 (|F_{1/2,\perp}|^2 + 3|F_{3/2,\perp}|^2) + |G_{1/2,0}|^2 (m_{\Lambda_b} - m_{\Lambda_c^*})^2 - q^2 (|G_{1/2,\perp}|^2 + 3|G_{3/2,\perp}|^2) \Big] . \quad (4.69)$$

Our results for the angular coefficients in eqs. (4.64)–(4.66) and eqs. (4.67)–(4.69) include the full m_ℓ dependence. We can compare them to the results for the fully differential decay rate in the limit $m_\ell \to 0$ as presented in [77]. We find complete agreement between our limit and the results of [77] when converting to the different basis of form factors as shown in eq. (B.16).

4.4 Prospects for the determination of the $\Lambda_b^0 \to \Lambda_c^{*+}$ form factors using LHCb data

Similarly to the mesonic $B \to D^{(*)}$ transitions, the most precise SM prediction for $R_{\Lambda_c^*}$ will arise from a combination of theoretical and experimental input. In this section, we investigate the sensitivity to the IW parameters from the decay $\Lambda_b^0 \to \Lambda_c^{*+} \mu^- \overline{\nu_\mu}$ in the present and future LHCb datasets when assuming a SM-like distribution[3]. To achieve this, we first produce a series of toy ensembles and subsequently fit the decay distribution to the simulated pseudo events. Estimates for the theoretical uncertainty on $R_{\Lambda_c^*}$ within the SM are then produced based on our fits.

4.4.1 Experimental situation

Two aspects of the experimental situation are needed to assess the experimental sensitivity. The reconstructed and selected signal yields of the decays $\Lambda_b^0 \to \Lambda_c(2625)^+ \mu^- \overline{\nu}_\mu$ and $\Lambda_b^0 \to$

[3] Note that a popular NP explanation for the present $R_{D^{(*)}}$ anomalies is a rescaling of the coupling associated with effective operator $\sim [\bar{c}\gamma^\mu(1-\gamma_5)b]\,[\overline{\nu}\gamma_\mu(1-\gamma_5)\ell]$. Such a rescaling would leave the angular distribution of $b \to c\ell\overline{\nu}$ decays used here invariant.

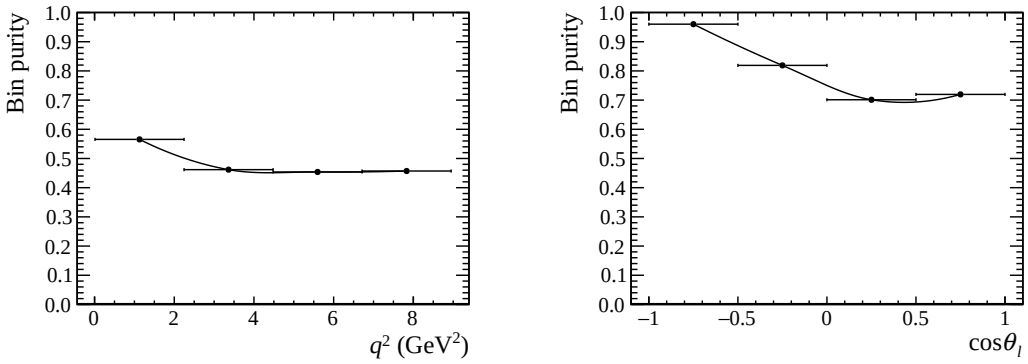

Figure 4.1: Purity as a function of q^2 and $\cos\theta_l$, defined as the fraction of candidates which belong in a particular kinematic bin. The purity for $\cos\theta_l$ is better than for q^2 due to the better resolution.

$\Lambda_c(2595)^+\mu^-\overline{\nu}_\mu$ and the resolution in q^2 and $\cos\theta_l$. We estimate the expected signal yields for a given luminosity by extrapolating from the numerical values quoted in Ref. [75], taking into the account the increased $b\overline{b}$ cross-section at 13 TeV [89]. We explore the sensitivity to parameters of interest as a function of the luminosity, starting from the current LHCb dataset, up to the luminosity expected at the end of the first LHCb upgrade [90].

A key factor which limits the precision of the experimental measurements is the resolution in q^2 and $\cos\theta_l$, induced by the unreconstructed neutrino. The resolution determines how finely the data is binned and introduces a statistical correlation between adjacent bins. At a hadron collider, the momentum of the neutrino can be deduced using the information of the Λ_b^0 flight direction and its mass, up to a two-fold ambiguity. The dominant effects on the resulting resolution originate from the measurement of the primary pp collision and Λ_b^0 vertices, as well the effect of choosing the wrong kinematic solution from the two available. In order to approximate the resolution of the LHCb detector, a sample of $\Lambda_b^0 \to \Lambda_c^{*+}\mu^-\overline{\nu}_\mu$ candidates are simulated using Pythia at 13 TeV [91, 92], with a required pseudo-rapidity of $2 < \eta < 5$, approximately corresponding to the LHCb acceptance. The vertices of the pp collision and Λ_b^0 decay are varied according to a resolution inspired from Ref. [93] and used in Ref. [94]. The resolutions of ± 20 μm in the x and y directions and ± 200 μm in the z direction (defined as the direction aligned with the LHC beam line) is used for the Λ_b^0 vertex. For the pp collision vertex, a resolution of ± 13 μm in x and y and ± 70 μm in z is assumed. With these new vertex positions the two kinematic solutions for the neutrino are then calculated, and one is chosen randomly.

The resulting purities with 4 q^2 bins and 4 $\cos\theta_l$ bins are shown in figure 4.1, where the purity is defined as the fraction of the number of candidates reconstructed correctly for a given q^2 bin. There is a better purity at negative $\cos\theta_l$, which is due to the interplay between q^2 and $\cos\theta_l$: at high q^2 the $\cos\theta_l$ resolution is poor, and in this region there is a positive $\cos\theta_l$ distribution. The resolution limits the number of bins and induces a statistical correlation between neighbouring bins, which is calculated based on the number of candidates which migrate between those two bins. In the 4×4 bins configuration, this correlation is around 10-30% in both q^2 and $\cos\theta_l$.

In addition to the above, precision measurements of b-hadrons branching fractions at the LHC require a well-measured normalisation channel to cancel the uncertainties related to the production. In principle one could normalise to a well measured B meson decay and take the ratio of production fractions. However, this method would inherit substantial systematic uncertainties, and therefore for this study the decay rate is normalised and only the shape information is used to determine the parameters of interest. This means that the absolute normalisation of the form factors cannot be constrained experimentally. As a consequence we do not report any sensitivity for the form factor parameter $\zeta(q^2_{\rm max})$, which corresponds to this absolute normalisation.

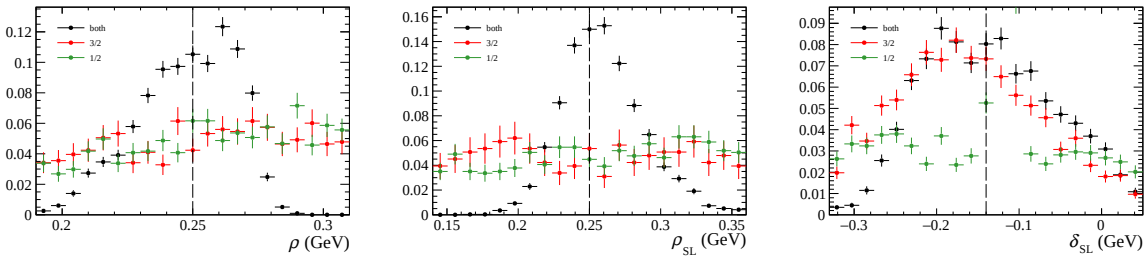

Figure 4.2: Distribution of the IW parameters as fitted from an ensemble of pseudo-experiments. The distributions are shown for the cases when one of the two Λ_c^{*+} states is fitted, as well as the combination of both.

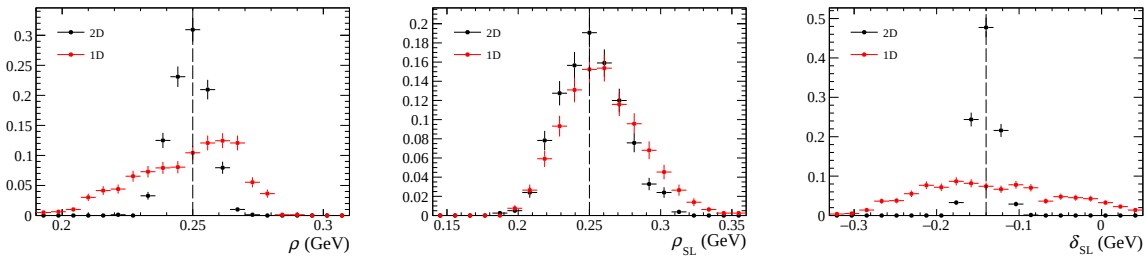

Figure 4.3: Distribution of the IW parameters as fitted from an ensemble of pseudo-experiments. The sensitivity is shown for fits to both the one-dimensional q^2 and two-dimensional $q^2 \times \cos\theta_l$ distributions.

4.4.2 Fits to the differential decay rate

We generate ensembles of pseudo-experiments according to the conditions outlined above, using both parameterisations of the IWFs given in section 4.3.1, and using the common benchmark points defined in section 4.3.2. We start by fitting the one-dimensional q^2 distribution of the $\Lambda_b^0 \to \Lambda_c(2625)^+\mu^-\overline{\nu}_\mu$ decay, $\Lambda_b^0 \to \Lambda_c(2595)^+\mu^-\overline{\nu}_\mu$ decay or a combination thereof. The resulting one-dimensional distributions of the form factor parameters are shown in figure 4.2. , with the two-dimensional distributions shown in appendix B.7. When fitting a single decay mode, we find that there is a degeneracy between the two slope parameters ρ and ρ_{SL} due to a strong correlation that is positive for the $\Lambda_b^0 \to \Lambda_c(2625)^+\mu^-\overline{\nu}_\mu$ decay and negative for the $\Lambda_b^0 \to \Lambda_c(2595)^+\mu^-\overline{\nu}_\mu$ decay. Only by combining both states in a single fit can the interference between the positive and negative correlation break this degeneracy.

In order to maximise the sensitivity to all three form factor parameters and make full use of the LHCb dataset, we investigate fits to the two-dimensional q^2 and $\cos\theta_l$. The resulting one-dimensional and two-dimensional distributions of the parameters are shown in appendix B.7. A comparison between the distributions of the IW parameters for the one- and two-dimensional fits are shown in figure 4.3. The results show that a two-dimensional fit improves the precision on all three parameters with reduced correlations between them. This strongly motivates a full two-dimensional fit to both Λ_c^{*+} states simultaneously for any future LHCb analysis to give the best possible precision on the form factor parameters.

4.4.3 Projected precision on the $R_{\Lambda_c^*}$ predictions

Finally, by using the expected precision on the form factors, one can calculate the precision on the ratio $R_{\Lambda_c^*}$, which denotes both the $R_{\Lambda_c(2595)^+}$ and $R_{\Lambda_c(2625)^+}$ ratios as they are derived from the same parameters and therefore have similar uncertainties. The precision as a function of the luminosity collected by the LHCb experiment is shown in figure 4.4. Assuming the

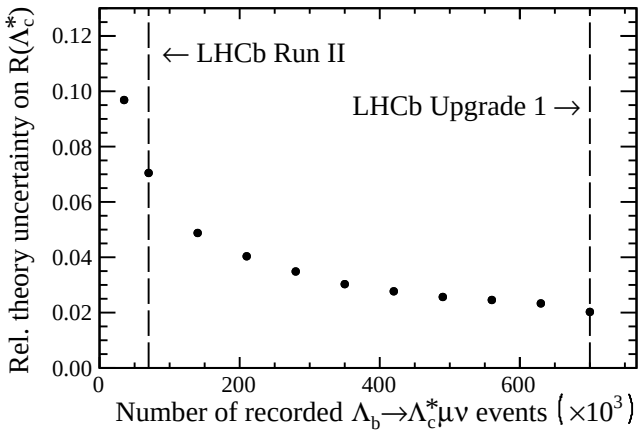

Figure 4.4: Expected theoretical precision of the $R_{\Lambda_c(2625)^+}$ ratio as a function of the data collected by the LHCb experiment.

exponential model[4] describes the data well, a ∼7% precision can be expected from run I+II data, and a 2% precision can be expected after upgrade 1 of the LHCb detector. For the linear model, we find in general smaller uncertainties than for the exponential model. Our estimates for the uncertainties ignore power suppressed terms in the HQET expansion and experimental systematic uncertainties, which could become relevant at that level of precision.

Similar to what has been done in the literature for R_{D^*}, we can estimate the impact of the dominant unknown $1/m_c^2$ corrections to the HQET relations on the theory predictions for the $R_{\Lambda_c^*}$. Following the discussion [30], we wish to separate the term involving the timelike form factors from the term that can be taken directly from data on the semimuonic decay mode. We therefore decompose

$$\frac{\mathrm{d}\Gamma_J^{(\tau)}}{\mathrm{d}q^2} = \frac{\mathrm{d}\Gamma_J^{(\tau,1)}}{\mathrm{d}q^2} + \frac{\mathrm{d}\Gamma_J^{(\tau,2)}}{\mathrm{d}q^2} \tag{4.70}$$

in two contributions

$$\frac{\mathrm{d}\Gamma_J^{(\tau,1)}}{\mathrm{d}q^2} = \frac{1}{3}\left(1-\frac{m_\tau^2}{q^2}\right)^2\left(2+\frac{m_\tau^2}{q^2}\right)\left.\frac{\mathrm{d}\Gamma^{(\ell)}}{q^2}\right|_{m_\ell\to 0}, \tag{4.71}$$

$$\frac{\mathrm{d}\Gamma_J^{(\tau,2)}}{\mathrm{d}q^2} = \begin{cases} \Gamma_0^{(\tau)}\left[|f_{1/2,t}|^2\,\frac{m_\tau^2}{q^2}\left(m_{\Lambda_b}-m_{\Lambda_c^*}\right)^2 + |g_{1/2,t}|^2\,\frac{m_\tau^2}{q^2}\left(m_{\Lambda_b}+m_{\Lambda_c^*}\right)^2\right] & J=1/2 \\ 2\,\Gamma_0^{(\tau)}\left[|F_{1/2,t}|^2\,\frac{m_\tau^2}{q^2}\left(m_{\Lambda_b}-m_{\Lambda_c^*}\right)^2 + |G_{1/2,t}|^2\,\frac{m_\tau^2}{q^2}\left(m_{\Lambda_b}+m_{\Lambda_c^*}\right)^2\right] & J=3/2 \end{cases}. \tag{4.72}$$

Note here that the $(\tau,1)$ terms are taken directly from data, while the $(\tau,2)$ terms rely on the HQET relations between the form factors for theoretical predictions. Correspondingly, we then decompose $R_{\Lambda_c^*} = R_{\Lambda_c^*,1} + R_{\Lambda_c^*,2}$ with

$$R_{\Lambda_c^*(J),i} = \frac{\int_{m_\tau^2}^{\left(m_{\Lambda_b}-m_{\Lambda_c^*}\right)^2}\mathrm{d}q^2\,\frac{\mathrm{d}\Gamma_J^{(\tau,i)}}{\mathrm{d}q^2}}{\int_{m_\mu^2}^{\left(m_{\Lambda_b}-m_{\Lambda_c^*}\right)^2}\mathrm{d}q^2\,\frac{\mathrm{d}\Gamma_J^{(\mu)}}{\mathrm{d}q^2}}. \tag{4.73}$$

[4]With exponential model we indicate the exponential parametrisation described in section 4.3.1 together with the benchmark points obtained in section 4.3.2.

We find that the relative contribution by the $(\tau, 1)$ term is both dominant and stable under variation of the slope parameters across our four benchmark points in the exponential model. We find that

$$R_{\Lambda_c(2595),1} \simeq 0.76 \cdot R_{\Lambda_c(2595)^+}\,, \qquad \text{and} \qquad R_{\Lambda_c(2625),1} \simeq 0.77 \cdot R_{\Lambda_c(2625)^+}\,. \tag{4.74}$$

For a conservative estimate, we can assume that the $1/m_c^2$ contributions yield 30% corrections to the HQET relations as estimated in [30]. Consequently, we would face an inherent theory uncertainty of $\sim 8\%$ for $R_{\Lambda_c(2595)}$ and up to $\sim 7\%$ for $R_{\Lambda_c(2625)}$. Given that projected statistical uncertainty in figure 4.4 are of similar size already with the full run II dataset, we come to the conclusion that our theoretical uncertainty estimates strongly motivate dedicated lattice QCD studies of the $\Lambda_b \to \Lambda_c^*$ form factors.

4.5 Conclusion

Motivated by the recent deviations in LFU in semileptonic $b \to s$ and $b \to c$ decays, we have provided the theoretical ingredients needed to constrain the theoretical uncertainty of the lepton universality ratios $R_{\Lambda_c(2595)^+}$ and $R_{\Lambda_c(2625)^+}$, collectively denoted as $R_{\Lambda_c^*}$.

To this end, we have improved and extended upon the work in [77]. We provide a new definition of the hadronic form factors, convenient for the decay observables, and work out formulae for $\mathcal{O}(\alpha_s)$ corrections to HQE. We then propose a parameterisation of the Isgur-Wise function informed from previous studies on the ground state $\Lambda_b^0 \to \Lambda_c^+$ transition [81] and perform a zero recoil sum rule to provide a benchmark point for these parameters to be used in a study of the sensitivity to these parameters for a future analysis of LHCb data. Last but not least, we provide the finite lepton mass terms for the two double differential decay distributions.

We investigated the benefits of fitting the two-dimensional $q^2 - \cos\theta_l$ distribution over fitting only the q^2 distribution, for either of the Λ_c^{*+} hadronic states and their combination. We find that fitting the angular information in addition to the q^2 spectrum is crucial to obtain sensitivity to the sub-leading Igsur-Wise function. In addition, we stress that a combined analysis of both Λ_c^{*+} states is necessary to break the degeneracy between the slopes of the leading and sub-leading Igsur-Wise functions. Finally, we show that by measuring the differential decay rate of $\Lambda_b^0 \to \Lambda_c^{*+}\mu^-\nu_\mu$, small statistical uncertainty for a data driven determination of the $R_{\Lambda_c^*}$ ratios can be achieved. Our results therefore motivate an LHCb analysis of the $\Lambda_b^0 \to \Lambda_c^{*+}\mu^-\nu_\mu$ double-differential decay rate and the subsequent experimental measurement of the $R_{\Lambda_c^*}$ ratios. On the other hand, we also demonstrate that the unknown $1/m^2$ terms in the form factors' expansion produce at present an irreducible uncertainty that is of the same order as the statistical uncertainty. This motivates further theoretical studies of the form factors, e.g. from lattice QCD.

Part III

Precise predictions within the Standard Model: neutral current processes

Chapter 5

On the Standard Model predictions for R_K and R_{K^*}

5.1 Introduction

The Lepton Flavour Universality (LFU) ratios

$$R_M[q^2_{\rm min},\ q^2_{\rm max}] = \frac{\displaystyle\int_{q^2_{\rm min}}^{q^2_{\rm max}} {\rm d}q^2 \frac{{\rm d}\Gamma(B\to M\mu^+\mu^-)}{{\rm d}q^2}}{\displaystyle\int_{q^2_{\rm min}}^{q^2_{\rm max}} {\rm d}q^2 \frac{{\rm d}\Gamma(B\to Me^+e^-)}{{\rm d}q^2}}\ , \tag{5.1}$$

where $q^2 = m^2_{\ell\ell}$, are very clean probes of physics beyond the Standard Model (SM): they have small theoretical uncertainties and are sensitive to possible new interactions that couple in a non-universal way to electrons and muons [95]. As already mentioned in section 2.4, a strong interest in the observable $R_{K^{(*)}}$ has recently been raised, given the $2.1-2.6\sigma$ deviations observed in [42, 43], that differs from the naïve expectation

$$R^{\rm (SM)}_{K^{(*)}} = 1 \tag{5.2}$$

by about 2.6σ. The interest is further raised by the combination of this anomaly with other $b\to s\ell^+\ell^-$ observables [49, 96], and by the independent hints of violations of LFU observed $B\to D^{(*)}\tau\nu_\ell$ decays [33, 36, 97].

While perturbative and non-perturbative QCD contributions cancel in $R_{K^{(*)}}$ (beside trivial kinematical factors), this is not necessarily the case for QED corrections. In particular, QED collinear singularities induce corrections of order $(\alpha/\pi)\log^2(m_B/m_\ell)$ to $b\to s\ell^+\ell^-$ transtions [17, 98, 99] that could easily imply 10% effects in $R_{K^{(*)}}$. The purpose of this work is to estimate these corrections and to precisely quantify up to which level a deviation of R_K or R_{K^*} from 1 can be considered a clean signal of physics beyond the SM.

5.2 QED corrections in R_M

A complete evaluation of QED corrections to $B\to M\ell^+\ell^-$ decay amplitudes is a non-trivial task, due to the interplay of perturbative and non-perturbative dynamics (see e.g. [100]). However, the problem is drastically simplified if we are only interested in the LFU ratios R_M, especially in the low dilepton invariant mass region, and if interested in possible deviations from eq. (5.2) exceeding 1%. In this case the problem is reduced to evaluating $\log(m_\ell)$ enhanced terms, whose

origin can be unambiguously traced to soft and collinear photon emission. The latter represents a universal correction factor [101, 102] that can be implemented, by means of appropriate convolution functions,[1] irrespective of the specific short-distance structure of the amplitude.

5.2.1 Universal radiation function

Following the above observation, the treatment of soft and collinear photon emission in $B \to M\ell^+\ell^-$ closely resemble that applied to $h \to 2e2\mu$ decays in Ref. [104]. The key observable we are interested in is the differential lepton-pair invariant-mass distribution

$$\mathcal{F}_M^\ell(q^2) = \frac{\mathrm{d}\Gamma(B \to M\ell^+\ell^-)}{\mathrm{d}q^2} \ . \tag{5.3}$$

The complete structure of infrared (IR) divergences in the decay is channel dependent [100]; however, the $\log(m_\ell)$ enhanced terms can be factorized and are independent from the spin of the meson M.

The leading QED corrections can be unambiguously identified working in the limit of massless leptons, retaining only the mass terms regulating collinear singularities. In this limit we define the radiator $\omega(x, x_\ell)$, that represents the probability density function that a dilepton system retains a fraction $\sqrt{x}$ of its original invariant mass after bremsstrahlung. Namely we define $x = q^2/q_0^2$, where q_0^2 is the initial dilepton invariant mass squared (pre bremsstrahlung), and we introduce the variable $x_\ell = 2m_\ell^2/q_0^2$ that regulates collinear singularities. In order to match the IR-safe observable directly probed in experiments, the integration range of x is determined by the requirement that the reconstructed B-meson mass ($m_B^{\rm rec}$), from the measurement of leptons and hadron momenta, is above a minimum value.

In order to regulate IR divergences, we introduce an (unphysical) IR-regulator x_* ($x_* \ll 1$), defined as the minimal detectable value of of $1-x$. The full radiator $\omega(x, x_\ell)$ is then decomposed as

$$\omega(x, x_\ell) = \omega_1(x, x_\ell)\theta(1 - x - x_*) + \omega_2(x, x_\ell, x_*)\delta(1 - x) \ , \tag{5.4}$$

where the explicit form of $\omega_{1,2}$ in the limit $(1 - x) \ll 1$ and $x_\ell, x_* \ll 1$ is

$$\begin{aligned} \omega_1(x, x_\ell) &= \frac{\alpha}{\pi}\frac{1}{1-x}\left[-2 + (1+x^2)\log\left(\frac{2x}{x_\ell}\right)\right] \ , \\ \omega_2(x, x_\ell, x_*) &= 1 - \frac{\alpha}{\pi}\left\{\frac{5}{4} - \frac{\pi^2}{3} + 2\log(x_*) + \left[\frac{3}{2} + 2\log(x_*)\right]\log\left(\frac{x_\ell}{2}\right)\right\} \ . \end{aligned} \tag{5.5}$$

The first term, ω_1, describes the real emission of a photon such that the lepton pair retains a fraction $\sqrt{x}$ of its invariant mass; the θ-function implements the corresponding IR regulator. The second term, ω_2, describes the events in which the soft radiation is below the IR regulator, as well as the effect of virtual corrections.

We have determined the structure of ω_1 by means of an explicit $O(\alpha)$ calculation of the real emission, while ω_2 has been determined by the condition

$$\omega_2(x, x_\ell, x_*) = 1 - \int_{2x_\ell}^{1-x^*} \mathrm{d}x \ \omega_1(x, x_\ell) \tag{5.6}$$

that, by construction, ensure the independence of the full radiator from the IR regulator and the normalization condition

$$\int_{2x_\ell}^{1} \mathrm{d}x \ \omega(x, x_\ell) = 1 \ . \tag{5.7}$$

[1] For a discussion about the implementation of universal QED corrections in a general EFT context see also Ref. [103].

The latter is valid up to finite (non log-enhanced) corrections of $O(\alpha/\pi)$ that define the accuracy of our approximation.

We can thus write the double differential distribution in terms of the invariant mass of the dilepton system before bremsstrahlung and $x = q^2/q_0^2$ as

$$\frac{\mathrm{d}^2\Gamma}{\mathrm{d}q_0^2\,\mathrm{d}x} = \mathcal{F}_M^{(0)}(q_0^2)\omega(x, x_\ell, x_*) \ , \tag{5.8}$$

where $\mathcal{F}_M^{(0)}(q_0^2)$ denotes the non-radiative spectrum. Starting from eq. (5.8) we can extract the double differential spectrum after radiative corrections. To this purpose, we first trade x for q^2, we then integrate over all the possible values of q_0^2 determined by the cut on $m_B^{\rm rec}$, namely[2]

$$q_0^2 \leq q_{0,\rm max}^2(q^2,\delta) = \frac{q^2}{\delta^2}\left[1 + (1-\delta^2)\frac{m_M^2}{m_B^2\delta^2 - q^2}\right] \ , \tag{5.9}$$

where $\delta = m_B^{\rm rec}/m_B < 1$. Proceeding this way we finally obtain:

$$\mathcal{F}_M^{\ell}(q^2) = \int_{q^2}^{q_{0,\rm max}^2} \frac{\mathrm{d}q_0^2}{q_0^2}\mathcal{F}_M^{(0)}(q_0^2)\ \omega\left(\frac{q^2}{q_0^2}, \frac{2m_\ell^2}{q_0^2}\right), \tag{5.10}$$

We stress that the result in eq. (5.10) includes both real and virtual QED corrections. The latter have been indirectly determined by the normalization condition for $\omega(x, x_\ell)$, that is the same condition applied in showering algorithms [105], and that follows from the safe IR behavior of the photon-inclusive dilepton spectrum.

Before concluding this section, we summarize below the size of neglected contributions and the accuracy of this calculation.

- As anticipated, we do not control $O(\alpha/\pi)$ virtual corrections that are regular in the limit $m_\ell \to 0$. The latter are expected to be safely below the 1% level.
- The calculation of the real emission has been done in the limit $m_\ell^2 \ll q^2$ that is certainly an excellent approximation in the electron case, while it is less good in the muon case; however, also in this case the neglected contributions are $O(\alpha/\pi)$ non log-enhanced terms.
- In the case of a charged meson in the final state, we should consider also the radiation from the meson leg. We have checked by means of an explicit calculation at $O(\alpha)$ (employing a generic hadronic matrix element) that the latter do not interfere with the radiation of the lepton legs at the leading-log level once we integrate over the leptonic angles.[3] The radiation of the meson leg can thus be considered separately by means of an independent radiation function. A quantification of its effect in the $B^+ \to K^+\ell^+\ell^-$ case is discussed in section 5.3.
- Independently of the charge of the meson, an additional contribution to the real radiation is due to structure-dependent terms (i.e. separately gauge-invariant amplitudes that vanish in the $E_\gamma \to 0$ limit). By construction, these amplitudes are free from soft singularities but could have collinear singularities. However, these vanishes after a symmetry integration over the leptonic angles for the same argument discussed above.
- In order to quantify the impact of radiative corrections we need a theoretical input for the non-radiative spectrum $\mathcal{F}_M^{(0)}(q_0^2)$, whose explicit expression for $B \to K$ and $B \to$

[2] In principle, from a pure kinematical point of view, the cut on $m_B^{\rm rec}$ allow q_0^2 values even exceeding the bound in eq. (5.9); however, this occurs only for non-soft and non-collinear emissions that are beyond our approximations.

[3] This happens because the leptonic current carries an overall neutral electric charge.

K^* transitions is discussed in section 5.2.2. From eq. (5.10) it is clear that, as long as $\mathcal{F}_M^\ell(q^2)/\mathcal{F}_M^{(0)}(q^2)$ is a smooth function of q^2, the relative impact of radiative corrections in R_M is insensitive to the dynamics responsible for the $B \to M\ell^+\ell^-$ decay.

5.2.2 Parameterization of the non-radiative spectrum

The choice of the radiative spectrum for the $B \to K^+\ell^+\ell^-$ decay is quite simple. In full generality we can write

$$\mathcal{F}_K^{(0)}(q^2) \propto \lambda^{3/2}(q^2) \left| f_+(q^2) \right|^2 \left[|a_9(q^2)|^2 + |a_{10}|^2 \right] \,, \tag{5.11}$$

where $\lambda(s) = (m_B^4 + m_K^4 + s^2 - 2m_K^2 m_B^2 - 2sm_B^2 - 2sm_K^2)/m_B^4$, $f_+(q^2)$ is the $B \to K$ vector form factor

$$\langle K(k)| \bar{s}\gamma_\mu b |B(p)\rangle = f_+(q^2)(p+k)^\mu + O(q^\mu) \tag{5.12}$$

and $a_9(q_0^2)$ and a_{10} denote the effective Wilson coefficients of the vector and the axial-vector components of the leptonic current [106]. For our numerical analysis we use the parameterization of the form factor and the numerical values of the Wilson coefficients from Ref. [106].

In order to provide an effective description of the non-perturbative distortion of the spectrum induced by the charmonium resonances, we modify the vector effective Wilson coefficient as follows

$$a_9(q^2) = a_9^{\text{pert}}(q^2) + \kappa_\psi \frac{q^2}{q^2 - m_\psi^2 + i m_\psi \, \Gamma_\psi} \tag{5.13}$$

where $\{m_\psi, \Gamma_\psi\}$ are the experimental mass and width of the $J/\psi(1S)$ state, and the value of the (real) effective coupling κ_ψ has been fixed in order to reproduce $\mathcal{B}(B \to K\psi)$ in the narrow width approximation. This description is certainly approximate (see e.g. the discussion in Ref. [107, 108]), but it provides a good estimate of the region where the $B \to K^+\ell^+\ell^-$ spectrum starts to vary rapidly with q^2, that is relevant in order to define the region of validity of our approach.

As far as the $B \to K^*\ell^+\ell^-$ is concerned, we proceed introducing the standard set of vector, axial, and tensor form factors

$$\langle K^*| \bar{s}\gamma_\mu b |B\rangle = \frac{2V(q^2)}{m_B + m_{K^*}} \varepsilon_{\mu\rho\sigma\tau} \epsilon^{*\rho} p^\sigma k^\tau, \tag{5.14}$$

$$\begin{aligned} \langle K^*| \bar{s}\gamma_\mu\gamma_5 b |B\rangle = i\epsilon^{*\rho} \Bigg[& 2m_V A_0(q^2) \frac{q_\mu q_\rho}{q^2} + (m_B + m_{K^*}) A_1(q^2) \left(g_{\mu\rho} - \frac{q_\mu q_\rho}{q^2} \right) \\ & - A_2(q^2) \frac{q_\rho}{m_B + m_{K^*}} \left((p+k)_\mu - \frac{\Delta m^2}{q^2} q_\mu \right) \Bigg], \end{aligned} \tag{5.15}$$

$$\langle K^*| \bar{s} i\sigma_{\mu\nu} q^\nu b |B)\rangle = -2T_1(q^2) \varepsilon_{\mu\rho\sigma\tau} \epsilon^{*\rho} p^\sigma k^\tau, \tag{5.16}$$

$$\begin{aligned} \langle K^*| \bar{s} i\sigma_{\mu\nu}\gamma_5 q^\nu b |B\rangle = & \, iT_2(q^2) \left[\epsilon_\mu^* \Delta m^2 - (\epsilon^* \cdot q)(p+k)_\mu \right] \\ & + iT_3(q^2) \left(\epsilon^* \cdot q \right) \left(q_\mu - \frac{q^2}{\Delta m^2} (p+k)_\mu \right), \end{aligned} \tag{5.17}$$

where $\Delta m^2 = m_B^2 - m_{K^*}^2$, whose numerical values are taken from Ref. [64] (and based on the original works in Ref. [109, 110]). With these we proceed evaluating the differential rate as, for instance, in Ref. [95].

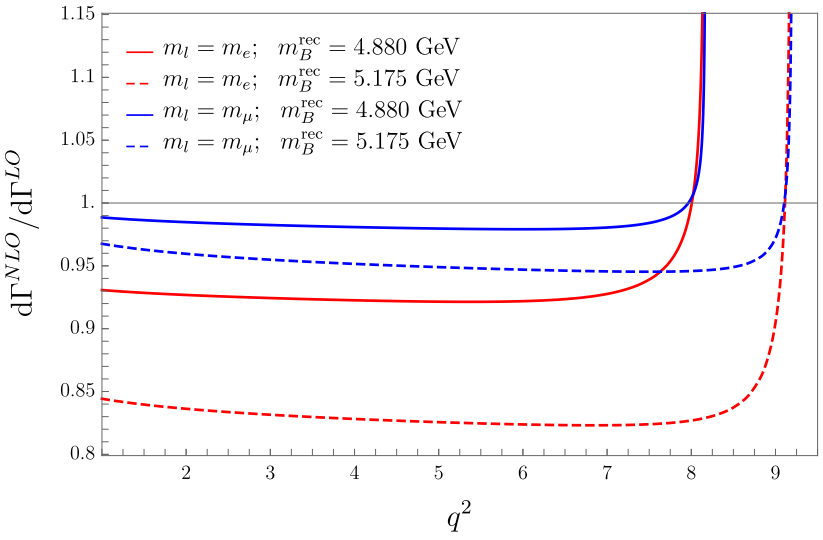

Figure 5.1: Relative impact of radiative correction in $B \to K^+\ell^+\ell^-$ decays for $q^2 \in [1, 9.5]$ GeV^2, with different cuts on the reconstructed mass and different lepton masses.

$B \to K\ell^+\ell^-$	$\ell = e$	$\ell = \mu$
$m_B^{\rm rec} = 4.880$ GeV	-7.6%	-1.8%
$m_B^{\rm rec} = 5.175$ GeV	-16.9%	-4.6%
$B \to K^*\ell^+\ell^-$	$\ell = e$	$\ell = \mu$
$m_B^{\rm rec} = 4.880$ GeV	-7.3%	-1.7%
$m_B^{\rm rec} = 5.175$ GeV	-16.7%	-4.5%

Table 5.1: Relative impact of radiative corrections for $q^2 \in [1, 6]$ GeV^2, with different cuts on the reconstructed mass and different lepton masses.

5.3 Numerical results

The relative impact of radiative corrections in $B \to K^+\ell^+\ell^-$, namely a plot of the ratio

$$\mathcal{R}_K^\ell(q^2) = \frac{\mathcal{F}_K^\ell(q^2)}{\mathcal{F}_K^{(0)}(q^2)}, \tag{5.18}$$

is shown in figure 5.1 in the region $q^2 \in [1, 9]$ GeV^2. The different colors correspond to different lepton masses (red for the electron and blue for the muon). Dashed and full lines correspond to different choices of the minimal cut on the reconstructed B-meson mass from the momenta of charged particles. We have choosen for the latter the two values used in Ref. [42] for the analysis of the electron modes ($m_B^{\rm rec} \geq 4.880$ GeV, full lines) or the muon modes ($m_B^{\rm rec} \geq 5.175$ GeV, dashed lines).

The first point to be noted in Fig. 5.1 is that $\mathcal{R}_K^\ell(q^2)$ is a smooth function for sufficiently low values of q^2, while a sudden rise appear close to the resonance region. The latter is a manifestation of the radiative return from the J/Ψ peak. The position where the J/Ψ contamination appears depends only from the cut imposed on $m_B^{\rm rec}$. Even for the looser cut applied in the electron case the region $q^2 \in [1, 6]$ GeV^2 is free from the J/Ψ contamination and can be estimated with good theoretical accuracy (see Fig. 5.2). To better quantify this statement we have explicitly checked that varying the phase of the effective coupling κ_ψ in eq. (5.13) leads to per-mill modifications to $\mathcal{R}_K^\ell(q^2)$ for $q^2 \leq 6$ GeV^2. We also have explicitly checked that the cut on $m_B^{\rm rec}$ eliminates

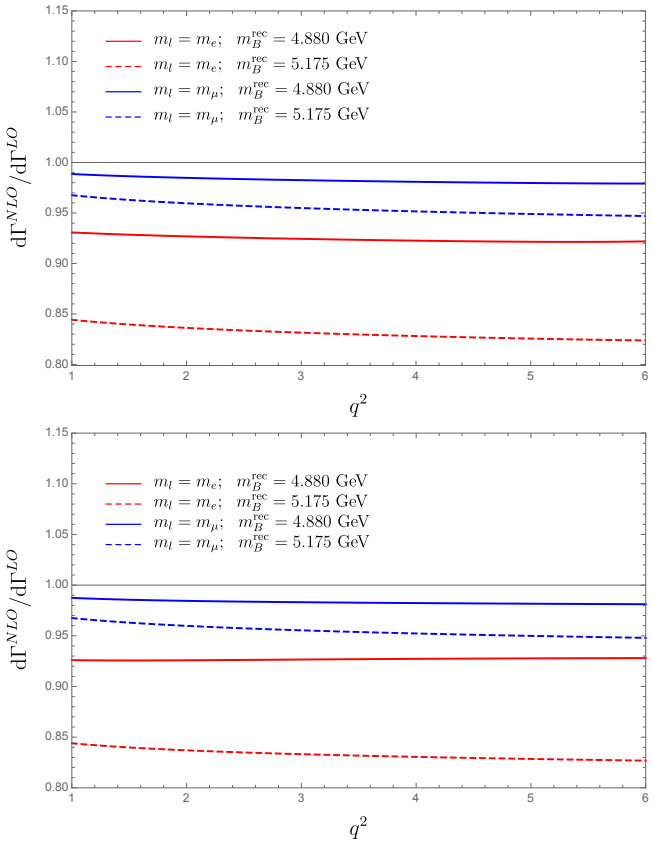

Figure 5.2: Relative impact of radiative correction in $B \to K\ell^+\ell^-$ (up) and in $B \to K^*\ell^+\ell^-$ (down) for $q^2 \in [1, 6]$ GeV^2, with different cuts on the reconstructed mass and different lepton masses. .

photons from the J/Ψ peak also when considering the full kinematics of the event, i.e. beyond the soft and collinear approximation on which we derived eq. (5.9).

The second point to be noted is that in the regular region of the spectrum radiative corrections reach (or even exceed) the 10% level for the electrons (as naively expected); however, the net effect in R_K is significantly smaller. Indeed the magnitude of the corrections is larger for electron vs. muons, but it increases for $m_B^{\rm rec} \to m_B$. This imply that the specific choice of $m_B^{\rm rec}$ cuts applied by the LHCb collaboration, i.e. a loose cut for the electrons and a tighter cut for the muons, give rise to a natural compensation of the QED corrections to R_K.

The integrated corrections that quantity the modifications to R_K are reported in table 5.1. Given the choice of $m_B^{\rm rec}$ applied in Ref. [42], we estimate that radiative corrections induce a *positive* shift of the central value of R_K of a about $\Delta R_K = +3\%$. This effect is taken into account by the LHCb collaboration, who estimated the impact of radiative corrections with PHOTOS [105], and properly corrected for in the result reported. We have explicitly checked that our estimate of ΔR_K is in agreement with that obtained with PHOTOS up to differences within $\pm 1\%$.[4]

In order to check the smallness of the non-log(m_ℓ) enhanced terms, in figure 5.2 we report the effect of the radiation from the meson leg, that is IR divergent but has no collinear singularities. We evaluated these terms developing the corresponding radiator function (see Ref. [103]), whose implementation depend only on $m_B^{\rm rec}$. As can be seen from figure 5.2, the results are well below the 1% level.

[4]We thank Rafael Silva Coutinho for a detailed comparison about the radiative corrections implemented in the LHCb analysis of R_K.

$m_B^{\rm rec} = 4.880$ GeV	-0.02%
$m_B^{\rm rec} = 5.175$ GeV	-0.18%

Table 5.2: Relative contribution of radiative corrections due emission from the meson leg, in the $B^+ \to K^+\ell^+\ell^-$ case, for $q^2 \in [1,6]\text{GeV}^2$.

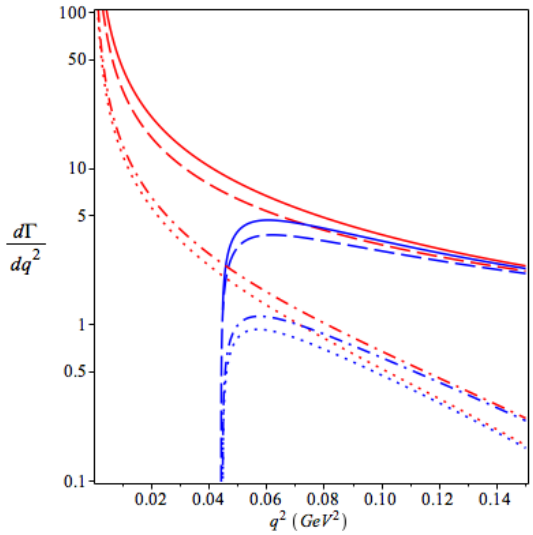

Figure 5.3: Contributions to $d\Gamma[B \to K^*\ell^+\ell^-(\gamma)]/dq^2$ (in arbitrary units) in the low q^2 region for $\ell = e$ (red) and $\ell = \mu$ (blue), before any cut in $m_B^{\rm rec}$. The full line is the photon-inclusive rate; the dashed line is the non-radiative FCNC rate; dotted and dash-dotted lines denote the contribution to the photon inclusive rate from $B \to K^* + \eta(\to \ell^+\ell^-\gamma)$ with (dash-dotted) and without (dots) interference with the soft radiation from the FCNC rate.

The impact of radiative corrections in the $B \to K^*\ell^+\ell^-$ decays is shown in figure 5.2 and summarized by the integrated values reported in Table 1. The situation is very similar to the $B^+ \to K^+\ell^+\ell^-$: employing the same $m_B^{\rm rec}$ cuts for electron and muon modes as in Ref. [42], we find that the net impact of radiative corrections is $\Delta R_{K^*} = +2.8\%$. Also in this case this effect is well described by PHOTOS.

5.4 SM predictions for R_{K^*} in the low q^2 region.

The prediction in the $0.045\ \text{GeV}^2 \le q^2 \le 1.1\ \text{GeV}^2$ bin is more delicate. The kinematical threshold of the muon mode, and the rapid (and flavour non-universal) variation of $d\Gamma/dq^2$ close to this threshold, imply larger theoretical uncertainties. First of all, even in absence of QED corrections, form-factor uncertainties do not cancel completely in this region. We estimate the latter to induce a ± 0.02 error (in agreement with Ref. [41]).

As far as QED corrections are concerned, a specific aspect of the near-threshold region is the sensitivity to light-hadron effects. Non-negligible extra contributions to the photon-inclusive rate are obtained by direct-emission amplitudes of the type $B \to K^*P^0 \to K^*\ell^+\ell^-\gamma$, where P^0 denotes an almost on-shell η or π^0 state. The η-mediated contribution turns out to be particularly sizeable given $\mathcal{B}(B \to K^*\eta) \approx 1.6 \times 10^{-5}$ and $\mathcal{B}(\eta \to e^+e^-\gamma) \approx 0.7\%$.[5] An illustration of the impact of the latter is shown in figure 5.3.

Some comments on the light-hadron contribution are in order:

[5] In absence of a lower cut on q^2 and $m_B^{\rm rec}$, the rate for $B \to K^*\eta \to K^*e^+e^-\gamma$ is about 30% of $\Gamma(B \to K^*e^+e^-;\ q^2 < 0.1)$.

i. This contribution is an irreducible part of the photon-inclusive rate (which is the only well-defined physical observable) and, as such, it must be included in the theoretical prediction of R_{K^*} (in the relevant kinematical region).

ii. The leading effect is necessarily a *decrease* of R_{K^*} compared to the non-radiative case (the radiative tails of electron and muon modes are both enhanced, but the effect is smaller in the muon case given the proximity to the phase-space border). The decrease of R_{K^*} is further enhanced by the looser $m_B^{\rm rec}$ cut on electron vs. muon modes.

iii. There is a non-negligible interference between the meson-mediated amplitude and the soft-photon emission of the genuine FCNC amplitude. This interference induces a (theoretical) uncertainty in estimating this effect given the unknown relative phases of the amplitudes. An additional source of uncertainty is provided by any other contribution of the type $B \to K^* \gamma + \gamma^* (\to e^+ e^-)$, for which we do not have a reliable normalization.

iv. Above the threshold region also the meson-mediated amplitude becomes lepton universal (figure 5.3), and the uncertainty of this contribution becomes negligible for $q^2 > 0.1$ GeV^2.

Taking into account the kinematical cuts $m_B^{\rm rec} = 4.500$ GeV (for $\ell = e$) and $m_B^{\rm rec} = 5.150$ GeV (for $\ell = \mu$), we estimate the meson-mediated contribution to yield[6]

$$\Delta_{\rm QED} R_{K^*}[0.045,\ 1.1] \approx -0.017\ . \tag{5.19}$$

Given the discussion above, we assign a conservative ± 0.02 error to the whole QED corrections in this region. Our final SM estimate is then

$$\begin{aligned} R_{K^*}[0.045, 1.1]^{\rm SM} &= 0.906 \pm 0.020\ {}_{\rm QED} \pm 0.020\ {}_{\rm FF} \\ &= 0.906 \pm 0.028\ {}_{\rm th}\ . \end{aligned} \tag{5.20}$$

It must be stressed that the (relatively) large theoretical uncertainty in (eq. (5.20)) is due to the definition of the bin, that starts at the di-muon threshold. Setting the lower threshold to 0.1 GeV^2 (a value that we advocate in view of future experimental analyses) we find

$$\begin{aligned} R_{K^*}[0.1, 1.1]^{\rm SM} &= 0.983 \pm 0.010\ {}_{\rm QED} \pm 0.010\ {}_{\rm FF} \\ &= 0.983 \pm 0.014\ {}_{\rm th}\ . \end{aligned} \tag{5.21}$$

5.5 Conclusions

The experimental result presented in [42, 43] stimulated a lot of theoretical activity [50, 57–59, 111–135]. In view of this result and, especially, in view of possible future experimental improvements in the determination of R_K or R_{K^*}, we have re-examined the SM predictions of these LFU ratios.

As we have show, $\log(m_\ell)$-enhanced QED corrections may induce sizable deviations from eq. (5.2), even up to 10%, depending on the specific cuts applied to define physical observables. In particular, a key role is played by the cuts on $q^2 = m_{\ell\ell}^2$ and on the reconstructed B-meson mass. The former is important to avoid rapidly varying regions in the dilepton spectrum (where the theoretical tools to compute QED corrections become unreliable), while the latter defines the physical IR cut-off of the rates. Employing the cuts presently applied by the LHCb Collaboration, the corrections in R_K do not exceed 3%. Moreover, their effect is well described (and corrected for in the experimental analysis) by existing Montecarlo codes.

[6] The result in eq. (5.19)) holds under the assumption that any contribution to the photon-inclusive electron rate with $q^2 < 0.045$ GeV^2 is subtracted (or corrected for) on the experimental side, otherwise the correction could be significantly larger.

According to our analysis, a deviation of R_K or R_{K^*} from 1 exceeding the 1% level, performed along the lines of Ref. [42] in the region 1 $\text{GeV}^2 < q^2 < 6$ GeV^2, would be a clear signal of physics beyond the Standard Model.

Part IV

Model building for the anomalies

Chapter 6

Semi-leptonic B-physics anomalies: a general EFT analysis within $U(2)^n$ flavour symmetry

6.1 Introduction

The set of deviations from the SM presented in section 2.4 have triggered a series of theoretical speculations about possible New Physics (NP) interpretations. In particular, attempts to provide a combined/coherent explanation for both charged- and neutral-current anomalies have been presented in Ref. [57–59, 125, 127, 128, 133, 136–140]. Among them, a particularly interesting class is that of models based on a $U(2)^n$ flavour symmetry, acting on the light generations of SM fermions [11, 141], and new massive vector mediators around the TeV scale (either colorless $SU(2)_L$ triplets [58], or $SU(2)_L$ doublet leptoquarks [125]). Beside providing a good description of low-energy data, these mediators could find a consistent UV completion in the context of strongly-interacting theories with new degrees of freedom at the TeV scale [134, 142].

While these NP interpretations are quite interesting, their compatibility with high-p_T data from the LHC and other precision low-energy observables is not trivial. On the one hand, it has been pointed out that high-p_T searches of resonances decaying into a $\tau\overline{\tau}$ pair ($pp \to \tau\overline{\tau} + X$) represent a very stringent constraint for a large class of model addressing the $R^{\tau/\ell}_{D^{(*)}}$ anomalies [143]. On the other hand, the consistency with LFU tests and the bounds on Lepton flavour Violation (LFV) from τ decays, after taking into account quantum corrections, seems to be problematic [144]. Last but not least, in all the explicit models constructed so far, a non-negligible amount of fine-tuning seems to be unavoidable in order to satisfy the constraints from B_s and B_d meson-antimeson mixing (see, in particular, Ref. [125, 134]).

The compatibility with collider searches is certainly a serious issue; however, it should not be over-emphasized especially in the context of strongly interacting theories, where the extrapolation from low-energy data to the on-shell production of the new states is subject to sizable uncertainties. On the contrary, the compatibility of these anomalies with other low-energy data is a question that can be addressed in a model-independent way using an appropriate Effective Field Theory (EFT) approach. The purpose of this work is to revisit the consistency and the compatibility of the anomalies reported in section 2.4 with other low-energy data, employing a general EFT approach based on the $U(2)^n$ flavour symmetry.

As it appeared clear from the first $U(2)^n$ based analyses [58, 125], the flavour symmetry alone is not enough to guarantee a natural explanation of B-physics anomalies in a general EFT approach. Additional dynamical assumptions are needed to explained the observed hierarchy among the various effective operators. Our goal is to discuss in general terms possible power-

counting schemes to justify these hierarchies and, within such schemes, to quantify the amount of fine-tuning necessary to obtain a satisfactory description of all low-energy data.

This chapter is organised as follows. In section 6.2 we define the low-energy EFT and provide a complete list of the four-fermion operators with the inclusion of at most one lepton spurion and one (or two) quark spurion(s) contributing to $\Delta F = 1$ (or $\Delta F = 2$) processes. The bounds on these operators from the relevant low-energy observables are discussed in section 7.4. In section 6.4.1 we analyse these bounds and determine a consistent power-counting scheme that allow us justify the observed hierarchies. In section 6.4.3 we discuss selected observables receiving leading contributions from operators with two lepton spurions (among which $R_K^{\mu/e}$), further testing the consistency of the proposed power-counting scheme. The final results, with a quantification of the fine-tuning needed to reconcile anomalies and bounds, are summarised in the Conclusions.

6.2 Setup

The EFT we are considering is characterised by the SM field content, the SM gauge symmetry $(SU(3)_c \times SU(2)_L \times U(1)_Y)$, and a global flavour symmetry $\mathcal{G}_{\rm flavour}$, that we can decompose as follows

$$\mathcal{G}_{\rm flavour} = U(2)_q \times U(2)_\ell \times \mathcal{G}_R \ . \tag{6.1}$$

The left-handed SM fermions (q_L^i and ℓ_L^i) are singlets under $\mathcal{G}_R$ and have the following transformation properties under $U(2)_q \times U(2)_\ell$:

$$Q \equiv (q_L^1, q_L^2) \sim (2,1) \ , \qquad q_{3L} \equiv q_L^3 \sim (1,1) \ , \tag{6.2}$$

$$L \equiv (\ell_L^1, \ell_L^2) \sim (1,2) \ , \qquad \ell_{3L} \equiv \ell_L^3 \sim (1,1) \ . \tag{6.3}$$

The third-generation right-handed fermions (t_R, b_R and τ_R) are all singlets of the complete group $\mathcal{G}_{\rm flavour}$. Various options are possible as far as the action of $\mathcal{G}_{\rm flavour}$ on the right-handed light-generation fermions is concerned. The simplest choice is the MFV-like [10] setting $\mathcal{G}_R = U(2)_{u_R} \times U(2)_{d_R} \times U(2)_{e_R}$, such that $E = (\mu_R, e_R)$ transforms as a doublet of $U(2)_{e_R}$, and similarly for right-handed light quarks. But other options, where μ_R and e_R belong to the same non-trivial representation of a non-Abelian subgroup, leads to equivalent results.

We further consider two breaking spurions of the flavour symmetry, V_Q and V_L, transforming, respectively, as (2,1) and (1,2) of $U(2)_q \times U(2)_\ell$. The structure of V_Q can be connected to the CKM matrix (V) up to an overall normalization factor [11]:

$$V_Q \equiv (V_{Q_1}, V_{Q_2}) = |V_Q| \times \left(\frac{V_{td}^*}{V_{ts}^*}, 1 \right) , \tag{6.4}$$

with $|V_Q|$ expected to be of $O(|V_{ts}|)$. In the case of V_L, in the absence of a clear connection to the entries in the lepton Yukawa couplings, and given the strong universality bounds in processes involving electrons, we assume the following hierarchical structure:

$$V_L \equiv (V_{L_1}, V_{L_2}) = |V_L| \times (0,1) \ , \tag{6.5}$$

with $|V_L| \ll 1$ (an estimate of the maximal allowed value for $|V_{L_1}/V_{L_2}|$ is presented in section 6.4.4).

So far we have not specified the flavour basis of the left-handed fermion doublets, or better how we define the $U(2)_q \times U(2)_\ell$ singlets. In the lepton case, the natural choice is provided by the charged-lepton mass-eigenstate basis (or by identifying τ_L as the $U(2)_\ell$ singlet). In the quark sector the situation is more ambiguous. In principle, any linear combination between down- and

	Operator	Relevant low-energy observables
$\mathcal{O}_{01}^{qq}$	$\left[\overline{q}_{3L}\gamma^\mu Q^i V_{Qi}^\dagger\right]^2$	ΔM_{B_d}, ΔM_{B_s}
$\mathcal{O}_{02}^{qq}$	$\left[\overline{q}_{3L}\sigma^a\gamma^\mu Q^i V_{Qi}^\dagger\right]^2$	ΔM_{B_d}, ΔM_{B_s}

Table 6.1: Four-quark operators contributing to $\Delta F = 2$ amplitudes with at most two quark spurions.

up-quark mass eigenstates is equally valid. For the sake of simplicity, we assume as reference basis the down-quark mass-eigenstate basis. This corresponds to identifying the $U(2)_q$ singlet and doublet as[1]

$$q_{3L} = \begin{pmatrix} V_{kb}^* u_L^k \\ b_L \end{pmatrix} \qquad \text{and} \qquad Q^i = \begin{pmatrix} V_{ki}^* u_L^k \\ d_L^i \end{pmatrix} , \quad i = \{1,2\} \equiv \{d,s\} \ . \tag{6.6}$$

A "natural" change of basis is equivalent to the following shift in q_{3L}

$$q_{3L} \to q'_{3L} = \ q_{3L} + \theta \ V_{Qi}^\dagger Q^i \ , \tag{6.7}$$

where θ is an $O(1)$ parameter. As a result, we can consider natural (non fine-tuned) the EFT constructions if operators without spurions and corresponding terms obtained with the replacement $q_{3L} \to V_{Qi}^\dagger Q^i$ have coefficients of similar size.

The basis of effective operators

In addition to the symmetries discussed above, we impose the conservation of baryon and lepton number, and we consider higher-dimensional operators up to dimension six. The EFT we are considering can thus be written as

$$\mathcal{L}_{\rm EFT} = \mathcal{L}_{\rm SM} + \frac{4G_F}{\sqrt{2}} \sum_i C_i \mathcal{O}_i \ , \tag{6.8}$$

using the Fermi scale, $v_F = (4G_F/\sqrt{2})^{-1/2} \approx 174$ GeV, as overall dimensional normalization factor. With such choice we reabsorb the value of the EFT effective scale (Λ) inside the Wilson coefficients, whose natural size in absence of specific suppression factors is $O(v_F^2/\Lambda^2)$.

The effective operators $\mathcal{O}_i$ can be separated into three main categories: i) operators with no fermion fields; ii) operators with two fermion fields (plus Higgs or gauge fields); iii) four-fermion operators. The first two categories contain a small number of operators and are not particularly interesting to the processes we are considering.[2] Within the class of four-fermion operators we can identify four interesting sub-categories, whose lists of operators, with the inclusion of at most one lepton spurion and one quark spurion (or two quark spurions in the case of $\Delta F = 2$ operators), are reported in tables 6.1–6.4. For each operator we indicate the low-energy processes that can provide the most stringent constraint.

In the case of semi-leptonic operators we do not list explicitly those with a pair of right-handed light quarks since they do not give rise to signatures different from those of the operators already

[1] In Eq. (6.6) we write explicitly the two electroweak doublet components of the doublets.

[2] As discussed in the introduction, we focus our attention only on low-energy processes. We do not include in this category precision electroweak tests at the Z-pole, which are sensitive to four-fermion operators at the one-loop level, but also to operators with a current and a Higgs current ($\overline{\psi}\gamma^\mu\psi H^\dagger D_\mu H$ or $\overline{\psi}_L\sigma_a\gamma^\mu\psi_L H^\dagger\sigma^a D_\mu H$) at the tree level. It is trivial to show that, adjusting the coefficients of the latter (in our framework these are free parameters unrelated to the four-fermion couplings) one can compensate the one-loop contributions discussed in [144] and have a good fit of the (high-energy) electroweak observables.

	Operator	Relevant low-energy processes
$\mathcal{O}^q_{01}$	$(\overline{q}_{3L}\gamma^\mu q_{3L})\,(\overline{\ell}_{3L}\gamma_\mu \ell_{3L})$	— ($\nu_\tau N \to \nu_\tau N$, $\Upsilon \to \tau\overline{\tau}$)
$\mathcal{O}^q_{02}$	$(\overline{q}_{3L}\sigma^a\gamma^\mu q_{3L})\,(\overline{\ell}_{3L}\sigma_a\gamma_\mu \ell_{3L})$	$b \to c\tau\overline{\nu}$
$\mathcal{O}^q_{03}$	$(\overline{q}_{3L}\gamma^\mu q_{3L})\left(\overline{L}_i\gamma_\mu L^i\right)$	— ($\nu_\ell N \to \nu_\ell N$, $\Upsilon \to \ell\bar{\ell}$)
$\mathcal{O}^q_{04}$	$(\overline{q}_{3L}\sigma^a\gamma^\mu q_{3L})\left(\overline{L}_i\sigma_a\gamma_\mu L^i\right)$	$b \to c\mu\overline{\nu}$
$\mathcal{O}^q_{05}$	$\left(\overline{Q}_i\gamma^\mu Q^i\right)(\overline{\ell}_{3L}\gamma_\mu \ell_{3L})$	— ($\nu_\tau N \to \nu_\tau N$, $\phi \to \tau\overline{\tau}$)
$\mathcal{O}^q_{06}$	$\left(\overline{Q}_i\sigma^a\gamma^\mu Q^i\right)(\overline{\ell}_{3L}\sigma_a\gamma_\mu \ell_{3L})$	$\tau \to K\nu$, $D \to \tau\nu$
$\mathcal{O}^q_{07}$	$\left(\overline{Q}_i\gamma^\mu Q^i\right)\left(\overline{L}_i\gamma_\mu L^i\right)$	— ($\nu_\ell N \to \nu_\ell N$, $\phi \to \ell\bar{\ell}$)
$\mathcal{O}^q_{08}$	$\left(\overline{Q}_i\sigma^a\gamma^\mu Q^i\right)\left(\overline{L}_i\sigma_a\gamma_\mu L^i\right)$	$K \to \ell\overline{\nu}$, $K \to \pi\ell\overline{\nu}$, $\pi \to \ell\overline{\nu}$
$\mathcal{O}^q_{11}$	$\left(\overline{q}_{3L}\gamma^\mu Q^i V^\dagger_{Qi}\right)(\overline{\ell}_{3L}\gamma_\mu \ell_{3L})$	$b \to s\tau\overline{\tau}$, $b \to s\nu\overline{\nu}$
$\mathcal{O}^q_{12}$	$\left(\overline{q}_{3L}\sigma^a\gamma^\mu Q^i V^\dagger_{Qi}\right)(\overline{\ell}_{3L}\sigma_a\gamma_\mu \ell_{3L})$	$b \to c\tau\overline{\nu}$, $b \to s\tau\overline{\tau}$, $b \to s\nu\overline{\nu}$, $\tau \to K\nu$
$\mathcal{O}^q_{13}$	$\left(\overline{q}_{3L}\gamma^\mu Q^i V^\dagger_{Qi}\right)\left(\overline{L}_i\gamma_\mu L^i\right)$	$b \to s\ell\bar{\ell}$, $b \to s\nu\overline{\nu}$
$\mathcal{O}^q_{14}$	$\left(\overline{q}_{3L}\sigma^a\gamma^\mu Q^i V^\dagger_{Qi}\right)\left(\overline{L}_i\sigma_a\gamma_\mu L^i\right)$	$b \to s\ell\bar{\ell}$, $b \to s\nu\overline{\nu}$
$\mathcal{O}^q_{21}$	$(\overline{q}_{3L}\gamma^\mu q_{3L})\left(\overline{\ell}_{3L}\gamma_\mu L^i V^\dagger_{Li}\right)$	$\Upsilon \to \tau\overline{\mu}$, $\eta_b \to \tau\mu$
$\mathcal{O}^q_{22}$	$(\overline{q}_{3L}\sigma^a\gamma^\mu q_{3L})\left(\overline{\ell}_{3L}\sigma_a\gamma_\mu L^i V^\dagger_{Li}\right)$	$\Upsilon \to \tau\overline{\mu}$, $\eta_b \to \tau\mu$
$\mathcal{O}^q_{23}$	$\left(\overline{Q}_i\gamma^\mu Q^i\right)\left(\overline{\ell}_{3L}\gamma_\mu L^i V^\dagger_{Li}\right)$	$\tau \to \mu\rho$, $\tau \to \mu\omega$
$\mathcal{O}^q_{24}$	$\left(\overline{Q}_i\sigma^a\gamma^\mu Q^i\right)\left(\overline{\ell}_{3L}\sigma_a\gamma_\mu L^i V^\dagger_{Li}\right)$	$\tau \to \mu\rho$, $\tau \to \mu\omega$
$\mathcal{O}^q_{31}$	$\left(\overline{q}_{3L}\gamma^\mu Q^i V^\dagger_{Qi}\right)\left(\overline{\ell}_{3L}\gamma_\mu L^i V^\dagger_{Li}\right)$	$B_s \to \tau\overline{\mu}$
$\mathcal{O}^q_{32}$	$\left(\overline{q}_{3L}\sigma^a\gamma^\mu Q^i V^\dagger_{Qi}\right)\left(\overline{\ell}_{3L}\sigma_a\gamma_\mu L^i V^\dagger_{Li}\right)$	$B_s \to \tau\overline{\mu}$

Table 6.2: Semi-leptonic four-fermion operators, with only left-handed currents and at most one lepton and/or one quark spurion. The processes listed between brackets do not give appreciable bounds and are reported only for completeness.

listed and, in addition, can be assumed to be suppressed under natural dynamical assumptions. For similar reasons, despite we have explicitly listed in tables 6.3–6.4 tensor operators, we will ignore their effects in the phenomenological analysis of $b \to c\tau\overline{\nu}$ and $b \to s\tau\overline{\tau}$ transitions.

In principle, the various effective operators mix under quantum corrections. However, as indicated in Eq. (6.8), we assume a rather low effective scale such that no large logarithms are involved in the renormalization-group (RG) evolution. This implies that in most cases these mixing effects can be neglected. The only exception are cases where an operator with a large coefficient (in particular those contributing to $R_{D^{(*)}}$) mixes into a strongly constrained one (such as those contributing to leptonic τ decays), as pointed out first in Ref. [144]. Since no large logarithms are involved, we take into account this effects directly at the matrix-element level (i.e. taking into account also one-loop matrix elements, when necessary).

6.3 Observables

In this Section, we analyse the main experimental constraints on the operators with at most one lepton spurion listed in the previous Section. These includes the non-vanishing constraints from R_D and R_{D^*}, and a long series of bounds from $\Delta F = 1$ and $\Delta F = 2$ processes, and τ decays. The discussion of selected observables receiving leading contributions from operators with two

	Operator	Relevant low-energy processes
$\mathcal{O}^q_{R1}$	$(\overline{q}_{3L}\gamma^\mu q_{3L})\,(\overline{\tau}_R\gamma_\mu\tau_R)$	— $(\Upsilon\to\tau\overline{\tau})$
$\mathcal{O}^q_{R2}$	$\left(\overline{q}_{3L}\gamma^\mu Q^i V^\dagger_{Qi}\right)(\overline{\tau}_R\gamma_\mu\tau_R)$	$b\to s\tau\overline{\tau}$
$\mathcal{O}^q_{R3}$	$\left(\overline{Q}_i\gamma^\mu Q^i\right)(\overline{\tau}_R\gamma_\mu\tau_R)$	— $(\tau N\to\tau N)$
$\mathcal{O}^q_{R4}$	$(\overline{q}_{3L}\gamma^\mu q_{3L})\left(\overline{E}_j\gamma_\mu E^j\right)$	— $(\Upsilon\to\ell\overline{\ell})$
$\mathcal{O}^q_{R5}$	$\left(\overline{q}_{3L}\gamma^\mu Q^i V^\dagger_{Qi}\right)\left(\overline{E}_j\gamma_\mu E^j\right)$	$b\to s\ell\overline{\ell}$
$\mathcal{O}^q_{R6}$	$\left(\overline{Q}_i\gamma^\mu Q^i\right)\left(\overline{E}_j\gamma_\mu E^j\right)$	— $(\phi\to\ell\overline{\ell})$
$\mathcal{O}^q_{S1}$	$\left(\overline{\ell}_{3L}\tau_R\right)\left(\overline{b}_R q_{3L}\right)$	$b\to c\tau\overline{\nu}$
$\mathcal{O}^q_{S2}$	$\left(\overline{\ell}_{3L}\tau_R\right)\left(\overline{b}_R Q^i V^\dagger_{Qi}\right)$	$b\to c\tau\overline{\nu}$, $b\to s\tau\overline{\tau}$
$\mathcal{O}^q_{S3}$	$\left(\overline{L}_i V^i_L\tau_R\right)\left(\overline{b}_R q_{3L}\right)$	$\eta_b\to\tau\overline{\mu}$
$\mathcal{O}^q_{T1}$	$\left(\overline{\ell}_{3L}\sigma_{\mu\nu}\tau_R\right)\left(\overline{b}_R\sigma^{\mu\nu} q_{3L}\right)$	$b\to c\tau\overline{\nu}$
$\mathcal{O}^q_{T2}$	$\left(\overline{\ell}_{3L}\sigma_{\mu\nu}\tau_R\right)\left(\overline{b}_R\sigma^{\mu\nu} Q^i V^\dagger_{Qi}\right)$	$b\to c\tau\overline{\nu}$, $b\to s\tau\overline{\tau}$
$\mathcal{O}^q_{T3}$	$\left(\overline{L}_i V^i_L\sigma_{\mu\nu}\tau_R\right)\left(\overline{b}_R\sigma^{\mu\nu} q_{3L}\right)$	$b\to c\tau\overline{\nu}$

Table 6.3: Semi-leptonic four-fermion operators, with leptonic right-handed and scalar currents, and at most one lepton and/or one quark spurion.

lepton spurions is postponed to section 6.4.3. Unless otherwise specified, the bounds should be interpreted as bounds on the C_i at the scale Λ (i.e. neglecting RG corrections between Λ and the electroweak scale).

6.3.1 Semi-leptonic $b\to c$ transitions

$B\to D\ell\overline{\nu}_\ell$

From the operators in table 6.2, the effective charged-current Lagrangian describing $b\to c$ semi-leptonic decays with light leptons is:[3]

$$\mathcal{L}(b\to c\ell\overline{\nu}_\ell) = -\frac{4G_F}{\sqrt{2}}V_{cb}\left(1+2C^q_{04}+2V_{Q_s}C^q_{14}\frac{V_{cs}}{V_{cb}}\right)(\overline{c}_L\gamma^\mu b_L)(\overline{\ell}_L\gamma_\mu\nu_{\ell L}). \tag{6.9}$$

Since the structure of the Lagrangian in eq. (6.9) is SM-like, the decay width of the process $B\to D\ell\overline{\nu}_\ell$ can simply written as

$$\Gamma(B\to D\ell\nu_\ell) = \Gamma^{\rm SM}(B\to D\ell\nu_\ell)^{\rm SM}\,|1+\delta_D|^2\ , \qquad \delta_D = 2C^q_{04}+2V_{Q_s}C^q_{14}\frac{V_{cs}}{V_{cb}}\ . \tag{6.10}$$

Using the SM prediction $\mathcal{B}(B\to D\mu\overline{\nu}_\mu)^{\rm SM} = (2.28\pm0.19)\ 10^{-2}$ [64], and the experimental result in Ref. [146], we derive the bound

$$\mathrm{Re}\left(C^q_{04}+V_{Q_s}C^q_{14}\frac{V_{cs}}{V_{cb}}\right) = -0.008\pm0.025\,, \tag{6.11}$$

which is compatible with the hypothesis of negligible NP effects in the light lepton channels.

[3] As anticipated, here and in $b\to c\tau\overline{\nu}_\tau$ we ignore the effects of tensor operators which are i) naturally suppressed in a wide class of NP models, and ii) whose effects are barely distinguishable from those of left-handed and scalar operators using the limited set of observables presently available. For a detailed discussion of charged-current transitions including also tensor operators we refer to Ref. [145].

	Operator	Relevant low-energy processes
$\mathcal{O}^\ell_{01}$	$\left(\overline{\ell}_{3L}\gamma^\mu\ell_{3L}\right)\left(\overline{\ell}_{3L}\gamma_\mu\ell_{3L}\right)$	— (flav. cons. leptonic curr.)
$\mathcal{O}^\ell_{02}$	$\left(\overline{\ell}_{3L}\sigma^a\gamma^\mu\ell_{3L}\right)\left(\overline{\ell}_{3L}\sigma_a\gamma_\mu\ell_{3L}\right)$	— (flav. cons. leptonic curr.)
$\mathcal{O}^\ell_{03}$	$\left(\overline{\ell}_{3L}\gamma^\mu\ell_{3L}\right)\left(\overline{L}_i\gamma_\mu L^i\right)$	— (flav. cons. leptonic curr.)
$\mathcal{O}^\ell_{04}$	$\left(\overline{\ell}_{3L}\sigma^a\gamma^\mu\ell_{3L}\right)\left(\overline{L}_i\sigma_a\gamma_\mu L^i\right)$	$\tau\to\ell\nu\overline{\nu}$
$\mathcal{O}^\ell_{11}$	$\left(\overline{\ell}_{3L}\gamma^\mu\ell_{3L}\right)\left(\overline{\ell}_{3L}\gamma_\mu L^i V^\dagger_{Li}\right)$	$\tau\to\ell\nu\overline{\nu}$
$\mathcal{O}^\ell_{12}$	$\left(\overline{\ell}_{3L}\sigma^a\gamma^\mu\ell_{3L}\right)\left(\overline{\ell}_{3L}\sigma_a\gamma_\mu L^i V^\dagger_{Li}\right)$	$\tau\to\ell\nu\overline{\nu}$
$\mathcal{O}^\ell_{13}$	$\left(\overline{\ell}_{3L}\gamma^\mu L^i V^\dagger_{Li}\right)\left(\overline{L}_j\gamma_\mu L^j\right)$	$\tau\to\ell\nu\overline{\nu}$, $\tau\to\ell'\ell\overline{\ell}$
$\mathcal{O}^\ell_{14}$	$\left(\overline{\ell}_{3L}\sigma^a\gamma^\mu L^i V^\dagger_{Li}\right)\left(\overline{L}_j\sigma_a\gamma_\mu L^j\right)$	$\tau\to\ell\nu\overline{\nu}$, $\tau\to\ell'\ell\overline{\ell}$
$\mathcal{O}^\ell_{R1}$	$\left(\overline{\ell}_{3L}\gamma^\mu\ell_{3L}\right)\left(\overline{E}_j\gamma_\mu E^j\right)$	— (flav. cons. leptonic curr.)
$\mathcal{O}^\ell_{R2}$	$\left(\overline{\ell}_{3L}\gamma^\mu L^i V^\dagger_{Li}\right)\left(\overline{E}_j\gamma_\mu E^j\right)$	$\tau\to\ell'\ell\overline{\ell}$
$\mathcal{O}^\ell_{S1}$	$\left(\overline{\ell}_{3L}E^j\right)\left(\overline{E}_j\ell_{3L}\right)$	— (flav. cons. leptonic curr.)
$\mathcal{O}^\ell_{S2}$	$\left(\overline{\ell}_{3L}E^j\right)\left(\overline{E}_j L^i V^\dagger_{Li}\right)$	$\tau\to\ell'\ell\overline{\ell}$
$\mathcal{O}^\ell_{T1}$	$\left(\overline{\ell}_{3L}\sigma_{\mu\nu}E^j\right)\left(\overline{E}_j\sigma^{\mu\nu}\ell_{3L}\right)$	— (flav. cons. leptonic curr.)
$\mathcal{O}^\ell_{T2}$	$\left(\overline{\ell}_{3L}\sigma_{\mu\nu}E^j\right)\left(\overline{E}_j\sigma^{\mu\nu}L^i V^\dagger_{Li}\right)$	$\tau\to\ell'\ell\overline{\ell}$

Table 6.4: Four-lepton operators

$B\to D^{(*)}\tau\overline{\nu}_\tau$

The effective Lagrangian relevant to semi-leptonic $b\to c$ decays with τ leptons in the final state is

$$\begin{aligned}\mathcal{L}(b\to c\tau\overline{\nu}_\tau) = -\frac{4G_F}{\sqrt{2}}V_{cb}\Bigg[&\left(1+2C^q_{02}+2V_{Q_s}C^q_{12}\frac{V_{cs}}{V_{cb}}\right)(\overline{c}_L\gamma^\mu b_L)(\overline{\tau}_L\gamma_\mu\nu_\tau)\\ &+\left(C^q_{S1}+V_{Q_s}C^q_{S2}\frac{V_{cs}}{V_{cb}}\right)(\overline{c}_L b_R)(\overline{\tau}_R\nu_{\tau L})\Bigg]\,.\end{aligned} \tag{6.12}$$

Contrary to the light lepton case, in the τ channel also the scalar operators $\mathcal{O}^q_{S1(2)}$ do appear and the decay amplitudes (and corresponding differential decay widths) cannot be expressed as a simple re-scaling of the SM ones.

Expanding to first order in the NP contributions, the $B\to D^{(*)}\tau\overline{\nu}_\tau$ differential decay widths can be decomposed as

$$\frac{\mathrm{d}\Gamma}{\mathrm{d}q^2}(B\to D^{(*)}\tau\overline{\nu}_\tau) = (1+2\Delta)\frac{\mathrm{d}\Gamma}{\mathrm{d}q^2}(B\to D^{(*)}\tau\overline{\nu}_\tau)_{\mathrm{SM}} + \Delta_{\,\mathrm{S}}\frac{\mathrm{d}\Gamma}{\mathrm{d}q^2}(B\to D^{(*)}\tau\overline{\nu}_\tau)_{\,\mathrm{VS}} + O(C_i^2)\,, \tag{6.13}$$

with

$$\Delta = 2\ \ \mathrm{Re}\left(C^q_{02}+2V_{Q_s}C^q_{12}\frac{V_{cs}}{V_{cb}}\right)\,,\qquad \Delta_{\mathrm{S}} =\ \mathrm{Re}\left(C^q_{S1}+V_{Q_s}C^q_{S2}\frac{V_{cs}}{V_{cb}}\right)\,. \tag{6.14}$$

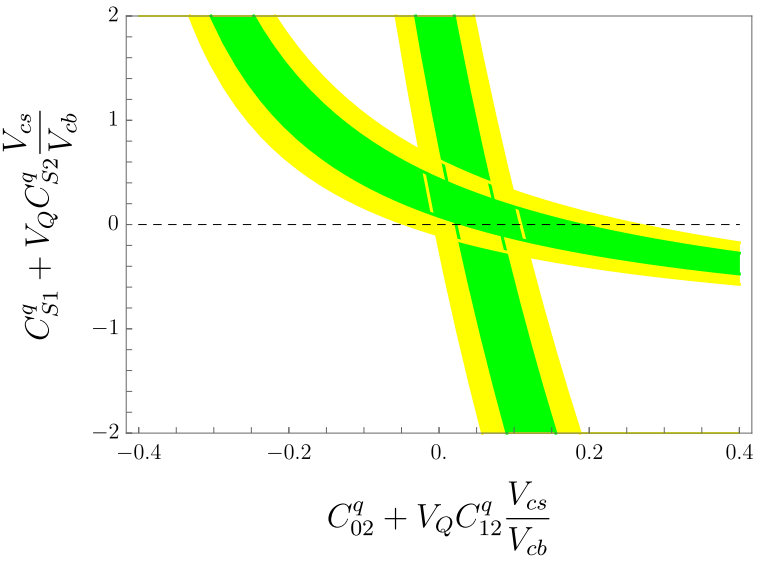

Figure 6.1: Parameter space allowed by the constraint on $\mathcal{B}(B \to D\tau\overline{\nu}_\tau)$ and $\mathcal{B}(B \to D^*\tau\overline{\nu}_\tau)$. The bands denotes 1 and 2σ limits (the C_i are assumed to be real).

Following Ref. [62], the two SM differential decay distribution can be written as[4]

$$\frac{\mathrm{d}\Gamma}{\mathrm{d}q^2}(B \to D\tau\overline{\nu}_\tau)_{\mathrm{SM}} = \frac{G_F^2\sqrt{\lambda}|V_{cb}|^2\left(m_\tau^2 - q^2\right)^2}{384\pi^3 m_B^3 q^6}\left[3f_0^2(q^2)m_\tau^2\left(m_B^2 - m_D^2\right)^2 + f_+^2\lambda\left(m_\tau^2 + 2q^2\right)\right], \tag{6.15}$$

$$\frac{\mathrm{d}\Gamma}{\mathrm{d}q^2}(B \to D^*\tau\overline{\nu}_\tau)_{\mathrm{SM}} = \frac{G_F^2\sqrt{\lambda}|V_{cb}|^2\left(m_\tau^2 - q^2\right)^2}{384\pi^3 m_B q^6}\Big[F_0^2\ m_B^2\left(m_\tau^2 + 2q^2\right) + q^2\left(F_\perp^2 + F_\parallel^2\right)\left(m_\tau^2 + 2q^2\right) + 3F_t^2\ m_B^2\ m_\tau^2\Big]. \tag{6.16}$$

The non-standard term $\frac{\mathrm{d}\Gamma}{\mathrm{d}q^2}(B \to D^{(*)}\tau\overline{\nu}_\tau)_{\mathrm{VS}}$ arise from the interference between the left-handed and the scalar operators. Its explicit expression in the D and D^* case is

$$\frac{\mathrm{d}\Gamma}{\mathrm{d}q^2}(B \to D\tau\overline{\nu}_\tau)_{\mathrm{VS}} = \frac{f_0^2 G_F^2\sqrt{\lambda}\ m_\tau|V_{cb}|^2\left(m_B^2 - m_D^2\right)^2\left(m_\tau^2 - q^2\right)^2}{64\pi^3 m_B^3 q^4(m_b - m_c)}, \tag{6.17}$$

$$\frac{\mathrm{d}\Gamma}{\mathrm{d}q^2}(B \to D^*\tau\overline{\nu}_\tau)_{\mathrm{VS}} = \frac{F_t^2 G_F^2\sqrt{\lambda}\ m_B\ m_\tau|V_{cb}|^2\left(m_\tau^2 - q^2\right)^2}{64\pi^3 q^4(m_b + m_c)}. \tag{6.18}$$

In principle, the best discrimination between scalar and left-handed contributions could be obtained by differential measurements of the two spectra, using the above formulae. So far these measurements are not available; however, a useful information can be derived also comparing the partial widths of two modes. The parameter space allowed by the experimental constraints [38] on $\mathcal{B}(B \to D\tau\nu_\tau)$ and $\mathcal{B}(B \to D^*\tau\nu_\tau)$ is shown in figure 6.1. As can be seen, the constraint on the scalar terms is quite weak. Still, it is interesting to note that present data are perfectly compatible with the absence of scalar terms, while pointing toward a non-negligible modification of the coefficient of the left-handed operator. As noted in Ref. [145], a significant improvement vs. the SM predictions can be obtained also with tensor operators, although with tensor operators

[4] See appendix C for the definition of the form factors

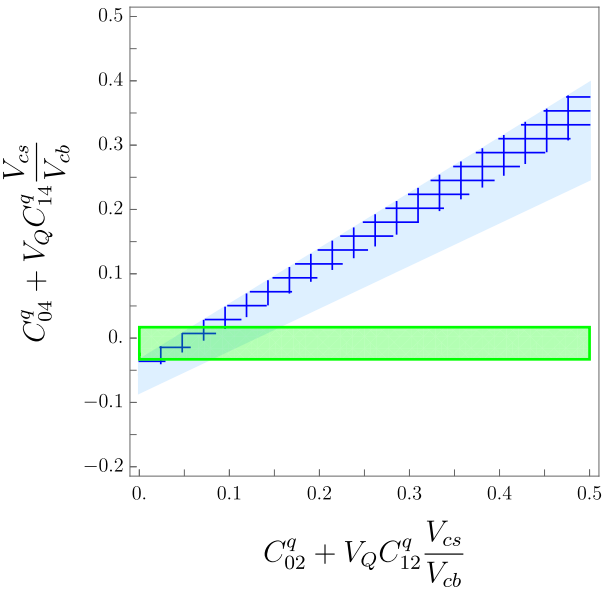

Figure 6.2: Parameter space allowed by the combination of the constraints given by the ratios R_D (blue region) and R_{D^*} (dashed region) in the hypothesis of negligible scalar current contributions. The horizontal band denotes the constraint from $\mathcal{B}(B \to D\mu\overline{\nu}_\ell)$.

only the overall fit of $\mathcal{B}(B \to D\tau\nu_\tau)$ and $\mathcal{B}(B \to D^*\tau\nu_\tau)$ data is clearly worse. For the sake of simplicity, and motivated by a large class of explicit NP constructions, in the following we will assume negligible NP effects in tensor operators.

As anticipated in the Introduction, the ratios $R_{D^{(*)}}^{\tau/\mu}$ play a crucial role in our analysis. Neglecting scalar terms, as suggested by figure 6.1, the parameter space allowed by these two ratios can easily be derived from eqs. (6.10) – (6.13) and is shown in figure 6.2. If we further take in account the bound in eq. (6.11), we deduce the following simple relation

$$\text{Re}\left(C_{02}^q + V_{Q_2} C_{12}^q \frac{V_{cs}}{V_{cb}}\right) = \frac{1}{4}\left[R_{D^{(*)}}^{\tau/\mu} - 1\right], \tag{6.19}$$

where we define

$$R_{D^{(*)}}^{\tau/\ell} = \frac{\mathcal{B}(B \to D^{(*)}\tau\overline{\nu})_{\text{exp}}/\mathcal{B}(B \to D^{(*)}\tau\overline{\nu})_{\text{SM}}}{\mathcal{B}(B \to D^{(*)}\ell\overline{\nu})_{\text{exp}}/\mathcal{B}(B \to D^{(*)}\ell\overline{\nu})_{\text{SM}}}\,. \tag{6.20}$$

If we combine the data from R_D and R_{D^*}, we obtain to the following limit

$$\text{Re}\left(C_{02}^q + V_{Q_2} C_{12}^q \frac{V_{cs}}{V_{cb}}\right) \;=\; 0.060 \pm 0.015\,. \tag{6.21}$$

6.3.2 Semi-leptonic $s \to u$ transitions

The semi-leptonic operators listed in table 6.2 generate also contributions to $s \to u$ transitions with τ and light leptons. The relevant effective Lagrangians, taking into account also the SM contributions, are

$$\mathcal{L}(s \to u\tau\nu) = -4\frac{G_F}{\sqrt{2}} V_{us}\left(1 + 2C_{06}^q + 2C_{12}^q V_{Q_s}\frac{V_{ub}}{V_{us}}\right)(\overline{u}_L\gamma_\mu s_L)(\overline{\tau}_L\gamma^\mu\nu_{\tau L})\,, \tag{6.22}$$

$$\mathcal{L}(s \to u\mu\nu) = -4\frac{G_F}{\sqrt{2}} V_{us}\left(1 + 2C_{08}^q + 2C_{14}^q V_{Q_s}\frac{V_{ub}}{V_{us}}\right)(\overline{u}_L\gamma_\mu s_L)(\overline{\mu}_L\gamma^\mu\nu_{\mu L})\,. \tag{6.23}$$

A particularly interesting observable to constrain the NP terms in these Lagrangians is the ratio $\mathcal{B}(\tau \to K\nu_\tau)/\mathcal{B}(K \to \mu\overline{\nu}_\mu)$, where the theoretical uncertainties on CKM elements and Kaon decay constant cancel out. Using the experimental results in [146] and the SM input in [147] we find

$$R_{sd}^{\tau/\mu} = \frac{\mathcal{B}(K \to \mu\overline{\nu}_\mu)^{\rm exp}/\mathcal{B}(K \to \mu\overline{\nu}_\mu)^{\rm SM}}{\mathcal{B}(\tau \to K\nu_\tau)^{\rm exp}/\mathcal{B}(\tau \to K\nu_\tau)^{\rm SM}} = 1.029 \pm 0.015 \ , \tag{6.24}$$

which allows us to obtain the following bound

$$\text{Re}\left[C_{08}^q - C_{06}^q + (C_{14}^q - C_{12}^q)\, V_{Q_s}\frac{V_{ub}}{V_{us}}\right] = 0.007 \pm 0.004 \ . \tag{6.25}$$

It is worth to stress that $R_{sd}^{\tau/\mu}$ or, equivalently, the comparison of the $|V_{us}|$ determination from τ vs. K decays is nothing but a test of LFU. Interestingly enough, present data exhibits a small tension with the SM prediction also in this case.

6.3.3 $\Delta F = 2$ processes

According to the operators in table 6.1, the effective Lagrangian relevant to $\Delta F = 2$ processes is

$$\mathcal{L}_{\Delta F=2}^{\rm NP} = -\frac{4G_F}{\sqrt{2}}\,(C_{01}^{qq} + C_{02}^{qq})\,(V_{Q_i}^*)^2\left[\left(\overline{b}_L\gamma^\mu d_L^i\right)^2 + \left(V_{ki}^*V_{j3}\right)^2\left(\overline{u}_L^j\gamma^\mu u_L^k\right)^2\right]. \tag{6.26}$$

Since the structure of the effective operators is the same as in the SM, we can conveniently encode all the NP effects via the ratios

$$R_{B_q}^{\Delta F=2} = \frac{\mathcal{A}\left(B_q \to \overline{B}_q\right)_{\rm SM+NP}}{\mathcal{A}\left(B_q \to \overline{B}_q\right)_{\rm SM}} \qquad \text{and} \qquad R_D^{\Delta F=2} = \frac{\mathcal{A}(D^0 \to \overline{D}^0)_{\rm SM+NP}}{\mathcal{A}(D^0 \to \overline{D}^0)_{\rm SM}} \ . \tag{6.27}$$

In the B-physics case we find

$$R_{B_q}^{\Delta F=2} = 1 + \frac{(C_{01}^{qq} + C_{02}^{qq})}{R_{\rm SM}^{\rm loop}}\left(\frac{V_{Q_q}^*}{V_{tb}^*V_{tq}}\right)^2 \ , \tag{6.28}$$

where[5]

$$R_{\rm SM}^{\rm loop} = \frac{\alpha_{em}}{16\pi s_w^2}S_0(x_t)\eta_B \approx 1.6 \times 10^{-3} \ . \tag{6.29}$$

Given the flavour structure of V_{Q_i}, we get very similar bounds from B_d and B_s mixing, while the bound from D^0 is weaker. In particular, from the constraint $R_{B_s} \in (0.86, 1.26)$ [148] we derive the bound

$$|V_{Q_d}|^2|C_{01}^{qq} + C_{02}^{qq}| < 6.7 \times 10^{-7} \ . \tag{6.30}$$

6.3.4 FCNC $b \to s$ transitions

$B \to K^{(*)}\mu\overline{\mu}$

The Lagrangian that encodes FCNC $b \to s$ transition for the light lepton channels is

$$\mathcal{L}(b \to s\ell\overline{\ell}) = -\frac{2G_F}{\sqrt{2}}\frac{\alpha_e}{2\pi}V_{ts}^*V_{tb}\left[(C_9 + \Delta C_9)\,\mathcal{O}_9 + (C_{10} + \Delta C_{10})\,\mathcal{O}_{10}\right] \ , \tag{6.31}$$

where $\mathcal{O}_9$ and $\mathcal{O}_{10}$ are defined in eq. (C.12) of appendix C.2, and the shifts of C_9 and C_{10} in term of the NP Wilson coefficients have the following form:

$$\Delta C_9 = \frac{2\pi(C_{13}^q + C_{14}^q + C_{R5}^q)V_{Q_s}}{\alpha_e V_{ts}^*V_{tb}} \ , \qquad \Delta C_{10} = -\frac{2\pi(C_{13}^q + C_{14}^q - C_{R5}^q)V_{Q_s}}{\alpha_e V_{ts}^*V_{tb}} \ . \tag{6.32}$$

[5] For analytic and numerical values of $S_0(x_t)$ ans η_B we refer to Ref. [13].

Inverting the relations above, we obtain an expression for the two combination of Wilson coefficients that appear in these channels as a function of the shifts ΔC_9 and ΔC_{10}. These shifts have been constrained in Ref. [49, 51, 96] from global fits of various $b \to s\mu\overline{\mu}$ observables (dominated by $B \to K^*\mu\overline{\mu}$ and $B \to K\mu\overline{\mu}$ data). Considering in particular the results in [49], namely $\Delta C_9 = -1.05 \pm 0.35$ and $\Delta C_{10} = 0.3 \pm 0.4$, we find

$$\text{Re}\left[(C_{13}^q + C_{14}^q + C_{R5}^q)V_{Q_s}\right] = (-4.9 \pm 1.7) \times 10^{-5} \,, \tag{6.33}$$

$$\text{Re}\left[(C_{13}^q + C_{14}^q - C_{R5}^q)V_{Q_s}\right] = (1.4 \pm 1.9) \times 10^{-5} \,. \tag{6.34}$$

$B \to K^{(*)}\tau\overline{\tau}$

In principle, $b \to s\tau\overline{\tau}$ transitions would be excellent probes of our EFT construction. However, the current experimental bounds [149] are too weak to draw significant constraints. For completeness, and in view of future data, we report here the relevant formulae.

The relevant effective Lagrangian can be expressed as

$$\mathcal{L}(b \to s\tau\overline{\tau}) = -\frac{2G_F}{\sqrt{2}}\frac{\alpha_e}{2\pi}V_{ts}^*V_{tb}\Big[\left(C_9 + \Delta C_9^\tau\right)\mathcal{O}_9 + \left(C_{10} + \Delta C_{10}^\tau\right)\mathcal{O}_{10} + C_S^\tau(\mathcal{O}_S - \mathcal{O}_P)\Big], \tag{6.35}$$

where the operators $\mathcal{O}_9$, $\mathcal{O}_{10}$, $\mathcal{O}_S$ and $\mathcal{O}_P$ are defined in eq. (C.12) with the identification $\ell = \tau$. In terms of the Wilson coefficients of the operators in tables 6.2–6.3, the NP contributions are given by

$$\Delta C_{9(10)}^\tau = \pm\,\frac{2\pi(C_{11}^q + C_{12}^q \pm C_{R2}^q)V_{Q_s}}{\alpha_e V_{ts}^*V_{tb}} \,, \qquad C_S^\tau = \frac{2\pi C_{S2}^q V_{Q_s}}{\alpha_e V_{ts}^*V_{tb}} \,. \tag{6.36}$$

$B \to K^{(*)}\nu\overline{\nu}$

From the operators in table 6.2 we get the following Lagrangian for $b \to s\nu\overline{\nu}$ transitions

$$\mathcal{L}(b \to s\nu\overline{\nu}) = -\frac{2G_F}{\sqrt{2}}\frac{\alpha_e}{2\pi}V_{ts}^*V_{tb}\left[\sum_{\ell=e,\mu}(C_\nu + \Delta C_{\nu_\ell})\mathcal{O}_{\nu_\ell} + (C_\nu + \Delta C_{\nu_\tau})\mathcal{O}_{\nu_\tau}\right] \tag{6.37}$$

where the operators $\mathcal{O}_{\nu_\ell}$ and $\mathcal{O}_{\nu_\tau}$ are defined starting from those in eq. (C.12) as

$$\mathcal{O}_{\nu_\ell(\nu_\tau)} = \mathcal{O}_9 - \mathcal{O}_{10}|_{\ell=\nu_\ell(\nu_\tau)} \,. \tag{6.38}$$

The shifts of the Wilson coefficients due to NP effects are

$$\Delta C_{\nu_\ell} = \frac{2\pi V_{Q_s}(C_{13}^q - C_{14}^q)}{\alpha_e V_{ts}^*V_{tb}} \,, \qquad \Delta C_{\nu_\tau} = \frac{2\pi V_{Q_s}(C_{11}^q - C_{12}^q)}{\alpha_e V_{ts}^*V_{tb}} \,. \tag{6.39}$$

Since the Lagrangian in eq. (6.37) has a SM-like structure, the differential decay widths for $B \to K^{(*)}\nu\overline{\nu}$ decays can be expressed as

$$\frac{\mathrm{d}\Gamma}{\mathrm{d}q^2}(B \to K^{(*)}\nu\overline{\nu}) = \frac{\mathrm{d}\Gamma}{\mathrm{d}q^2}(B \to K^{(*)}\nu\overline{\nu})^{\text{SM}}\left(\frac{2}{3}\left|1 + \frac{\Delta C_{\nu_\ell}}{C_\nu}\right|^2 + \frac{1}{3}\left|1 + \frac{\Delta C_{\nu_\tau}}{C_\nu}\right|^2\right) \,. \tag{6.40}$$

In the case, the SM spectrum can be be read from eq. (C.19) setting $C_9 = -C_{10} = C_\nu$, $C_S = 0$ and $m_\ell = 0$. Using the SM $C_\nu = -6.35$ [150] and the hadronic form factors in [22], from the experimental bound in [146] we obtain

$$0 < \text{Re}\left(\frac{\Delta C_{\nu_\tau}}{C_\nu}\right) < 2.17 \,, \tag{6.41}$$

in the limit $|\Delta C_{\nu_\ell}| \ll |\Delta C_{\nu_\tau}|$. This implies in turn

$$\text{Re}\left[V_{Q_s}(C_{11}^q - C_{12}^q)\right] < 6.69 \times 10^{-4} \,. \tag{6.42}$$

6.3.5 Leptonic τ decays

$\tau \to \ell\nu\overline{\nu}$

The effective Lagrangian generating $\tau \to \mu\nu\overline{\nu}$ decay amplitudes at the tree level is

$$\mathcal{L}(\tau \to \mu\nu\overline{\nu}) = -\frac{4G_F}{\sqrt{2}}\{(1+2C_{04}^{\ell})(\overline{\nu}_{\tau_L}\gamma^{\lambda}\tau_L)(\overline{\mu}_L\gamma_{\lambda}\nu_{\mu_L}) + V_{L_{\mu}}[(3C_{12}^{\ell} - C_{11}^{\ell})(\overline{\nu}_{\tau_L}\gamma^{\lambda}\tau_L)(\overline{\mu}_L\gamma_{\lambda}\nu_{\tau_L}) + (3C_{14}^{\ell} - C_{13}^{\ell})(\overline{\nu}_{\mu_L}\gamma^{\lambda}\tau_L)(\overline{\mu}_L\gamma_{\lambda}\nu_{\mu_L}) + (C_{14}^{\ell} - C_{13}^{\ell})(\overline{\nu}_{e_L}\gamma^{\lambda}\tau_L)(\overline{\mu}_L\gamma_{\lambda}\nu_{e_L})]\}. \tag{6.43}$$

Since the interacting structure is the same occurring within the SM, the decay width can be simply written as

$$\Gamma(\tau \to \mu\nu\overline{\nu}) = \Gamma^{\rm SM}(\tau \to \mu\nu_{\tau}\overline{\nu}_{\mu}) \times \left|1 + 2C_{04}^{\ell}\right|^2 , \tag{6.44}$$

where $\Gamma^{\rm SM}(\tau \to \mu\nu_{\tau}\overline{\nu}_{\mu})$ is given in [147]. We can now consider the observable $R_{\tau}^{\tau/\ell}$, defined as

$$R_{\tau}^{\tau/\ell_{1,2}} = \frac{\mathcal{B}(\tau \to \ell_{2,1}\nu\overline{\nu})_{\rm exp}/\mathcal{B}(\tau \to \ell_{2,1}\nu\overline{\nu})_{\rm SM}}{\mathcal{B}(\mu \to e\nu\overline{\nu})_{\rm exp}/\mathcal{B}(\mu \to e\nu\overline{\nu})_{\rm SM}} , \tag{6.45}$$

whose value can be extracted from [38]:

$$R_{\tau}^{\tau/\mu} = 1.0020 \pm 0.0030 , \qquad R_{\tau}^{\tau/e} = 1.0058 \pm 0.0030 . \tag{6.46}$$

This allows us to constrain with very good precision $\mathrm{Re}(C_{04}^{\ell})$.

Given the strength of these constraints (that affect a combination of C_i not parametrically suppressed by spurions), in this case it is necessary to take into account also the effect of radiative corrections [144]. The latter are identical for SM and NP amplitudes below the electroweak scale, i.e. they factorise in Eq. (6.44). This implies that we can directly translate the experimental bounds (6.46) into a constraint on $\mathrm{Re}(C_{04}^{\ell})$ renormalised at the electroweak scale:

$$\mathrm{Re}\left[C_{04}^{\ell}\left(M_W\right)\right] = (5 \pm 7) \times 10^{-4} . \tag{6.47}$$

On the contrary, radiative corrections are different for SM and NP amplitudes above the electroweak scale. In particular, a sizeable contribution to $\tau \to \mu\nu_{\tau}\overline{\nu}_{\mu}$ is generated by the semileptonic operators contributing to $R_{D^{(*)}}$. To a first approximation, this effect can be taken into account by the leading contribution to the RG evolution of C_{04}^{ℓ} [144]

$$C_{04}^{\ell}\left(M_W\right) = C_{04}^{\ell}\left(\Lambda\right) + \frac{3y_t^2}{8\pi^2}|V_{tb}|^2\left[C_{02}^{q}\left(\Lambda\right) + V_Q C_{12}^{q}\left(\Lambda\right)\right] \times \left[\log\left(\frac{\Lambda^2}{m_t^2}\right) + \frac{1}{2}\right] . \tag{6.48}$$

Using this result, and setting $\Lambda \approx 1$ TeV, the constrain in eq. (6.21) becomes

$$\mathrm{Re}\left[C_{04}^{\ell}(\Lambda)\right] = -\left(0.79 \pm 0.09_{\tau} \pm 0.2_{R_D}\right) \times 10^{-2} , \tag{6.49}$$

where we have explicitly separated the small error due to eq. (6.47) and the sizable error due to the input value of $C_{02}^{q}(\Lambda)$ or, equivalently, due to $R_{D^{(*)}}$. The fact that we need a non-vanishing value for $C_{04}^{\ell}(\Lambda)$ in order to cancel the large NP contribution generated by $C_{02}^{q}(\Lambda)$ necessarily signals a fine tuning in the EFT. The minimum amount of this fine-tuning is $\approx 10\%$, that is what we deduce comparing the central value of $C_{04}^{\ell}(\Lambda)$ with the error determined by eq. (6.47). The fine-tuning would increase if the central value of $C_{04}^{\ell}(\Lambda)$ were not natural. However, this can be avoided with the power-counting scheme that we will introduce in section 6.4.1.

$\tau \to \ell\bar{\ell}\ell'$

The purely leptonic LFV decays $\tau \to \ell\bar{\ell}\ell'$, which are highly suppressed in the SM, arises naturally in our framework due to the operators $\mathcal{O}_{13}^{\ell}$ and $\mathcal{O}_{14}^{\ell}$ in table 6.4. The corresponding effective Lagrangian is:

$$\begin{aligned}\mathcal{L}(\tau \to \ell^i \ell\bar{\ell}) = -\frac{4G_F}{\sqrt{2}}\Big[&(C_{13}^{\ell} + C_{14}^{\ell})V_L^i(\bar{\ell}_L^i\gamma_\mu\tau_L)(\bar{\ell}_L\gamma^\mu\ell_L) + C_{R2}^{\ell}V_L^i(\bar{\ell}_L^i\gamma_\mu\tau_L)(\bar{\ell}_{jR}\gamma^\mu\ell_R) \\ &+ C_{T2}^{\ell}V_L^i(\bar{\ell}_R\sigma_{\mu\nu}\tau_L)(\bar{\ell}_L^i\sigma^{\mu\nu}\ell_R)\Big].\end{aligned} \tag{6.50}$$

In the $\tau \to \mu e\bar{e}$ case we get

$$\Gamma(\tau \to \mu e\bar{e}) = \left(|C_{13}^{\ell} + C_{14}^{\ell}|^2 + |C_{R2}^{\ell}|^2 + |C_{T2}^{\ell}|^2\right)|V_L|^2\tilde{\Gamma}(\tau \to \mu e\bar{e}) \ , \tag{6.51}$$

where $\tilde{\Gamma}(\tau \to \mu e\bar{e}) = \Gamma(\tau \to \mu\bar{\nu}\nu)$ in the limit $m_e \to 0$. From the experimental bound $\mathcal{B}(\tau \to \bar{e}e\mu)^{\rm exp} < 1.8 \times 10^{-8}$ [146] we obtain

$$|V_L|\sqrt{\left(|C_{13}^{\ell} + C_{14}^{\ell}|^2 + |C_{R2}^{\ell}|^2 + |C_{T2}^{\ell}|^2\right)} < 3.2 \times 10^{-4} \ . \tag{6.52}$$

An almost identical bound is obtained from $\mathcal{B}(\tau \to 3\mu)^{\rm exp} < 2.1 \times 10^{-8}$.

6.3.6 Semi-leptonic LFV transitions

$B \to \tau\bar{\mu}$

The leading contributions to the semi-leptonic LFV $b \to d\tau\mu$ transitions can be computed in terms of the following effective Lagrangian

$$\mathcal{L}^{\rm NP}(b \to d\tau\bar{\mu}) = -\frac{4G_F}{\sqrt{2}}\left(C_{31}^{q} + C_{32}^{q}\right)V_{Q_d}V_L(\bar{d}_L\gamma^\mu b_L)(\bar{\tau}_L\gamma_\mu\mu_L) \ , \tag{6.53}$$

that in the $B \to \tau\mu$ case leads to

$$\Gamma\left(B \to \tau\bar{\mu}\right) = \left(C_{31}^{q} + C_{32}^{q}\right)^2\left|V_Q\right|^2|V_L|^2\,\frac{G_F^2 f_B^2\sqrt{\lambda(m_B^2 + m_\tau^2 + m_\mu^2)}}{8\pi m_B^3}\left[m_B^2\left(m_\tau^2 + m_\mu^2\right) - \left(m_\tau^2 - m_\mu^2\right)^2\right] \ . \tag{6.54}$$

Using $f_B = (207^{+17}_{-9})$ MeV [151] and the current experimental bound $\mathcal{B}(B \to \tau\mu) < 2.2 \times 10^{-5}$ [146] we obtain

$$|C_{31}^{q} + C_{32}^{q}||V_L V_{Q_d}| < 1.8 \times 10^{-3} \ . \tag{6.55}$$

$\tau \to \mu\omega$ and $\tau \to \mu\rho$

Semi-leptonic LFV transitions can occur in τ decays via the following effective Lagrangian

$$\mathcal{L}\left(\tau \to \mu V\right) = -\frac{4G_F}{\sqrt{2}}V_L\left[\left(C_{23}^{q} - C_{24}^{q}\right)\left(\bar{u}_L\gamma^\mu u_L\right) + \left(C_{23}^{q} + C_{24}^{q}\right)\left(\bar{d}_L\gamma^\mu d_L\right)\right]\left(\bar{\tau}_L\gamma_\mu\mu_L\right) \ . \tag{6.56}$$

The two most interesting cases are $V = \rho$ and $V = \omega$, which allow us to constrain separately the Wilson coefficients C_{23}^{q} and C_{24}^{q}. The decay widths of these two processes are:

$$\begin{aligned}\Gamma\left(\tau \to \mu\rho\right) &= \frac{G_F^2}{8\pi}|C_{24}^{q}|^2|V_L|^2 f_\rho^2\,\frac{\sqrt{\lambda(m_\tau^2, m_\rho^2, m_\mu^2)}}{m_\tau^3}\left[(m_\tau^2 - m_\mu^2)^2 + m_\rho^2(m_\tau^2 + m_\mu^2 - 2m_\rho^2)\right] \ , \\ \Gamma\left(\tau \to \mu\omega\right) &= \frac{G_F^2}{8\pi}|C_{23}^{q}|^2|V_L|^2 f_\omega^2\,\frac{\sqrt{\lambda(m_\tau^2, m_\omega^2, m_\mu^2)}}{m_\tau^3}\left[(m_\tau^2 - m_\mu^2)^2 + m_\omega^2(m_\tau^2 + m_\mu^2 - 2m_\omega^2)\right] \ .\end{aligned} \tag{6.57}$$

Using the decay constant for both ω and ρ mesons in [152] and the experimental bounds in [146] we get the following limits

$$|C_{24}^q||V_L| < 1.4 \times 10^{-4} \qquad \text{from} \qquad \mathcal{B}(\tau \to \mu\rho) < 1.8 \times 10^{-8} \,, \tag{6.58}$$

$$|C_{23}^q||V_L| < 3.2 \times 10^{-4} \qquad \text{from} \qquad \mathcal{B}(\tau \to \mu\omega) < 4.7 \times 10^{-8} \,. \tag{6.59}$$

$\Upsilon \to \tau\overline{\mu}$ and $\eta_b \to \tau\overline{\mu}$

As listed in tables 6.2–6.3, in principle LFV decays of $b\bar{b}$ bound states are also possible. The Lagrangian relevant to these processes is

$$\mathcal{L}(b \to b\tau\mu) = -\frac{4G_F}{\sqrt{2}} V_L \left[(C_{21}^q + C_{22}^q) \left(\bar{b}_L \gamma^\mu b_L\right) \left(\overline{\tau}_L \gamma_\mu \mu_L\right) + C_{S3}^q (\bar{b}_L b_R)(\overline{\tau}_R \mu_L) \right] . \tag{6.60}$$

In the $\Upsilon \to \tau\mu$ case we find

$$\Gamma\left(\Upsilon \to \tau\mu\right) = \frac{G_F^2}{24\pi} |C_{21}^q + C_{22}^q|^2 |V_L|^2 f_\Upsilon^2 \frac{\sqrt{\lambda(m_\Upsilon^2, m_\tau^2, m_\mu^2)}}{m_\Upsilon^3} \left[2m_\Upsilon^4 - m_\Upsilon^2 (m_\tau^2 + m_\mu^2) - (m_\tau^2 - m_\mu^2)^2 \right] . \tag{6.61}$$

From the experimental bound $\mathcal{B}(\Upsilon \to \tau\overline{\mu}) < 6 \times 10^{-6}$ [146], using $f_\Upsilon = (684.4 \pm 4.6)$ MeV [152], we get

$$|C_{21}^q + C_{22}^q||V_L| < 0.52 \,. \tag{6.62}$$

The bound in eq. (6.62) is significantly weaker than all LFV bounds discussed so far, despite the stringent experimental limit on $\mathcal{B}(\Upsilon \to \tau\overline{\mu})$. This is trivial consequence of the fact that, contrary to τ and B mesons, the Υ does not decay via weak interactions. It is then easy to verify that the constraints following from the $O(1\%)$ experimental bound on $\mathcal{B}(\eta_b \to \mu\overline{\mu})$ are irrelevant.

6.4 Consistency of the EFT construction

6.4.1 Power-counting scheme

We are now ready to discuss the consistency of the EFT construction for the leading four-fermion operators listed in section 6.2. The constraints on the Wilson coefficients obtained by comparison with data, as discussed in section 7.4, are summarised in table 6.5. Assuming a non-vanishing value for the combination of C_i contributing to $R_{D^{(*)}}$, the construction can be considered consistent if we are able to justify, via appropriate re-scaling of the fields (motivated by dynamical assumptions), the strong suppression of all the other terms in table 6.5.

Inspired by the explicit dynamical models proposed in the literature, we assume a generic framework where the NP sector is coupled preferentially to third generation SM fermions (i.e. the $\mathcal{G}_{\text{flavour}}$ singlets), while the coupling to the light SM fermions are suppressed by small mixing angles (as suggested e.g. in [58, 117]). As a result of this hypothesis, we re-scale the light SM fermion fields as following

$$Q_L^i \to \epsilon_L^q Q_L^i \,, \qquad L^i \to \epsilon_L^\ell L^i \,, \qquad E_R^i \to \epsilon_R^\ell E_R \,, \tag{6.63}$$

every time these fields appear in bilinear combinations without spurions. Furthermore, given the underlying dynamics is potentially different in quark and lepton sectors, we introduce the flavour-blind re-scaling factor $r_{q\ell}$, which allow us to enhance (suppress) the relative weight of leptonic (four-quark) operators vs. semi-leptonic ones. Finally, as far as the size of the spurions are concerned, we perform the following re-scaling:

$$|V_Q| \to \epsilon_q' |V_{ts}| \qquad\qquad |V_L| \to \epsilon_\ell' \,. \tag{6.64}$$

Process	Combination	Constraint	Parametric scaling	Order of magnitude
$R_{D^{(*)}}$	$\text{Re}\left(C^q_{02} + V_{Q_s} C^q_{12} \frac{V_{cs}}{V_{cb}}\right)$	0.060 ± 0.015	1	10^{-1}
$B \to D\mu\nu_\mu$	$\text{Re}\left(C^q_{04} + V_{Q_s} C^q_{14} \frac{V_{cs}}{V_{cb}}\right)$	$-(0.8 \pm 2.5) \times 10^{-2}$	$\left(\epsilon^\ell_L\right)^2$	10^{-2}
$\tau \to \mu\nu\overline{\nu}$	$\text{Re}\left(C^\ell_{04}\right)$	$-(7.9 \pm 2.2) \times 10^{-3}$	$\left(\epsilon^\ell_L\right)^2 r_{q\ell}$	$10^{-2}\, r_{q\ell}$
$R^{\tau/\mu}_{sd}$	$\text{Re}\left[C^q_{08} - C^q_{06} + (C^q_{14} - C^q_{12})\lvert V_{Q_s} V_{ub}/V_{us}\rvert\right]$	$(0.7 \pm 0.4) \times 10^{-2}$	$\left(\epsilon^q_L\right)^2$	$\leq 10^{-2}$
$\tau \to \mu ee$ $\tau \to 3\mu$	$\lvert V_L\rvert \times \left(\lvert C^\ell_{13} + C^\ell_{14}\rvert^2 + \right.$ $\left. + C^\ell_{R2}\rvert^2 + \lvert C^\ell_{T2}\rvert^2\right)^{1/2}$	$\leq 3.2 \times 10^{-4}$	$\epsilon'_\ell \left(\epsilon^\ell_{L,R}\right)^2 r_{q\ell}$	$10^{-3} \left(\frac{\epsilon'_\ell}{0.1}\right) r_{q\ell}$
$\tau \to \rho\mu$	$\lvert C^q_{24}\rvert \lvert V_L\rvert$	$\leq 1.4 \times 10^{-4}$	$\epsilon'_\ell (\epsilon^q_L)^2$	$\leq 10^{-3} \left(\frac{\epsilon'_\ell}{0.1}\right)$
$\tau \to \omega\mu$	$\lvert C^q_{23}\rvert \lvert V_L\rvert$	$\leq 3.2 \times 10^{-4}$	$\epsilon'_\ell (\epsilon^q_L)^2$	$\leq 10^{-3} \left(\frac{\epsilon'_\ell}{0.1}\right)$
$B \to K\nu\overline{\nu}$	$\text{Re}(C^q_{11} - C^q_{12})$	$< -1.6 \times 10^{-2}$	ϵ'_q	$10^{-2} \left(\frac{\epsilon'_q}{0.1}\right)$
$B^0 - \overline{B}^0$	$\lvert C^{qq}_{01} + C^{qq}_{02}\rvert$	$\leq 0.42 \times 10^{-3}$	$\left(\epsilon'_q\right)^2 r^{-1}_{q\ell}$	$10^{-3} \left(\frac{\epsilon'_q}{0.1}\right)^2 r^{-1}_{q\ell}$
$B \to K^{(*)}\mu\overline{\mu}$	$\text{Re}\left(C^q_{13} + C^q_{14}\right)$ $\text{Re}\left(C^q_{R5}\right)$	$-(0.8 \pm 0.3) \times 10^{-3}$ $-(0.4 \pm 0.3) \times 10^{-3}$	$\epsilon'_q \left(\epsilon^\ell_L\right)^2$ $\epsilon'_q \left(\epsilon^\ell_R\right)^2$	$10^{-3} \left(\frac{\epsilon'_q}{0.1}\right)$
$B_d \to \tau\mu$	$\lvert C^q_{31} + C^q_{32}\rvert$	$\leq 4.5 \times 10^{-2}$	$\epsilon'_q \epsilon'_\ell$	$10^{-3} \left(\frac{\epsilon'_q \epsilon'_\ell}{10^{-2}}\right)$

Table 6.5: Most relevant constraints on the Wilson coefficients, as obtained in section 7.4. In the last two columns we report the parametric scaling of the (leading) Wilson coefficients, according to the rules defined in section 6.4.1, and the order of magnitude following from the overall EFT scale and the choice of the ϵ_i reported in Eqs. (6.65)–(6.66).

As discussed in section 6.2, in absence of a specific alignment of the $U(2)_q$ singlets to left-handed bottom or top quarks, we expect $|V_Q| = O(|V_{ts}|)$. The parameter ϵ'_q is thus a measure of the tuning in the (quark) flavour space. On the contrary, V_L parametrises the unknown size of the spurion in the lepton sector.

By construction, the only combination in table 6.5 without ϵ_i suppression is the one contributing to $R_{D^{(*)}}$. This allows us to determine the overall scale of the EFT. From the central value of the $R_{D^{(*)}}$ anomaly we deduce

$$\Lambda \approx (0.06)^{-1/2} v_F \approx 700 \text{ GeV} \tag{6.65}$$

or a natural size of $O(10^{-1})$ for the C_i in absence of ϵ_i factors.

A non-vanishing NP contribution to $R_{D^{(*)}}$ necessarily implies a non-vanishing value for $C^\ell_{04}(\Lambda)$ to cancel NP contributions in $\tau \to \mu\nu\overline{\nu}$. As discussed in Section 6.3.5, this fact necessarily implies a fine-tuning of at least 10%, obtained by comparing error and central value of $C^\ell_{04}(\Lambda)$. This fine-tuning does not increase if the central value of $C^\ell_{04}(\Lambda)$ is natural, that is what we obtain setting $\left(\epsilon^\ell_L\right)^2 r_{q\ell} = O(10^{-1})$. More generally, we find that all entries in table 6.5 have the correct order of magnitude for the following choice of parameters

$$\epsilon^\ell_L \approx 0.3\ , \qquad \epsilon^q_L \leq 0.3\ , \qquad \epsilon'_\ell \leq 0.1\ , \tag{6.66}$$

and

$$\epsilon'_q \approx 0.1 \ , \qquad r_{q\ell} = O(1) \ . \tag{6.67}$$

Using these reference values we determine the numerical scaling reported in the last column of table 6.5. Setting $\epsilon'_\ell = 0.1$, that is the preferred value for a natural solution of the R_K anomaly (see section 6.4.3), a residual fine-tuning appears in the operators contributing to LFV τ decays; however, this tuning is less severe that the one occurring in C^ℓ_{04} and the experimental bounds can easily be satisfied setting a slightly smaller value for ϵ^q_L.

A second significant source of tuning is the one implied by the smallness of ϵ'_q, that is a necessary consequence of both $\Delta F = 2$ and $b \to s$ FCNC constraints. Given the different parametric dependence of these constraints from ϵ^q_L and $r_{q\ell}$, is not possible to obtain a good fit to all data for larger values of ϵ'_q. This implies that the EFT requires a non-negligible tuning in flavour space, namely a $O(10\%)$ alignment of the $U(2)_q$ singlets to left-handed bottom quarks.

We finally address the issue of the stability of this modified power counting scheme under radiative corrections. Being not associated to spurions of the flavour symmetry, the value of ϵ^ℓ_L and ϵ^q_L cannot be arbitrarily small. Indeed, even if we do not introduce operators with light quarks at the heavy scale Λ, these are radiatively generated at lower scales (as pointed out in Ref. [144]). On general grounds, for $\Lambda \sim 1$ TeV, we expect the construction to be radiatively stable if

$$\left(\epsilon^{q(\ell)}_L\right)^2 > \frac{N_C}{16\pi^2} \log(\Lambda^2/m_t^2) \approx 7\% \ . \tag{6.68}$$

We have explicitly verified that, adopting the numerical values in eq. (6.66), loop contributions compete with initial conditions only in the case of C^ℓ_{04}, while they are numerically subleading for the other combinations of Wilson coefficients in table 6.5.

6.4.2 Constraints from direct searches

Given the low value of the effective scale in eq. (6.65), a relevant question to address is the compatibility of this EFT construction with the absence of NP signals from high-p_T searches of resonances decaying into a $\tau\overline{\tau}$ pair [143].

Let us fist consider the problem from a pure EFT point of view. In this case, the bounds from $\sigma(pp \to \tau\overline{\tau} + X)$ can be expressed as bounds on the (un-suppressed) operator

$$\Delta\mathcal{L}_{bb\tau\tau} = -\frac{1}{\Lambda^2} \left(\overline{b}_L\gamma_\mu b_L\right)\left(\overline{\tau}_L\gamma_\mu\tau_L\right) \ . \tag{6.69}$$

According to the analysis of [143], where a recasting different ATLAS searches for $\tau^+\tau^-$ resonances has been performed, the present bound on the effective scale of this operator is $\Lambda > 0.62\,\text{TeV}$. Since this value is slightly below the value in eq. (6.65), it indicates that the NP construction we are considering is not trivially excluded by direct searches (although it should soon manifest itself with non-standard signals at high energies).

On the other hand, we stress that a naïve application of the EFT to analyse high-p_T constraints is highly questionable. Indeed at LHC energies the possible mediators responsible for the effective interaction in eq. (6.69) can be produced on-shell, with a significant change in the signal/background ratio depending on the specific mediator involved (such as color-less vectors or leptoquarks) and, most important, depending on the width of such mediator. This fact has already been noted in Ref. [58, 143], where the connections between low- and high-energy data, for models addressing the $B-$physics anomalies, have been analysed employing specific simplified models. According to the detailed analysis of Ref. [143], present bounds on $pp \to \tau\overline{\tau} + X$ do not rule out UV completions for the EFT we are considering, provided the corresponding TeV mediators have sufficiently large decay widths, as expected in strongly interacting theories. The only case that it is in clear tension with $pp \to \tau\overline{\tau} + X$ data is the case of narrow ($\Gamma/M < 10\%$) color-less vector mediators (i.e. Z' and W').

6.4.3 Processes starting at $O(|V_L|^2)$

So far we restricted the attention to processes with at most one V_L spurion. A complete analysis of all the operators appearing at $O(|V_L|^2)$ is beyond the scope of our analysis. However, there are two interesting LFU ratios receiving leading contributions at $O(|V_L|^2)$ that is worth to analyse to further tests the consistency of the EFT: $R_{K^{(*)}}$, and a similar μ/e ratio in $\tau \to \ell\nu\overline{\nu}$ decays.

The LFU ratio $R_{K^{(*)}}$

The $O(|V_L|^2)$ operators generating a breaking of LFU at the tree-level in $b \to s\ell\overline{\ell}$ decays have the form

$$\mathcal{O}_{13}^{q-2} = \left(\overline{q}_{3L}\gamma^\mu Q^i V_{Qi}^\dagger\right)\left(V_{Lj}\overline{L}_j\gamma_\mu L^i V_{Li}^\dagger\right) , \tag{6.70}$$

$$\mathcal{O}_{14}^{q-2} = \left(\overline{q}_{3L}\sigma^a\gamma^\mu Q^i V_{Qi}^\dagger\right)\left(V_{Lj}\overline{L}_j\sigma_a\gamma_\mu L^i V_{Li}^\dagger\right) . \tag{6.71}$$

Using the notations of section 6.3.4, these would generate the following non-universal shift in the $\ell = \mu$ case

$$\Delta C_9^\mu = -\Delta C_{10}^\mu = \frac{|V_Q|\left[\left(C_{13}^{q-2}\right)_\mu + \left(C_{14}^{q-2}\right)_\mu\right]}{\frac{\alpha}{2\pi}|V_{ts}^* V_{tb}|} = \left(0.8\times 10^3\right)\times O\left[\epsilon'_q(\epsilon'_\ell)^2\right] , \tag{6.72}$$

where on the r.h.s. we have indicated the parametric scaling as defined in the previous Section. The central value of $R_K^{\rm exp}$ can be obtained for $\Delta C_9^\mu = -\Delta C_{10}^\mu \approx -1.0$ [49]. As can be seen, this value can naturally be obtained for $\epsilon'_q \approx \epsilon'_\ell \approx 0.1$, i.e. in absence of further fine-tuning compared to what determined from the leading operators.

LFU violations in $\tau \to \ell\nu\overline{\nu}$ decays

At $O(|V_L|^2)$ one can generate a violation of μ/e universality in $\tau \to \ell\nu\overline{\nu}$, which is experimentally strongly constrained. The relevant operator is

$$\mathcal{O}_{04}^{\ell-2} = \left(\overline{\ell}_{3L}\sigma^a\gamma^\mu\ell_{3L}\right)\left(V_{Lj}\overline{L}_j\sigma_a\gamma_\mu L^i V_{Li}^\dagger\right) , \tag{6.73}$$

that leads to

$$\frac{\Gamma(\tau\to\mu\nu\overline{\nu})}{\Gamma(\tau\to e\nu\overline{\nu})} = \left[\frac{\Gamma(\tau\to\mu\nu\overline{\nu})}{\Gamma(\tau\to e\nu\overline{\nu})}\right]_{\rm SM}\times\left|1+2C_{04}^{\ell-2}|V_L|^2\right|^2 . \tag{6.74}$$

Using $\Gamma(\tau\to\mu\nu\overline{\nu})^{\rm exp}/\Gamma(\tau\to e\nu\overline{\nu})^{\rm exp} = 0.9762\pm 0.0028$ and $\Gamma(\tau\to\mu\nu\overline{\nu})_{\rm SM}/\Gamma(\tau\to e\nu\overline{\nu})^{\rm SM} = 0.9726$ we find

$$\mathrm{Re}\left(C_{04}^{\ell-2}|V_L|^2\right) = (0.95\pm 0.70)\times 10^{-3} , \tag{6.75}$$

which is perfectly consistent with the power-counting expectation $\mathrm{Re}\left(C_{04}^{\ell-2}|V_L|^2\right) = 10^{-3}$ obtained for $\epsilon'_\ell \approx 0.1$.

6.4.4 Upper bound on $|V_{L_1}/V_{L_2}|$

We conclude this Section with a naïve estimate of the maximal value of $|V_{L_1}/V_{L_2}|$ (or the electron component of the lepton spurion), which can be regarded as a tuning in the lepton-flavour space of the EFT. Assuming $|V_L| = \epsilon'_\ell = O(0.1)$, as required to explain the $R_{K^{(*)}}$ anomaly, the $|V_{L_1}/V_{L_2}|$ ratio is strongly bounded by $\mu \to e$ LFV processes. Employing the power-counting scheme defined in section 6.4.1, the bounds dictated by the present experimental bounds on

$\mu \to e$ conversion in Nuclei and $\mathcal{B}(\mu \to 3e)$ turn out to be very similar. Focusing on the latter, the power-counting scheme implies

$$\mathcal{A}(\mu \to 3e) \propto (\epsilon'_\ell)^2 (\epsilon^\ell_L)^2 \left(\frac{V_{L_1}}{V_{L_2}}\right)^2 \ . \tag{6.76}$$

Taking into account also the overall-suppression scale we get

$$\mathcal{B}(\mu \to 3e) \approx 10^{-8} \times \left(\frac{\epsilon'_\ell}{10^{-1}}\right)^4 \left(\frac{\epsilon^\ell_L}{0.3}\right)^4 \left|\frac{V_{L_1}}{V_{L_2}}\right|^2 < 1.0 \times 10^{-12} \ , \tag{6.77}$$

where the last inequality corresponds to the present experimental constraint [146]. As can be seen, for $|V_{L_1}/V_{L_2}| < 0.01$ the experimental bound is satisfied. This ratio is significantly smaller than the corresponding $|V_{Q_d}/V_{Q_s}|$ ratio in the quark sector, but it is not unnatural given the observed hierarchies in the charged lepton mass matrix ($m_e/m_\mu \approx 5 \times 10^{-3}$).

6.5 Conclusions

In this chapter we have analysed the consistency of the $R_{D^{(*)}}$ and $R_{K^{(*)}}$ anomalies with all available low-energy observables, in the context of an EFT based on the $U(2)_q \times U(2)_\ell \times \mathcal{G}_R$ flavour symmetry defined in eq. (6.1). The $R_{D^{(*)}}$ anomaly, if interpreted as a signal of NP, necessarily points toward a low effective scale for the EFT, slightly below 1 TeV. As a result, despite the MFV-like protection implied by the flavour symmetry, the latter is not enough to guarantee a natural consistency of the EFT with the tight constraints from various low-energy processes (most notably precision measurements in B and τ physics). However, as we have shown, a consistent picture for all low-energy observables can be obtained under the additional dynamical assumption that the NP sector is coupled preferentially to third generation SM fermions (or the singlets of the flavour symmetry).

In the EFT context, this dynamical assumptions can be realised in general terms via the rescaling of fields (and operators) that we have identified in section 6.4.1. This rescaling of the field leads to a modified power counting, and the resulting EFT turns out to be rather coherent. Still some tuning of the EFT parameters is necessary in order to satisfy constraints from processes involving light quarks and leptons. More precisely, we have identified two main sources of tuning, both quantifiable around the 10% level. The first one is an alignment in (quark) flavour space: the flavour singlets need to be closely aligned to left-handed bottom quarks in order to satisfy the constraints from $B_{s(d)}$ mixing. The second one is a $O(10\%)$ cancellation of two independent terms in order to justify the absence of NP effects in $\mathcal{B}(\tau \to \mu\nu\overline{\nu})$. Modulo these two tunings, the EFT allows us to accommodate non-vanishing NP contributions to $R_{D^{(*)}}$ and $R_{K^{(*)}}$ at the level of present anomalies, and contributions to the other observables below (or within) current uncertainties for natural values of the other free parameters, as summarised in table 6.5.

The analysis of all existing bounds presented in section 6.4 can also be used to identify which are the most promising observables to obtain further evidences of NP in this framework. In addition to the model-independent confirmation of the anomalies in other B decays (both charged and netural-current transitions), the EFT construction has allowed us to identify there particularly interesting sets of observables in τ decays.

I. LFV τ decays. The branching ratios of both purely leptonic and semi-leptonic LFV τ decays can easily exceed the 10^{-9} level.

II. Precision measurements of $\mathcal{B}(\tau \to \ell\nu\overline{\nu})$. Violations of μ/e universality and, more generally, deviations from the SM predictions in $\mathcal{B}(\tau \to \ell\nu\overline{\nu})$ are expected at the few per-mil level.

III. The determination of $|V_{us}|$ from τ decays. Due to the breaking of LFU, the $|V_{us}|$ determination from τ vs. K decays can differ at the 1% level.

While the first two categories have already been widely discussed in the literature (see e.g. Ref. [58, 144]), the last one has been identified for the first time by the present analysis. In all these cases NP effects are expected just below current experimental sensitivities. Improved measurements of these observables could therefore provide a very valuable tool to provide further evidences or to falsify this framework in the near future.

Chapter 7

Probing Lepton Flavour Universality with $K \to \pi\nu\overline{\nu}$ decays

7.1 Introduction

The pattern of deviations from the SM presented in section 2.4 have triggered a series of theoretical speculations about possible NP interpretations. In particular, attempts to provide a combined/coherent explanation for both charged- and neutral-current anomalies have been presented in Ref. [57–59,125,127,128,133,134,136–140,142,153,154]. One of the puzzling aspects of present anomalies is that they have been seen only in semileptonic B decays and are quite large compared to the corresponding SM amplitudes. On the contrary, no evidences of deviations from the SM have been seen so far in the precise (per-mil) tests of LFU performed in semileptonic K and π decays, in purely leptonic τ decays, and in electroweak precision observables. The most natural assumption to address this apparent paradox is the hypothesis that the NP responsible for the breaking of LFU is coupled mainly to the third generation of quarks and leptons, with some small (but non-negligible) mixing with the light generations [58, 117, 153]. Within this paradigm, a motivated class of models are those based on a $U(2)_q \times U(2)_\ell$ flavour symmetry acting on the light generations of SM fermions [11, 141], that turns out to be quite successful in addressing these anomalies while satisfying all existing bounds [153].

If NP is coupled mainly to third generation fermions, it is very difficult to detect it in K decays, which necessarily imply a transition among light quarks and, in most cases, also imply light leptons in the final states. The only exception in this respect is provided by $K \to \pi\nu\overline{\nu}$ decays, which involve third-generation leptons in the final state – the τ neutrinos. As we will show in the following, this fact implies that $K \to \pi\nu\overline{\nu}$ decays are a very sensitive probe of the most motivated models addressing the hints of LFU violations in B physics, as already pointed out in Ref. [125, 155] in specific models. On the one hand, $\mathcal{B}(K \to \pi\nu\overline{\nu})$ could exhibit $O(1)$ deviations from the SM predictions in a large area of the parameter space of such models. On the other hand, even in absence of large deviations, improved measurements (or constraints) on $\mathcal{B}(K \to \pi\nu\overline{\nu})$ would provide a very valuable model-building information.

The chapter is organised as follows: in section 7.2 we briefly review the main formulae to evaluate $\mathcal{B}(K \to \pi\nu\overline{\nu})$ within and beyond the SM. In section 7.3 we discuss the Effective Field Theory (EFT) approach to LFU violations based on the $U(2)_q \times U(2)_\ell$ flavour symmetry and, in that framework, we analyse the possible impact on $K \to \pi\nu\overline{\nu}$ decays. In section 7.4 we focus in particular on the expected correlations between $K \to \pi\nu\overline{\nu}$, the $R_{D^{(*)}}$ anomaly, and $B \to K^{(*)}\nu\overline{\nu}$, which turn out to be closely related observables (impact and constraints from other observables are briefly mentioned at the end of the section). The results are summarised in the Conclusions.

7.2 The $K \to \pi\nu\overline{\nu}$ decays

Here we briefly summarise the main steps to predict $\mathcal{B}(K^+ \to \pi^+\nu\overline{\nu})$ and $\mathcal{B}(K_L \to \pi^0\nu\overline{\nu})$ within and beyond the SM, taking into account possible violations of LFU. The effective Lagrangian describing short-distance FCNC interactions of the type $d_L^i \to d_L^j\nu\overline{\nu}$ is

$$\mathcal{L}_{\text{eff}} = \frac{4G_F}{\sqrt{2}}\frac{\alpha}{2\pi}V_{ti}^*V_{tj}C_{ij,\ell}\left(\overline{d}_L^i\gamma_\mu d_L^j\right)(\overline{\nu}_\ell\gamma^\mu\nu_\ell)\,, \tag{7.1}$$

where α is the fine-structure constant, and V_{ij} are the elements of the CKM matrix. For $s_L \to d_L\nu_\ell\overline{\nu}_\ell$, the Wilson coefficient in the SM reads

$$C_{sd,\ell}^{\text{SM}} = -\frac{1}{s_w^2}\left(X_t + \frac{V_{cs}^*V_{cd}}{V_{ts}^*V_{td}}X_c^\ell\right), \tag{7.2}$$

where X_t and X_c^ℓ are the loop functions for the top and charm contributions, respectively, and s_w is the sine of the weak mixing angle.

The branching ratio for $K^+ \to \pi^+\nu\overline{\nu}$ in the SM, summing over the three neutrino species, can be written as [156]

$$\mathcal{B}(K^+ \to \pi^+\nu\overline{\nu})_{\text{SM}} = \frac{\kappa_+(1+\Delta_{\text{em}})}{3}\sum_{\ell=e,\mu,\tau}\left|\frac{V_{ts}^*V_{td}}{\lambda^5}X_t + \frac{V_{cs}^*V_{cd}}{\lambda}\left(\frac{X_c^\ell}{\lambda^4} + \delta P_c^\ell\right)\right|^2, \tag{7.3}$$

where λ is the Cabibbo angle, $\kappa_+ = (5.173 \pm 0.025)\times 10^{-11}(\lambda/0.225)^8$, $\Delta_{\text{em}} = -0.003$ is a QED correction [157], and $\delta P_{c,u}^\ell \approx 0.04 \pm 0.02$ is the long-distance contribution from light quark loops [158]. The numerical value of the loop functions are $X_t = 1.481 \pm 0.009$ and $P_c = \frac{1}{3}\sum_\ell X_c^\ell/\lambda^4 = 0.365 \pm 0.012$ [159].[1]

Within the SM the CP-violating decay $K_L \to \pi^0\nu\overline{\nu}$ is lepton-flavour universal. However, in order to take into account possible violation of LFU beyond the SM, we can conveniently write its branching ratio as

$$\mathcal{B}(K_L \to \pi^0\nu\overline{\nu})_{\text{SM}} = \frac{\kappa_L}{3}\sum_{\ell=e,\mu,\tau}\text{Im}\left(\frac{V_{ts}^*V_{td}}{\lambda^5}X_t\right)^2, \tag{7.4}$$

where $\kappa_L = (2.231 \pm 0.013)\times 10^{-10}(\lambda/0.225)^8$.

In the class of NP models we will consider, the short-distance contributions to $K \to \pi\nu\overline{\nu}$ amplitudes are still left-handed but lepton flavour non-universal. The general expressions for the branching ratios in presence of such non-standard contributions can simply be obtained replacing the function X_t in eq. (7.3) and eq. (7.4) by

$$X(C_{sd,\ell}^{\text{NP}}) = X_t + C_{sd,\ell}^{\text{NP}}\,s_w^2, \tag{7.5}$$

where $C_{sd,\ell}^{\text{NP}}$ is the new physics contribution to the Wilson coefficient in eq. (7.1).

Using the most recent determinations of the input parameters, the SM predictions for the two branching ratios are [161]

$$\mathcal{B}(K^+ \to \pi^+\nu\overline{\nu})_{\text{SM}} = (8.4 \pm 1.0)\times 10^{-11}, \tag{7.6}$$

$$\mathcal{B}(K_L \to \pi^0\nu\overline{\nu})_{\text{SM}} = (3.4 \pm 0.6)\times 10^{-11}. \tag{7.7}$$

[1] The NLO values of the individual X_c^ℓ can be found e.g. in [160].

The dominant source of error in eq. (7.6) and eq. (7.7) comes from the uncertainty in the CKM matrix elements, and from the charm contribution.

The current experimental bounds are [146]

$$\mathcal{B}(K^+ \to \pi^+ \nu\overline{\nu})_{\rm exp} = 17.3^{+11.5}_{-10.5} \times 10^{-11}, \tag{7.8}$$

$$\mathcal{B}(K_L \to \pi^0 \nu\overline{\nu})_{\rm exp} \leq 2.6 \times 10^{-8} \qquad (90\%\,{\rm CL}). \tag{7.9}$$

The branching ratio of the charged mode is expected to be measured with a precision of 10%, relative to the SM prediction, by the on-going NA62 experiment at CERN [162]. A search for the challenging neutral mode at the SM level is the ultimate goal of the KOTO experiment at JPARC [163].

7.3 The EFT approach to LFU violations based on $U(2)_q \times U(2)_\ell$

As already anticipated, the B-physics anomalies observed so far point toward NP coupled mainly to the third generation of SM fermions with some small (but non-negligible) mixing with the light generations. In addition, all effects observed so far are well compatible with NP only involving left-handed currents. Left-handed four-fermion operators are also the most natural candidates to build a connection between anomalies in charged and neutral current semileptonic processes. These observations have led to identify the EFT approach based on the $U(2)_q \times U(2)_\ell$ flavour symmetry as a a convenient framework (both successful and sufficiently general) to analyse B-physics anomalies and discuss possible correlations with other low-energy observables [58, 142, 153].

The EFT is based on the assumption that the first two generations of left-handed quarks and leptons transform as doublets of $U(2)_q \times U(2)_\ell$ while the third generation and the right-handed fermions are singlets

$$Q \equiv (q^1_L, q^2_L) \sim (2,1), \qquad q^3_L \sim (1,1), \tag{7.10}$$

$$L \equiv (\ell^1_L, \ell^2_L) \sim (1,2), \qquad \ell^3_L \sim (1,1). \tag{7.11}$$

Motivated by the observed pattern of the quark mass matrices, it is further assumed that the leading breaking terms of this flavour symmetry are two spurion doublets, $V_q \sim (2,1)$ and $V_\ell \sim (1,2)$, that give rise to the mixing between the third generation and the other two [11] (additional sub-leading breaking terms are needed to generate the masses of the light generations and the corresponding mixing structures [11]).

This symmetry and symmetry-breaking pattern implies $|V_{3i}| \approx |V_{i3}| \approx V_q^{(i)}$, up to model-dependent parameters of order one. As a starting point, it is convenient to work in the down-quark mass basis, where the left-handed singlet and doublet fields read

$$q^b_L = \begin{pmatrix} V^*_{j3} u^j_L \\ b_L \end{pmatrix}, \qquad Q^i_L = \begin{pmatrix} V^*_{ji} u^j_L \\ d^i_L \end{pmatrix}, \qquad (i = 1,2). \tag{7.12}$$

In this basis, one can set

$$V_q \propto (V^*_{td}, V^*_{ts}) \equiv \hat{V}_q, \tag{7.13}$$

with the proportionality constant real and of order one. In the lepton sector, the size of the spurion V_ℓ is a free parameter, since it has no direct connection to the lepton Yukawa couplings.[2] Given that processes involving electrons are SM-like to a very high accuracy, we will assume $V_\ell = (0, \epsilon_\ell)$ with $|\epsilon_\ell| \ll 1$.

[2] It is worth stressing that in the lepton sector a different breaking pattern, i.e. a leading breaking controlled by a triplet of $U(2)_\ell$, rather than a doublet, is also a viable option.

The choice of the down-quark mass basis to identify singlets and doublets of the (quark) flavour symmetry is somehow arbitrary. In particular, the singlets do not need to be aligned with bottom quarks. On general grounds we expect

$$q_{3L} \equiv q_L^b + \theta_q e^{i\phi_q}\, \hat{V}_q^\dagger \cdot Q_L \ , \tag{7.14}$$

were $\theta_q e^{i\phi_q}$ is the complex $O(1)$ parameter that controls this possible mis-alignment: $\theta_q \to 0$ in case of alignment to the down-quark mass basis, while $\theta_q e^{i\phi_q} \to 1$ in the case of alignment to the up-quark mass basis. Given the absence of deviations from the SM in CP-violating observables, it is natural to expect ϕ_q to be close to 0 or π (θ_q is defined to be real and positive). Similarly, in the lepton sector we define

$$\ell_{3L} \equiv \ell_L^3 + V_\ell^\dagger \cdot L \ . \tag{7.15}$$

We shall describe NP effects through an EFT based on the following hypotheses:

1. the field content below the NP scale $\Lambda > (G_F)^{-1/2}$ is the SM one;
2. the Lagrangian is invariant under the flavour symmetry $U(2)_q \times U(2)_\ell$, apart from the breaking induced by the spurions V_q and V_ℓ;
3. NP is directly coupled only to left-handed quark and lepton singlets in flavour space (i.e. only operators containing only q_{3L} or ℓ_{3L} fields are affected by tree-level matching conditions at the NP scale Λ).

Given these assumptions, we can identify only two independent operators of dimension six affected by NP and contributing to semileptonic decays at the tree level, namely the electroweak singlet and triplet current-current interactions,

$$\mathcal{L}_{\text{eff}} = -\frac{1}{\Lambda^2}(\overline{q}_{3L}\gamma_\mu\sigma^a q_{3L})(\overline{\ell}_{3L}\gamma^\mu\sigma^a\ell_{3L}) - \frac{c_{13}}{\Lambda^2}(\overline{q}_{3L}\gamma_\mu q_{3L})(\overline{\ell}_{3L}\gamma^\mu\ell_{3L}) \ . \tag{7.16}$$

The normalisation of the triplet operator in (7.16) has been chosen in order to generate a constructive interference with the SM in charged-current amplitudes, as suggested by $b \to c\tau\overline{\nu}_\tau$ data. The overall-scale of this operator defines the NP scale Λ, while c_{13} denotes the ratio between the singlet and triplet Wilson coefficients.

7.4 Physical observables

7.4.1 The $R_{D^{(*)}}$ anomaly

The averages of the τ/ℓ universality ratios ($\ell = \mu, e$) in $b \to c$ transitions measured by BaBar [39], Belle [35] and LHCb [36], are

$$R_{D^*} \equiv \frac{\mathcal{B}(B \to D^*\tau\overline{\nu}_\tau)_{\text{exp}}/\mathcal{B}(B \to D^*\tau\overline{\nu}_\tau)_{\text{SM}}}{\mathcal{B}(B \to D^*\ell\overline{\nu}_\ell)_{\text{exp}}/\mathcal{B}(B \to D^*\ell\overline{\nu}_\ell)_{\text{SM}}} = 1.23 \pm 0.07\,, \tag{7.17}$$

$$R_D \equiv \frac{\mathcal{B}(B \to D\tau\overline{\nu}_\tau)_{\text{exp}}/\mathcal{B}(B \to D\tau\overline{\nu}_\tau)_{\text{SM}}}{\mathcal{B}(B \to D\ell\overline{\nu}_\ell)_{\text{exp}}/\mathcal{B}(B \to D\ell\overline{\nu}_\ell)_{\text{SM}}} = 1.35 \pm 0.16\,. \tag{7.18}$$

These two results can be combined into a single observable that parametrises the violation of LFU in charged currents (assuming a purely left-handed structure):

$$R_{D^{(*)}} = 1.24 \pm 0.07. \tag{7.19}$$

Only the triplet operator in eq. (7.16) contributes to $b \to c\tau\overline{\nu}_\tau$ decays via the following effective interaction

$$\mathcal{L}^{\text{NP}}_{b\to c\tau\overline{\nu}_\tau} = -\frac{2}{\Lambda^2}\Big[V_{cb} + \theta_q e^{-i\phi_q}(V_{cs}V_{ts}^* + V_{cd}V_{td}^*)\Big](\overline{c}_L\gamma^\mu b_L)(\overline{\tau}_L\gamma_\mu\nu_\tau)\,. \tag{7.20}$$

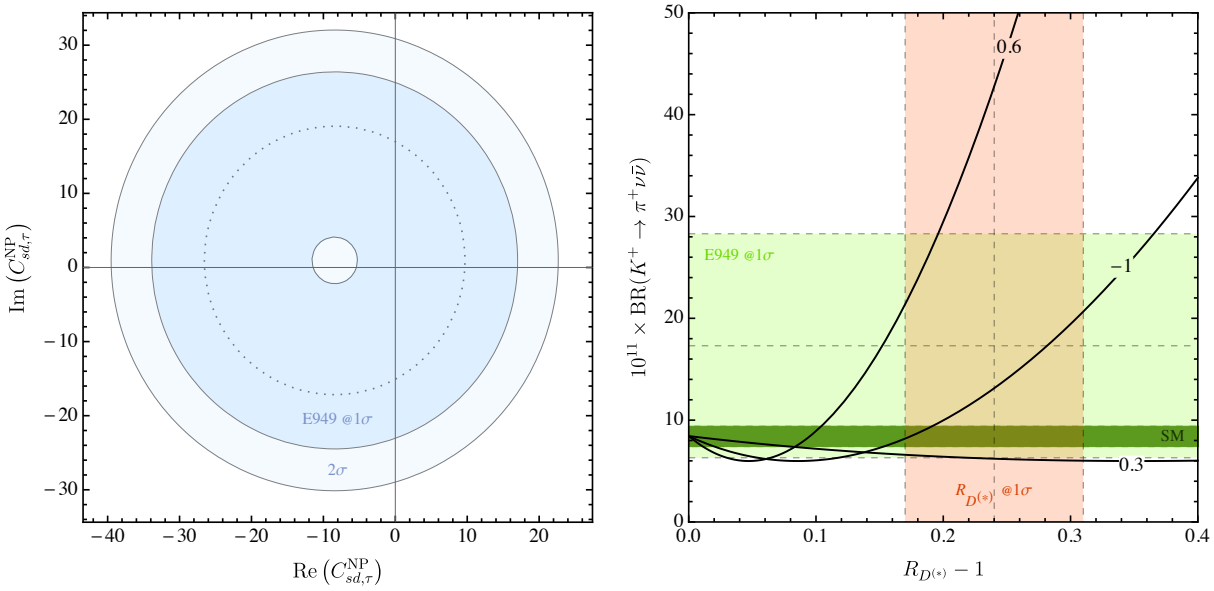

Figure 7.1: Left: allowed range for the real and imaginary parts of the NP Wilson coefficient $C^{\mathrm{NP}}_{sd,\tau}$. Right: correlation between $\mathcal{B}(K^+ \to \pi^+ \nu\overline{\nu})$ and $R_{D^{(*)}}$ for different values of the parameter θ_q (with $\phi_q = c_{13} = 0$); the coloured regions are the experimental measurements at $1\,\sigma$, the dark green band is the SM prediction.

The branching ratio for the processes $B \to D^{(*)}\tau\overline{\nu}$ is then modified as follows by the triplet operator (using CKM unitarity and setting $V_{tb} = 1$)

$$\mathcal{B}(B \to D^{(*)}\tau\overline{\nu}) = \mathcal{B}(B \to D^{(*)}\tau\overline{\nu})_{\mathrm{SM}} \left|1 + R_0 \left(1 - \theta_q e^{-i\phi_q}\right)\right|^2 \tag{7.21}$$

where we have defined

$$R_0 = \frac{1}{\Lambda^2}\frac{1}{\sqrt{2}G_F}. \tag{7.22}$$

In the limit where we neglect sub-leading terms suppressed by the small leptonic spurion, NP does not affect $\mathcal{B}(B \to D^{(*)}\ell\overline{\nu})$ for the light leptons. This allows us to fix the overall scale of NP via the relation

$$\left[R^{\tau/\mu}_{D^{(*)}} - 1\right] \approx 2R_0(1 - \theta_q \cos\phi_q) = 0.24 \pm 0.07\,. \tag{7.23}$$

The reference effective scale of NP, obtained for $\theta_q \to 0$, is $\Lambda_0 \approx 700\,\mathrm{GeV}$. Notice that higher scales of NP can be obtained if $\theta_q = O(1)$ and $\cos\phi_q < 0$, obtaining in this way a better compatibility with constraints from direct searches [143] and electroweak precision tests [144,164]. On the other hand, the NP contribution to $R_{D^{(*)}}$ vanishes in the case of alignment of the flavour symmetry to up-type quarks ($\theta_q \to 1, \phi_q \to 0$).

7.4.2 LFU violating contributions to $K \to \pi\nu\overline{\nu}$

The operators eq. (7.16) contribute to $s \to d\nu\overline{\nu}$ transitions through the term proportional to the V_q spurion in eq. (7.14),

$$\mathcal{L}^{\mathrm{NP}}_{s\to d\nu\overline{\nu}} = \frac{1 - c_{13}}{\Lambda^2}\theta_q^2\, V^*_{ts}V_{td}(\overline{s}_L\gamma_\mu d_L)(\overline{\nu}_\tau\gamma_\mu\nu_\tau). \tag{7.24}$$

Neglecting, in first approximation, the NP contribution to $s \to d\nu_\ell\overline{\nu}_\ell$ ($\ell = e, \mu$) amplitudes, we can write

$$\begin{aligned}
\mathcal{B}(K^+ \to \pi^+\nu\overline{\nu}) &= 2\mathcal{B}(K^+ \to \pi^+\nu_e\overline{\nu}_e)_{\rm SM} + \mathcal{B}(K^+ \to \pi^+\nu_\tau\overline{\nu}_\tau)_{\rm SM}\left|1 + \frac{R_0\,\theta_q^2(1-c_{13})}{(\alpha/\pi)C_{sd,\tau}^{{\rm SM},eff}}\right|^2 , \\
\mathcal{B}(K_L \to \pi^0\nu\overline{\nu}) &= 2\mathcal{B}(K_L \to \pi^0\nu_e\overline{\nu}_e)_{\rm SM} + \mathcal{B}(K_L \to \pi^0\nu_\tau\overline{\nu}_\tau)_{\rm SM}\left|1 - \frac{R_0\,\theta_q^2(1-c_{13})}{(\alpha/\pi)(X_t/s_w^2)}\right|^2 ,
\end{aligned} \tag{7.25}$$

where $C_{sd,\tau}^{{\rm SM},eff} \approx -8.5 \times e^{0.11i}$ includes also the long-distance contributions of eq. (7.3).

The current allowed range from the experimental result eq. (7.8) for the real and imaginary parts of the Wilson coefficient $C_{sd,\tau}^{\rm NP}$ in a generic NP model is shown in figure 7.1 (left). In our case this translates into the constraint

$$|R_0\,\theta_q^2(1-c_{13})| \lesssim 0.1 \ . \tag{7.26}$$

As expected, the constraint vanishes in the limit $c_{13} \to 1$, where triplet and singlet NP contributions to $s \to d\nu\overline{\nu}$ amplitudes cancel each other. However, it must be stressed that there is no symmetry reason to expect $c_{13} = 1$. Even if $c_{13} = 1$ holds as tree-level matching condition in the EFT (such as e.g. in the lepto-quark models of Ref. [125, 154]), one expects $c_{13} \neq 1$ beyond the tree level [125]. For $c_{13} \neq 1$ the result in eq. (7.26) implies a severe constraint on the maximal value of θ_q, assuming eq. (7.23) is satisfied. For $|c_{13} - 1| \ll 1$ one finds $|\theta_q| \lesssim 1/|c_{13} - 1|$.

Expressing R_0 in terms of the measured value of $R_{D^{(*)}}$ (and the unknown parameters θ_q and ϕ_q) we can rewrite the previous expression as a relation between $R_{D^{(*)}}$ and $\mathcal{B}(K \to \pi\nu\overline{\nu})$ as follows

$$\mathcal{B}(K^+ \to \pi^+\nu\overline{\nu}) \approx \mathcal{B}(K^+ \to \pi^+\nu\overline{\nu})_{\rm SM}\Big[1 - 14\,[R_{D^{(*)}} - 1]\theta_q^2 f_q + 165\,[R_{D^{(*)}} - 1]^2\theta_q^4 f_q^2\Big] , \tag{7.27}$$

where $f_q \equiv (1 - c_{13})/(1 - \theta_q \cos\phi_q)$, and where we neglected higher orders in R_0 from eq. (7.23). This correlation is shown in figure 7.1 (right), for different values of the free parameters. As can be seen, for $\theta_q = O(1)$ the solution of the $R_{D^{(*)}}$ anomaly can imply sizeable deviations in $\mathcal{B}(K^+ \to \pi^+\nu\overline{\nu})$ compared to the SM. The dependence of $\mathcal{B}(K^+ \to \pi^+\nu\overline{\nu})$ on the parameter θ_q, with $R_{D^{(*)}}$ fixed as in eq. (7.23), is shown by the blue lines in Figure 7.2 (right) for the two values of the phase $\phi_u = 0$ and π, and for different values of the singlet contribution c_{13}. Notice that for $c_{13} > 1$ the branching ratio is always enhanced with respect to the SM prediction.

The neutral mode $K_L \to \pi^0\nu\overline{\nu}$ is purely CP-violating and constrains only the imaginary part of the amplitude. The present bound on the NP Wilson coefficient from eq. (7.9) is roughly 10 times weaker than the one from the K^+ mode.

7.4.3 Correlations between $B \to K^{(*)}\nu\overline{\nu}$ and $K \to \pi\nu\overline{\nu}$

Also $b \to s\nu\overline{\nu}$ transitions are described by the Lagrangian eq. (7.1), with $C_{bs}^{\rm SM} = -X_t/s_w^2 \approx -6.4$. Notice that the charm contribution is not relevant in this case. Both charged and neutral $B \to K^{(*)}\nu\overline{\nu}$ decays set bounds on the New Physics Wilson coefficient, with the stronger constraints coming from the B^+ modes. In the SM, the branching ratios are [165]

$$\mathcal{B}(B^+ \to K^+\nu\overline{\nu})_{\rm SM} = 3.94 \times 10^{-6}\left|\frac{V_{ts}V_{tb}^*}{0.04}\right|^2 , \tag{7.28}$$

$$\mathcal{B}(B^+ \to K^{+*}\nu\overline{\nu})_{\rm SM} = 9.82 \times 10^{-6}\left|\frac{V_{ts}V_{tb}^*}{0.04}\right|^2 , \tag{7.29}$$

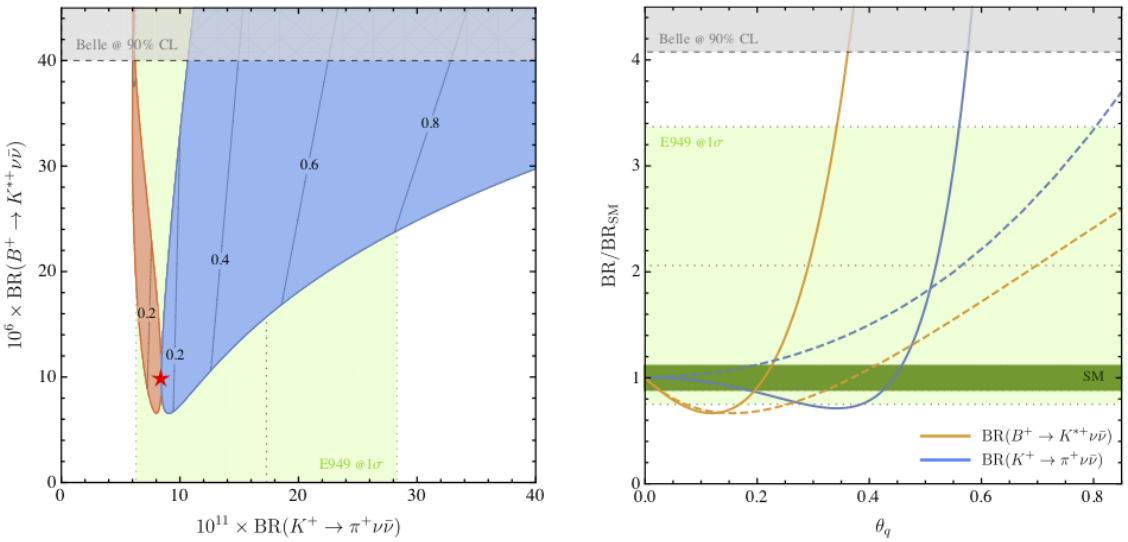

Figure 7.2: Left: correlation of $\mathcal{B}(K^+ \to \pi^+\nu\bar{\nu})$ with $\mathcal{B}(B^+ \to K^{*+}\nu\bar{\nu})$, having imposed $R_{D^{(*)}} = 1.25$. The red (blue) colored region is for $c_{13} = 0$ ($c_{13} = 2$). We also show isolines of θ_q, and the red star is the SM point. Right: branching ratios for $K^+ \to \pi^+\nu\bar{\nu}$ and $B^+ \to K^{*+}\nu\bar{\nu}$, normalised to the SM values, as functions of θ_q. The solid (dashed) lines correspond to $c_{13} = 0$, $\phi_q = 0$ ($c_{13} = 2$, $\phi_q = \pi$).

to be compared with the experimental bounds [146]

$$\mathcal{B}(B^+ \to K^+\nu\bar{\nu}) \leq 1.7 \times 10^{-5} \quad @\ 90\%\ \mathrm{CL}\ , \tag{7.30}$$

$$\mathcal{B}(B^+ \to K^{+*}\nu\bar{\nu}) \leq 4.0 \times 10^{-5} \quad @\ 90\%\ \mathrm{CL}\ . \tag{7.31}$$

In the presence of the operators of eq. (7.16) the branching ratios are modified as follows

$$\mathcal{B}(B \to K^{(*)}\nu\bar{\nu}) = \mathcal{B}(B \to K^{(*)}\nu\bar{\nu})_{\mathrm{SM}} \left[\frac{2}{3} + \frac{1}{3}\left|1 - \frac{\pi s_w^2 R_0}{\alpha X_t}\theta_q e^{i\phi_q}(1 - c_{13})\right|^2\right] . \tag{7.32}$$

As for $K \to \pi\nu\bar{\nu}$, we can obtain a direct connection to the charged-current anomaly expressing R_0 in terms of $R_{D^{(*)}}$:

$$\mathcal{B}(B \to K^{(*)}\nu\bar{\nu}) \approx \mathcal{B}(B \to K^{(*)}\nu\bar{\nu})_{\mathrm{SM}}\Big(1 - 21[R_{D^{(*)}} - 1]\theta_q \cos\phi_q f_q + 320[R_{D^{(*)}} - 1]^2\theta_q^2 f_q^2\Big). \tag{7.33}$$

Figure 7.2 (right) shows the dependence of $\mathcal{B}(B^+ \to K^{*+}\nu\bar{\nu})$ on θ_q, with $R_{D^{(*)}}$ fixed to the central value of the experimental measurement, and for two different values of ϕ_q and c_{13}.

The deviations from the SM expectations in the two FCNC neutrino modes are closely correlated, as described by the following relation

$$\frac{\Delta\mathcal{B}(K^+ \to \pi^+\nu\bar{\nu})}{\Delta\mathcal{B}(B \to K^{(*)}\nu\bar{\nu})} \approx \frac{2}{3} \times \frac{\theta_q}{\cos\phi_q} \times \frac{1 - 12\,[R_{D^{(*)}} - 1]\theta_q^2 f_q}{1 - 15[R_{D^{(*)}} - 1]\,\frac{\theta_q f_q}{\cos\phi_q}}\,, \tag{7.34}$$

where $\Delta\mathcal{B} = \frac{\mathcal{B} - \mathcal{B}_{\mathrm{SM}}}{\mathcal{B}_{\mathrm{SM}}}$, and as illustrated in figure 7.2. Notice that for small θ_q this correlation does not depend on the measured value of $R_{D^{(*)}}$. The constraints from $B \to K^{(*)}\nu\bar{\nu}$ can severely limit the deviations in $K \to \pi\nu\bar{\nu}$. This fact is well known in the literature, independently of

the relation with the LFU B anomalies, see e.g. [166, 167]. If $c_{13} < 1$, the NP contributions interfere constructively with the SM amplitude in the first branching ratio, and destructively in the second one. As a consequence, in this case $\mathcal{B}(K^+ \to \pi^+ \nu\overline{\nu})$ is always suppressed, with deviations of up to -30% with respect to the SM value. The opposite is true when $c_{13} > 1$. Also, the constraints are more stringent when $\cos\phi_q$ is positive, since in this case the effective scale of new physics is lower. For negative $\cos\phi_q$ and $c_{13} > 1$, in particular, the constraint from $B \to K^{(*)}\nu\overline{\nu}$ becomes irrelevant, and large deviations can be expected in $\mathcal{B}(K^+ \to \pi^+\nu\overline{\nu})$ (within the limits of eq. (7.8)).

7.4.4 Constraints and connections to other observables

$b \to s\ell^+\ell^-$. FCNC processes that involve the light generations of leptons are suppressed by the spurion V_ℓ in our framework. While LFU violation in these modes is a general prediction following from eq. (7.15), the exact size of these effects depends on the unknown parameter ϵ_ℓ (and, more generally, by the assumption on the breaking of the $U(2)_\ell$ lepton flavour symmetry). The NP contributions to the Wilson coefficients C_9 and C_{10} of the semileptonic $b \to s\mu^+\mu^-$ Lagrangian

$$\mathcal{L}_{\text{eff}}^{b\to s\mu\mu} = \frac{4G_F}{\sqrt{2}}\frac{\alpha}{4\pi}V_{tb}^* V_{ts}\left[C_{9,\mu}(\bar{b}_L\gamma_\mu s_L)(\overline{\mu}\gamma^\mu\mu) + C_{10,\mu}(\bar{b}_L\gamma_\mu s_L)(\overline{\mu}\gamma^\mu\gamma_5\mu)\right] \tag{7.35}$$

read

$$C_{9,\mu}^{\text{NP}} = -C_{10,\mu}^{\text{NP}} = -\frac{\pi}{\alpha}R_0\theta_q e^{i\phi_q}(1+c_{13})|\epsilon_\ell|^2\,. \tag{7.36}$$

Global fits of these Wilson coefficients, performed after the recent measurement of the LFU ratio R_{K^*} [43], in the case of NP coupled to left-handed currents only, yields $C_{9,\mu}^{\text{NP}} = -C_{10,\mu}^{\text{NP}} = -0.64 \pm 0.18$ [41, 48, 52, 54, 168]. From this result, fixing the overall scale of NP from eq. (7.23), it follows that $|\epsilon_\ell|\,(1+c_{13}) \approx 0.1$ up to an $O(1)$ factor depending on θ_q and ϕ_q. Since the sign of C_9^{NP} must be negative to fit the $b \to s\ell\overline{\ell}$ anomalies, it follows that $(1-c_{13})\cos\phi_q > 0$.

$b \to s\tau^+\tau^-$. FCNC decays of B mesons with a $\tau^+\tau^-$ pair in the final state arise at leading order in the breaking of $U(2)_q \times U(2)_\ell$. This implies that these processes can be directly related both to the $R_{D^{(*)}}$ anomalies, and to the two neutrino modes discussed above. The current experimental limits on $\mathcal{B}(B \to K\tau^+\tau^-)$ are four orders of magnitude larger than the corresponding SM prediction (which lies in the 10^{-7} range). The Belle II experiment is expected to improve these limits by at least one order of magnitude, reaching the 10^{-4} level [169]. While the value predicted in the SM would still be out of reach, this sensitivity could be interesting in the NP framework introduced above. The relevant NP Wilson coefficient are $C_{9,\tau}^{\text{NP}} = -C_{10,\tau}^{\text{NP}} = C_{9,\mu}^{\text{NP}}/|\epsilon_\ell|^2$, and the branching ratio depends quadratically on $R_0(1+c_{13})$ in the limit where the NP contribution is large. Setting $R_{D^{(*)}}$ to the central value in eq. (7.23), and imposing the constraints on θ_q from $\mathcal{B} \to K^{(*)}\nu\overline{\nu}$ and $K \to \pi\nu\overline{\nu}$, one gets an enhancement of a factor $10^2 \div 10^3$ in $\mathcal{B}(B \to K\tau^+\tau^-)$ if $\left|\frac{1-c_{13}}{1+c_{13}}\right| \lesssim 20\%$ (which is a rather natural choice of parameters). Finally, it is interesting to note that the observation of $b \to s\tau^+\tau^-$ transitions, together with $s \to d\nu\overline{\nu}$ and $b \to s\nu\overline{\nu}$, would allow to fix the three dimensionless parameters c_{13}, θ_q, and ϕ_q entering the Lagrangian eq. (7.16), thus completely determining the leading free parameters of the EFT.

$\tau \to K\nu$. The $s \to u$ analogue of $B \to D^{(*)}\tau\overline{\nu}$ is the tau decay $\tau \to K\nu$, which is generated at tree-level in the SM, and gets a contribution from the charged-current interaction eq. (7.16). The total branching ratio in presence of NP can be written as

$$\mathcal{B}(\tau \to K\nu) = \mathcal{B}(\tau \to K\nu)_{\text{SM}}\left|1 - R_0\frac{V_{ub}V_{ts}}{\lambda}\theta_q(e^{i\phi} - \theta_q)\right|^2\,. \tag{7.37}$$

The measured value is $\mathcal{B}(\tau \to K\nu)_{\rm exp} = (6.9 \pm 0.1) \times 10^{-3}$, which has to be compared with the SM prediction $\mathcal{B}(\tau \to K\nu)_{\rm SM} = (7.1 \pm 0.1) \times 10^{-3}$. This translates into a loose bound on the scale of NP [$R_0\theta_q(1-\theta_q) \lesssim 20$ for $\phi_q = 0$].

Loop effects. The running from the scale Λ to the electroweak scale, starting from the NP semileptonic Lagrangian eq. (7.16), does generate non-vanishing contributions to four-quark and four-lepton operators. The contributions to $K - \overline{K}$ and $B_s - \overline{B}_s$ mixing, as well as to flavour-changing $Zq\overline{q}$ interactions, are suppressed at least by the τ mass, and turn out to be several orders of magnitude below present experimental constraints.

It is on the other hand known that running effects due to quark loops, leading to purely leptonic operators [144,164], are potentially more problematic because of precise constraints from leptonic τ decays. In concrete models, additional UV contributions to the same effective operators will arise from the matching at the scale Λ. These contributions can help satisfying the τ decay constraints, but can also constitute a problem for meson mixing. On general grounds, satisfying all the constraints in a concrete UV completion that incorporates both the $b \to c\tau\overline{\nu}$ and $b \to s\ell^+\ell^-$ anomalies is not straightforward. However, as shown in [153], this result can be achieved with a moderate tuning of parameters. Given the model-dependence of the radiative constraints, we do not take them into account in the present analysis whose main focus are semileptonic decays.

7.5 Conclusions

Recent B-physics data hints toward violations of Lepton Flavour Universality in charged- and neutral-current semileptonic processes. The most natural explanation of these phenomena, if both will be confirmed as evidences of physics beyond the SM, is the hypothesis of a new interaction in the TeV range that couples mainly to third-generation fermions. If a CKM-like relation connects NP effects in B and K physics, it is natural to expect sizeable deviations from the SM in $K \to \pi\nu\overline{\nu}$ decays, which are the only $s \to d$ transitions that involve third-generation leptons in the final state.

To quantify possible NP effects in $K \to \pi\nu\overline{\nu}$ decays in sufficiently general terms, being motivated by present B-physics anomalies, we have considered an EFT based on the hypothesis of a $U(2)_q \times U(2)_\ell$ flavour symmetry acting on the light generations of left-handed fermions, broken in the quark sector by the small CKM-like spurion V_q connecting third and light generations (and similarly broken by a small spurion V_ℓ in the lepton sector). We further assumed that NP is coupled only to the left-handed third generation flavour-singlets (q_{3L} and ℓ_{3L}). Because of the freedom in the choice of the flavour basis, the spurions $V_{q,\ell}$ can enter the definition of the flavour singlets with an arbitrary mixing parameter of order one. The latter control the communication of NP effects from processes with third-generation fermions only, to processes with light generations. This set-up is not the most general one compatible with the $U(2)_q \times U(2)_\ell$ flavour symmetry, but it covers a wide class of the most motivated explicit models so far proposed to address B-physics anomalies.

In this framework, we focused our attention to semileptonic transitions involving only τ leptons and τ neutrinos. These processes are completely determined by four real parameters: the overall scale of the new interactions Λ, the two model-dependent real (mixing) parameters θ_q and ϕ_q defining the (quark) flavour basis, and the relative strength of the electroweak-triplet and -singlet NP interactions c_{13}. The measurement of the LFU ratios $R_{D^{(*)}}$ can be used to fix the NP scale Λ in terms of θ_q and ϕ_q. This allows in turn to study the neutrino FCNC transitions $K \to \pi\nu\overline{\nu}$ and $B \to K^{(*)}\nu\overline{\nu}$, as well as $B \to K^{(*)}\tau^+\tau^-$, as functions of the three remaining parameters naturally expected to be of $O(1)$.

We have shown that, for natural values of the free parameters, sizeable and closely correlated deviations from the SM of both neutrino modes are expected. The electroweak triplet operator alone necessarily causes a suppression of $\mathcal{B}(K^+ \to \pi^+ \nu\overline{\nu})$, due to the interference of NP with the SM amplitude which is always destructive. This suppression could be as large as 30%, relative the SM value. If, on the other hand, also an electroweak singlet interaction is present, arbitrary modifications of $\mathcal{B}(K^+ \to \pi^+ \nu\overline{\nu})$ are possible. The strongest constraint on the allowed size of these deviations comes from the present bounds on $\mathcal{B}(B \to K^{(*)} \nu\overline{\nu})$ which, however, do not exclude $O(1)$ enhancements in $\mathcal{B}(K^+ \to \pi^+ \nu\overline{\nu})$, as illustrated in Figure 7.2.

Order of magnitude enhancements of $b \to s\tau^+\tau^-$ compared to the SM are possible in this class of NP models. However, these transitions are very challenging from the experimental point of view. In principle, the combined measurement of $R_{D^{(*)}}$, $\mathcal{B}(K^+ \to \pi^+ \nu\overline{\nu})$, $\mathcal{B}(B \to K^{(*)} \nu\overline{\nu})$, and $\mathcal{B}(B \to K\tau^+\tau^-)$ would allow to completely determine the leading parameters of the EFT. The correlation with other observables is less straightforward: violations of μ/e universality in $b \to s\ell\overline{\ell}$ transitions are a natural prediction of this framework; however, their size and the correlation with NP effects in the neutrino modes are controlled by additional free parameters.

Summarising, $K \to \pi\nu\overline{\nu}$ decays could be significantly affected by the non-standard LFU-violating interactions hinted by present B-physics data. The forthcoming measurement of $\mathcal{B}(K^+ \to \pi^+ \nu\overline{\nu})$ by the NA62 experiment at CERN will provide an important insight on this class of NP models. The general expectation is a sizeable deviation from the SM, that, however, could result also into a significant suppression. Should a deviation from the SM prediction be observed in this channel, its correlation with NP effects in $\mathcal{B}(B \to K^{(*)} \nu\overline{\nu})$ and, possibly, $\mathcal{B}(B \to K\tau^+\tau^-)$, would allow to reveal the flavour structure of this new interaction.

Chapter 8

A three-site gauge model for flavour hierarchies and flavour anomalies

8.1 Introduction

A common origin of the two set of anomalies presented in section 2.4 is not obvious, but is very appealing from the theoretical point of view. Severals attempts to provide a combined explanation of the two effects have been presented in the recent literature [57–59, 125, 127, 128, 133, 134, 136, 137, 139, 140, 142, 153, 154, 170–173]. Among them, a class of particularly motivated models are those based on TeV-scale new physics (NP) coupled mainly to the third generation of SM fermions, with subleading effects on the light generations controlled by an approximate $\mathrm{U}(2)_\mathrm{Q}\times\mathrm{U}(2)_\mathrm{L}$ flavour symmetry [11]. As recently shown in [174] (see also [58,125,153]), an EFT) based on this flavour symmetry allows us to account for the observed semileptonic LFU anomalies taking into account the tight constraints from other low-energy data [144, 164]. Moreover, the EFT fit singles out the case of a vector leptoquark (LQ) field $U_\mu \sim (\mathbf{3},\mathbf{1})_{2/3}$, originally proposed in [125], as the simplest and most successful framework with a single TeV-scale mediator (taking into account also the direct bounds from high-energy searches [143]).

While the results of Ref. [174] are quite encouraging, the EFT solution and the simplified models require an appropriate UV completion. In particular, the vector LQ mediator could be a composite state of a new strongly interacting sector, as proposed in [125, 142], or a massive gauge boson of a spontaneously broken gauge theory, as proposed in [175–177]. In this work we follow the latter direction.

Ultraviolet completions for the vector LQ mediator U_μ naturally point toward variations of the Pati-Salam (PS) gauge group, PS=$\mathrm{SU}(4)\times\mathrm{SU}(2)_\mathrm{L}\times\mathrm{SU}(2)_\mathrm{R}$ [178], that contains a massive gauge field with these quantum numbers. The original PS model does not work since the (flavour-blind) LQ field has to be very heavy in order to satisfy the tight bounds from the coupling to the light generations. An interesting proposal to overcome this problem has been put forward in Ref. [176], with an extension of the PS gauge group and the introduction of heavy vector-like fermions, such that the LQ boson couples to SM fermions only as a result of a specific mass mixing between exotic and SM fermions.

A weakness of most of the explicit SM extensions proposed so far to address the B-physics anomalies, including the proposal of Ref. [176], is the fact that the flavour structure of the models is somehow ad hoc. This should be contrasted with the EFT solution of Ref. [174], which seems to point toward a common origin between flavour anomalies and the hierarchies of the SM Yukawa couplings. In this work we try to address these problems together, proposing a model that is not only able to address the anomalies, but is also able to explain in a natural way the observed flavour hierarchies.

The model we propose is a three-site version of the original PS model. At high energies, the gauge group is $\mathrm{PS}^3 \equiv \mathrm{PS}_1 \times \mathrm{PS}_2 \times \mathrm{PS}_3$, where each PS group acts on a single fermion family. The spontaneous symmetry breaking (SSB) down to the SM group occurs in a series of steps characterized by different energy scales, whichf allow us to decouple the heavy exotic fields coupled to the first two generations at very high energies. As a result, the gauge group controlling TeV-scale dynamics contains a LQ field that is coupled mainly to the third generation (see figure 8.1). A key aspect of this construction is the hypothesis that electroweak symmetry breaking (EWSB) occurs via a Higgs field sitting only on the third-generation site: this assumption allows us to derive the hierarchical structure of the Yukawa couplings as a consequence of the hierarchies of the vacuum expectation values (VEVs) controlling the breaking of the initial gauge group down to the SM. In particular, the $\mathrm{U}(2)_\mathrm{Q} \times \mathrm{U}(2)_\mathrm{L}$ global flavour symmetry appears as a subgroup of an approximate flavour symmetry of the system emerging at low energies [$\mathrm{U}(2)^5$]. Last but not least, the localization of the Higgs field on the third-generation site provides a natural screening mechanism for the Higgs mass term against the heavy energy scales related to the symmetry breaking of the heavy fields coupled to the light generations.

8.2 The model

The gauge symmetry of the model holding at high energies is $\mathrm{PS}^3 \equiv \mathrm{PS}_1 \times \mathrm{PS}_2 \times \mathrm{PS}_3$, where

$$\mathrm{PS}_i = \mathrm{SU}(4)_i \times [\mathrm{SU}(2)_\mathrm{L}]_i \times [\mathrm{SU}(2)_\mathrm{R}]_i \ . \tag{8.1}$$

The fermion content is the same as in the SM plus three right-handed neutrinos, such that each fermion family is embedded in left- and right-handed multiplets of a given PS_i subgroup:

$$\Psi_L^{(i)} \sim (\mathbf{4}, \mathbf{2}, \mathbf{1})_i \,, \qquad \Psi_R^{(i)} \sim (\mathbf{4}, \mathbf{1}, \mathbf{2})_i \,. \tag{8.2}$$

The subindex $i = 1, 2, 3$ denotes the site that, before any symmetry breaking, can be identified with the generation index.

The SM gauge group is a subgroup of the diagonal group, $\mathrm{PS}_{\mathrm{diag}} = \mathrm{PS}_{1+2+3}$, which corresponds to the original PS gauge group. The SSB breaking $\mathrm{PS}^3 \to$ SM occurs in a series of steps at different energy scales (see figure 8.1) with appropriate scalar fields acquiring non-vanishing VEVs, as described below.

I. High-scale *vertical breaking* [$\mathrm{PS}_1 \to \mathrm{SM}_1$].
At some heavy scale, $\Lambda_1 > 10^3$ TeV, the PS_1 group is broken to SM_1, where

$$\mathrm{SM}_i = \mathrm{SU}(3)_i \times [\mathrm{SU}(2)_\mathrm{L}]_i \times [\mathrm{U}(1)_\mathrm{Y}]_i \ , \tag{8.3}$$

by the VEV of a scalar field $\Sigma_1 \sim (\mathbf{4}, \mathbf{1}, \mathbf{2})_1$, charged only under PS_1 (or localized on the first site). Via this breaking 9 gauge fields with exotic quantum numbers (6 LQ fields, a $W_R^\pm$, and a Z', all coupled only to the first generation) acquire a heavy mass and decouple.

II. *Horizontal breaking* 1–2 [$\mathrm{SM}_1 \times \mathrm{PS}_2 \to \mathrm{SM}_{1+2}$].
Gauge fields on different sites are broken to their diagonal subgroup via appropriate *link* fields, or scalar bilinears. On both links (1–2 and 2–3) we introduce the following set of link fields

$$\begin{aligned} \Phi_{ij}^L &\sim (\mathbf{1}, \mathbf{2}, \mathbf{1})_i \times (\mathbf{1}, \overline{\mathbf{2}}, \mathbf{1})_j \ , \\ \Phi_{ij}^R &\sim (\mathbf{1}, \mathbf{1}, \mathbf{2})_i \times (\mathbf{1}, \mathbf{1}, \overline{\mathbf{2}})_j \ , \\ \Omega_{ij} &\sim (\mathbf{4}, \mathbf{2}, \mathbf{1})_i \times (\overline{\mathbf{4}}, \overline{\mathbf{2}}, \mathbf{1})_j \ , \end{aligned} \tag{8.4}$$

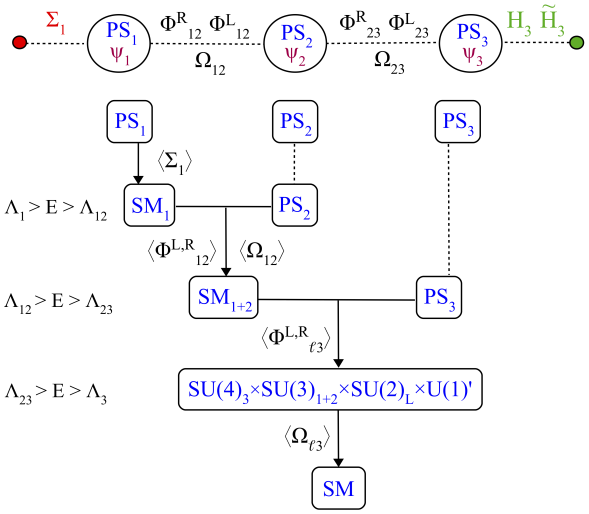

Figure 8.1: Moose diagram of the model (up) and symmetry breaking sequence.

such that

$$\begin{aligned}
\langle \Phi^L_{ij} \rangle \neq 0 &\Rightarrow [\mathrm{SU}(2)_\mathrm{L}]_i \times [\mathrm{SU}(2)_\mathrm{L}]_j \to [\mathrm{SU}(2)_\mathrm{L}]_{i+j} \ , \\
\langle \Phi^R_{ij} \rangle \neq 0 &\Rightarrow [\mathrm{SU}(2)_\mathrm{R}]_i \times [\mathrm{SU}(2)_\mathrm{R}]_j \to [\mathrm{SU}(2)_\mathrm{R}]_{i+j} \ , \\
\langle \Omega_{ij} \rangle \neq 0 &\Rightarrow \begin{cases} \mathrm{SU}(4)_i \times \mathrm{SU}(4)_j \to \mathrm{SU}(4)_{i+j} \\ [\mathrm{SU}(2)_\mathrm{L}]_i \times [\mathrm{SU}(2)_\mathrm{L}]_j \to [\mathrm{SU}(2)_\mathrm{L}]_{i+j} \end{cases} .
\end{aligned}$$

At a scale $\Lambda_{12} < \Lambda_1$ the 1–2 link fields acquire a VEV. As a result, the vertical breaking occurring on the first site is mediated also to the second site, and the gauge symmetry is reduced to $\mathrm{SM}_{1+2} \times \mathrm{PS}_3$.

Thanks to this second breaking, 9 exotic gauge fields coupled mainly to the second generation, and 12 SM-like gauge fields coupled in a non-universal way to the first two families acquire a heavy mass and can be integrated out. Below the scale Λ_{12} the residual dynamical gauge sector is invariant under a global $\mathrm{U}(2)^5$ flavour symmetry acting on the first two generations of SM fermions[1].

At this stage there is still no local coupling between the fermions of the first two generations and the scalar fields sitting on the third site (H_3 and $\widetilde{H}_3$) that contain the SM Higgs. In other words, we have not yet generated an effective Yukawa coupling for the light generations.

The hierarchy between Λ_1, Λ_{12}, and the VEVs of the 1–2 link fields does not need to be specified. The lower bound on the lowest of such scales, that we fix to be 10^3 TeV, is set by the tight limits on flavour-changing neutral currents involving the first two generations (most notably K–$\overline{K}$ and D–$\overline{D}$ mixing [179], and $K_L \to \mu e$ [180]). With this choice, we can ignore the effect of $d \geq 6$ effective operators generated at this scale.

III. *Horizontal breaking* 2–3 [$\mathrm{SM}_{1+2} \times \mathrm{PS}_3 \to \mathrm{SM}$].
The scale characterizing the dynamics of the 2–3 link fieds is $\Lambda_{23} \sim 10^2$ TeV. We assume a specific hierarchy among this scale and the VEVs of the link fields:

$$\Lambda_{23} > \langle \Phi^{L,R}_{23} \rangle > \langle \Omega_{23} \rangle \equiv \Lambda_3 \sim 1 \text{ TeV} \ . \tag{8.5}$$

[1] At $E < \Lambda_{12}$ mass terms for the right-handed neutrinos of the first two generations are allowed. We thus integrate out also $\nu^R_{1,2}$ remaining with 5 independent species of massless fermions charged under SM_{1+2}.

This hierarchy is a key ingredient to generate the correct pattern for the Yukawa couplings (discussed in detail below) and, at the same time, address the flavour anomalies.
At energies $\langle \Phi_{23}^{L,R} \rangle > E > \Lambda_3$ we can decouple a $W_L^{\pm}$, a $W_R^{\pm}$, and two Z' fields with mass of $\mathcal{O}(10\text{ TeV})$, that are too heavy to be probed at colliders and have no impact on flavour physics because of the $\mathrm{U}(2)^5$ flavour symmetry.

Below Λ_{23}, the dynamical gauge group is reduced to

$$\mathcal{G} = \mathrm{SU}(4)_3 \times \mathrm{SU}(3)_{1+2} \times \mathrm{SU}(2)_\mathrm{L} \times \mathrm{U}(1)' \,. \tag{8.6}$$

This symmetry group is structurally similar to the one proposed in [176], but its action on SM fermions is different: with the exception of $\mathrm{SU}(2)_\mathrm{L}$, all the other subgroups are flavour non-universal. In particular, the action of $\mathrm{U}(1)'$ coincides with the SM hypercharge on the first two families and with T_R^3 on the third family. The final breaking $\mathcal{G} \to \text{SM}$ gives rise to 15 massive gauge bosons with mass of $\mathcal{O}(1\text{ TeV})$: 6 LQ fields, 8 colorons (i.e. a color octet), and a Z'. By construction, the LQ is coupled only to the third generation, as desired in order to address the flavour anomalies.

IV. Low-scale *vertical breaking* [EWSB].
The electroweak symmetry breaking is achieved by an effective $\mathrm{SU}(2)_\mathrm{L}$ scalar doublet, emerging as a light component from the following two set of fields

$$H_3 \sim (\mathbf{15}, \mathbf{2}, \overline{\mathbf{2}})_3 \,, \qquad \widetilde{H}_3 \sim (\mathbf{1}, \mathbf{2}, \overline{\mathbf{2}})_3 \,, \tag{8.7}$$

localized on the third site.

In the absence of Yukawa couplings, the full Lagrangian of the proposed model is invariant under the accidental global $[\mathrm{U}(1)_{3B+L}]_i$ symmetries, corresponding to the individual fermion number for each family. The Yukawas explicitly break these symmetries, leaving the diagonal combination $\mathrm{U}(1)_{3B+L}$ unbroken. After the SSB of the PS group to the SM one, this accidental symmetry combines with the $[\mathrm{U}(1)_{B-L}]_i$ generators in $\mathrm{SU}(4)_i$, leaving two unbroken global U(1) symmetries, $\mathrm{U}(1)_B\colon\ B = X_{3B+L} + 1/\sqrt{6}\,T^{15}$ and $\mathrm{U}(1)_L\colon\ L = X_{3B+L} - 3/\sqrt{6}\,T^{15}$ (with $T^{15} \equiv T_1^{15} + T_2^{15} + T_3^{15}$). These two symmetries correspond to baryon and lepton numbers and are responsible of keeping the proton stable.

8.2.1 Yukawa structure

The flavour structure observed at low energies emerges as a consequence of the localization of fermions and scalars on different sites. Given the Higgs fields in eq. (8.7), the only renormalizable (unsuppressed) Yukawa interaction at high energies is

$$\mathcal{L}_{\text{Yuk}}^{\text{ren}} = y_3\,\mathrm{Tr}\left\{\overline{\Psi}_L^{(3)} H_3 \Psi_R^{(3)}\right\} + \widetilde{y}_3\,\mathrm{Tr}\left\{\overline{\Psi}_L^{(3)} \widetilde{H}_3\, \Psi_R^{(3)}\right\} + \text{ h.c.}$$

and similarly for the conjugate fields H_3^c and $\widetilde{H}_3^c$. The EWSB breaking induced by $\langle H_3 \rangle$ and $\langle \widetilde{H}_3 \rangle$, with $\langle H_3 \rangle$ aligned along the T^{15} generator of SU(4), allows us to generate four independent SM-like Yukawa couplings for the third generation fermions with different SM quantum numbers.

As anticipated, below the scale Λ_{12} the dynamical gauge sector is invariant under a global $\mathrm{U}(2)^5$ flavour symmetry acting on the first two generations of SM fermions:

$$\Psi_F^{(\ell)} \equiv \left(\Psi_F^{(1)}, \Psi_F^{(2)}\right) \,, \qquad F = \{F_L, F_R\} \,, \tag{8.8}$$

with $F_L = Q_L, L_L$ and $F_R = U_R, D_R, E_R$. Effective Yukawa couplings for these fields are generated below the scale Λ_{23} (see discussion in Section 8.2.2). At dimension-five, the following

effective operators are generated

$$\mathcal{L}_{\rm Yuk}^{d=5} = \frac{\widetilde{y}^F_{3\ell}}{\Lambda_{23}} \,{\rm Tr}\left\{\overline{\Psi}^{(\ell)}_{F_L}\,\Omega_{\ell 3}\,\widetilde{H}_3\,\Psi^{(3)}_R\right\} + \text{ h.c.} \tag{8.9}$$

Note that, while the $\mathrm{U}(2)^5$ flavour symmetry is exact in the gauge sector, this is not the case for the scalar sector. In particular, the Ω_{23} link field is expected to acquire a non-negligible mixing with Ω_{12} of order $\epsilon_{12} = \langle\Omega_{12}\rangle/\Lambda_{12} \ll 1$ (and similarly for the other link fields). This is why we denote $\Omega_{\ell 3}$ (rather than Ω_{23}) its dynamical component for $E < \Lambda_{12}$. Strictly speaking, at this stage we should also treat separately the components of $\Omega_{\ell 3}$ along the SM_{1+2} sub-groups of PS_{1+2}; however, we leave this tacitly implied.

As a result of $\mathcal{L}_{\rm Yuk}^{d=5}$, at low energies two spurions of the $\mathrm{U}(2)_{\rm Q} \times \mathrm{U}(2)_{\rm L} \in \mathrm{U}(2)^5$ flavour symmetry appear. These spurions (transforming as $\mathbf{2}_Q$ and $\mathbf{2}_L$, respectively) control the left-handed mixing between third- and light-generations. Up to $\mathcal{O}(1)$ parameters, the size of the $\mathbf{2}_Q$ spurion can be deduced from the size of the 3–2 mixing in the CKM matrix [11], implying

$$\langle\Omega_{\ell 3}\rangle/\Lambda_{23} \sim |V_{ts}| \approx 4 \times 10^{-2}\ . \tag{8.10}$$

Masses and mixing for the first two generations are obtained from subleading spurions appearing at the dimension-six level,

$$\mathcal{L}_{\rm Yuk}^{d=6} = \frac{\widetilde{y}^F_{\ell}}{\Lambda_{23}^2} \,{\rm Tr}\left\{\overline{\Psi}^{(\ell)}_{F_L}\Phi^L_{\ell 3}\,\widetilde{H}_3\,\Phi^R_{3\ell}\Psi^{(\ell)}_{F_R}\right\} + \text{ h.c.} \tag{8.11}$$

Adding these symmetry breaking terms to the ones in eq. (8.9), we get the following Yukawa pattern

$$Y_f = \begin{pmatrix} y^f_\ell \frac{\langle\Phi^L_{\ell 3}\rangle\langle\Phi^R_{3\ell}\rangle}{\Lambda^2_{23}} & y^f_{3\ell}\frac{\langle\Omega_{\ell 3}\rangle}{\Lambda_{23}} \\ 0 & y^f_3 \end{pmatrix}\ , \tag{8.12}$$

where the $y^f_{\ell,3\ell,3}$ are obtained by y_3, $\widetilde{y}_3$, and $\widetilde{y}^F_{\ell,3\ell}$, normalizing the components of $\langle H_3\rangle$ and $\langle\widetilde{H}_3\rangle$ to v. This structure leads to a very good description of the SM Yukawa couplings in terms of $\mathcal{O}(1)$ parameters and VEV ratios. The natural scale for the $d = 6$ terms is

$$\frac{\langle\Phi^L_{\ell 3}\rangle\langle\Phi^R_{3\ell}\rangle}{\Lambda^2_{23}} \sim y_c(v) = \frac{m_c(v)}{v} \approx 5 \times 10^{-3}\ . \tag{8.13}$$

A detailed discussion of the scalar sector of the model is beyond the scope of this work. However, it is worth stressing that the various scale hierarchies are partially stabilized by the different localization of the fields (or by the initial gauge symmetry). In particular, because of eq. (8.10), corrections to the Higgs mass term proportional to Λ^2_{23} are suppressed by $|V_{ts}|^2$, hence they are effectively of $\mathcal{O}(1\ \mathrm{TeV}^2)$.

8.2.2 Origin of the effective Yukawa operators

The effective Yukawa operators in Section 8.2.1 cannot be generated using only the link fields so far introduced, assuming a renormalizable structure at high energies, but can be generated integrating out additional heavy fermions or heavy scalar fields with vanishing VEV. In particular, we envisage the following three main options:

i) *New link fields.* Adding the following set of (scalar) link fields,

$$\Delta_{ij} \sim (\mathbf{4},\mathbf{2},\mathbf{1})_i \times \left(\overline{\mathbf{4}},\mathbf{1},\overline{\mathbf{2}}\right)_j\ , \tag{8.14}$$

with vanishing VEV, we can generate all the effective Yukawa operators at the tree-level via appropriate triple and quartic scalar couplings with the other link fields, and (renormalizable) Yukawa-type interactions with the chiral fermions.

ii) *Vector-like fermions.* The following set of vector-like fermions,

$$\begin{aligned} &\chi_{L/R} \sim (\mathbf{4},\mathbf{2},\mathbf{1})_3 \ , \\ &\chi'_{L/R} \sim (\mathbf{4},\mathbf{1},\mathbf{1})_i \times (\mathbf{1},\mathbf{2},\mathbf{1})_3 \ , \\ &\chi''_{L/R} \sim (\mathbf{4},\mathbf{1},\mathbf{1})_i \times (\mathbf{1},\mathbf{1},\mathbf{2})_3 \ , \end{aligned} \tag{8.15}$$

is sufficient to induce the desired operators at the tree-level via appropriate new Yukawa-type interactions with the link fields and the chiral fermions.

iii) *Mixed solution.* An interesting mixed solution consists on having a single extra vector-like fermion and a single additional link field,

$$\begin{aligned} \Delta_{12} &\sim (\mathbf{4},\mathbf{2},\mathbf{1})_1 \times \left(\overline{\mathbf{4}},\mathbf{1},\overline{\mathbf{2}}\right)_2 \ , \\ \chi_{L/R} &\sim (\mathbf{4},\mathbf{2},\mathbf{1})_3 \ . \end{aligned} \tag{8.16}$$

This way the vector-like fermion is responsible of generating the operator in eq. (8.9), while the operator in eq. (8.11) is induced integrating out the new link field.

Other possibilities to generate these operators, in particular via loops of extra scalars and fermions, are also possible. Similarly to the case of the scalar potential, a detailed discussion of the dynamics of these heavy fields is beyond the scope of this work. On the other hand, it is important discuss in general terms the nature of the higher-dimensional operators, bilinear in the SM fermion fields, generated below the Λ_{23} scale upon integration of generic heavy dynamics. The only two hypotheses we need to assume are that: i) this dynamics respect the $\mathrm{U}(2)^5$ flavour symmetry; ii) only the link fields in (eq. (8.4)) break this symmetry via their VEV. These two hypotheses are sufficient to ensure a constrained structure for the corresponding EFT, leading to a well-defined pattern of NP effects at low energies.

The higher dimensional operators can be divided into two main classes:

i) $\mathrm{U}(2)$ *preserving operators.* A large set of operators in this category are those containing SM fields only, belonging to the so-called SMEFT [181]. Other operators contain $\mathrm{U}(2)^5$-conserving contractions of the link fields, or field-strength tensors of the TeV-scale exotic gauge fields. In both cases, the $\mathrm{U}(2)^5$ protection and the large effective scale ($\Lambda_{23} \sim 10^2$ TeV) imply marginal effects in low-energy phenomenology.

ii) $\mathrm{U}(2)$ *breaking operators.* Contrary to the previous case, these operators necessarily involve link fields, namely $\Omega_{\ell 3}$, $\Phi^L_{\ell 3}$ and $\Phi^R_{\ell 3}$. Restricting the attention to the fermion bilinears, it is easy to show that dimension-5 operators involve only heavy-light fermions and a single $\Omega_{\ell 3}$ field. These are the Yukawa operators in (eq. (8.9)), and operators that reduce to these ones after using the equations of motion.

At dimension six we find operators involving light fermions only and two link fields. The chirally-violating ones are the Yukawa terms in eq. (8.11). The chirally-preserving ones necessarily involve two powers of the same link field. Terms bilinear in $\Phi^L_{\ell 3}$ and $\Phi^R_{\ell 3}$ modify the couplings of the heavy $W^\pm_L$, $W^\pm_R$, Z' with mass of $\mathcal{O}(10\ \mathrm{TeV})$. Given the heavy masses of these fields, and the smallness of the $\mathrm{U}(2)$ breaking, these terms are irrelevant for low-energy phenomenology. We thus conclude that, beside the Yukawa couplings, the only additional effective fermion bilinears generated by integrating out heavy dynamics at the scale Λ_{23} are operators of the type

$$\frac{i\,C^{(0)}_\Omega}{\Lambda^2_{23}}\ \mathrm{Tr}\{\Omega^\dagger_{\ell 3} D^\mu \Omega_{\ell 3}\}(\overline{\Psi}^{(\ell)}_{F_L}\gamma_\mu \Psi^{(\ell)}_{F_L}) \ , \tag{8.17}$$

$$\frac{i\,C^{(4)}_\Omega}{\Lambda^2_{23}}\ \mathrm{Tr}\{\Omega^\dagger_{\ell 3} T^\alpha D^\mu \Omega_{\ell 3}\}(\overline{\Psi}^{(\ell)}_{F_L} T_\alpha \gamma_\mu \Psi^{(\ell)}_{F_L}) \ , \tag{8.18}$$

and analogous terms where T^α is replaced by a $\mathrm{SU}(2)_\mathrm{L}$ generator or a combination of $\mathrm{SU}(2)_\mathrm{L}$ and SU(4) generators, and finally terms obtained substituting $\Psi^{(\ell)}_{F_L}$ with $\Psi^{(\ell)}_{F_R}$.

f After SSB, the operators (8.17)–(8.18) induce small modifications to the couplings among the TeV-scale gauge bosons and first- and second-generation fermions. As we discuss in section 8.3, this effect plays a fundamental role in the explanation of the (subleading) $b \to s\ell\bar{\ell}$ anomalies. On the contrary, the effect of the analogous operators with right-handed fermions are severely constrained by $B_s \to \ell\ell$ ($\ell = e, \mu$). It is quite natural to find heavy dynamics that, in first approximation, induces only the left-handed operators and not the right-handed counterparts. This is for instance the case of the vector-like fermions in eq. (8.15) and eq. (8.16). In what follows we include the the operators (8.17)–(8.18) in our analysis and neglect the right-handed ones.

8.2.3 Gauge boson spectrum at the TeV scale

In what follows we focus on the last step of the breaking chain discussed above, namely the $\mathcal{G} \to$ SM breaking, that controls low-energy phenomenology and high-p_T physics. We denote the gauge couplings respectively by $g_c^{(3)}$, $g_c^{(l)}$, g_L, and g'_B and the gauge fields by $H^\alpha_{3\,\mu}$, $H^a_{l\,\mu}$, W^i_μ and B', with $\alpha = 1, \ldots, 15$, $a = 1, \ldots, 8$, and $i = 1, 2, 3$. As discussed above, this symmetry breaking is triggered by the VEV of $\Omega_{\ell 3}$, which can be decomposed as $\Omega_{\ell 3} \overset{\mathcal{G}}{\sim} \left(\overline{\mathbf{4}}, \mathbf{3}, \mathbf{3}\right)_{1/6} \oplus \left(\overline{\mathbf{4}}, \mathbf{1}, \mathbf{3}\right)_{-1/2} \oplus \left(\overline{\mathbf{4}}, \mathbf{3}, \mathbf{1}\right)_{1/6} \oplus \left(\overline{\mathbf{4}}, \mathbf{1}, \mathbf{1}\right)_{-1/2}$. We assume that the scalar potential is such that $\Omega_{\ell 3}$ only takes a VEV along the $\mathrm{SU}(2)_\mathrm{L}$-preserving directions, denoted as $\Omega_3 \equiv \left(\overline{\mathbf{4}}, \mathbf{3}, \mathbf{1}\right)_{1/6}$ and $\Omega_1 \equiv \left(\overline{\mathbf{4}}, \mathbf{1}, \mathbf{1}\right)_{-1/2}$, while the $\mathrm{SU}(2)_\mathrm{L}$-triplet components become heavy and decouple. We have:

$$\langle \Omega_3 \rangle = \frac{1}{\sqrt{2}} \begin{pmatrix} \omega_3 & 0 & 0 \\ 0 & \omega_3 & 0 \\ 0 & 0 & \omega_3 \\ 0 & 0 & 0 \end{pmatrix}, \quad \langle \Omega_1 \rangle = \frac{1}{\sqrt{2}} \begin{pmatrix} 0 \\ 0 \\ 0 \\ \omega_1 \end{pmatrix}, \tag{8.19}$$

with $\omega_{1,3}$ assumed to be of $\mathcal{O}$(TeV). These scalar fields can be decomposed under the unbroken SM subgroup as $\Omega_3 \sim (\mathbf{8}, \mathbf{1})_0 \oplus (\mathbf{1}, \mathbf{1})_0 \oplus (\mathbf{3}, \mathbf{1})_{2/3}$ and $\Omega_1 \sim (\overline{\mathbf{3}}, \mathbf{1})_{-2/3} \oplus (\mathbf{1}, \mathbf{1})_0$. So, after removing the Goldstones, we end up with a real color octect, one real and one complex singlet, and a complex leptoquark.

The resulting gauge spectrum is the same as in the model proposed in Ref. [176]. The massive gauge bosons are a vector leptoquark, a color octect, and a neutral gauge boson, transforming under the SM subgroup as: $U \sim (\mathbf{3}, \mathbf{1})_{2/3}$, $G' \sim (\mathbf{8}, \mathbf{1})_0$, and $Z' \sim (\mathbf{1}, \mathbf{1})_0$. These are given by the following combinations of the original gauge fields:

$$\begin{aligned} U^{1,2,3}_\mu &= \frac{1}{\sqrt{2}} \left(H^{9,11,13}_{3\,\mu} - i H^{10,12,14}_{3\,\mu} \right), \\ G'^{\,a}_\mu &= \frac{g_c^{(l)}}{g'_c} H^a_{l\,\mu} - \frac{g_c^{(3)}}{g'_c} H^a_{3\,\mu}, \\ Z'_\mu &= \frac{g_c^{(3)}}{g'_Z} H^{15}_{3\,\mu} - \sqrt{\frac{2}{3}} \frac{g'_B}{g'_Z} B'_\mu, \end{aligned} \tag{8.20}$$

with $g'_c = \sqrt{(g_c^{(3)})^2 + (g_c^{(l)})^2}$, $g'_Z = \sqrt{(g_c^{(3)})^2 + \frac{2}{3}(g'_B)^2}$, and their masses read

$$\begin{aligned} M_U &= \frac{g_c^{(3)}}{2} \sqrt{\omega_1^2 + \omega_3^2}, \qquad M_{G'} = \frac{1}{\sqrt{2}} g'_c \omega_3, \\ M_{Z'} &= \frac{3}{2\sqrt{6}} g'_Z \sqrt{\omega_1^2 + \frac{\omega_3^2}{3}}. \end{aligned} \tag{8.21}$$

For the phenomenological analysis, it is useful to define the following combination, $C_U \equiv v^2\,(g_c^{(3)})^2/4M_{U_3}^2 = v^2/(\omega_1^2+\omega_3^2)$, which quantifies the overall strength of the NP effects mediated by the vectors at low energies.

The combinations orthogonal to G'^a_μ and Z'_μ are the (massless) SM gauge fields G^a_μ and B_μ, with couplings

$$g_c = \frac{g_c^{(l)}\, g_c^{(3)}}{g'_c}\ , \qquad g_Y = \frac{g'_B g_c^{(3)}}{g'_Z}\ . \tag{8.22}$$

At the matching scale, $\mu \approx 1$ TeV, we have $g_c = 1.02$ and $g_Y = 0.363$. From these relations it is clear that $g_c^{(3)}, g_c^{(l)} > g_c$ and $g_c^{(3)}, g'_B > g_Y$, with one of the NP couplings approaching the SM value from above in the limit when the other becomes large. Hence, it follows that $g_c^{(3)}, g_c^{(l)} \gg g'_B$.

A key difference between the model presented here and the one in Ref. [176] is found in the couplings of the extra gauge bosons to fermions. In the SU(4) eigenstate basis (denoted by primed fields) these are given by

$$\begin{aligned}
\mathcal{L}_L \ \supset\ & \frac{g_c^{(3)}}{\sqrt{2}}\, U^\mu\, \overline{q}'_L N_U^L \gamma_\mu\, \ell'_L + \ \text{h.c.} \\
& + g_c\, G'^a_\mu\, \overline{q}'_L\, N_{G'}\, \gamma^\mu\, T^a\, q'_L \\
& + \frac{g_Y}{2\sqrt{6}}\, Z'_\mu \left(3\, \overline{\ell}'_L\, N_{Z'}\, \gamma^\mu\, \ell'_L - \overline{q}'_L\, N_{Z'}\, \gamma^\mu\, q'_L \right) , \\
\mathcal{L}_R \ \supset\ & \frac{g_c^{(3)}}{\sqrt{2}}\, U^\mu \left(\overline{u}'_R N_U^R \gamma_\mu\, \nu'_R + \overline{d}'_R N_U^R \gamma_\mu\, e'_R \right) + \ \text{h.c.} \\
& + g_c\, G'^a_\mu \left(\overline{u}'_R\, N_{G'}\, \gamma^\mu\, T^a\, u'_R + \overline{d}'_R\, N_{G'}\, \gamma^\mu\, T^a\, d'_R \right) \\
& + \frac{g_Y}{2\sqrt{6}}\, Z'_\mu \left[3\, \overline{\nu}'_R\, N_{Z'}^{(-)}\, \gamma^\mu\, \nu'_R + 3\, \overline{e}'_R\, N_{Z'}^{(+)}\, \gamma^\mu\, e'_R \right. \\
& \left. - \overline{u}'_R N_{Z'}^{(+)} \gamma^\mu\, u'_R - \overline{d}'_R N_{Z'}^{(-)} \gamma^\mu\, d'_R \right] ,
\end{aligned} \tag{8.23}$$

where we have defined the following matrices in flavour space ($N_c = 3\,(1)$ for quarks (leptons))

$$\begin{aligned}
N_U^{L,R} &= \text{diag}\,(0,0,1)\ , \qquad N_{G'} = \text{diag}\left(\frac{g_c^{(l)}}{g_c^{(3)}}, \frac{g_c^{(l)}}{g_c^{(3)}}, -\frac{g_c^{(3)}}{g_c^{(l)}} \right) , \\
N_{Z'}^{(\pm)} &= N_{Z'} \pm \frac{2g'_B}{3g_c^{(3)}} N_c\, \mathbf{1}\,, \quad N_{Z'} = \text{diag}\left(\frac{2g'_B}{3g_c^{(3)}}, \frac{2g'_B}{3g_c^{(3)}}, -\frac{g_c^{(3)}}{g'_B} \right) ,
\end{aligned}$$

which encode the non-universality of the couplings. The effective operators in eqs. (8.17)–(8.18) generate small additional couplings to the left-handed components of the light families, almost aligned to the second generation. This effect is particular relevant for the U^μ couplings, where

$$N_U^L \to N_U^L \approx \text{diag}\,(0,\epsilon,1)\ , \tag{8.24}$$

with $\epsilon \equiv -1/2\ C_\Omega^{(4)}\, \omega_1\omega_3/\Lambda_{23}^2$, while N_U^R remains unchanged.

For phenomenological applications we need to rewrite these interactions in the fermion mass-eigenstate basis. This is achieved by rotating the fermion fields with the unitary matrices $V_{f_{L(R)}}$, defined by $Y_f = V_{f_L}^\dagger\ \text{diag}(Y_f) V_{f_R}$. As a result of the Yukawa structure in eq. (8.12), flavour-mixing terms in the right-handed currents can be neglected (the corresponding diagonalization matrices become identity matrices in the limit of vanishing light-fermion masses). However, due to the arbitrariness in the normalization of quark and lepton fields inside the SU(4) spinors in eq. (8.2), a freedom remains in the relative phase between left- and right-handed charged

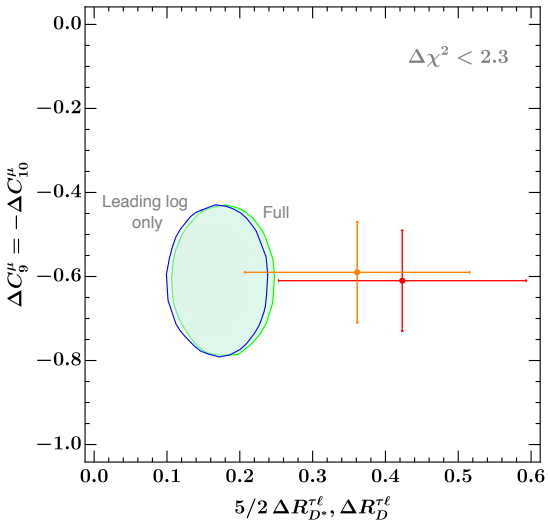

Figure 8.2: Model prediction for $\Delta C_9^\mu = -\Delta C_{10}^\mu$, $\Delta R_{D^*}^{\tau\ell}$, and $\Delta R_D^{\tau\ell}$ for the $\Delta\chi^2 \leq 2.3$ (1σ) fit region: in blue including only the logarithmic contribution in eq. (8.28), and in green including also the non-logarithmic corrections. The 1σ experimental data are shown by the two crosses. Predictions and results for $\Delta R_{D^*}^{\tau\ell}$ (red cross) are scaled by 5/2 compared to $\Delta R_D^{\tau\ell}$ (orange cross), since our model predicts $\Delta R_D^{\tau\ell} \approx 5/2 \times \Delta R_{D^*}^{\tau\ell}$.

currents. Assuming no other sources of CP violation beside the CKM matrix, we restrict this phase (θ_{LR}) to assume the discrete values $\{0, \pi\}$.

The left-handed flavour rotations can be written as

$$\begin{aligned} q'_L &= V_d\, q_L \equiv V_d \begin{pmatrix} V^\dagger{}_{\rm CKM}\, u_L \\ d_L \end{pmatrix} , \\ \ell'_L &= V_e\, \ell_L \equiv V_e \begin{pmatrix} U^\dagger{}_{\rm PMNS}\, \nu_L \\ e_L \end{pmatrix} , \end{aligned} \tag{8.25}$$

where $V_{d,e}$ are unitary matrices. As a result of these rotations, flavour-changing terms appear in the couplings of U_3, G' and Z' to left-handed fermions. Because of the approximate $\mathrm{U}(2)^5$ flavour symmetry, we expect both V_d and V_e to be close to the identity matrix; for simplicity, we assume them to be real and set to zero the rotations involving the first family:

$$V_d = \begin{pmatrix} 1 & 0 & 0 \\ 0 & \cos\theta_{bs} & \sin\theta_{bs} \\ 0 & -\sin\theta_{bs} & \cos\theta_{bs} \end{pmatrix} , \quad V_e = \begin{pmatrix} 1 & 0 & 0 \\ 0 & \cos\theta_{\tau\mu} & \sin\theta_{\tau\mu} \\ 0 & -\sin\theta_{\tau\mu} & \cos\theta_{\tau\mu} \end{pmatrix} . \tag{8.26}$$

Because of eq. (8.10), both θ_{bs} and $\theta_{\tau\mu}$ are naively expected to be of $\mathcal{O}(|V_{ts}|)$. However, in order to avoid the strong bounds from B_s-mixing, we assume $y^d_{3\ell}/y^d_3 \ll 1$, such that $\theta_{bs} \ll |V_{ts}|$.

8.3 Phenomenological analysis

Low-energy constraints. The low-energy phenomenology of the model can be described in terms of $\{C_U, \epsilon, \theta_{\tau\mu}, \theta_{bs}\}$ and the discrete parameter θ_{LR}. The list of relevant low-energy observables, with their explicit expression in terms of four-fermion effective operators, is given in Table II of Ref. [174]. An important difference is the appearence of effective charged-current scalar operators from the right-handed terms in (eq. (8.23)). These have a negligible impact

in $B \to D^* \tau\nu$, but are non-negligible in $B \to D\tau\nu$. Using the results in Ref. [29] for the matrix-elements of the $(\bar{b}_R c_L)(\bar{\nu}_L \tau_R)$ operator, we obtain in the limit $\theta_{\tau\mu}, \theta_{bs} \to 0$

$$\begin{aligned} \Delta R^{\tau\ell}_{D^*} &= R^{\tau\ell}_{D^*} - 1 \approx 2[1 - 0.12\cos(\theta_{LR})] C_U \ , \\ \Delta R^{\tau\ell}_{D} &= R^{\tau\ell}_{D} - 1 \approx 2[1 - 1.5\cos(\theta_{LR})] C_U \ , \end{aligned} \tag{8.27}$$

with $R^{\tau\ell}_{D^{(*)}}$ defined as in Ref. [174]. In order to maximize the correction to $R^{\tau\ell}_{D^{(*)}}$ we set $\theta_{LR} = \pi$. This implies the relation $\Delta R^{\tau\ell}_{D} \approx 5/2 \times \Delta R^{\tau\ell}_{D^*}$, that is well consistent with present data [35–37, 39].

Having fixed θ_{LR}, we determine the remaining four parameters from a global fit. At the best fit point we obtain $\chi^2_{\rm min} \approx 9$, which gives a very good fit compared to the SM, for which $\chi^2_{\rm SM} \approx 46$. A typical set of parameters providing a good fit to data is given by $C_U = 0.03$, $\epsilon = -0.02$, $\theta_{\tau\mu} = -0.05$ and $\theta_{bs} = 0.05\, V_{ts}$. This can be obtained for instance from the benchmark point: $g^{(3)}_c = 3$ and $M_{U_3} \approx 2$ TeV, with $M_{G'}$ and $M_{Z'}$ ranging between 1.5 and 3 TeV (depending on the ω_1/ω_3 ratio).

The potential of the model to explain the anomalies in $b \to s\ell\bar{\ell}$ (that we express as deviations in the Wilson coefficients $C_{9,10}$, defined as in [49, 96]) and in $R^{\tau\ell}_{D^{(*)}}$ (for which we adopt the updated SM prediction in [30, 31, 182]) is depicted in figure 8.2. A good fit to $b \to s\ell\bar{\ell}$ data can only be achieved when considering the dimension-six operator eq. (8.17), whose effect is encoded in ϵ. Interestingly, the best fit value for ϵ is perfectly consistent with that of the dimension-six contributions in the Yukawa couplings.

While the model significantly reduces the tension with data, predicting a non-trivial correlation between $R^{\tau\ell}_{D}$ and $R^{\tau\ell}_{D^*}$ (see caption of figure 8.2), the central value of these two observables cannot be achieved due to the constraints from LFU tests in τ physics and $\mathcal{B}(B_{c,u} \to \tau\nu)$. The LFU tests yield per-mille constraints on the modifications of W and Z couplings to τ leptons (δg^W_τ and $\delta g^Z_{\tau_L,\nu_\tau}$)[2]. These quantities arise in our model from one-loop diagrams involving SM fermions and LQ fields[3], whose (leading) result at $\mathcal{O}(y_t^2)$ is

$$\begin{aligned} \delta g^W_\tau / g^W_\ell &= \frac{3\, y_t^2}{16\pi^2}\, C_U \left(\frac{1}{2} + \log \frac{m_t^2}{M_U^2} \right) , \\ \delta g^Z_{\nu_\tau} / g^Z_{\nu_\ell} &= \frac{3\, y_t^2}{8\pi^2}\, C_U \left(1 + \log \frac{m_t^2}{M_U^2} \right) . \end{aligned} \tag{8.28}$$

These expressions agree in the logarithmic part with the EFT results in [144, 164, 183]. However, having a complete model, we have been able to compute also the non-logarithmic terms which are non-negligible and partially alleviate the tensions with LFU tests in τ physics (see figure 8.2). As far as $\mathcal{B}(B_{c,u} \to \tau\nu)$ are concerned, at the best fit point we predict a $\sim 60\%$ enhancement over the SM, which is perfectly consistent with present data.

Another important constraint is obtained from $B_{s,d}$ mixing. Contributions to these observables arise in our model from the tree-level exchange of the coloron and the Z', as well as from one-loop box diagrams involving the vector leptoquark. All these contributions are proportional to the down-type rotation angle $|\theta_{bs}|$. Allowing for ($U(2)^5$ preserving) deviations of up to $\mathcal{O}(10\%)$ in $B_{s,d}$ mixing leads to the bound $|\theta_{bs}| \lesssim 0.1\, |V_{ts}|$, forcing a flavour-alignment in the down-quark sector. As a result of this alignment, contributions to $D - \overline{D}$ mixing from coloron and Z' exchange turn out to be below the present limits and do not give any relevant bound.

[2] The dominant constrain arises from the bound on $|g^W_\tau / g^W_\mu|$, for which we use the value reported in [38]

[3] An additional contribution to $\delta g^Z_{\tau_L,\nu_\tau}$ arises in our model from the mixing of the lowest-lying Z' and the SM Z; however, this receives a parametric suppression of $\mathcal{O}(s^2_W\, g'_B/g^{(3)}_c\, M^2_Z/M^2_{Z'})$ and turns out to be negligible.

The vector leptoquark does not contribute significantly to $B \to K^{(*)}\nu\overline{\nu}$ nor to $\tau \to 3\mu$, while the approximate down-alignment in the quark sector required from B_s mixing renders the Z' contribution to $B \to K^{(*)}\nu\overline{\nu}$ negligibly small. The Z' contributes at tree-level to $\tau \to 3\mu$. However, since its coupling to muons is suppressed, the constraints from these processes only become relevant when the leptonic mixing angle $\theta_{\tau\mu}$ becomes large, effectively setting the bound $|\theta_{\tau\mu}| \lesssim 0.1$.

High-p_T searches. The masses of the lightest exotic vector bosons predicted by the model are expected to lie around the TeV scale, and are therefore constrained by direct searches at LHC. The phenomenology for these searches is very similar to the one discussed in the model of Ref. [176], so we only highlight the main aspects.

• $\boldsymbol{U}$**.** The vector LQ is subject to the bounds coming from QCD pair production and from tau pair production at high-energies (i.e. $pp \to \tau\overline{\tau} + X$), generated by t–channel exchange [143]. As in Ref. [176], the most stringent constraint is set by leptoquark pair production, which implies $M_U \gtrsim 1.3$ TeV. This expression is obtained by recasting [184] the CMS search in Ref. [185] and translates to $C_U \lesssim 0.08$ for $g_c^{(3)} = 3$.

• $\boldsymbol{G'}$**.** Given the large couplings and relatively low mass of the coloron, di-jet searches at LHC can offer an important test of the validity of the model. However, current limits [186] rely on bump searches that become less sensitive when the coloron width is large. This is the case in our model, where we find $\Gamma_{G'}/M_{G'} = 0.22$ for $g_c^{(3)} = 3$, if we assume that the only available decay channels are those to SM quarks. For large widths, the coloron signal is diluted into the QCD background allowing the model to avoid current bounds [**?**].

• $\boldsymbol{Z'}$**.** As already mentioned, the Z' couplings to light generations appear strongly suppressed compared to the third-generation ones. This renders the Z' Drell-Yan production at LHC sufficiently small to evade the strong bounds from di-lepton resonance searches [187].

• **Heavy scalars.** The minimal model discussed in Section 8.2.3 presents a rich scalar sector, whose phenomenological analysis depends significantly on the details of the scalar potential and is beyond the scope of the present letter. Nevertheless, we do not expect it to yield tensions with data in large areas of the parameter space.

8.4 Summary and conclusions

If unambiguously confirmed as beyond-the-SM signals, the recent B-physics anomalies would lead to a significant shift in our understanding of fundamental interactions. They could imply abandoning the assumption of flavour universality of gauge interactions, which implicitly holds in the SM and in its most popular extensions. In this chapter we have presented a model where the idea of flavour non-universal gauge interactions is pushed to its extreme consequences, with an independent gauge group for each fermion family.

The idea of the (flavour-blind) SM gauge group being the result of a suitable breaking of a flavour non-universal gauge symmetry, holding at high energies, has already been proposed in the past as a possible explanation for the observed flavour hierarchies (see e.g. [11, 188]). Interestingly, constructions of this type naturally arise in higher-dimensional models (see e.g. [189]) with fermion fields localized on different four-dimensional branes, the multi-site gauge group being the deconstructed version of a single higher-dimensional gauge symmetry [190].

As we have shown, a three-site Pati-Salam gauge symmetry, with a suitable symmetry breaking sector, could describe in a natural way the observed Yukawa hierarchies and explain at the same time the recent B-physics anomalies, while being consistent with the tight constraints

from other low- and high-energy measurements. The model we present exhibits a rich TeV-scale phenomenology that can be probed in the near future by high-p_T experiments at the LHC.

Conclusions

The flavour structure of the SM is rather peculiar. It follows from the observation that the interaction basis and the mass basis do not coincide. This is due to the Yukawa terms, which arise when we introduce the Higgs scalar field. As a consequence, the quark families defined in the interaction with the gauge bosons mix between each other; the magnitude of such mixing is encoded in the CKM mixing matrix.
From direct measurements of the elements of the CKM matrix, we can see that they obey a strict hierarchy: the diagonal entries are almost one, while the off-diagonal ones are rather small and complex. In other terms, the CKM matrix does not differ strongly from the identity. At the same time, quark and charged-lepton masses are very hierarchical, with values that vary from the MeV range of the first generation to the 174 GeV of the top quark.
Such peculiar structure leads to very specific predictions, such as the strong suppression of FCNC amplitudes, and their link to the off-diagonal elements of the CKM matrix. This structure, and the corresponding predictions, can easily be falsified if we imagine any kind of NP beyond the SM. Therefore, testing at which extent the CKM description of the mixing in the quark sector of the SM holds, grants a clean probe of the SM itself.
Many experiments in the last years attempted such task, helping to put bounds to the possible NP scale. Only recently a few measurements provided some surprising results. In particular, the processes exhibiting some apparent deviations from the SM predictions are the semileptonic decays $b \to c\ell\overline{\nu}_\ell$ and $b \to s\ell^+\ell^-$. The former happens in the SM through a charged-current tree-level transition, while the latter arises at the loop level.
The deviations from the SM become manifest when comparing the transitions with different lepton species, so-called lepton-universality ratios. In particular, for the $b \to c\ell\overline{\nu}_\ell$ the leptonic final states with taus and muons are compared, leading to a 3.7σ discrepancy with respect to the SM. Instead, in the $b \to s\ell^+\ell^-$ channel, decays with either muon or electron are studied. Global fits to the data available have been performed, pointing to a combined deviation even at the level of 5σ, accordingly to the NP scenario considered.
Taken together, this pattern of anomaly represents a challenging and exciting framework to be studied. The most natural approach is twofold. On the one hand, a deeper and more complete understanding of SM prediction for the interesting observables is needed; moreover, efforts must be made to interface with experiments and their needs. On the other hand, a model building approach can help to disentangle which kind of heavy particles may be responsible of the pattern of anomalies. Examples of this two complementary approaches have been presented in this thesis.
In Part II we focused on the charged current anomalies. Here we have shown two examples of the first approach. In chapter 3 we discussed the strategies to reduce the background for the $B \to D\ell\nu_\ell$ decays to be applied in upcoming analysis. Through this study we have been able to propose a new strategy to determine R_D in an independent way from the previous measurements. Such strategy could represent an interesting and new approach soon to be adopted by B factories such as Belle II. On the same line, in chapter 4 we have proposed a new observable to probe

lepton flavour universality violation, namely the $R(\Lambda_c^*) = \mathcal{B}(\Lambda_b \to \Lambda_c^* \tau\nu)/\mathcal{B}(\Lambda_b \to \Lambda_c^* \ell\nu)$ ratio. Throughout the first complete analysis of these barionic decays, we have demonstrated that the SM prediction for $R(\Lambda_c^*)$ can be controlled using HQET results and future data. A feasibility study for this observable has also been presented, showing that that $R(\Lambda_c^*)$ can be measured with high accuracy at LHCb in the near future.
In Part III we have investigated the anomalies in flavour changing neutral currents. In chapter 5 we have presented the first SM prediction for the universality ratios $R_{K^{(*)}}$ taking into account QED corrections. Our analysis demonstrates that the theoretical error on $R_{K^{(*)}}$, defined and extracted from data using the procedure adopted by LHCb, does not exceed the 1% level. These observables are therefore of key importance in view of future high-statistics data.
Various model-building approach aimed to describe the anomalies and infer conclusions for future observables have been presented in Part IV. In chapter 6 we explored the possibility to coherently explain both anomalies through an EFT approach based to the flavour symmetry $U(2)^5$. We have shown that such solution is viable if we allow a moderate fine tuning in $B_{s(d)}$ mixing and in the tau leptonic decays. A general consequence of this EFT approach is the prediction of visible deviations from the SM both in leptonic and hadronic τ decays. Using the same EFT approach, in chapter 7 we have explored the connections between the anomalies and kaon physics. We have shown that $K \to \pi\nu\nu$ decays are potentially sensitive to the same operators responsible for the anomalies, although the connection suffers of $\mathcal{O}(1)$ unknown free parameters. The latter could be determined by a combined analysis of $B \to K^{(*)}\nu\overline{\nu}$ and $B \to K\tau^+\tau^-$ channels. In chapter 8 we have presented one of the first attempt to build a UV complete model for a vector leptoquark, as leading mediator for the anomalies. Our construction is rather peculiar but effective: through a particular choice of the starting gauge group and the symmetry-breaking sector we end up with a low-energy theory which not only reproduces quite well data on the anomalies, but it also provides a natural explanation of the hierarchy of the Yukawa couplings. Interestingly enough, a few implications of this specific UV construction are quite different than all other models proposed so far. These include a non-trivial relation between R_D and R_{D^*} and a possible large enhancement of $\mathcal{B}(B \to \tau\nu)$.

Appendix A

Appendix to Chapter 2

A.1 $\overline{B} \to P$ form factors

The hadronic matrix element for the vector current between two pseudoscalar states is commonly (e.g. [65]) expressed in terms of two form factor

$$\langle P(k)|\,\bar{c}\gamma^\mu b\,|\overline{B}(p)\rangle = f_+(q^2)\left[(p+k)^\mu - \frac{M_B^2 - M_P^2}{q^2}q^\mu\right] + f_0(q^2)\frac{M_B^2 - M_P^2}{q^2}q^\mu\,. \tag{A.1}$$

In the above, $q^\mu \equiv p^\mu - k^\mu$. In the limit $q^2 \to 0$ one finds a relation between the two form factors in the form of

$$f_+(0) = f_0(0)\,, \tag{A.2}$$

otherwise A.1 would diverge.

While the heavy quark limit can be used as a guiding principle to parametrize both form factors, we prefer not to apply it. Instead, we follow the BCL ansatz [65] and write

$$\begin{aligned} f_+(q^2) &= \frac{f_+(0)}{1 - q^2/M^2_{R(1^-)}}\left[1 + \sum_{k=1}^{3}\alpha_k^+ z^k(q^2; t_+, 0)\right]\,, \\ f_0(q^2) &= \frac{f_+(0)}{1 - q^2/M^2_{R(0^+)}}\left[1 + \sum_{k=1}^{2}\alpha_k^0 z^k(q^2, t_+, 0)\right]\,, \end{aligned} \tag{A.3}$$

	$f_+(0\,\mathrm{GeV}^2)$	$f_+(4\,\mathrm{GeV}^2)$	$f_+(8\,\mathrm{GeV}^2)$	$f_+(t_-)$	$f_0(4\,\mathrm{GeV}^2)$	$f_0(8\,\mathrm{GeV}^2)$	$f_0(t_-)$
				mean			
	0.665	0.798	0.972	1.177	0.729	0.810	0.901
				covariance matrix			
$f_+(0\,\mathrm{GeV}^2)$	1.128×10^{-3}	1.042×10^{-3}	9.230×10^{-4}	7.727×10^{-4}	1.093×10^{-3}	1.063×10^{-3}	1.045×10^{-3}
$f_+(4\,\mathrm{GeV}^2)$	1.042×10^{-3}	1.079×10^{-3}	1.108×10^{-3}	1.123×10^{-3}	1.026×10^{-3}	1.017×10^{-3}	1.021×10^{-3}
$f_+(8\,\mathrm{GeV}^2)$	9.230×10^{-4}	1.108×10^{-3}	1.331×10^{-3}	1.576×10^{-3}	9.307×10^{-4}	9.511×10^{-4}	9.865×10^{-4}
$f_+(t_-)$	7.727×10^{-4}	1.123×10^{-3}	1.576×10^{-3}	2.112×10^{-3}	8.108×10^{-4}	8.681×10^{-4}	9.425×10^{-4}
$f_0(4\,\mathrm{GeV}^2)$	1.093×10^{-3}	1.026×10^{-3}	9.307×10^{-4}	8.108×10^{-4}	1.126×10^{-3}	1.165×10^{-3}	1.210×10^{-3}
$f_0(8\,\mathrm{GeV}^2)$	1.063×10^{-3}	1.017×10^{-3}	9.511×10^{-4}	8.681×10^{-4}	1.165×10^{-3}	1.283×10^{-3}	1.410×10^{-3}
$f_0(t_-)$	1.045×10^{-3}	1.021×10^{-3}	9.865×10^{-4}	9.425×10^{-4}	1.210×10^{-3}	1.410×10^{-3}	1.635×10^{-3}

Table A.1: Mean values and covariance matrix for the data points reconstructed from [21] at $q^2 \in \{0\,\mathrm{GeV}^2, 4\,\mathrm{GeV}^2, 8\,\mathrm{GeV}^2, t_- = (M_B^2 - M_D^2)\}$.

	$f_+(18\,\mathrm{GeV}^2)$	$f_+(22\,\mathrm{GeV}^2)$	$f_+(26\,\mathrm{GeV}^2)$	$f_0(18\,\mathrm{GeV}^2)$	$f_0(22\,\mathrm{GeV}^2)$	$f_0(26\,\mathrm{GeV}^2)$
			mean			
	1.016	1.971	6.443	0.417	0.609	0.961
			covariance matrix			
$f_+(18\,\mathrm{GeV}^2)$	3.492×10^{-3}	1.997×10^{-3}	1.648×10^{-3}	1.067×10^{-3}	2.904×10^{-4}	1.096×10^{-4}
$f_+(22\,\mathrm{GeV}^2)$	1.997×10^{-3}	3.371×10^{-3}	6.193×10^{-3}	2.123×10^{-4}	2.167×10^{-4}	1.294×10^{-4}
$f_+(26\,\mathrm{GeV}^2)$	1.648×10^{-3}	6.193×10^{-3}	7.419×10^{-2}	2.064×10^{-3}	1.139×10^{-3}	1.346×10^{-3}
$f_0(18\,\mathrm{GeV}^2)$	1.067×10^{-3}	2.123×10^{-4}	2.064×10^{-3}	8.478×10^{-4}	4.266×10^{-4}	3.150×10^{-4}
$f_0(22\,\mathrm{GeV}^2)$	2.904×10^{-4}	2.167×10^{-4}	1.139×10^{-3}	4.266×10^{-4}	3.923×10^{-4}	4.009×10^{-4}
$f_0(26\,\mathrm{GeV}^2)$	1.096×10^{-4}	1.294×10^{-4}	1.346×10^{-3}	3.150×10^{-4}	4.009×10^{-4}	6.467×10^{-4}

Table A.2: Mean values and covariance matrix for the data points reconstructed from [20] at $q^2 \in \{18\,\mathrm{GeV}^2, 22\,\mathrm{GeV}^2, 26\,\mathrm{GeV}^2\}$.

where $M_{R(1^-)}$ and $M_{R(0^+)}$ denote the masses of the low-lying resonances with spin/parity quantum numbers $J = 1^-$ and $J = 0^+$, respectively. Note the use of $f_+(0)$ in the parametrization of $f_0(q^2)$, which automatically fulfills the equation of motion A.2. In the parametrization A.3, we make use of the conformal mapping from q^2 to z, where

$$z(q^2; t_+, t_0) = \frac{\sqrt{t_+ - q^2} - \sqrt{t_+ - t_0}}{\sqrt{t_+ - q^2} - \sqrt{t_+ - t_0}}\,. \tag{A.4}$$

Following [65] we impose $\mathrm{Im}\, f_+(q^2) = (q^2 - t_+)^{3/2}$ close to the pair-production threshold $t_+ \equiv (M_B + M_D)^2$. This leads to a relation between the expansion parameters α_k^+:

$$\alpha_3^+ = \frac{1}{3} \sum_{k=1}^{K-1} (-1)^k k\, \alpha_k^+\,. \tag{A.5}$$

$\boldsymbol{\overline{B} \to D}$ The lattice QCD results as presented in [21] follow the BCL parametrization, however, they do not automatically fulfill the equation of motion eq. (A.2). We therefore reconstruct lattice data points for four different choices of q^2 (see table A.1), and fit our choice of the parametrization to these reconstructed points. We use $M_{R(1^-)} = 6.330$GeV and $M_{R(0^+)} = 6.420$GeV as in [21].

$\boldsymbol{\overline{B} \to \pi}$ The lattice QCD results as presented in [20] follow the BCL parametrization. However, they do not automatically fulfill the equation of motion eq. (A.2). Moreover, for the form factor $f_0(q^2)$, no pole for a low-lying resonance scalar resonance is used. We therefore reconstruct lattice data points for three different choices of q^2 in the domain for which lattice data point had been obtained (see table A.2). In addition, we use the results of a recent Light-Cone Sum Rules (LCSR) study [66] for the form factor f_+ at $q^2 = \{0, 10\}\,\mathrm{GeV}^2$. The LCSR results provide, beyond the form factor f_+, also its first and second derivatives with respect to q^2. We fit our choice of the parametrization to the aforementioned constraints. We use $M_{R(1^-)} = 5.325$GeV and $M_{R(0^+)} = 5.540$GeV.

A.2 Scalar Products

In order to facilitate the comparison with our results, we list here all scalar products that emerge in the calculation of 3.21.

The scalar products involving p are

$$p \cdot q = \frac{M_B^2 + q^2 - M_D^2}{2}\,, \tag{A.6}$$

$$p \cdot q_{[\tau]} = \frac{(1-\beta_\tau)(M_B^2 + q^2 - M_D^2) - \beta_\tau\sqrt{\lambda}\cos\theta_{[\tau]}}{2} \tag{A.7}$$

$$\begin{aligned} p \cdot q_{[\mu]} = \frac{1}{2}\beta_{\nu\overline{\nu}}\Big[&(M_B^2 + q^2 - M_D^2)((1-\beta_\tau) + \beta_\tau\cos\theta^*_{[\mu]} \\ &- \sqrt{\lambda}(\beta_\tau + (1-\beta_\tau)\cos\theta^*_{[\mu]})\cos\theta_{[\tau]} \\ &+ \sqrt{\lambda}\sqrt{\frac{1}{2} - \beta_\tau}\sin\theta^*_{[\mu]}\sin\theta_\tau\cos\phi\Big]\,. \end{aligned} \tag{A.8}$$

The scalar product involving q read

$$q \cdot q_{[\tau]} = (1-\beta_\tau)q^2\,, \tag{A.9}$$

$$q \cdot q_{[\mu]} = \beta_{\nu\overline{\nu}}((1-\beta_\tau) + \beta_\tau\cos\theta^*_{[\mu]})q^2\,, \tag{A.10}$$

$$\begin{aligned} q \cdot q_{[\overline{\nu}_\mu]} = \frac{1}{2}\Big[&(1-\beta_{\nu\overline{\nu}})(1-\beta_\tau) - \beta_{\nu\overline{\nu}}(1-\beta_\tau)\cos\theta^{**}_{[\overline{\nu}_\mu]} \\ &- \beta_\tau(\beta_{\nu\overline{\nu}} - (1-\beta_{\nu\overline{\nu}})\cos\theta^{**}_{[\overline{\nu}_\mu]})\cos\theta^*_{[\mu]} \\ &- 2\sqrt{\frac{1}{2} - \beta_{\nu\overline{\nu}}}\beta_\tau\sin\theta^*_{[\mu]}\sin\theta^{**}_{[\overline{\nu}_\mu]}\cos\phi^{**}\Big]q^2\,. \end{aligned} \tag{A.11}$$

For scalar products involving $q_{[\tau]}$ we find

$$q_{[\tau]} \cdot q_{[\mu]} = \beta_{\nu\overline{\nu}}q^2_{[\tau]}\,, \tag{A.12}$$

$$q_{[\tau]} \cdot q_{[\overline{\nu}_\mu]} = \frac{1}{2}\big[(1-\beta_{\nu\overline{\nu}}) - \beta_{\nu\overline{\nu}}\cos\theta^{**}_{[\overline{\nu}_\mu]}\big]q^2_{[\tau]}\,. \tag{A.13}$$

For the antisymmetric tensors we obtain

$$\varepsilon(p, q, q_{[\mu]}, q_{[\overline{\nu}_\mu]}) = \frac{\beta_{\nu\overline{\nu}}\beta_\tau\sqrt{\frac{1}{2} - \beta_\tau}}{2}\sqrt{\lambda}q^2\sin\theta^*_{[\mu]}\sin\theta_{[\tau]}\sin\phi\,, \tag{A.14}$$

In all of the above, we abbreviate

$$\beta_\tau = \frac{q^2 + q^2_{[\tau]}}{2q^2}\,, \qquad\qquad \beta_{\nu\overline{\nu}} = \frac{q^2_{[\tau]} + q^2_{[\nu_\tau\overline{\nu}_\mu]}}{2q^2_{[\tau]}}\,. \tag{A.15}$$

A.3 Results for the Legendre Ansatz in $P_3(y)$

The mean values and covariance matrices for the Legendre moments in the PDFs $P_3(y)$ of $\overline{B} \to D\tau(\to \mu\overline{\nu}\nu)\overline{\nu}$ and $\overline{B} \to \pi\tau(\to \mu\overline{\nu}\nu)\overline{\nu}$ decays are listed in tables A.3 and A.4, respectively.

c_k	-5.02×10^{-1}	-4.82×10^{-1}	7.41×10^{-1}	-1.98×10^{-1}	-1.71×10^{-1}	1.85×10^{-1}	-9.99×10^{-2}	1.99×10^{-2}	2.67×10^{-2}	-3.22×10^{-2}	1.45×10^{-2}	2.46×10^{-3}
k	1	2	3	4	5	6	7	8	9	10	11	12
1	5.22×10^{-7}	-6.69×10^{-7}	-4.86×10^{-7}	1.05×10^{-6}	-3.07×10^{-7}	-2.92×10^{-7}	2.84×10^{-7}	-1.28×10^{-7}	1.54×10^{-8}	3.84×10^{-8}	-4.05×10^{-8}	1.27×10^{-8}
2	-6.69×10^{-7}	1.33×10^{-6}	-7.86×10^{-8}	-1.75×10^{-6}	1.52×10^{-6}	-5.29×10^{-9}	-6.93×10^{-7}	4.86×10^{-7}	-1.59×10^{-7}	-3.22×10^{-8}	8.67×10^{-8}	-5.88×10^{-8}
3	-4.86×10^{-7}	-7.86×10^{-8}	1.94×10^{-6}	-1.11×10^{-6}	-1.74×10^{-6}	2.05×10^{-6}	-2.31×10^{-7}	-7.24×10^{-7}	5.56×10^{-7}	-2.21×10^{-7}	3.3×10^{-9}	8.87×10^{-8}
4	1.05×10^{-6}	-1.75×10^{-6}	-1.11×10^{-6}	4.09×10^{-6}	-1.78×10^{-6}	-2.56×10^{-6}	2.89×10^{-6}	-4.67×10^{-7}	-8.47×10^{-7}	7.25×10^{-7}	-3.16×10^{-7}	2.88×10^{-8}
5	-3.07×10^{-7}	1.52×10^{-6}	-1.74×10^{-6}	-1.78×10^{-6}	4.94×10^{-6}	-1.94×10^{-6}	-3.15×10^{-6}	3.43×10^{-6}	-5.29×10^{-7}	-9.97×10^{-7}	8.51×10^{-7}	-3.7×10^{-7}
6	-2.92×10^{-7}	-5.29×10^{-9}	2.05×10^{-6}	-2.56×10^{-6}	-1.94×10^{-6}	5.89×10^{-6}	-2.37×10^{-6}	-3.58×10^{-6}	3.93×10^{-6}	-6.18×10^{-7}	-1.12×10^{-6}	9.4×10^{-7}
7	2.84×10^{-7}	-6.93×10^{-7}	-2.31×10^{-7}	2.89×10^{-6}	-3.15×10^{-6}	-2.37×10^{-6}	6.9×10^{-6}	-2.75×10^{-6}	-4.06×10^{-6}	4.45×10^{-6}	-7.26×10^{-7}	-1.23×10^{-6}
8	-1.28×10^{-7}	4.86×10^{-7}	-7.24×10^{-7}	-4.67×10^{-7}	3.43×10^{-6}	-3.58×10^{-6}	-2.75×10^{-6}	7.84×10^{-6}	-3.1×10^{-6}	-4.57×10^{-6}	4.97×10^{-6}	$-8.\times10^{-7}$
9	1.54×10^{-8}	-1.59×10^{-7}	5.56×10^{-7}	-8.47×10^{-7}	-5.29×10^{-7}	3.93×10^{-6}	-4.06×10^{-6}	-3.1×10^{-6}	8.75×10^{-6}	-3.44×10^{-6}	-5.04×10^{-6}	5.46×10^{-6}
0	3.84×10^{-8}	-3.22×10^{-8}	-2.21×10^{-7}	7.25×10^{-7}	-9.97×10^{-7}	-6.18×10^{-7}	4.45×10^{-6}	-4.57×10^{-6}	-3.44×10^{-6}	9.68×10^{-6}	-3.81×10^{-6}	-5.51×10^{-6}
11	-4.05×10^{-8}	8.67×10^{-8}	3.3×10^{-9}	-3.16×10^{-7}	8.51×10^{-7}	-1.12×10^{-6}	-7.26×10^{-7}	4.97×10^{-6}	-5.04×10^{-6}	-3.81×10^{-6}	1.06×10^{-5}	-4.14×10^{-6}
12	1.27×10^{-8}	-5.88×10^{-8}	8.87×10^{-8}	2.88×10^{-8}	-3.7×10^{-7}	9.4×10^{-7}	-1.23×10^{-6}	$-8.\times10^{-7}$	5.46×10^{-6}	-5.51×10^{-6}	-4.14×10^{-6}	1.15×10^{-5}

Table A.3: Mean values and covariance matrix for the Legendre moments $c_k^{(3)}$ in the parametrization of the PDF $P_3(y)$ in the Decay $\overline{B} \to D\tau(\to \mu\overline{\nu}\nu)\overline{\nu}$. We use $k \leq 12$.

c_k	-5.2×10^{-1}	-3.6×10^{-1}	6.14×10^{-1}	-3.02×10^{-1}	6.0×10^{-2}	6.47×10^{-2}	-1.18×10^{-1}	1.09×10^{-1}	-6.88×10^{-2}	2.31×10^{-2}	1.11×10^{-2}	$-3.\times10^{-2}$
k	1	2	3	4	5	6	7	8	9	10	11	12
1	6.58×10^{-7}	-7.83×10^{-7}	-5.16×10^{-7}	1.03×10^{-6}	-4.39×10^{-7}	-4.1×10^{-12}	1.7×10^{-7}	-2.17×10^{-7}	1.69×10^{-7}	-8.57×10^{-8}	5.91×10^{-9}	3.7×10^{-8}
2	-7.83×10^{-7}	1.62×10^{-6}	-2.61×10^{-7}	-1.79×10^{-6}	1.74×10^{-6}	-4.72×10^{-7}	-2.72×10^{-7}	4.94×10^{-7}	-4.59×10^{-7}	2.78×10^{-7}	-8.51×10^{-8}	-6.28×10^{-8}
3	5.16×10^{-7}	-2.61×10^{-7}	2.24×10^{-6}	-1.04×10^{-6}	-1.83×10^{-6}	$2.\times10^{-6}$	-5.54×10^{-7}	-2.55×10^{-7}	4.78×10^{-7}	-4.5×10^{-7}	2.7×10^{-7}	-7.25×10^{-8}
4	1.03×10^{-6}	-1.79×10^{-6}	-1.04×10^{-6}	4.14×10^{-6}	-1.93×10^{-6}	-2.14×10^{-6}	2.58×10^{-6}	-9.36×10^{-7}	-6.37×10^{-8}	4.21×10^{-7}	-4.79×10^{-7}	3.73×10^{-7}
5	-4.39×10^{-7}	1.74×10^{-6}	-1.83×10^{-6}	-1.93×10^{-6}	5.3×10^{-6}	-2.28×10^{-6}	-2.71×10^{-6}	3.21×10^{-6}	-1.22×10^{-6}	-9.6×10^{-9}	5.19×10^{-7}	-6.59×10^{-7}
6	-4.1×10^{-12}	-4.72×10^{-7}	$2.\times10^{-6}$	-2.14×10^{-6}	-2.28×10^{-6}	6.14×10^{-6}	-2.55×10^{-6}	-3.21×10^{-6}	3.72×10^{-6}	-1.35×10^{-6}	-1.12×10^{-7}	6.54×10^{-7}
7	1.7×10^{-7}	-2.72×10^{-7}	-5.54×10^{-7}	2.58×10^{-6}	-2.71×10^{-6}	-2.55×10^{-6}	7.03×10^{-6}	-2.91×10^{-6}	-3.57×10^{-6}	4.09×10^{-6}	-1.45×10^{-6}	-1.11×10^{-7}
8	-2.17×10^{-7}	4.94×10^{-7}	-2.55×10^{-7}	-9.36×10^{-7}	3.21×10^{-6}	-3.21×10^{-6}	-2.91×10^{-6}	8.05×10^{-6}	-3.41×10^{-6}	-3.92×10^{-6}	4.56×10^{-6}	-1.68×10^{-6}
9	1.69×10^{-7}	-4.59×10^{-7}	4.78×10^{-7}	-6.37×10^{-8}	-1.22×10^{-6}	3.72×10^{-6}	-3.57×10^{-6}	-3.41×10^{-6}	9.09×10^{-6}	-3.79×10^{-6}	-4.39×10^{-6}	5.1×10^{-6}
10	-8.57×10^{-8}	2.78×10^{-7}	-4.5×10^{-7}	4.21×10^{-7}	-9.6×10^{-9}	-1.35×10^{-6}	4.09×10^{-6}	-3.92×10^{-6}	-3.79×10^{-6}	9.99×10^{-6}	-4.11×10^{-6}	-4.83×10^{-6}
11	5.91×10^{-9}	-8.51×10^{-8}	2.7×10^{-7}	-4.79×10^{-7}	5.19×10^{-7}	-1.12×10^{-7}	-1.45×10^{-6}	4.56×10^{-6}	-4.39×10^{-6}	-4.11×10^{-6}	1.09×10^{-5}	-4.5×10^{-6}
12	3.7×10^{-8}	-6.28×10^{-8}	-7.25×10^{-8}	3.73×10^{-7}	-6.59×10^{-7}	6.54×10^{-7}	-1.11×10^{-7}	-1.68×10^{-6}	5.1×10^{-6}	-4.83×10^{-6}	-4.5×10^{-6}	1.19×10^{-5}

Table A.4: Mean values and covariance matrix for the Legendre moments $c_k^{(3)}$ in the parametrization of the PDF $P_3(y)$ in the Decay $\overline{B}\to\pi\tau(\to\mu\overline{\nu}\nu)\overline{\nu}$. We use $k\leq 12$.

Appendix B

Appendix to Chapter 4

B.1 Details on the Rarita-Schwinger object

We describe a $J^P = 3/2^-$ state by the spin-3/2 projection u^α of a generic Rarita-Schwinger object $u^\alpha_{\rm RS}(k,\eta) = \eta^\alpha u(k)$,

$$\begin{aligned} u^\alpha_{(3/2)}(k,\eta,s_c) &= \left[\eta^\alpha - \frac{1}{3}\left(\gamma^\alpha + \frac{k^\alpha}{m_{\Lambda_c^*}}\right)\not{\eta}\right] u(k,s_c) \\ &= \left[g^\alpha{}_\beta - \frac{1}{3}\left(\gamma^\alpha + \frac{k^\alpha}{m_{\Lambda_c^*}}\right)\gamma_\beta\right] u^\beta_{\rm RS}(k,\eta(\lambda),s_c) \\ &\equiv \left[P_{3/2}\right]^\alpha{}_\beta\, u^\beta_{\rm RS}(k,\eta(\lambda),s_c)\,. \end{aligned} \tag{B.1}$$

In the above, $u(k,s_c)$ denotes a spin-$1/2^+$ spinor of four momentum k and rest-frame helicity $s_c = \pm 1/2$, and η denotes a polarization vector with $J^P = 1^-$. Likewise, we can also characterise the $J^P = 1/2^-$ state in term of the projection onto the spin-1/2 component as:

$$u^\alpha_{(1/2)}(k,\eta,s_c) = \frac{1}{3}\left[\gamma^\alpha + \frac{k^\alpha}{m_{\Lambda_c^*}}\right]\not{\eta}\; u(k,s_c) \tag{B.2}$$

$$= \frac{1}{3}\left[\gamma^\alpha + \frac{k^\alpha}{m_{\Lambda_c^*}}\right]\gamma_\beta\; u^\beta_{\rm RS}(k,\eta(\lambda),s_c) \tag{B.3}$$

$$\equiv \left[P_{1/2}\right]^\alpha{}_\beta\, u^\beta_{\rm RS}(k,\eta(\lambda),s_c)\,. \tag{B.4}$$

The Rarita-Schwinger object fulfills the equation of motion

$$\left[i\varepsilon_{\mu\alpha\beta\sigma}\gamma^5\gamma^\mu k^\sigma - im\,\sigma_{\alpha\beta}\right] u^\beta(k) = 0\,. \tag{B.5}$$

By virtue of the equations of motions, the following identities hold

$$k^\alpha u^{\rm RS}_\alpha(k,\eta,s_c) = 0 = \eta(t)^\alpha u^{\rm RS}_\alpha(k,\eta,s_c) \tag{B.6}$$

while for the spin 3/2 projection u_α of a Rarita-Schwinger object, the following relations are also true:

$$\gamma^\alpha u^{(3/2)}_\alpha(k,\eta,s_c) = 0\,, \tag{B.7}$$

$$-i\sigma^{\alpha\beta}\, u^{(3/2)}_\alpha(k,\eta,s_c) = u^\beta_{(3/2)}(k,\eta,s_c)\,. \tag{B.8}$$

The completeness relation for the 3/2 spinor read

$$\sum_{\lambda(')s_c(')} u^{\alpha}(k,\eta(\lambda),s_c)\overline{u}^{\alpha'}(k,\eta(\lambda'),s_c') = (\not{k}+m_{\Lambda_c^*})\Big[-g^{\alpha\alpha'}+\frac{k^{\alpha}k^{\alpha'}}{m^2_{\Lambda_c^*}} + \frac{1}{3}\left(\gamma^{\alpha}-\frac{k^{\alpha}}{m_{\Lambda_c^*}}\right)\left(\gamma^{\alpha'}+\frac{k^{\alpha'}}{m_{\Lambda_c^*}}\right)\Big], \tag{B.9}$$

while for the 1/2 spinor we have:

$$\sum_{\lambda(')s_c(')} u^{\alpha}_{1/2}(k,\eta(\lambda),s_c)\overline{u}^{\alpha'}_{1/2}(k,\eta(\lambda'),s_c') = -\frac{1}{3}(\not{k}+m_{\Lambda_c^*})\left(\gamma^{\alpha}-\frac{k^{\alpha}}{m_{\Lambda_c^*}}\right)\left(\gamma^{\alpha'}+\frac{k^{\alpha'}}{m_{\Lambda_c^*}}\right) \tag{B.10}$$

B.2 Details on the form factor definitions

The spin structures $\Gamma^{\alpha\mu}_{J,i}$ that contribute to the transition $\Lambda_b \to \Lambda_c^*$ are listed in the following. For the final state $\Lambda_c(2595)^+$ and for the vector current ($J=V$) we find :

$$\begin{aligned}
\Gamma^{\alpha\mu}_{V,(1/2,t)} &= \frac{\sqrt{4m_{\Lambda_b}m_{\Lambda_c^*}}}{\sqrt{s_+}}\frac{2m_{\Lambda_c^*}}{\sqrt{s_+s_-}}p^{\alpha}\frac{m_{\Lambda_b}-m_{\Lambda_c^*}}{\sqrt{q^2}}\frac{q^{\mu}}{\sqrt{q^2}},\\
\Gamma^{\alpha\mu}_{V,(1/2,0)} &= \frac{\sqrt{4m_{\Lambda_b}m_{\Lambda_c^*}}}{\sqrt{s_-}}\frac{2m_{\Lambda_c^*}}{\sqrt{s_+s_-}}p^{\alpha}\frac{m_{\Lambda_b}+m_{\Lambda_c^*}}{s_+}\left[(p+k)^{\mu}-\frac{m^2_{\Lambda_b}-m^2_{\Lambda_c^*}}{q^2}q^{\mu}\right],\\
\Gamma^{\alpha\mu}_{V,(1/2,\perp)} &= \frac{\sqrt{4m_{\Lambda_b}m_{\Lambda_c^*}}}{\sqrt{s_-}}\frac{2m_{\Lambda_c^*}}{\sqrt{s_+s_-}}p^{\alpha}\left[\gamma^{\mu}-\frac{2m_{\Lambda_c^*}}{s_+}p^{\mu}-\frac{2m_{\Lambda_b}}{s_+}k^{\mu}\right],
\end{aligned} \tag{B.11}$$

while for the axialvector current ($J=A$) we obtain:

$$\begin{aligned}
\Gamma^{\alpha\mu}_{A,(1/2,t)} &= \frac{\sqrt{4m_{\Lambda_b}m_{\Lambda_c^*}}}{\sqrt{s_-}}\frac{2m_{\Lambda_c^*}}{\sqrt{s_+s_-}}p^{\alpha}\frac{m_{\Lambda_b}+m_{\Lambda_c^*}}{\sqrt{q^2}}\frac{q^{\mu}}{\sqrt{q^2}},\\
\Gamma^{\alpha\mu}_{A,(1/2,0)} &= \frac{\sqrt{4m_{\Lambda_b}m_{\Lambda_c^*}}}{\sqrt{s_+}}\frac{2m_{\Lambda_c^*}}{\sqrt{s_+s_-}}p^{\alpha}\frac{m_{\Lambda_b}-m_{\Lambda_c^*}}{s_-}\left[(p+k)^{\mu}-\frac{m^2_{\Lambda_b}-m^2_{\Lambda_c^*}}{q^2}q^{\mu}\right],\\
\Gamma^{\alpha\mu}_{A,(1/2,\perp)} &= \frac{\sqrt{4m_{\Lambda_b}m_{\Lambda_c^*}}}{\sqrt{s_+}}\frac{2m_{\Lambda_c^*}}{\sqrt{s_+s_-}}p^{\alpha}\left[\gamma^{\mu}+\frac{2m_{\Lambda_c^*}}{s_-}p^{\mu}-\frac{2m_{\Lambda_b}}{s_-}k^{\mu}\right].
\end{aligned} \tag{B.12}$$

In the case of the final state $\Lambda_c(2625)^+$, for the vector current ($J=V$) we obtain:

$$\begin{aligned}
\Gamma^{\alpha\mu}_{V,(1/2,t)} &= \frac{\sqrt{4m_{\Lambda_b}m_{\Lambda_c^*}}}{\sqrt{s_+}}\frac{2m_{\Lambda_c^*}}{\sqrt{s_+s_-}}p^{\alpha}\frac{m_{\Lambda_b}-m_{\Lambda_c^*}}{\sqrt{q^2}}\frac{q^{\mu}}{\sqrt{q^2}},\\
\Gamma^{\alpha\mu}_{V,(1/2,0)} &= \frac{\sqrt{4m_{\Lambda_b}m_{\Lambda_c^*}}}{\sqrt{s_-}}\frac{2m_{\Lambda_c^*}}{\sqrt{s_+s_-}}p^{\alpha}\frac{m_{\Lambda_b}+m_{\Lambda_c^*}}{s_+}\left[(p+k)^{\mu}-\frac{m^2_{\Lambda_b}-m^2_{\Lambda_c^*}}{q^2}q^{\mu}\right],\\
\Gamma^{\alpha\mu}_{V,(1/2,\perp)} &= \frac{\sqrt{4m_{\Lambda_b}m_{\Lambda_c^*}}}{\sqrt{s_-}}\frac{2m_{\Lambda_c^*}}{\sqrt{s_+s_-}}p^{\alpha}\left[\gamma^{\mu}-\frac{2m_{\Lambda_c^*}}{s_+}p^{\mu}-\frac{2m_{\Lambda_b}}{s_+}k^{\mu}\right],\\
\Gamma^{\alpha\mu}_{V,(3/2,\perp)} &= \frac{\sqrt{4m_{\Lambda_b}m_{\Lambda_c^*}}}{\sqrt{s_-}}\frac{-4i\varepsilon^{\alpha\mu pk}}{\sqrt{s_+s_-}}\gamma_5+\Gamma_{V,(1/2,\perp)},
\end{aligned} \tag{B.13}$$

while for the axialvector current ($J = A$) we use

$$\begin{aligned}
\Gamma^{\alpha\mu}_{A,(1/2,t)} &= \frac{\sqrt{4m_{\Lambda_b}m_{\Lambda_c^*}}}{\sqrt{s_-}}\,\frac{2m_{\Lambda_c^*}}{\sqrt{s_+s_-}}p^\alpha\,\frac{m_{\Lambda_b}+m_{\Lambda_c^*}}{\sqrt{q^2}}\,\frac{q^\mu}{\sqrt{q^2}}\,,\\
\Gamma^{\alpha\mu}_{A,(1/2,0)} &= \frac{\sqrt{4m_{\Lambda_b}m_{\Lambda_c^*}}}{\sqrt{s_+}}\,\frac{2m_{\Lambda_c^*}}{\sqrt{s_+s_-}}p^\alpha\,\frac{m_{\Lambda_b}-m_{\Lambda_c^*}}{s_-}\left[(p+k)^\mu-\frac{m^2_{\Lambda_b}-m^2_{\Lambda_c^*}}{q^2}q^\mu\right]\,,\\
\Gamma^{\alpha\mu}_{A,(1/2,\perp)} &= \frac{\sqrt{4m_{\Lambda_b}m_{\Lambda_c^*}}}{\sqrt{s_+}}\,\frac{2m_{\Lambda_c^*}}{\sqrt{s_+s_-}}p^\alpha\left[\gamma^\mu+\frac{2m_{\Lambda_c^*}}{s_-}p^\mu-\frac{2m_{\Lambda_b}}{s_-}k^\mu\right]\,,\\
\Gamma^{\alpha\mu}_{A,(3/2,\perp)} &= \frac{\sqrt{4m_{\Lambda_b}m_{\Lambda_c^*}}}{\sqrt{s_+}}\,\frac{-4i\varepsilon^{\alpha\mu pk}}{\sqrt{s_+s_-}}\gamma_5-\Gamma_{A,(1/2,\perp)}\,.
\end{aligned}\tag{B.14}$$

Note that we adopted the convention $\varepsilon^{0123} = -\varepsilon_{0123} = +1$ for the Levi-Civita tensor.

In the above a recurring term fulfills

$$\overline{u}_\alpha(k)\frac{-2m_{\Lambda_c^*}}{\sqrt{s_+s_-}}p^\alpha = \overline{u}_\alpha(k)\eta^\alpha(0)\,.\tag{B.15}$$

To conclude, we also provide the matching between our form factor definitions and the ones in [77]:

$$\begin{aligned}
F_{1/2,t}(q^2(w)) &= +\frac{\sqrt{w-1}}{\sqrt{2}(r-1)}(w+1)\left[(r-1)l_{V_1}+(rw-1)l_{V_2}+(r-w)l_{V_3}-l_{V_4}\right]\,,\\
F_{1/2,0}(q^2(w)) &= +\frac{\sqrt{w+1}}{\sqrt{2}(1+r)}\left[(r+1)(w-1)l_{V_1}+(w^2-1)(rl_{V_2}+l_{V_3})+(w-r)l_{V_4}\right]\,,\\
F_{1/2,\perp}(q^2(w)) &= -\frac{\sqrt{w+1}}{2\sqrt{2}}\left[2(1-w)l_{V_1}+l_{V_4}\right]\,,\\
F_{3/2,\perp}(q^2(w)) &= -\frac{\sqrt{w+1}}{2\sqrt{2}}l_{V_4}\,,\\
G_{1/2,t}(q^2(w)) &= +\frac{\sqrt{w+1}}{\sqrt{2}(r+1)}(w-1)\left[(r+1)l_{A_1}+(rw-1)l_{A_2}+(r-w)l_{A_3}-l_{A_4}\right]\,,\\
G_{1/2,0}(q^2(w)) &= +\frac{\sqrt{w-1}}{\sqrt{2}(1-r)}\left[(r-1)(w+1)l_{A_1}+(w^2-1)(rl_{A_2}+l_{A_3})+(w-r)l_{A_4}\right]\,,\\
G_{1/2,\perp}(q^2(w)) &= -\frac{\sqrt{w-1}}{2\sqrt{2}}\left[-2(1+w)l_{A_1}+l_{A_4}\right]\,,\\
G_{3/2,\perp}(q^2(w)) &= +\frac{\sqrt{w-1}}{2\sqrt{2}}l_{A_4}\,,
\end{aligned}\tag{B.16}$$

with $r = m_{\Lambda_c^*}/m_{\Lambda_b}$.
We worked out the matching between out convention and [77] also for the form factors of $\Lambda_b \to \Lambda_c(2595)^+$ transitions. This is slightly more involved since our approach and the approach of [77] for the spin $1/2^-$ projection of the Rarita-Schwinger object differ. We find it convenient to use:

$$\sum_{\lambda_c',s_c'} C^{1/2,s_c}_{\lambda_c',s_c'}\,\overline{u}^{(1/2)}_\alpha(k,\eta(\lambda_c'),s_c')p^\alpha = -\frac{1}{\sqrt{3}}\overline{u}(k,s_c)\gamma^5\left(\frac{1}{m_{\Lambda_c^*}}k\cdot q+\not{q}\right)\,,\tag{B.17}$$

with the $C^{1/2,s_c}_{\lambda_c',s_c'}$ being the Clebsch-Gordan coefficients for $j_1 \oplus j_2 = 1 \oplus 1/2$ angular momentum. Using eq. (B.17), the matching between our form factors for the $\Lambda_b \to \Lambda_c(2595)^+$ transition and the ones in [77] reads:

$$\begin{aligned}
f_{1/2,t}(q^2(w)) &= +\sqrt{\frac{3}{2}}\frac{\sqrt{w-1}}{r-1}\left[(r+1)d_{V_1} + (rw-1)d_{V_2} + (r-w)d_{V_3}\right] , \\
f_{1/2,0}(q^2(w)) &= +\sqrt{\frac{3}{2}}\frac{\sqrt{w+1}}{r+1}\left[(r-1)d_{V_1} + (w-1)(rd_{V_2} + d_{V3})\right] , \\
f_{1/2,\perp}(q^2(w)) &= -\sqrt{\frac{3}{2}}\sqrt{w+1}\, d_{V_1} , \\
g_{1/2,t}(q^2(w)) &= +\sqrt{\frac{3}{2}}\frac{\sqrt{w+1}}{r+1}\left[(r-1)d_{A_1} + (rw-1)d_{A_2} + (r-w)d_{A_3}\right] , \\
g_{1/2,0}(q^2(w)) &= +\sqrt{\frac{3}{2}}\frac{\sqrt{w-1}}{r-1}\left[(r+1)d_{A_1} + (w+1)(rd_{A_2} + d_{A_3})\right] , \\
g_{1/2,\perp}(q^2(w)) &= -\sqrt{\frac{3}{2}}\sqrt{w-1}\, d_{A_1} .
\end{aligned} \tag{B.18}$$

B.3 Helicity Amplitudes

B.3.1 $1/2^+ \to 1/2^-$

For the scalar current, defined as

$$h_S^\alpha(s_b, s_c, \lambda_c) \equiv \overline{u}^\alpha(k, \eta(\lambda_c), s_c) u(p, s_b) , \tag{B.19}$$

we find the following non vanishing terms:

$$\frac{1}{\sqrt{2}} h_S^\alpha(-1/2,-1/2,+1) = h_S^\alpha(-1/2,+1/2,0) = \frac{\sqrt{2}}{3}\sqrt{s_+}\eta^{*\alpha}(+1) , \tag{B.20}$$

$$\frac{1}{\sqrt{2}} h_S^\alpha(+1/2,+1/2,-1) = h_S^\alpha(+1/2,-1/2,0) = \frac{\sqrt{2}}{3}\sqrt{s_+}\eta^{*\alpha}(-1) , \tag{B.21}$$

$$-h_S^\alpha(+1/2,-1/2,+1) = \sqrt{2} h_S^\alpha(+1/2,+1/2,0) = \frac{\sqrt{2}}{3}\sqrt{s_+}\eta^{*\alpha}(0) , \tag{B.22}$$

$$-h_S^\alpha(-1/2,+1/2,-1) = \sqrt{2} h_S^\alpha(-1/2,-1/2,0) = \frac{\sqrt{2}}{3}\sqrt{s_+}\eta^{*\alpha}(0) . \tag{B.23}$$

For the pseudoscalar current current, defined as

$$h_P^\alpha(s_b, s_c, \lambda_c) \equiv \overline{u}^\alpha(k, \eta(\lambda_c), s_c)\gamma_5 u(p, s_b) , \tag{B.24}$$

one finds:

$$\frac{1}{\sqrt{2}} h_P^\alpha(-1/2,-1/2,+1) = -h_P^\alpha(-1/2,+1/2,0) = +\frac{\sqrt{2}}{3}\sqrt{s_-}\eta^{*\alpha}(+1) , \tag{B.25}$$

$$-\frac{1}{\sqrt{2}} h_P^\alpha(+1/2,+1/2,-1) = h_P^\alpha(+1/2,-1/2,0) = +\frac{\sqrt{2}}{3}\sqrt{s_-}\eta^{*\alpha}(-1) , \tag{B.26}$$

$$h_P^\alpha(+1/2,-1/2,+1) = -\sqrt{2} h_P^\alpha(+1/2,+1/2,0) = +\frac{\sqrt{2}}{3}\sqrt{s_-}\eta^{*\alpha}(0) , \tag{B.27}$$

$$-h_P^\alpha(-1/2,+1/2,-1) = \sqrt{2} h_P^\alpha(-1/2,-1/2,0) = +\frac{\sqrt{2}}{3}\sqrt{s_-}\eta^{*\alpha}(0) . \tag{B.28}$$

For the vector current

$$h^{\alpha}_{V,\lambda_q}(s_b,s_c,\lambda_c) \equiv \overline{u}^{\alpha}(k,\eta(\lambda_c),s_c)\not{\epsilon}^{*}(\lambda_q)u(p,s_b)\,, \tag{B.29}$$

we identify

$$h^{\alpha}_{V,t}(s_b,s_c,\lambda_c) = \frac{m_{\Lambda_b}-m_{\Lambda_c^*}}{\sqrt{q^2}}h^{\alpha}_{S}(s_b,s_c,\lambda_c)\,. \tag{B.30}$$

For the transverse polarisation we find:

$$-\frac{1}{\sqrt{2}}h^{\alpha}_{V,-1}(+1/2,-1/2,+1) = h^{\alpha}_{V,-1}(+1/2,+1/2,0) = +\frac{2}{3}\sqrt{s_-}\eta^{*\alpha}(+1)\,, \tag{B.31}$$

$$-\frac{1}{\sqrt{2}}h^{\alpha}_{V,+1}(-1/2,+1/2,-1) = h^{\alpha}_{V,+1}(-1/2,-1/2,0) = +\frac{2}{3}\sqrt{s_-}\eta^{*\alpha}(-1)\,, \tag{B.32}$$

$$h^{\alpha}_{V,+1}(-1/2,-1/2,+1) = -\sqrt{2}h^{\alpha}_{V,+1}(-1/2,+1/2,0) = +\frac{2}{3}\sqrt{s_-}\eta^{*\alpha}(0)\,, \tag{B.33}$$

$$h^{\alpha}_{V,-1}(+1/2,+1/2,-1) = -\sqrt{2}h^{\alpha}_{V,-1}(+1/2,-1/2,0) = +\frac{2}{3}\sqrt{s_-}\eta^{*\alpha}(0)\,. \tag{B.34}$$

For the longitudinal polarisation we find:

$$\frac{1}{\sqrt{2}}h^{\alpha}_{V,0}(-1/2,-1/2,+1) = -h^{\alpha}_{V,0}(-1/2,+1/2,0) = \frac{\sqrt{2}}{3}\frac{m_{\Lambda_b}+m_{\Lambda_c^*}}{\sqrt{q^2}}\sqrt{s_-}\eta^{*\alpha}(+1)\,, \tag{B.35}$$

$$\frac{1}{\sqrt{2}}h^{\alpha}_{V,0}(+1/2,+1/2,-1) = -h^{\alpha}_{V,0}(+1/2,-1/2,0) = \frac{\sqrt{2}}{3}\frac{m_{\Lambda_b}+m_{\Lambda_c^*}}{\sqrt{q^2}}\sqrt{s_-}\eta^{*\alpha}(-1)\,, \tag{B.36}$$

$$-h^{\alpha}_{V,0}(+1/2,-1/2,+1) = \sqrt{2}h^{\alpha}_{V,0}(+1/2,+1/2,0) = \frac{\sqrt{2}}{3}\frac{m_{\Lambda_b}+m_{\Lambda_c^*}}{\sqrt{q^2}}\sqrt{s_-}\eta^{*\alpha}(0)\,, \tag{B.37}$$

$$-h^{\alpha}_{V,0}(-1/2,+1/2,-1) = \sqrt{2}h^{\alpha}_{V,0}(-1/2,-1/2,0) = \frac{\sqrt{2}}{3}\frac{m_{\Lambda_b}+m_{\Lambda_c^*}}{\sqrt{q^2}}\sqrt{s_-}\eta^{*\alpha}(0)\,. \tag{B.38}$$

Similarly for the axialvector current

$$h^{\alpha}_{A,\lambda_q}(s_b,s_c,\lambda_c) \equiv \overline{u}^{\alpha}(k,\eta(\lambda_c),s_c)\not{\epsilon}^{*}(\lambda_q)\gamma_5 u(p,s_b)\,, \tag{B.39}$$

we identify

$$h^{\alpha}_{A,t}(s_b,s_c,\lambda_c) = -\frac{m_{\Lambda_b}+m_{\Lambda_c^*}}{\sqrt{q^2}}h^{\alpha}_{P}(s_b,s_c,\lambda_c)\,. \tag{B.40}$$

For the transverse polarisation we find

$$\frac{1}{\sqrt{2}}h^{\alpha}_{A,-1}(+1/2,-1/2,+1) = -h^{\alpha}_{A,-1}(+1/2,+1/2,0) = +\frac{2}{3}\sqrt{s_+}\eta^{*\alpha}(+1)\,, \tag{B.41}$$

$$-\frac{1}{\sqrt{2}}h^{\alpha}_{A,+1}(-1/2,+1/2,-1) = h^{\alpha}_{A,+1}(-1/2,-1/2,0) = +\frac{2}{3}\sqrt{s_+}\eta^{*\alpha}(-1)\,, \tag{B.42}$$

$$h^{\alpha}_{A,+1}(-1/2,-1/2,+1) = -\sqrt{2}h^{\alpha}_{A,+1}(-1/2,+1/2,0) = +\frac{2}{3}\sqrt{s_+}\eta^{*\alpha}(0)\,, \tag{B.43}$$

$$-h^{\alpha}_{A,-1}(+1/2,+1/2,-1) = \sqrt{2}h^{\alpha}_{A,-1}(+1/2,-1/2,0) = +\frac{2}{3}\sqrt{s_+}\eta^{*\alpha}(0)\,. \tag{B.44}$$

For the longitudinal polarization we find

$$-\frac{1}{\sqrt{2}}h^{\alpha}_{A,0}(-1/2,-1/2,+1) = h^{\alpha}_{A,0}(-1/2,+1/2,0) = +\frac{\sqrt{2}}{3}\frac{m_{\Lambda_b}-m_{\Lambda_c^*}}{\sqrt{q^2}}\sqrt{s_+}\eta^{*\alpha}(+1)\,, \tag{B.45}$$

$$\frac{1}{\sqrt{2}}h^{\alpha}_{A,0}(+1/2,+1/2,-1) = -h^{\alpha}_{A,0}(+1/2,-1/2,0) = +\frac{\sqrt{2}}{3}\frac{m_{\Lambda_b}-m_{\Lambda_c^*}}{\sqrt{q^2}}\sqrt{s_+}\eta^{*\alpha}(-1)\,, \tag{B.46}$$

$$-h^{\alpha}_{A,0}(+1/2,-1/2,+1) = \sqrt{2}h^{\alpha}_{A,0}(+1/2,+1/2,0) = +\frac{\sqrt{2}}{3}\frac{m_{\Lambda_b}-m_{\Lambda_c^*}}{\sqrt{q^2}}\sqrt{s_+}\eta^{*\alpha}(0)\,, \tag{B.47}$$

$$h^{\alpha}_{A,0}(-1/2,+1/2,-1) = -\sqrt{2}h^{\alpha}_{A,0}(-1/2,-1/2,0) = +\frac{\sqrt{2}}{3}\frac{m_{\Lambda_b}-m_{\Lambda_c^*}}{\sqrt{q^2}}\sqrt{s_+}\eta^{*\alpha}(0)\,. \tag{B.48}$$

Using the above expressions, we can now list the helicity amplitudes for the transition $\Lambda_b \to \Lambda_c(2595)^+$. For the vector current we find the following non-zero helicity amplitudes:

$$+\mathcal{A}_V^{(1/2)}(+1/2,+1/2,0) = +\mathcal{A}_V^{(1/2)}(-1/2,-1/2,0) = -\sqrt{\frac{1}{3}}f_{1/2,0}\frac{m_{\Lambda_b}+m_{\Lambda_c^*}}{\sqrt{q^2}}\sqrt{4m_{\Lambda_b}m_{\Lambda_c^*}}\,, \tag{B.49}$$

$$+\mathcal{A}_V^{(1/2)}(+1/2,+1/2,t) = +\mathcal{A}_V^{(1/2)}(-1/2,-1/2,t) = -\sqrt{\frac{1}{3}}f_{1/2,t}\frac{m_{\Lambda_b}-m_{\Lambda_c^*}}{\sqrt{q^2}}\sqrt{4m_{\Lambda_b}m_{\Lambda_c^*}}\,, \tag{B.50}$$

$$+\mathcal{A}_V^{(1/2)}(+1/2,-1/2,-1) = +\mathcal{A}_V^{(1/2)}(-1/2,+1/2,+1) = -\sqrt{\frac{2}{3}}f_{1/2,\perp}\sqrt{4m_{\Lambda_b}m_{\Lambda_c^*}}\,. \tag{B.51}$$

For the axialvector current we find similarly

$$+\mathcal{A}_A^{(1/2)}(+1/2,+1/2,0) = -\mathcal{A}_A^{(1/2)}(-1/2,-1/2,0) = -\sqrt{\frac{1}{3}}g_{1/2,0}\frac{m_{\Lambda_b}-m_{\Lambda_c^*}}{\sqrt{q^2}}\sqrt{4m_{\Lambda_b}m_{\Lambda_c^*}}\,, \tag{B.52}$$

$$+\mathcal{A}_A^{(1/2)}(+1/2,+1/2,t) = -\mathcal{A}_A^{(1/2)}(-1/2,-1/2,t) = -\sqrt{\frac{1}{3}}g_{1/2,t}\frac{m_{\Lambda_b}+m_{\Lambda_c^*}}{\sqrt{q^2}}\sqrt{4m_{\Lambda_b}m_{\Lambda_c^*}}\,, \tag{B.53}$$

$$+\mathcal{A}_A^{(1/2)}(+1/2,-1/2,-1) = -\mathcal{A}_A^{(1/2)}(-1/2,+1/2,+1) = +\sqrt{\frac{2}{3}}g_{1/2,\perp}\sqrt{4m_{\Lambda_b}m_{\Lambda_c^*}}\,. \tag{B.54}$$

In the heavy quark expansion, if we use eq. (4.10) for the vector current, we calculated the following helicitity amplitudes:

$$\begin{aligned}\mathcal{A}_V(+1/2,+1/2,0) = +\mathcal{A}_V(-1/2,-1/2,0) = \\ -\sqrt{\frac{1}{3}}\frac{m_{\Lambda_b}+m_{\Lambda_c^*}}{\sqrt{q^2}}\frac{\sqrt{s_+}}{m_{\Lambda_b}m_{\Lambda_c^*}}\Bigg\{\Bigg[s_-\left(C_1(\overline{w})+\frac{s_+(C_2(\overline{w})m_{\Lambda_c^*}+C_3(\overline{w})m_{\Lambda_b})}{2m_{\Lambda_b}m_{\Lambda_c^*}(m_{\Lambda_b}+m_{\Lambda_c^*})}\right) \\ +\frac{m_{\Lambda_b}-m_{\Lambda_c^*}}{m_{\Lambda_b}+m_{\Lambda_c^*}}\left(\frac{m_{\Lambda_b}^2-m_{\Lambda_c^*}^2+q^2}{2m_{\Lambda_b}}\overline{\Lambda}-\frac{m_{\Lambda_b}^2-m_{\Lambda_c^*}^2-q^2}{2m_{\Lambda_c^*}}\overline{\Lambda}'\right)\Bigg]\zeta \\ -2(m_{\Lambda_b}-m_{\Lambda_c^*})\zeta_{\rm SL}\Bigg\}\,,\end{aligned} \tag{B.55}$$

$$\mathcal{A}_V(+1/2,+1/2,t) = +\mathcal{A}_V(-1/2,-1/2,t) = \\ - \sqrt{\frac{1}{3}} \frac{m_{\Lambda_b} - m_{\Lambda_c^*}}{\sqrt{q^2}} \frac{\sqrt{s_-}}{m_{\Lambda_b} m_{\Lambda_c^*}} \left\{ \left[C_1(\overline{w}) s_+ \right.\right. \\ + \frac{m_{\Lambda_b} + m_{\Lambda_c^*}}{m_{\Lambda_b} - m_{\Lambda_c^*}} \left(\frac{m_{\Lambda_b}^2 - m_{\Lambda_c^*}^2 + q^2}{2 m_{\Lambda_b}} \left(\overline{\Lambda} + \frac{C_2(\overline{w}) s_+}{m_{\Lambda_b} + m_{\Lambda_c^*}} \right) \right. \\ \left.\left. \left. - \frac{m_{\Lambda_b}^2 - m_{\Lambda_c^*}^2 - q^2}{2 m_{\Lambda_c^*}} \left(\overline{\Lambda}' - \frac{C_3(\overline{w}) s_+}{m_{\Lambda_b} + m_{\Lambda_c^*}} \right) \right) \right] \zeta - 2 \frac{\left(m_{\Lambda_b} + m_{\Lambda_c^*}\right)^2}{m_{\Lambda_b} - m_{\Lambda_c^*}} \zeta_{\mathrm{SL}} \right\}, \tag{B.56}$$

$$\mathcal{A}_V(+1/2,-1/2,+1) = +\mathcal{A}_V(-1/2,+1/2,-1) = -\sqrt{\frac{2}{3}} \frac{\sqrt{s_+}}{m_{\Lambda_b} m_{\Lambda_c^*}} \left\{ \left[C_1(\overline{w}) s_- \right.\right. \\ \left.\left. + \frac{3 m_{\Lambda_b}^2 + m_{\Lambda_c^*}^2 - q^2}{2 m_{\Lambda_b}} \overline{\Lambda} - \frac{m_{\Lambda_b}^2 + 3 m_{\Lambda_c^*}^2 - q^2}{2 m_{\Lambda_c^*}} \overline{\Lambda}' \right] \zeta - 2 m_{\Lambda_b} \zeta_{\mathrm{SL}} \right\}, \tag{B.57}$$

while for the axial vector current in eq. (4.15) we obtain:

$$\mathcal{A}_A(+1/2,+1/2,0) = -\mathcal{A}_A(-1/2,-1/2,0) = \\ - \sqrt{\frac{1}{3}} \frac{m_{\Lambda_b} - m_{\Lambda_c^*}}{\sqrt{q^2}} \frac{\sqrt{s_-}}{m_{\Lambda_b} m_{\Lambda_c^*}} \left\{ \left[s_+ \left(C_1(\overline{w}) - \frac{s_-(C_2(\overline{w}) m_{\Lambda_c^*} + C_3(\overline{w}) m_{\Lambda_b})}{2 m_{\Lambda_b} m_{\Lambda_c^*} (m_{\Lambda_b} - m_{\Lambda_c^*})} \right) \right.\right. \\ \left. + \frac{m_{\Lambda_b} + m_{\Lambda_c^*}}{m_{\Lambda_b} - m_{\Lambda_c^*}} \left(\frac{m_{\Lambda_b}^2 - m_{\Lambda_c^*}^2 + q^2}{2 m_{\Lambda_b}} \overline{\Lambda} - \frac{m_{\Lambda_b}^2 - m_{\Lambda_c^*}^2 - q^2}{2 m_{\Lambda_c^*}} \overline{\Lambda}' \right) \right] \zeta \\ \left.\left. - 2 (m_{\Lambda_b} + m_{\Lambda_c^*}) \zeta_{\mathrm{SL}} \right\}, \tag{B.58}$$

$$\mathcal{A}_A(+1/2,+1/2,t) = -\mathcal{A}_A(-1/2,-1/2,t) = -\sqrt{\frac{1}{3}} \frac{m_{\Lambda_b} + m_{\Lambda_c^*}}{\sqrt{q^2}} \frac{\sqrt{s_+}}{m_{\Lambda_b} m_{\Lambda_c^*}} \left\{ \left[C_1(\overline{w}) s_- \right.\right. \\ + \frac{m_{\Lambda_b} - m_{\Lambda_c^*}}{m_{\Lambda_b} + m_{\Lambda_c^*}} \left(\frac{m_{\Lambda_b}^2 - m_{\Lambda_c^*}^2 + q^2}{2 m_{\Lambda_b}} \left(\overline{\Lambda} - \frac{C_2(\overline{w}) s_+}{m_{\Lambda_b} - m_{\Lambda_c^*}} \right) \right. \\ \left.\left. \left. - \frac{m_{\Lambda_b}^2 - m_{\Lambda_c^*}^2 - q^2}{2 m_{\Lambda_c^*}} \left(\overline{\Lambda}' + \frac{C_3(\overline{w}) s_+}{m_{\Lambda_b} + m_{\Lambda_c^*}} \right) \right) \right] \zeta - 2 \frac{\left(m_{\Lambda_b} - m_{\Lambda_c^*}\right)^2}{m_{\Lambda_b} + m_{\Lambda_c^*}} \zeta_{\mathrm{SL}} \right\}, \tag{B.59}$$

$$\mathcal{A}_A(+1/2,-1/2,+1) = -\mathcal{A}_A(-1/2,+1/2,-1) = \sqrt{\frac{2}{3}} \frac{\sqrt{s_-}}{m_{\Lambda_b} m_{\Lambda_c^*}} \left\{ \left[C_1(\overline{w}) s_+ \right.\right. \\ \left.\left. + \frac{3 m_{\Lambda_b}^2 + m_{\Lambda_c^*}^2 - q^2}{2 m_{\Lambda_b}} \overline{\Lambda} - \frac{m_{\Lambda_b}^2 + 3 m_{\Lambda_c^*}^2 - q^2}{2 m_{\Lambda_c^*}} \overline{\Lambda}' \right] \zeta + 2 m_{\Lambda_b} \zeta_{\mathrm{SL}} \right\}. \tag{B.60}$$

B.3.2 $1/2^+ \to 3/2^-$

We list here the $\Lambda_b \to \Lambda_c(2625)^+$ helicity amplitudes for various currents. For the scalar current

$$h_S^{\alpha}(s_b, s_c, \lambda_c) \equiv \overline{u}^{\alpha}(k, \eta(\lambda_c), s_c) u(p, s_b) \tag{B.61}$$

one finds the non-vanishing helicity amplitudes as follows:

$$\frac{\sqrt{2}}{3}h_S^\alpha(+1/2,+1/2,+1)=\sqrt{2}h_S^\alpha(-1/2,-1/2,+1)=h_S^\alpha(-1/2,+1/2,0)=\frac{\sqrt{2}}{3}\sqrt{s_+}\eta^{*\alpha}(+1)\,, \tag{B.62}$$

$$\frac{\sqrt{2}}{3}h_S^\alpha(-1/2,-1/2,-1)=\sqrt{2}h_S^\alpha(+1/2,+1/2,-1)=h_S^\alpha(+1/2,-1/2,0)=\frac{\sqrt{2}}{3}\sqrt{s_+}\eta^{*\alpha}(-1)\,, \tag{B.63}$$

$$h_S^\alpha(+1/2,-1/2,+1)=\frac{1}{\sqrt{2}}h_S^\alpha(+1/2,+1/2,0)=\frac{\sqrt{2}}{3}\sqrt{s_+}\eta^{*\alpha}(0)\,, \tag{B.64}$$

$$h_S^\alpha(-1/2,+1/2,-1)=\frac{1}{\sqrt{2}}h_S^\alpha(-1/2,-1/2,0)=\frac{\sqrt{2}}{3}\sqrt{s_+}\eta^{*\alpha}(0)\,. \tag{B.65}$$

For the pseudoscalar current

$$h_P^\alpha(s_b,s_c,\lambda_c)\equiv\overline{u}^\alpha(k,\eta(\lambda_c),s_c)\gamma_5 u(p,s_b) \tag{B.66}$$

one finds similarly:

$$-\frac{\sqrt{2}}{3}h_P^\alpha(+1/2,+1/2,+1)=\sqrt{2}h_P^\alpha(-1/2,-1/2,+1)=h_P^\alpha(-1/2,+1/2,0)=+\frac{\sqrt{2}}{3}\sqrt{s_-}\eta^{*\alpha}(+1)\,, \tag{B.67}$$

$$-\frac{\sqrt{2}}{3}h_P^\alpha(-1/2,-1/2,-1)=\sqrt{2}h_P^\alpha(+1/2,+1/2,-1)=h_P^\alpha(+1/2,-1/2,0)=-\frac{\sqrt{2}}{3}\sqrt{s_-}\eta^{*\alpha}(-1)\,, \tag{B.68}$$

$$h_P^\alpha(+1/2,-1/2,+1)=\frac{1}{\sqrt{2}}h_P^\alpha(+1/2,+1/2,0)=-\frac{\sqrt{2}}{3}\sqrt{s_-}\eta^{*\alpha}(0)\,, \tag{B.69}$$

$$h_P^\alpha(-1/2,+1/2,-1)=\frac{1}{\sqrt{2}}h_P^\alpha(-1/2,-1/2,0)=+\frac{\sqrt{2}}{3}\sqrt{s_-}\eta^{*\alpha}(0)\,. \tag{B.70}$$

For the vector current we investigate

$$h_{V,\lambda_q}^\alpha(s_b,s_c,\lambda_c)\equiv\overline{u}^\alpha(k,\eta(\lambda_c),s_c)\not{\epsilon}^*(\lambda_q)u(p,s_b)\,, \tag{B.71}$$

and identify

$$h_{V,t}^\alpha(s_b,s_c,\lambda_c)=\frac{m_{\Lambda_b}-m_{\Lambda_c^*}}{\sqrt{q^2}}h_S^\alpha(s_b,s_c,\lambda_c)\,. \tag{B.72}$$

For the transverse polarizations we find:

$$-\frac{\sqrt{2}}{3}h^{\alpha}_{V,+1}(-1/2,+1/2,+1)=\sqrt{2}h^{\alpha}_{V,-1}(+1/2,-1/2,+1)=h^{\alpha}_{V,-1}(+1/2,+1/2,0)=-\frac{2}{3}\sqrt{s_-}\eta^{*\alpha}(+1)\,, \tag{B.73}$$

$$\frac{\sqrt{2}}{3}h^{\alpha}_{V,-1}(+1/2,-1/2,-1)=\sqrt{2}h^{\alpha}_{V,+1}(-1/2,+1/2,-1)=h^{\alpha}_{V,+1}(-1/2,-1/2,0)=-\frac{2}{3}\sqrt{s_-}\eta^{*\alpha}(-1)\,, \tag{B.74}$$

$$h^{\alpha}_{V,+1}(-1/2,-1/2,+1)=\frac{1}{\sqrt{2}}h^{\alpha}_{V,+1}(-1/2,+1/2,0)=-\frac{2}{3}\sqrt{s_-}\eta^{*\alpha}(0)\,, \tag{B.75}$$

$$h^{\alpha}_{V,-1}(+1/2,+1/2,-1)=\frac{1}{\sqrt{2}}h^{\alpha}_{V,-1}(+1/2,-1/2,0)=-\frac{2}{3}\sqrt{s_-}\eta^{*\alpha}(0)\,. \tag{B.76}$$

For the longitudinal polarization we find

$$\begin{aligned}\frac{\sqrt{2}}{3}h^{\alpha}_{V,0}(+1/2,+1/2,+1)=\sqrt{2}h^{\alpha}_{V,0}(-1/2,-1/2,+1)&=h^{\alpha}_{V,0}(-1/2,+1/2,0)\\&=\frac{\sqrt{2}}{3}\frac{m_{\Lambda_b}+m_{\Lambda_c^*}}{\sqrt{q^2}}\sqrt{s_-}\eta^{*\alpha}(+1)\,,\end{aligned} \tag{B.77}$$

$$\begin{aligned}\frac{\sqrt{2}}{3}h^{\alpha}_{V,0}(-1/2,-1/2,-1)=\sqrt{2}h^{\alpha}_{V,0}(+1/2,+1/2,-1)&=h^{\alpha}_{V,0}(+1/2,-1/2,0)\\&=\frac{\sqrt{2}}{3}\frac{m_{\Lambda_b}+m_{\Lambda_c^*}}{\sqrt{q^2}}\sqrt{s_-}\eta^{*\alpha}(-1)\,,\end{aligned} \tag{B.78}$$

$$h^{\alpha}_{V,0}(+1/2,-1/2,+1)=\frac{1}{\sqrt{2}}h^{\alpha}_{V,0}(+1/2,+1/2,0)=\frac{\sqrt{2}}{3}\frac{m_{\Lambda_b}+m_{\Lambda_c^*}}{\sqrt{q^2}}\sqrt{s_-}\eta^{*\alpha}(0)\,, \tag{B.79}$$

$$h^{\alpha}_{V,0}(-1/2,+1/2,-1)=\frac{1}{\sqrt{2}}h^{\alpha}_{V,0}(-1/2,-1/2,0)=\frac{\sqrt{2}}{3}\frac{m_{\Lambda_b}+m_{\Lambda_c^*}}{\sqrt{q^2}}\sqrt{s_-}\eta^{*\alpha}(0)\,. \tag{B.80}$$

For the axialvector current we investigate

$$h^{\alpha}_{A,\lambda_q}(s_b,s_c,\lambda_c)\equiv\overline{u}^{\alpha}(k,\eta(\lambda_c),s_c)\not{\epsilon}^*(\lambda_q)\gamma_5 u(p,s_b)\,, \tag{B.81}$$

and identify

$$h^{\alpha}_{A,t}(s_b,s_c,\lambda_c)=-\frac{m_{\Lambda_b}+m_{\Lambda_c^*}}{\sqrt{q^2}}h^{\alpha}_{P}(s_b,s_c,\lambda_c)\,. \tag{B.82}$$

For the transverse polarizations we find:

$$\begin{aligned}-\frac{\sqrt{2}}{3}h^{\alpha}_{A,+1}(-1/2,+1/2,+1)=\sqrt{2}h^{\alpha}_{A,-1}(+1/2,-1/2,+1)&=h^{\alpha}_{A,-1}(+1/2,+1/2,0)\\&=\frac{2}{3}\sqrt{s_+}\eta^{*\alpha}(+1)\,,\end{aligned} \tag{B.83}$$

$$\begin{aligned}-\frac{\sqrt{2}}{3}h^{\alpha}_{A,-1}(+1/2,-1/2,-1)=\sqrt{2}h^{\alpha}_{A,+1}(-1/2,+1/2,-1)&=h^{\alpha}_{A,+1}(-1/2,-1/2,0)\\&=-\frac{2}{3}\sqrt{s_+}\eta^{*\alpha}(-1)\,,\end{aligned} \tag{B.84}$$

$$h^{\alpha}_{A,+1}(-1/2,-1/2,+1)=\frac{1}{\sqrt{2}}h^{\alpha}_{A,+1}(-1/2,+1/2,0)=-\frac{2}{3}\sqrt{s_+}\eta^{*\alpha}(0)\,, \tag{B.85}$$

$$h^{\alpha}_{A,-1}(+1/2,+1/2,-1)=\frac{1}{\sqrt{2}}h^{\alpha}_{A,-1}(+1/2,-1/2,0)=+\frac{2}{3}\sqrt{s_+}\eta^{*\alpha}(0)\,. \tag{B.86}$$

For the longitudinal polarization we find

$$-\frac{\sqrt{2}}{3}h^{\alpha}_{A,0}(+1/2,+1/2,+1)=\sqrt{2}h^{\alpha}_{A,0}(-1/2,-1/2,+1)=h^{\alpha}_{A,0}(-1/2,+1/2,0)$$
$$=-\frac{\sqrt{2}}{3}\frac{m_{\Lambda_b}-m_{\Lambda_c^*}}{\sqrt{q^2}}\sqrt{s_+}\eta^{*\alpha}(+1)\,, \tag{B.87}$$

$$-\frac{\sqrt{2}}{3}h^{\alpha}_{A,0}(-1/2,-1/2,-1)=\sqrt{2}h^{\alpha}_{A,0}(+1/2,+1/2,-1)=h^{\alpha}_{A,0}(+1/2,-1/2,0)$$
$$=+\frac{\sqrt{2}}{3}\frac{m_{\Lambda_b}-m_{\Lambda_c^*}}{\sqrt{q^2}}\sqrt{s_+}\eta^{*\alpha}(-1)\,, \tag{B.88}$$

$$h^{\alpha}_{A,0}(+1/2,-1/2,+1)=\frac{1}{\sqrt{2}}h^{\alpha}_{A,0}(+1/2,+1/2,0)=+\frac{\sqrt{2}}{3}\frac{m_{\Lambda_b}-m_{\Lambda_c^*}}{\sqrt{q^2}}\sqrt{s_+}\eta^{*\alpha}(0)\,, \tag{B.89}$$

$$h^{\alpha}_{A,0}(-1/2,+1/2,-1)=\frac{1}{\sqrt{2}}h^{\alpha}_{A,0}(-1/2,-1/2,0)=-\frac{\sqrt{2}}{3}\frac{m_{\Lambda_b}-m_{\Lambda_c^*}}{\sqrt{q^2}}\sqrt{s_+}\eta^{*\alpha}(0)\,. \tag{B.90}$$

For the vector current we find the following non-zero helicity amplitudes:

$$+\mathcal{A}_V^{(3/2)}(+1/2,+3/2,+1)=+\mathcal{A}_V^{(3/2)}(-1/2,-3/2,-1)=-2F_{3/2,\perp}\sqrt{4\,m_{\Lambda_b}\,m_{\Lambda_c^*}}\,, \tag{B.91}$$

$$+\mathcal{A}_V^{(3/2)}(+1/2,+1/2,0)=+\mathcal{A}_V^{(3/2)}(-1/2,-1/2,0)=+\sqrt{\frac{2}{3}}F_{1/2,0}\frac{m_{\Lambda_b}+m_{\Lambda_c^*}}{\sqrt{q^2}}\sqrt{4\,m_{\Lambda_b}\,m_{\Lambda_c^*}}\,, \tag{B.92}$$

$$+\mathcal{A}_V^{(3/2)}(+1/2,+1/2,t)=+\mathcal{A}_V^{(3/2)}(-1/2,-1/2,t)=+\sqrt{\frac{2}{3}}F_{1/2,t}\frac{m_{\Lambda_b}-m_{\Lambda_c^*}}{\sqrt{q^2}}\sqrt{4\,m_{\Lambda_b}\,m_{\Lambda_c^*}}\,, \tag{B.93}$$

$$+\mathcal{A}_V^{(3/2)}(+1/2,-1/2,-1)=+\mathcal{A}_V^{(3/2)}(-1/2,+1/2,+1)=-\frac{2}{\sqrt{3}}F_{1/2,\perp}\sqrt{4\,m_{\Lambda_b}\,m_{\Lambda_c^*}}\,. \tag{B.94}$$

For the axialvector current we find similarly

$$+\mathcal{A}_A^{(3/2)}(+1/2,+3/2,+1)=-\mathcal{A}_A^{(3/2)}(-1/2,-3/2,-1)=-2G_{3/2,\perp}\sqrt{4\,m_{\Lambda_b}\,m_{\Lambda_c^*}}\,, \tag{B.95}$$

$$+\mathcal{A}_A^{(3/2)}(+1/2,+1/2,0)=-\mathcal{A}_A^{(3/2)}(-1/2,-1/2,0)=+\sqrt{\frac{2}{3}}G_{1/2,0}\frac{m_{\Lambda_b}-m_{\Lambda_c^*}}{\sqrt{q^2}}\sqrt{4\,m_{\Lambda_b}\,m_{\Lambda_c^*}}\,, \tag{B.96}$$

$$+\mathcal{A}_A^{(3/2)}(+1/2,+1/2,t)=-\mathcal{A}_A^{(3/2)}(-1/2,-1/2,t)=+\sqrt{\frac{2}{3}}G_{1/2,t}\frac{m_{\Lambda_b}+m_{\Lambda_c^*}}{\sqrt{q^2}}\sqrt{4\,m_{\Lambda_b}\,m_{\Lambda_c^*}}\,, \tag{B.97}$$

$$+\mathcal{A}_A^{(3/2)}(+1/2,-1/2,-1)=-\mathcal{A}_A^{(3/2)}(-1/2,+1/2,+1)=+\frac{2}{\sqrt{3}}G_{1/2,\perp}\sqrt{4\,m_{\Lambda_b}\,m_{\Lambda_c^*}}\,. \tag{B.98}$$

In the heavy quark expansion, the helicity amplitudes related to the vector current eq. (4.10)

read

$$\mathcal{A}_V(+1/2,+3/2,+1) = +\,\mathcal{A}_V(-1/2,-3/2,-1) = +2\frac{\sqrt{s_+}}{m_{\Lambda_b}}\zeta_{\rm SL}\,, \tag{B.99}$$

$$\begin{aligned}\mathcal{A}_V(+1/2,+1/2,0) = &+\,\mathcal{A}_V(-1/2,-1/2,0) = +\sqrt{\frac{2}{3}}\,\frac{m_{\Lambda_b}+m_{\Lambda_c^*}}{\sqrt{q^2}}\,\frac{\sqrt{s_+}}{m_{\Lambda_b}m_{\Lambda_c^*}}\,\Bigg\{\Bigg[s_-\Bigg(C_1(\overline{w})\\ &+ s_+\frac{C_2(\overline{w})m_{\Lambda_c^*}+C_3(\overline{w})m_{\Lambda_b}}{2m_{\Lambda_b}m_{\Lambda_c^*}(m_{\Lambda_b}+m_{\Lambda_c^*})}\Bigg)+\frac{m_{\Lambda_b}-m_{\Lambda_c^*}}{m_{\Lambda_b}+m_{\Lambda_c^*}}\Bigg(\frac{m_{\Lambda_b}^2-m_{\Lambda_c^*}^2+q^2}{2m_{\Lambda_b}}\overline{\Lambda}\\ &-\frac{m_{\Lambda_b}^2-m_{\Lambda_c^*}^2-q^2}{2m_{\Lambda_c^*}}\overline{\Lambda}'\Bigg)\Bigg]\zeta+(m_{\Lambda_b}-m_{\Lambda_c^*})\zeta_{\rm SL}\Bigg\}\,,\end{aligned} \tag{B.100}$$

$$\begin{aligned}\mathcal{A}_V(+1/2,+1/2,t) = &+\,\mathcal{A}_V(-1/2,-1/2,t) = +\sqrt{\frac{2}{3}}\,\frac{m_{\Lambda_b}-m_{\Lambda_c^*}}{m_{\Lambda_b}m_{\Lambda_c^*}}\,\frac{\sqrt{s_-}}{\sqrt{q^2}}\,\Bigg\{\Bigg[s_+\\ &+\frac{m_{\Lambda_b}+m_{\Lambda_c^*}}{m_{\Lambda_b}-m_{\Lambda_c^*}}\left(\frac{m_{\Lambda_b}^2-m_{\Lambda_c^*}^2+q^2}{2m_{\Lambda_b}}\left(\overline{\Lambda}+\frac{C_2(\overline{w})s_+}{m_{\Lambda_b}+m_{\Lambda_c^*}}\right)\right.\\ &\left.-\frac{m_{\Lambda_b}^2-m_{\Lambda_c^*}^2-q^2}{2m_{\Lambda_c^*}}\left(\overline{\Lambda}'-\frac{C_3(\overline{w})s_+}{m_{\Lambda_b}+m_{\Lambda_c^*}}\right)\right)\Bigg]\zeta+\frac{(m_{\Lambda_b}+m_{\Lambda_c^*})^2}{m_{\Lambda_b}-m_{\Lambda_c^*}}\zeta_{\rm SL}\Bigg\}\,,\end{aligned} \tag{B.101}$$

$$\begin{aligned}\mathcal{A}_V(+1/2,-1/2,-1) = &+\,\mathcal{A}_V(-1/2,+1/2,+1) = -\sqrt{\frac{4}{3}}\,\frac{\sqrt{s_+}}{m_{\Lambda_b}m_{\Lambda_c^*}}\,\Bigg\{\Bigg[s_-C_1(\overline{w})\\ &-\frac{3m_{\Lambda_b}^2+m_{\Lambda_c^*}^2-q^2}{2m_{\Lambda_b}}\overline{\Lambda}+\frac{m_{\Lambda_b}^2+3m_{\Lambda_c^*}^2-q^2}{2m_{\Lambda_c^*}}\overline{\Lambda}'\Bigg]\zeta+m_{\Lambda_b}\zeta_{\rm SL}\Bigg\}\,,\end{aligned} \tag{B.102}$$

while for the axial vector current eq. (4.15), we obtain

$$\mathcal{A}_A(+1/2,+3/2,-1) = -\,\mathcal{A}_A(-1/2,-3/2,+1) = 2\frac{\sqrt{s_-}}{m_{\Lambda_b}}\zeta_{\rm SL}\,, \tag{B.103}$$

$$\begin{aligned}\mathcal{A}_A(+1/2,+1/2,0) = &-\,\mathcal{A}_A(-1/2,-1/2,0) = +\sqrt{\frac{2}{3}}\,\frac{m_{\Lambda_b}-m_{\Lambda_c^*}}{\sqrt{q^2}}\,\frac{\sqrt{s_-}}{m_{\Lambda_b}m_{\Lambda_c^*}}\,\Bigg\{\Bigg[s_+\Bigg(C_1(\overline{w})\\ &-s_-\frac{C_2(\overline{w})m_{\Lambda_c^*}+C_3(\overline{w})m_{\Lambda_b}}{2m_{\Lambda_b}m_{\Lambda_c^*}(m_{\Lambda_b}+m_{\Lambda_c^*})}\Bigg)+\Bigg(\frac{m_{\Lambda_b}^2-m_{\Lambda_c^*}^2+q^2}{2m_{\Lambda_b}}\overline{\Lambda}\\ &-\frac{m_{\Lambda_b}^2-m_{\Lambda_c^*}^2-q^2}{2m_{\Lambda_c^*}}\overline{\Lambda}'\Bigg)\frac{(m_{\Lambda_b}+m_{\Lambda_c^*})}{m_{\Lambda_b}-m_{\Lambda_c^*}}\Bigg]\zeta+(m_{\Lambda_b}+m_{\Lambda_c^*})\zeta_{\rm SL}\Bigg\}\,,\end{aligned} \tag{B.104}$$

$$\begin{aligned}\mathcal{A}_A(+1/2,+1/2,t) = &-\,\mathcal{A}_A(-1/2,-1/2,t) = +\sqrt{\frac{2}{3}}\,\frac{m_{\Lambda_b}+m_{\Lambda_c^*}}{\sqrt{q^2}}\,\frac{\sqrt{s_+}}{m_{\Lambda_b}m_{\Lambda_c^*}}\,\Bigg\{\Bigg[s_-\\ &+\frac{(m_{\Lambda_b}-m_{\Lambda_c^*})}{m_{\Lambda_b}+m_{\Lambda_c^*}}\left(\frac{m_{\Lambda_b}^2-m_{\Lambda_c^*}^2+q^2}{2m_{\Lambda_b}}\left(\overline{\Lambda}-\frac{C_2(\overline{w})s_-}{m_{\Lambda_b}-m_{\Lambda_c^*}}\right)\right.\\ &\left.-\frac{m_{\Lambda_b}^2-m_{\Lambda_c^*}^2-q^2}{2m_{\Lambda_c^*}}\left(\overline{\Lambda}'+\frac{C_3(\overline{w})s_-}{m_{\Lambda_b}-m_{\Lambda_c^*}}\right)\right)\Bigg]\zeta+\frac{(m_{\Lambda_b}-m_{\Lambda_c^*})^2}{m_{\Lambda_b}+m_{\Lambda_c^*}}\zeta_{\rm SL}\Bigg\}\,,\end{aligned} \tag{B.105}$$

$$\mathcal{A}_A(+1/2,-1/2,+1) = -\,\mathcal{A}_A(-1/2,+1/2,-1) = +\sqrt{\frac{4}{3}}\,\frac{\sqrt{s_-}}{m_{\Lambda_b}m_{\Lambda_c^*}}\,\Bigg\{\Bigg[s_+C_1(\overline{w})$$

$$+\frac{3m_{\Lambda_b}^2+m_{\Lambda_c^*}^2-q^2}{2m_{\Lambda_b}}\overline{\Lambda}-\frac{m_{\Lambda_b}^2+3m_{\Lambda_c^*}^2-q^2}{2m_{\Lambda_c^*}}\overline{\Lambda}'\Big]\zeta+m_{\Lambda_b}\zeta_{\rm SL}\Big\}\,. \quad \text{(B.106)}$$

B.4 Details on the Kinematics

We choose the z axis along the flight direction of the Λ_c^*. Thus, in the rest frame of the Λ_b^0 (B-RF) one has

$$p^\mu\big|_{\text{B-RF}}=(m_{\Lambda_b^0},0,0,0)\,, \quad \text{(B.107)}$$
$$q^\mu\big|_{\text{B-RF}}=(q^0,0,0,-|\vec{q}|)\,, \quad \text{(B.108)}$$
$$k^\mu\big|_{\text{B-RF}}=(m_{\Lambda_b^0}-q^0,0,0,+|\vec{q}|)\,. \quad \text{(B.109)}$$

We chose to describe the decay through the invariants q^2 and obtain

$$q^0\big|_{B-RF}=\frac{m_{\Lambda_b}^2-m_{\Lambda_c^*}^2+q^2}{2m_{\Lambda_b}}\,,\qquad |\vec{q}|\big|_{B-RF}=\frac{\sqrt{\lambda(m_{\Lambda_b}^2,m_{\Lambda_c^*}^2,q^2)}}{2m_{\Lambda_b}}\,, \quad \text{(B.110)}$$

where λ is the usual Källén function.

The description of the Λ_c^* involves a spin-1 polarization vector $\eta(m)$ along the positive z direction. According to [191] we can use

$$\eta(\pm)|_{B-RF}=(0,\mp1,-i,0)/\sqrt{2}\,, \quad \text{(B.111)}$$
$$\eta(0)|_{B-RF}=(|\vec{q}|,0,0,m_{\Lambda_b}-q^0)/m_{\Lambda_c^*}\,. \quad \text{(B.112)}$$

In order to facilitate the calculation we introduce artificial polarization vectors $\varepsilon(n)$ which fulfill the following relations:

$$\varepsilon(n)\cdot q=0 \qquad n=\pm,0 \quad \text{(B.113)}$$
$$\varepsilon(n)\cdot\varepsilon^\dagger(n')=g_{nn'} \qquad g_{nn'}=\text{diag}(+,-,-,-)\text{ for }n,n'=t,+,-,0 \quad \text{(B.114)}$$
$$\varepsilon(n)_\mu\varepsilon^\dagger(n')_\nu g_{nn'}=g_{\mu\nu}\,. \quad \text{(B.115)}$$

Within the $\ell\nu$ rest frame these relations are fulfilled by the set

$$\varepsilon^\mu(t)\big|_{\ell\nu-RF}=(1,0,0,0)\,, \quad \text{(B.116)}$$
$$\varepsilon^\mu(\pm)\big|_{\ell\nu-RF}=(0,\pm1,-i,0)/\sqrt{2}\,, \quad \text{(B.117)}$$
$$\varepsilon^\mu(0)\big|_{\ell\nu-RF}=(0,0,0,-1)\,. \quad \text{(B.118)}$$

Using a boost along z, one obtains in the B rest frame

$$\varepsilon^\mu(t)\big|_{B-RF}=(q^0,0,0,-|\vec{q}|)/\sqrt{q^2}=q^\mu/\sqrt{q^2}\,, \quad \text{(B.119)}$$
$$\varepsilon^\mu(0)\big|_{B-RF}=(+|\vec{q}|,0,0,-q_0)/\sqrt{q^2}\,, \quad \text{(B.120)}$$

while the $\varepsilon(\pm)$ remain invariant under that boost. Comments are due on the choice of the polarization vectors, especially the signs of $\varepsilon^z(0)$ as well as $\varepsilon^y(\pm)$. These haven been adopted to obtain longitudinal and right-handed/left-handed polarization of the $\ell\nu$ system, which moves along the *negative* z-axis. The phase convention is as in [191].

B.5 Explicit Spinor Representations

In the course of the calculations we need to use explicit representations of spinors for an arbitrary momentum and fixed helicity in their rest frame. In the chiral representation of Dirac spinors, one obtains for a u spinor with momentum p^μ,

$$p^\mu = (p^0, |\vec{p}|\sin\theta\cos\phi, |\vec{p}|\sin\theta\sin\phi, |\vec{p}|\cos\theta), \tag{B.121}$$

with $p^2 = m^2$ and helicity $h = \pm 1/2$ in their respective rest frames [191]

$$u(p, h = +1/2) = \frac{\gamma^0}{\sqrt{2(p^0+m)}} \begin{bmatrix} +(p^0+m-|\vec{p}|) & \cos(\theta/2) & \\ +(p^0+m-|\vec{p}|) & \sin(\theta/2) & \exp(+i\phi) \\ +(p^0+m+|\vec{p}|) & \cos(\theta/2) & \\ +(p^0+m+|\vec{p}|) & \sin(\theta/2) & \exp(+i\phi) \end{bmatrix} \tag{B.122}$$

$$u(p, h = -1/2) = \frac{\gamma^0}{\sqrt{2(p^0+m)}} \begin{bmatrix} -(p^0+m+|\vec{p}|) & \sin(\theta/2) & \exp(-i\phi) \\ +(p^0+m+|\vec{p}|) & \cos(\theta/2) & \\ -(p^0+m-|\vec{p}|) & \sin(\theta/2) & \exp(-i\phi) \\ +(p^0+m-|\vec{p}|) & \cos(\theta/2) & \end{bmatrix}. \tag{B.123}$$

B.6 Formulae

For the Levi-Civita tensor we use the convention

$$\varepsilon^{0123} = -\varepsilon_{0123} = +1\,. \tag{B.124}$$

In this convention one has

$$\mathrm{tr}\,\gamma^\mu\gamma^\nu\gamma^\rho\gamma^\sigma\gamma_5 = -4i\varepsilon^{\mu\nu\rho\sigma} \tag{B.125}$$

$$\varepsilon^{\alpha\beta\mu\nu}\varepsilon_{\alpha\beta\rho\sigma} = -2(\delta^\mu_\rho\delta^\nu_\sigma - \delta^\mu_\sigma\delta^\nu_\rho) \tag{B.126}$$

$$\sigma_{\mu\nu}\gamma_5 = \frac{i}{2}\varepsilon_{\mu\nu\alpha\beta}\sigma^{\alpha\beta} \tag{B.127}$$

B.7 Additional material on the sensitivity study

We show in Fig. B.1 the distributions of the Isgur-Wise parameters resulting from a two-dimensional fit to both q^2 and $\cos\theta_l$, comparing ensembles of pseudo-experiments using only the $\Lambda_c(2595)^+$, only the $\Lambda_c(2625)^+$, or both. In Fig. B.2 we investigate the correlations between the Isgur-Wise parameters resulting from a two-dimensional fit to q^2 and $\cos\theta_l$ of the three sets of pseudo-experiments. In particular, the leftmost plots demonstrate how only a simultaneous fit to both Λ_c^{*+} states can solve the degeneracy between the two slope parameters. Moreover, both $\Lambda_c(2595)^+$ and $\Lambda_c(2625)^+$ data sets are individually sensitive to the δ_{SL} parameter, but a simultaneous fit provides much better precision.

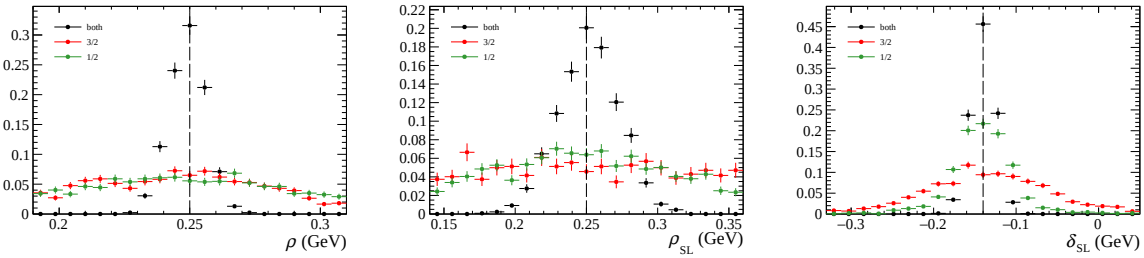

Figure B.1: Distribution of the Isgur-Wise parameters as fitted from an ensemble of pseudo-experiments. The distributions are shown for the cases when one of the two Λ_c^{*+} states is fitted, as well as the combination of both. Both q^2 and $\cos\theta_l$ are fitted simultaneously.

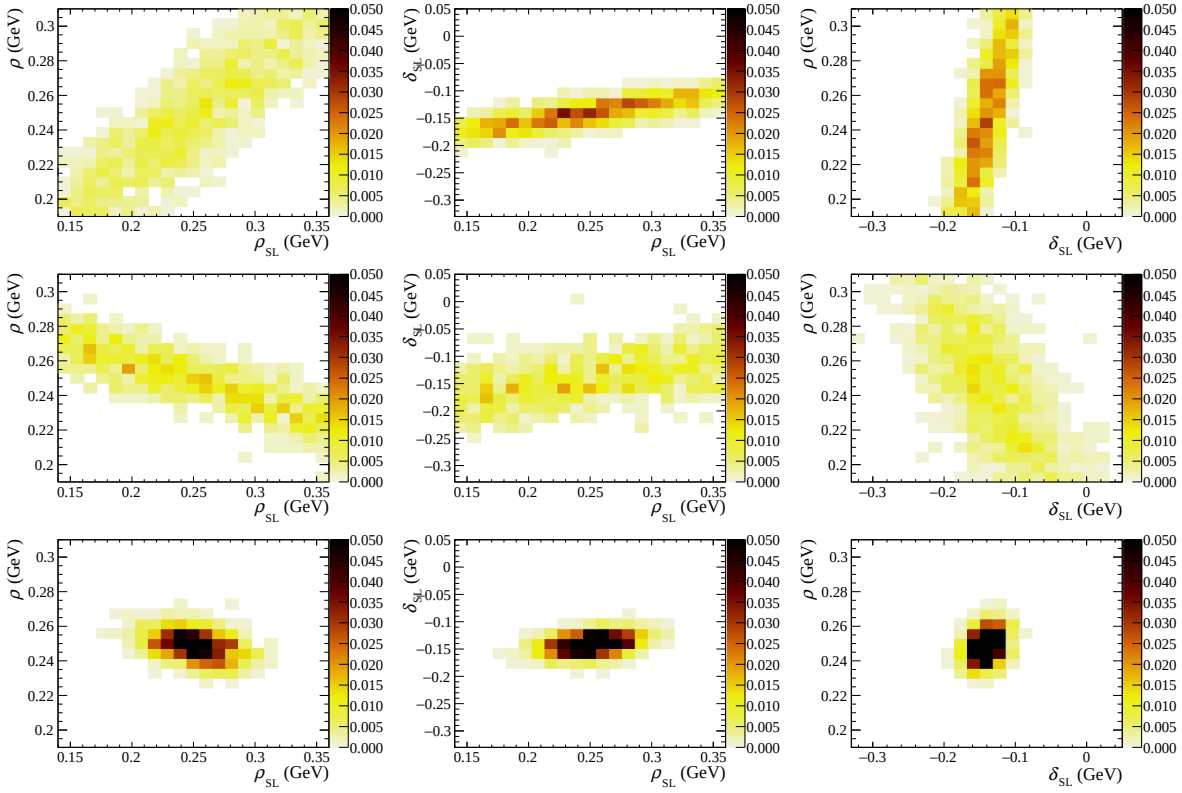

Figure B.2: Two-dimensional distributions of the Isgur-Wise parameters as fitted from an ensemble of pseudoexperiments. Both q^2 and $\cos\theta_l$ are fitted simultaneously. Only simulated $\Lambda_c(2595)^+$ and $\Lambda_c(2625)^+$ data are used for the pseudoexperiments shown in the first and second row, respectively. Both states are fitted in the pseudoexperiments shown in the third row.

Appendix C

Appendix to Chapter 6

C.1 Hadronic Form Factors for $B \to V$ or $B \to P$ transitions

We need to express explicitly the hadronic matrix elements through Lorentz invariant form factors. for $B \to P$ transitions, where P is any pseudo-scalar meson, we have [62]:

$$\langle P(k)|\overline{q}_i\gamma_\mu b|\overline{B}(p)\rangle = \left[(p+k)_\mu - \frac{m_B^2 - m_P^2}{q^2}q_\mu\right] f_+(q^2) + q_\mu \frac{m_B^2 - m_P^2}{q^2} f_0(q^2) \tag{C.1}$$

$$\langle P(k)|[\overline{q}_i b](\mu)|\overline{B}(p)\rangle = \frac{1}{m_b(\mu) - m_{q_i}(\mu)} q^\mu \langle P(k)|\overline{q}_i\gamma_\mu b|\overline{B}(p)\rangle = \frac{m_B^2 - m_P^2}{m_b(\mu) - m_{q_i}(\mu)} f_0(q^2). \tag{C.2}$$

Instead, for $B \to V$ transitions, where V is a vector meson, we use:

$$\langle V(k,\eta)|\overline{q}_i\gamma_\mu b|\overline{B}(p)\rangle = i\epsilon_{\mu\nu\rho\sigma}\eta^{\nu *}p^\rho k^\sigma \frac{2V(q^2)}{m_B + m_V}, \tag{C.3}$$

$$\begin{aligned}\langle V(k,\eta)|\overline{q}_i\gamma_\mu\gamma_5 b|\overline{B}(p)\rangle &= \eta_\mu^*(m_B + m_V)A_1(q^2) - (p+k)_\mu(\eta^*\cdot q)\frac{A_2(q^2)}{m_B + m_V} \\ &\quad - q_\mu(\eta^*\cdot q)\frac{2m_V}{q^2}[A_3(q^2) - A_0(q^2)],\end{aligned} \tag{C.4}$$

$$\begin{aligned}\langle V(k,\eta)|[\overline{q}_i\gamma_5 b](\mu)|\overline{B}(p)\rangle &= -\frac{1}{m_b(\mu) + m_{q_i}(\mu)} q_\mu \langle V(k,\eta)|\overline{q}_i\gamma_\mu\gamma_5 b|\overline{B}(p)\rangle \\ &= (\eta^*\cdot q)\frac{2m_V}{m_b(\mu) + m_{q_i}(\mu)} A_0(q^2).\end{aligned} \tag{C.5}$$

where we can express $A_3(q^2)$ as:

$$A_3(q^2) = \frac{m_B + m_V}{2m_V}A_1(q^2) - \frac{m_B - m_V}{2m_V}A_2(q^2), \tag{C.6}$$

and we changed the form factors basis in

$$V(q^2) = \frac{m_B(m_B + m_V)}{\sqrt{2\lambda}}F_\perp, \tag{C.7}$$

$$A_1(q^2) = \frac{m_B}{\sqrt{2}(m_B + m_V)}F_\parallel, \tag{C.8}$$

$$A_2(q^2) = -\frac{2m_V m_B^2(m_B + m_V)}{\lambda}F_0(q^2) + \frac{m_B(m_B + m_V)(m_B^2 - m_V^2 - q^2)}{\sqrt{2}\lambda}A_1(q^2), \tag{C.9}$$

$$A_0(q^2) = \frac{m_B^2}{\sqrt{\lambda}}F_t(q^2). \tag{C.10}$$

C.2 Differential decay width for $B \to K\ell\bar{\ell}$

In this Appendix we intend to give the complete expression for the differential decay width of the process $B \to K\ell\bar{\ell}$, where $\ell = \mu, \tau, \nu$. For this purpose we keep the full dependence from the lepton mass, which gives a non negligible contribution in the case $\ell = \tau$.
The most general Lagrangian that arises from the operators in tables 6.2–6.3 assumes the form:

$$\mathcal{L}(b \to s\ell\bar{\ell}) = -\frac{2G_F}{\sqrt{2}}\frac{\alpha_e}{2\pi}V_{ts}^* V_{tb}\left[C_9\mathcal{O}_9 + C_{10}\mathcal{O}_{10} + C_S(\mathcal{O}_S - \mathcal{O}_P)\right], \tag{C.11}$$

where the operators are defined as

$$\begin{aligned} \mathcal{O}_9 &= (\bar{s}\gamma_\mu P_L b)(\bar{\ell}\gamma_\mu \ell) \quad & \mathcal{O}_{10} &= (\bar{s}\gamma_\mu P_L)b(\bar{\ell}\gamma_\mu\gamma_5\ell), \\ \mathcal{O}_S &= (\bar{s}P_R b)(\ell\bar{\ell}) & \mathcal{O}_P &= (\bar{s}P_R b)(\bar{\ell}\gamma_5\ell). \end{aligned} \tag{C.12}$$

By mean of explicit calculation, we can write the double differential decay width as

$$\frac{\mathrm{d}^2\Gamma}{\mathrm{d}\cos\theta\ \mathrm{d}q^2} = a_\ell + b_\ell\cos\theta + c_\ell\cos^2\theta \tag{C.13}$$

and the coefficients are

$$\begin{aligned} \frac{4a_\ell}{\Gamma_0} =& (|C_9|^2 + |C_{10}|^2)f_+^2\lambda + 4|C_{10}|^2\frac{m_\ell^2}{q^2}\left[f_0^2(m_B^2 - m_K^2)^2 - f_+^2\lambda\right] \\ & - \frac{4C_S C_{10} f_0^2 m_\ell (m_B^2 - m_K^2)^2}{m_b - m_s} + \frac{2C_S^2 f_0^2 (m_B^2 - m_K^2)^2(q^2 - 2m_\ell^2)}{(m_b - m_s)^2}, \end{aligned} \tag{C.14}$$

$$\frac{b_\ell}{\Gamma_0} = \frac{C_S C_9 f_+ f_0 \sqrt{\lambda} m_\ell (m_B^2 - m_K^2)\beta_\ell}{m_b - m_s}, \tag{C.15}$$

$$\frac{4c_\ell}{\Gamma_0} = -\beta_\ell^2\lambda f_+^2\left(|C_9|^2 + |C_{10}|^2\right). \tag{C.16}$$

where

$$\beta_\ell = \sqrt{1 - \frac{4m_\ell^2}{q^2}}, \qquad \Gamma_0 = \frac{\alpha_e^2 G_F^2 \sqrt{\lambda}\beta_\ell |V_{tb}V_{ts}^*|^2}{512\ \pi^5 m_B^3}, \tag{C.17}$$

$$\lambda = m_B^4 + m_K^4 + q^4 - 2m_B^2 q^2 - 2m_K^2 q^2 - 2m_B^2 m_K^2. \tag{C.18}$$

Performing the angular integration we get the following differential decay width:

$$\begin{aligned} \frac{\mathrm{d}\Gamma}{\mathrm{d}q^2}(B \to K\ell\bar{\ell}) =& \frac{\Gamma_0}{6}\left[(|C_9|^2 + |C_{10}|^2)(3 - \beta_\ell^2)f_+^2\lambda + 12|C_{10}|^2\frac{m_\ell^2}{q^2}\left(f_0^2(m_B^2 - m_K^2)^2 - f_+^2\lambda\right)\right] \\ & - 2\Gamma_0 C_S C_{10}\frac{f_0^2 m_\ell\left(m_B{}^2 - m_K^2\right)^2}{m_b - m_s} + \Gamma_0 C_S^2\frac{f_0^2\left(m_B^2 - m_K^2\right)^2\left(q^2 - 2m_\ell^2\right)}{(m_b - m_s)^2} \end{aligned} \tag{C.19}$$

Scientific publications

1. M.Bordone, C.Cornella, J. Fuentes-Martín, G.Isidori, *Low-energy signatures of the PS^3 model: from B-physics anomalies to LFV*, [arxiv:1805.09328[hep-ph]]
2. P. Böer, M.Bordone, E.Graverini, P. Owen, M. Rotondo, D.van Dyk, *Testing lepton flavour universality in semileptonic $\Lambda_b \to \Lambda_c^*$ decays*, [arxiv:1801.08367[hep-ph]]
3. M.Bordone, C.Cornella, J. Fuentes-Martín, G.Isidori, *A three-site gauge model for flavor hierarchies and flavor anomalies*, **Phys.Lett. B779 (2018) 317-323** , [arxiv:1712.01368[hep-ph]]
4. M.Bordone, D.Buttazzo, G.Isidori, J.Monnard, *Probing Lepton flavour universality with $K \to \pi\nu\overline{\nu}$ decays*, **Eur.Phys.J. C77 (2017) no.9, 618**, [arxiv:1705.10729[hep-ph]]
5. M.Bordone, G.Isidori, S. Trifinopoulus, *Semi-leptonic B-physics anomalies: a general EFT anlysis within the $U(2)^n$ flavor symmetry*, **Phys.Rev. D96 (2017) no.1, 015038**, [arxiv:1702.07238[hep-ph]]
6. C.Biggio, M.Bordone, L.Di Luzio, G.Ridolfi, *Massive vectors and loop observables: the $g-2$ case*, **JHEP 1610 (2016) 002**, [arXiv:1607.07621[hep-ph]]
7. M.Bordone, G.Isidori, A.Pattori, *On the Standard Model predictions for R_K and R_{K^*}*, **Eur.Phys.J. C76 (2016) no.8, 440**, [arXiv:1605.07633[hep-ph]]
8. M.Bordone, G.Isidori, D. van Dyk, *Impact of leptonic τ decays on the distribution of $B \to P\mu\overline{\nu}$ decays*, **Eur.Phys.J. C76 (2016) no.7, 360**, [arXiv:1602.06143[hep-ph]]
9. M.Bordone, A.Greljo, G.Isidori, M.Marzocca, A.Pattori, *Higgs Pseudo Observables and Radiative Corrections*, **Eur.Phy.J. C75 (2015) no.8, 385**, [arXiv:1507.02555[hep-ph]]
10. C.Biggio and M.Bordone, *Minimal muon magnetic moment*, **JHEP 1502(2015) 099**, [arXiv:1411.6799[hep-ph]]

Acknowledgements

During the four years of my Ph.D. I met many people who helped me going through this very complicated and exciting period of my life and I feel it is my duty to thank them for what they have done for me.
The first one is Gino. I have to thank you for giving me the opportunity of coming to Zürich and having this fantastic experience working in your group. You have been a wise and helpful guide, always available to give me advice when I needed it. And I'm not only referring to the work side which of course is very important, but also to the teachings you gave me which I will use and apply in every day life.
In the last few years I had the honour to meet many people who joined our working group and they all left their mark: being in such a rich environment helped me to grow as a physicist and as a person, and this is priceless.
Among everyone, I have to spend a few words for Danny, who has been a valuable teacher and guide for two years of my Ph.D., being willing to share his knowledge, projects and ideas with me. I am very happy that our collaboration goes beyond your time here in Zürich and that I have found in you a very good friend.
I also want to thank Dario for sharing the office with me and having been both a precious colleague and a friend. Without you everything would have been much more boring.
I'm grateful to Javier for sharing the uncertain moments that characterise the last year of Ph.D. and for always telling me that everything was going to be fine.
Last but not least I want to thank Claudia, who I met a few months ago but became immediately a good friend and loyal work ally. Thanks for sharing with me the bad and good moments, and for having helped me in a difficult moment of my life.

Apart from Gino's group, I must also thank the LHCb group, which has been a second family to me.
Certainly a special thank goes to Federica and Annarita, who are two special friends I know I can always count on. It is a priviledge to have friends like you to laugh or just complain (with me a lot of complaining) or gossip every time I need it.
To Iaroslava I want to say that our friendship turned out to be unexpected and precious. I appreciated so much our Friday evening chats and all our girlish conversations and I'm very proud of being responsible of your not so formal Italian vocabulary.
I am very happy to have met Andrea, because I enjoyed our physics exchange and our close friendship. I found in you someone who I can consider as an acquired brother.
And now it's Rafael's turn: I found every conversation or discussion we had on physics very stimulating and I enjoyed trying to steal any bit of non public information I could. But of course I also treasure the fun moments, and the friendship we built. On this regard, I also mention Marianna. I am very happy to have met such good friends like you two: you teach me every day that even in our job, it is possible to have bonds and everything can be sorted out. Thanks for being so inspiring.

I also want to thank Patrick for being such a good friend and having always been there for me when I needed it.
Of course a special place is occupied by Davide: I extremely enjoyed our friendship, your enthusiasm in every situation and of course, last but not least, our lunch breaks spent playing volley.

Among the people I met at the university I want to thank Marianna for having always been there for me. Thanks for the support and help you gave me in every situation. And of course here it comes Francesco, our late evenings in the office with all our chats and laughs are invaluable.
I want also to thank Chiara for all the gossip and the fun, and Riccardo for cooking an amazing pizza and the time that we spent and enjoyed together.

Apart from my work at university I am very happy to have joined for two years the VBC Oerlikon D2 volleyball team: I started again to play a sport I love and I met fantastic people. So I feel obliged to mention all my team-mates: Mira, Aina, Alice, Annette, Berlinde, Esther, Janine, Mary, Sabrina, Nici and Andrea and of course our trainer Martin. Thanks for giving me the fun and the excitement during the matches, and also for the chats and advice you were always ready to give me. Being in contact with people outside my research field helped me many times to complete shut the work out of my mind and to keep in mind that there are many things in life which are more important than work.

Last, a very special thank goes to my family. You are the reason why I managed to go through this path; you have always being ready to help, listen, give advice and tell me that I could make it. I have the gift to have someone like you who push me to go always further and look for new challenges and improvements in my life with the confidence that I will be able to do whatever I aim to. This gift you are giving me everyday is one of the most precious thing I have in my life and I will never thank you enough for this.

Ringraziamenti

Durante i quattro anni del mio dottorato ho conosciuto molte persone che mi hanno aiutato a superare questo periodo della mia vita molto complicato ed entusiasmante ed è mio dovere ringraziarle per quello che hanno fatto per me.
La prima di queste persone è Gino. Devo ringraziarti per avermi dato l'opportunità di venire a Zurigo ed avere la fantastica esperienza di lavorare nel tuo gruppo. Sei stato una guida saggia e incoraggiante, sempre disponibile ad aiutarmi quando ne ho avuto bisogno. E non mi riferisco solamente al lato lavorativo che ovviamente è molto importante, ma anche agli insegnamenti che mi hai dato che posso utilizzare nella vita di tutti i giorni.
Negli ultimi anni ho avuto l'onore di conoscere molte persone che si sono unite nel nostro gruppo e tutte loro hanno lasciato un proprio segno: far parte di un ambiente cosí ricco mi ha aiutato a crescere sia a livello professionale che personale e questo non ha prezzo.
Tra tutti, devo spendere qualche parola per Danny, che è stato un prezioso insegnante e una guida per due anni del mio dottorato, condividendo conoscienza, progetti e idee con me. Sono molto contenta che la nostra collaborazione vada oltre il tempo che hai trascorso a Zurigo e che in te ho trovato un ottimo amico.
Voglio anche ringraziare Dario per aver condiviso con me l'ufficio ed essere stato un collega e amico prezioso. Senza di te tutto sarebbe stato molto più noioso.
Sono grata ad Javier per aver condiviso i momenti di incertezza che caratterizzano l'ultimo anno di dottorato per avermi ripetuto ogni volta che tutto sarebbe andato per il meglio.
Infine, voglio ringraziare Claudia, che ho conosciuto qualche mese fa ma che è diventata da subito una buona amica e una alleata sul lavoro. Grazie per aver condiviso con me i momenti buoni e quelli cattivi e per avermi aiutata in un momento difficile della mia vita.

A parte il gruppo di Gino, devo ringraziare il gruppo di LHCb, che per me è stato come una seconda famiglia.
Sicuramente un ringraziamento speciale va a Federica ed Annarita, che sono due amiche speciali su cui so di poter sempre contare. È un privilegio avere due amiche come voi con cui ridere, lamentarsi (con me molto) o spettegolare ogni volta che ne ho bisogno.
A Iaroslava voglio dire he la nostra amicizia si è rivelata inaspettata e preziosa. Ho apprezzato molto le nostre chiacchierate del Venerdì sera e le nostre chiacchiere da ragazze e sono molto fiera di essere responsabile del tuo vocabolario non molto formale di parole italiane.
Sono molto felice di aver conosciuto Andrea, perchè ho apprezzato i nostri scambi sulla fisica e la nostra amicizia. Ho trovato in te un fratello acquisito.
Ed ora è il turno di Rafael: ogni conversazione o discussione lavorativa è stata molto stimolante e mi sono divertita nel cercare di rubare ogni piccola informazione non pubblica. Ovviamente faccio tesoro dei momenti di divertimento e della amicizia che abbiamo costruito. A proposito di questo, voglio anche menzionare Marianna. Sono molto contenta di aver incontrato due buoni amici come voi: ogni giorno mi insegnate che anche col nostro lavoro è possibile avere legami e che si può trovare una soluzione.

Voglio anche ringraziare Patrick per essere un buon amico ed esserci sempre stato ogni volta che ho avuto bisogno.
Un posto speciale è occupato da Davide: grazie per la nostra amicizia, il tuo entusiasmo e per le pause pranzo spese a giocare a pallavolo.

Tra le persone che ho conosciuto all'università c'è Marianna, che per me cè sempre stata. Hai ascoltato tutti i problemi che ho avuto e hai sempre cercato una soluzione. Avere un'amica come te è un privilegio. Ed ovviamente ringrazio anche Francesco, le nostre chiacchierate serali in ufficio non hanno valore.
Voglio anche ringraziare Chiara per esserci divertite insieme e per la certezza che tu fossi sempre disponibile a spettegolare, e ringrazio Riccardo per cucinare una pizza spettacolare e per il tempo che abbiamo passato insieme.

A parte la sfera lavorativa, sono molto contenta di essermi unita per due anni alla squadra di pallavolo VBC Oerlikon D2: ho cominciato nuovamente a giocare ad uno sport che amo e ho incontrato persone fantastiche. Quindi mi sembra d'obbligo menzionare le mie compagne di squadra: Mira, Aina, Alice, Annette, Berlinde, Esther, Janine, Mary, Sabrina, Nici and Andrea e ovviamente il nostro allenatore Martin. Vi ringrazio per il divertimento e l'adrenalina durante le partite, e anche per le chiacchierate ed i consigli che siete sempre stati pronti a darmi. Avere un rapporto così bello con persone al di fuori del mio ambito lavorativo mi ha aiutata molte volte a dimenticarmi del lavoro e a ricordarmi sempre che nella vita ci sono molte cose che sono più importanti del lavoro.

In ultimo, un ringraziamento molto speciale va alla mia famiglia. Voi siete la ragione per cui sono riuscita a completare questo percorso; siete sempre stati pronti ad aiutare, ascoltarmi e consigliarmi e a ripetermi che ce l'avrei fatta. Ho il dono di avere persone come voi nella mia vita che mi spinge sempre a fare di più e a cercare nuove sfide e miglioramenti, con la sicurezza che sarò in grado di fare qualsiasi cosa io desideri. Questo regalo che voi mi fate ogni giorno è una delle cose più preziose che ho nella mia vita e per questo non vi ringrazierò mai abbastanza.

Bibliography

[1] N. Cabibbo, "Unitary Symmetry and Leptonic Decays," *Phys. Rev. Lett.* **10** (1963) 531–533. [,648(1963)].

[2] M. Kobayashi and T. Maskawa, "CP Violation in the Renormalizable Theory of Weak Interaction," *Prog. Theor. Phys.* **49** (1973) 652–657.

[3] R. Kowalewski and T. Mannel, "Semileptonic bottom hadron decays and the determination of V_{cb} and V_{ub}," in *Review of Particle Physics (RPP)*, vol. C38, p. 090001. 2014.

[4] B. Pontecorvo, "Neutrino Experiments and the Problem of Conservation of Leptonic Charge," *Sov. Phys. JETP* **26** (1968) 984–988. [Zh. Eksp. Teor. Fiz.53,1717(1967)].

[5] B. Pontecorvo, "Mesonium and anti-mesonium," *Sov. Phys. JETP* **6** (1957) 429. [Zh. Eksp. Teor. Fiz.33,549(1957)].

[6] B. Pontecorvo, "Inverse beta processes and nonconservation of lepton charge," *Sov. Phys. JETP* **7** (1958) 172–173. [Zh. Eksp. Teor. Fiz.34,247(1957)].

[7] Z. Maki, M. Nakagawa, and S. Sakata, "Remarks on the unified model of elementary particles," *Prog. Theor. Phys.* **28** (1962) 870–880. [,34(1962)].

[8] **Particle Data Group** Collaboration, C. Patrignani *et al.*, "Review of Particle Physics," *Chin. Phys.* **C40** no. 10, (2016) 100001. including the 2017 partial update.

[9] **UTfit** Collaboration, "Unitary triangle fit," 2016. http://www.utfit.org/UTfit/ResultsSummer2016SM.

[10] G. D'Ambrosio, G. F. Giudice, G. Isidori, and A. Strumia, "Minimal flavor violation: An Effective field theory approach," *Nucl. Phys.* **B645** (2002) 155–187, arXiv:hep-ph/0207036 [hep-ph].

[11] R. Barbieri, G. Isidori, J. Jones-Perez, P. Lodone, and D. M. Straub, "$U(2)$ and Minimal Flavour Violation in Supersymmetry," *Eur. Phys. J.* **C71** (2011) 1725, arXiv:1105.2296 [hep-ph].

[12] A. J. Buras, P. Gambino, M. Gorbahn, S. Jager, and L. Silvestrini, "Universal unitarity triangle and physics beyond the standard model," *Phys. Lett.* **B500** (2001) 161–167, arXiv:hep-ph/0007085 [hep-ph].

[13] G. Buchalla, A. J. Buras, and M. E. Lautenbacher, "Weak decays beyond leading logarithms," *Rev. Mod. Phys.* **68** (1996) 1125–1144, arXiv:hep-ph/9512380 [hep-ph].

[14] A. Sirlin, "Radiative corrections to g(v)/g(mu) in simple extensions of the su(2) x u(1) gauge model," *Nucl. Phys.* **B71** (1974) 29–51.

[15] A. Sirlin, "Current Algebra Formulation of Radiative Corrections in Gauge Theories and the Universality of the Weak Interactions," *Rev. Mod. Phys.* **50** (1978) 573. [Erratum: Rev. Mod. Phys.50,905(1978)].

[16] C. Bobeth, M. Misiak, and J. Urban, "Photonic penguins at two loops and m_t dependence of $BR[B \to X_s l^+ l^-]$," *Nucl. Phys.* **B574** (2000) 291–330, arXiv:hep-ph/9910220 [hep-ph].

[17] T. Huber, E. Lunghi, M. Misiak, and D. Wyler, "Electromagnetic logarithms in $\overline{B} \to X_s l^+ l^-$," *Nucl. Phys.* **B740** (2006) 105–137, arXiv:hep-ph/0512066 [hep-ph].

[18] C. Bobeth, M. Gorbahn, T. Hermann, M. Misiak, E. Stamou, and M. Steinhauser, "$B_{s,d} \to l^+ l^-$ in the Standard Model with Reduced Theoretical Uncertainty," *Phys. Rev. Lett.* **112** (2014) 101801, arXiv:1311.0903 [hep-ph].

[19] T. Hermann, M. Misiak, and M. Steinhauser, "Three-loop QCD corrections to $B_s \to \mu^+ \mu^-$," *JHEP* **12** (2013) 097, arXiv:1311.1347 [hep-ph].

[20] **Fermilab Lattice, MILC** Collaboration, J. A. Bailey *et al.*, "$|V_{ub}|$ from $B \to \pi \ell \nu$ decays and (2+1)-flavor lattice QCD," *Phys. Rev.* **D92** no. 1, (2015) 014024, arXiv:1503.07839 [hep-lat].

[21] **HPQCD** Collaboration, H. Na, C. M. Bouchard, G. P. Lepage, C. Monahan, and J. Shigemitsu, "$B \to D \ell \nu$ form factors at nonzero recoil and extraction of $|V_{cb}|$," *Phys. Rev.* **D92** no. 5, (2015) 054510, arXiv:1505.03925 [hep-lat].

[22] **HPQCD** Collaboration, C. Bouchard, G. P. Lepage, C. Monahan, H. Na, and J. Shigemitsu, "Rare decay $B \to K \ell^+ \ell^-$ form factors from lattice QCD," *Phys. Rev.* **D88** no. 5, (2013) 054509, arXiv:1306.2384 [hep-lat]. [Erratum: Phys. Rev.D88,no.7,079901(2013)].

[23] R. R. Horgan, Z. Liu, S. Meinel, and M. Wingate, "Lattice QCD calculation of form factors describing the rare decays $B \to K^* \ell^+ \ell^-$ and $B_s \to \phi \ell^+ \ell^-$," *Phys. Rev.* **D89** no. 9, (2014) 094501, arXiv:1310.3722 [hep-lat].

[24] R. R. Horgan, Z. Liu, S. Meinel, and M. Wingate, "Rare B decays using lattice QCD form factors," *PoS* **LATTICE2014** (2015) 372, arXiv:1501.00367 [hep-lat].

[25] A. Bharucha, D. M. Straub, and R. Zwicky, "$B \to V \ell^+ \ell^-$ in the Standard Model from light-cone sum rules," *JHEP* **08** (2016) 098, arXiv:1503.05534 [hep-ph].

[26] A. Khodjamirian, T. Mannel, and Y. M. Wang, "$B \to K \ell^+ \ell^-$ decay at large hadronic recoil," *JHEP* **02** (2013) 010, arXiv:1211.0234 [hep-ph].

[27] C. Bobeth, M. Chrzaszcz, D. van Dyk, and J. Virto, "Long-distance effects in $B \to K^* \ell\ell$ from Analyticity," arXiv:1707.07305 [hep-ph].

[28] M. E. Luke, "Effects of subleading operators in the heavy quark effective theory," *Phys. Lett.* **B252** (1990) 447–455.

[29] S. Fajfer, J. F. Kamenik, and I. Nisandzic, "On the $B \to D^* \tau \overline{\nu}_\tau$ Sensitivity to New Physics," *Phys. Rev.* **D85** (2012) 094025, arXiv:1203.2654 [hep-ph].

[30] D. Bigi, P. Gambino, and S. Schacht, "$R(D^*)$, $|V_{cb}|$, and the Heavy Quark Symmetry relations between form factors," *JHEP* **11** (2017) 061, arXiv:1707.09509 [hep-ph].

[31] D. Bigi and P. Gambino, "Revisiting $B \to D\ell\nu$," *Phys. Rev.* **D94** no. 9, (2016) 094008, arXiv:1606.08030 [hep-ph].

[32] **MILC** Collaboration, J. A. Bailey *et al.*, "B?D?? form factors at nonzero recoil and —V_{cb}— from 2+1-flavor lattice QCD," *Phys. Rev.* **D92** no. 3, (2015) 034506, arXiv:1503.07237 [hep-lat].

[33] **Belle** Collaboration, M. Huschle *et al.*, "Measurement of the branching ratio of $\overline{B} \to D^{(*)} \tau^- \overline{\nu}_\tau$ relative to $\overline{B} \to D^{(*)} \ell^- \overline{\nu}_\ell$ decays with hadronic tagging at Belle," *Phys. Rev.* **D92** no. 7, (2015) 072014, arXiv:1507.03233 [hep-ex].

[34] **Belle** Collaboration, Y. Sato *et al.*, "Measurement of the branching ratio of $\overline{B}^0 \to D^{*+} \tau^- \overline{\nu}_\tau$ relative to $\overline{B}^0 \to D^{*+} \ell^- \overline{\nu}_\ell$ decays with a semileptonic tagging method," *Phys. Rev.* **D94** no. 7, (2016) 072007, arXiv:1607.07923 [hep-ex].

[35] **Belle** Collaboration, S. Hirose *et al.*, "Measurement of the τ lepton polarization and $R(D^*)$ in the decay $\overline{B} \to D^* \tau^- \overline{\nu}_\tau$," *Phys. Rev. Lett.* **118** no. 21, (2017) 211801, arXiv:1612.00529 [hep-ex].

[36] **LHCb** Collaboration, R. Aaij *et al.*, "Measurement of the ratio of branching fractions $\mathcal{B}(\overline{B}^0 \to D^{*+} \tau^- \overline{\nu}_\tau)/\mathcal{B}(\overline{B}^0 \to D^{*+} \mu^- \overline{\nu}_\mu)$," *Phys. Rev. Lett.* **115** no. 11, (2015) 111803, arXiv:1506.08614 [hep-ex]. [Addendum: Phys. Rev. Lett.115,no.15,159901(2015)].

[37] **LHCb** Collaboration, R. Aaij *et al.*, "Measurement of the $B^0 \to D^{*-} \tau^+ \nu_\tau$ branching fraction using three-prong τ decays," arXiv:1711.02505 [hep-ex].

[38] Y. Amhis *et al.*, "Averages of b-hadron, c-hadron, and τ-lepton properties as of summer 2016," arXiv:1612.07233 [hep-ex]. and following updates.

[39] **BaBar** Collaboration, J. P. Lees *et al.*, "Measurement of an Excess of $\overline{B} \to D^{(*)} \tau^- \overline{\nu}_\tau$ Decays and Implications for Charged Higgs Bosons," *Phys. Rev.* **D88** no. 7, (2013) 072012, arXiv:1303.0571 [hep-ex].

[40] M. Bordone, G. Isidori, and A. Pattori, "On the Standard Model predictions for R_K and R_{K^*}," *Eur. Phys. J.* **C76** no. 8, (2016) 440, arXiv:1605.07633 [hep-ph].

[41] B. Capdevila, A. Crivellin, S. Descotes-Genon, J. Matias, and J. Virto, "Patterns of New Physics in $b \to s\ell^+\ell^-$ transitions in the light of recent data," arXiv:1704.05340 [hep-ph].

[42] **LHCb** Collaboration, R. Aaij *et al.*, "Test of lepton universality using $B^+ \to K^+ \ell^+ \ell^-$ decays," *Phys. Rev. Lett.* **113** (2014) 151601, arXiv:1406.6482 [hep-ex].

[43] **LHCb** Collaboration, R. Aaij *et al.*, "Test of lepton universality with $B^0 \to K^{*0} \ell^+ \ell^-$ decays," *JHEP* **08** (2017) 055, arXiv:1705.05802 [hep-ex].

[44] **LHCb** Collaboration, R. Aaij *et al.*, "Angular analysis of the $B^0 \to K^{*0} \mu^+ \mu^-$ decay using 3 fb^{-1} of integrated luminosity," *JHEP* **02** (2016) 104, arXiv:1512.04442 [hep-ex].

[45] **Belle** Collaboration, S. Wehle *et al.*, "Lepton-Flavor-Dependent Angular Analysis of $B \to K^* \ell^+ \ell^-$," *Phys. Rev. Lett.* **118** no. 11, (2017) 111801, arXiv:1612.05014 [hep-ex].

[46] **ATLAS** Collaboration, M. Aaboud *et al.*, "Angular analysis of $B_d^0 \to K^* \mu^+ \mu^-$ decays in pp collisions at $\sqrt{s} = 8$ TeV with the ATLAS detector," arXiv:1805.04000 [hep-ex].

[47] **CMS** Collaboration, V. Khachatryan *et al.*, "Angular analysis of the decay $B^0 \to K^{*0} \mu^+ \mu^-$ from pp collisions at $\sqrt{s} = 8$ TeV," *Phys. Lett.* **B753** (2016) 424–448, arXiv:1507.08126 [hep-ex].

[48] W. Altmannshofer, P. Stangl, and D. M. Straub, "Interpreting Hints for Lepton Flavor Universality Violation," *Phys. Rev.* **D96** no. 5, (2017) 055008, arXiv:1704.05435 [hep-ph].

[49] S. Descotes-Genon, L. Hofer, J. Matias, and J. Virto, "Global analysis of $b \to s\ell\ell$ anomalies," *JHEP* **06** (2016) 092, arXiv:1510.04239 [hep-ph].

[50] T. Hurth, F. Mahmoudi, and S. Neshatpour, "Global fits to $b \to s\ell\ell$ data and signs for lepton non-universality," *JHEP* **12** (2014) 053, arXiv:1410.4545 [hep-ph].

[51] T. Hurth, F. Mahmoudi, and S. Neshatpour, "On the anomalies in the latest LHCb data," *Nucl. Phys.* **B909** (2016) 737–777, arXiv:1603.00865 [hep-ph].

[52] M. Ciuchini, A. M. Coutinho, M. Fedele, E. Franco, A. Paul, L. Silvestrini, and M. Valli, "On Flavourful Easter eggs for New Physics hunger and Lepton Flavour Universality violation," *Eur. Phys. J.* **C77** no. 10, (2017) 688, arXiv:1704.05447 [hep-ph].

[53] M. Ciuchini, M. Fedele, E. Franco, S. Mishima, A. Paul, L. Silvestrini, and M. Valli, "$B \to K^* \ell^+ \ell^-$ decays at large recoil in the Standard Model: a theoretical reappraisal," *JHEP* **06** (2016) 116, arXiv:1512.07157 [hep-ph].

[54] G. D'Amico, M. Nardecchia, P. Panci, F. Sannino, A. Strumia, R. Torre, and A. Urbano, "Flavour anomalies after the R_{K^*} measurement," *JHEP* **09** (2017) 010, arXiv:1704.05438 [hep-ph].

[55] **Belle** Collaboration, P. Hamer *et al.*, "Search for $B^0 \to \pi^- \tau^+ \nu_\tau$ with hadronic tagging at Belle," *Phys. Rev.* **D93** no. 3, (2016) 032007, arXiv:1509.06521 [hep-ex].

[56] A. Celis, M. Jung, X.-Q. Li, and A. Pich, "Sensitivity to charged scalars in $\boldsymbol{B \to D^{(*)} \tau \nu_\tau}$ and $\boldsymbol{B \to \tau \nu_\tau}$ decays," *JHEP* **01** (2013) 054, arXiv:1210.8443 [hep-ph].

[57] R. Alonso, B. Grinstein, and J. M. Camalich, "Lepton universality violation and lepton flavor conservation in B-meson decays," *JHEP* **10** (2015) 184, arXiv:1505.05164 [hep-ph].

[58] A. Greljo, G. Isidori, and D. Marzocca, "On the breaking of Lepton Flavor Universality in B decays," *JHEP* **07** (2015) 142, arXiv:1506.01705 [hep-ph].

[59] L. Calibbi, A. Crivellin, and T. Ota, "Effective Field Theory Approach to $b \to s\ell\ell'$, $B \to K^* \nu\overline{\nu}$ and $B \to D^{(*)} \tau\nu$ with Third Generation Couplings," *Phys. Rev. Lett.* **115** (2015) 181801, arXiv:1506.02661 [hep-ph].

[60] **Particle Data Group** Collaboration, K. A. Olive *et al.*, "Review of Particle Physics," *Chin. Phys.* **C38** (2014) 090001.

[61] R. Dutta, A. Bhol, and A. K. Giri, "Effective theory approach to new physics in $b \to u$ and $b \to c$ leptonic and semileptonic decays," *Phys. Rev.* **D88** no. 11, (2013) 114023, arXiv:1307.6653 [hep-ph].

[62] D. Becirevic, S. Fajfer, I. Nisandzic, and A. Tayduganov, "Angular distributions of $\overline{B} \to D^{(*)}\ell\overline{\nu}_\ell$ decays and search of New Physics," arXiv:1602.03030 [hep-ph].

[63] M. Bordone, G. Isidori, and D. van Dyk, "Impact of leptonic τ decays on the distribution of $B \to P\mu\overline{\nu}$ decays," *Eur. Phys. J.* **C76** no. 7, (2016) 360, arXiv:1602.06143 [hep-ph].

[64] D. van Dyk *et al.*, "EOS - A HEP Program for Flavour Observables,". http://github.com/eos/eos.

[65] C. Bourrely, I. Caprini, and L. Lellouch, "Model-independent description of B —¿ pi l nu decays and a determination of —V(ub)—," *Phys. Rev.* **D79** (2009) 013008, arXiv:0807.2722 [hep-ph]. [Erratum: Phys. Rev.D82,099902(2010)].

[66] I. Sentitemsu Imsong, A. Khodjamirian, T. Mannel, and D. van Dyk, "Extrapolation and unitarity bounds for the $B \to \pi$ form factor," *JHEP* **02** (2015) 126, arXiv:1409.7816 [hep-ph].

[67] N. Metropolis, A. W. Rosenbluth, M. N. Rosenbluth, A. H. Teller, and E. Teller, "Equation of state calculations by fast computing machines," *J. Chem. Phys.* **21** (1953) 1087–1092.

[68] W. K. Hastings, "Monte Carlo Sampling Methods Using Markov Chains and Their Applications," *Biometrika* **57** (1970) 97–109.

[69] M. Bordone, G. Isidori, and D. van Dyk, "Monte Carlo pseudo events for the decays $\overline{B} \to P\mu X_{\overline{\nu}}$, $P = D, \pi$,".

[70] F. Beaujean, M. Chrzaszcz, N. Serra, and D. van Dyk, "Extracting Angular Observables without a Likelihood and Applications to Rare Decays," *Phys. Rev.* **D91** no. 11, (2015) 114012, arXiv:1503.04100 [hep-ex].

[71] A. Khodjamirian, T. Mannel, N. Offen, and Y. M. Wang, "$B \to \pi\ell\nu_l$ Width and $|V_{ub}|$ from QCD Light-Cone Sum Rules," *Phys. Rev.* **D83** (2011) 094031, arXiv:1103.2655 [hep-ph].

[72] **LHCb** Collaboration, R. Aaij *et al.*, "Measurement of b-hadron production fractions in 7 TeV pp collisions," *Phys. Rev.* **D85** (2012) 032008, arXiv:1111.2357 [hep-ex].

[73] **LHCb** Collaboration, R. Aaij *et al.*, "Study of the kinematic dependences of Λ_b^0 production in pp collisions and a measurement of the $\Lambda_b^0 \to \Lambda_c^+ \pi^-$ branching fraction," *JHEP* **08** (2014) 143, arXiv:1405.6842 [hep-ex].

[74] W. Detmold, C. Lehner, and S. Meinel, "$\Lambda_b \to p\ell^-\overline{\nu}_\ell$ and $\Lambda_b \to \Lambda_c\ell^-\overline{\nu}_\ell$ form factors from lattice QCD with relativistic heavy quarks," *Phys. Rev.* **D92** no. 3, (2015) 034503, arXiv:1503.01421 [hep-lat].

[75] **LHCb** Collaboration, R. Aaij *et al.*, "Measurement of the shape of the $\Lambda_b^0 \to \Lambda_c^+ \mu^- \overline{\nu}_\mu$ differential decay rate," *Phys. Rev.* **D96** no. 11, (2017) 112005, arXiv:1709.01920 [hep-ex].

[76] A. F. Falk, "Hadrons of arbitrary spin in the heavy quark effective theory," *Nucl. Phys.* **B378** (1992) 79–94.

[77] A. K. Leibovich and I. W. Stewart, "Semileptonic Lambda(b) decay to excited Lambda(c) baryons at order Lambda(QCD) / m(Q)," *Phys. Rev.* **D57** (1998) 5620–5631, arXiv:hep-ph/9711257 [hep-ph].

[78] S. Meinel and G. Rendon, "Lattice QCD calculation of form factors for $\Lambda_b \to \Lambda(1520)\ell^+\ell^-$ decays," *PoS* **LATTICE2016** (2016) 299, arXiv:1608.08110 [hep-lat].

[79] T. Feldmann and M. W. Y. Yip, "Form Factors for $Lambda_b \to \Lambda$ Transitions in SCET," *Phys. Rev.* **D85** (2012) 014035, arXiv:1111.1844 [hep-ph]. [Erratum: Phys. Rev.D86,079901(2012)].

[80] M. Neubert, "Heavy quark symmetry," *Phys. Rept.* **245** (1994) 259–396, arXiv:hep-ph/9306320 [hep-ph].

[81] E. E. Jenkins, A. V. Manohar, and M. B. Wise, "The Baryon Isgur-Wise function in the large N(c) limit," *Nucl. Phys.* **B396** (1993) 38–52, arXiv:hep-ph/9208248 [hep-ph].

[82] A. V. Manohar and M. B. Wise, "Heavy quark physics," *Camb. Monogr. Part. Phys. Nucl. Phys. Cosmol.* **10** (2000) 1–191.

[83] M. A. Shifman, N. G. Uraltsev, and A. I. Vainshtein, "V(cb) from OPE sum rules for heavy flavor transitions," *Phys. Rev.* **D51** (1995) 2217, arXiv:hep-ph/9405207 [hep-ph]. [Erratum: Phys. Rev.D52,3149(1995)].

[84] I. I. Y. Bigi, M. A. Shifman, N. G. Uraltsev, and A. I. Vainshtein, "Sum rules for heavy flavor transitions in the SV limit," *Phys. Rev.* **D52** (1995) 196–235, arXiv:hep-ph/9405410 [hep-ph].

[85] A. Czarnecki, K. Melnikov, and N. Uraltsev, "Complete O (alpha-s**2) corrections to zero recoil sum rules for B —¿ D* transitions," *Phys. Rev.* **D57** (1998) 1769–1775, arXiv:hep-ph/9706311 [hep-ph].

[86] T. Mannel and D. van Dyk, "Zero-recoil sum rules for $\Lambda_b \to \Lambda_c$ form factors," *Phys. Lett.* **B751** (2015) 48–53, arXiv:1506.08780 [hep-ph].

[87] P. Gambino, T. Mannel, and N. Uraltsev, "B-¿ D* Zero-Recoil Formfactor and the Heavy Quark Expansion in QCD: A Systematic Study," *JHEP* **10** (2012) 169, arXiv:1206.2296 [hep-ph].

[88] C. Bobeth, G. Hiller, and G. Piranishvili, "Angular distributions of $\overline{B} \to \overline{K}\ell^+\ell^-$ decays," *JHEP* **12** (2007) 040, arXiv:0709.4174 [hep-ph].

[89] **LHCb** Collaboration, R. Aaij *et al.*, "Measurement of the b-quark production cross-section in 7 and 13 TeV pp collisions," *Phys. Rev. Lett.* **118** no. 5, (2017) 052002, arXiv:1612.05140 [hep-ex]. [Erratum: Phys. Rev. Lett.119,no.16,169901(2017)].

[90] **LHCb collaboration** Collaboration, I. e. a. Bediaga, "Framework TDR for the LHCb Upgrade: Technical Design Report," Tech. Rep. CERN-LHCC-2012-007. LHCb-TDR-12, Apr, 2012. https://cds.cern.ch/record/1443882.

[91] T. Sjöstrand, S. Mrenna, and P. Skands, "PYTHIA 6.4 physics and manual," *JHEP* **05** (2006) 026, arXiv:hep-ph/0603175 [hep-ph].

[92] T. Sjöstrand, S. Mrenna, and P. Skands, "A brief introduction to PYTHIA 8.1," *Comput. Phys. Commun.* **178** (2008) 852–867, arXiv:0710.3820 [hep-ph].

[93] **LHCb Collaboration** Collaboration, B.-M. et al", *LHCb VELO (VErtex LOcator): Technical Design Report*. Technical Design Report LHCb. CERN, Geneva, 2001. http://cds.cern.ch/record/504321.

[94] G. Ciezarek, A. Lupato, M. Rotondo, and M. Vesterinen, "Reconstruction of semileptonically decaying beauty hadrons produced in high energy pp collisions," *JHEP* **02** (2017) 021, arXiv:1611.08522 [hep-ex].

[95] G. Hiller and F. Kruger, "More model-independent analysis of $b \to s$ processes," *Phys. Rev.* **D69** (2004) 074020, arXiv:hep-ph/0310219 [hep-ph].

[96] W. Altmannshofer and D. M. Straub, "Implications of $b \to s$ measurements," in *Proceedings, 50th Rencontres de Moriond Electroweak Interactions and Unified Theories (La Thuile, Italy, March 14-21, 2015)*. arXiv:1503.06199 [hep-ph].

[97] **BaBar** Collaboration, J. P. Lees *et al.*, "Evidence for an excess of $\overline{B} \to D^{(*)}\tau^-\overline{\nu}_\tau$ decays," *Phys. Rev. Lett.* **109** (2012) 101802, arXiv:1205.5442 [hep-ex].

[98] T. Huber, T. Hurth, and E. Lunghi, "Inclusive $\overline{B} \to X_s\ell^+\ell^-$: complete angular analysis and a thorough study of collinear photons," *JHEP* **06** (2015) 176, arXiv:1503.04849 [hep-ph].

[99] T. Huber, T. Hurth, and E. Lunghi, "Logarithmically Enhanced Corrections to the Decay Rate and Forward Backward Asymmetry in $\overline{B} \to X_s\ell^+\ell^-$," *Nucl. Phys.* **B802** (2008) 40–62, arXiv:0712.3009 [hep-ph].

[100] J. Gratrex, M. Hopfer, and R. Zwicky, "Generalised helicity formalism, higher moments and the $B \to K_{J_K}(\to K\pi)\bar{\ell}_1\ell_2$ angular distributions," *Phys. Rev.* **D93** no. 5, (2016) 054008, arXiv:1506.03970 [hep-ph].

[101] D. R. Yennie, S. C. Frautschi, and H. Suura, "The infrared divergence phenomena and high-energy processes," *Annals Phys.* **13** (1961) 379–452.

[102] S. Weinberg, "Infrared photons and gravitons," *Phys. Rev.* **140** (1965) B516–B524.

[103] G. Isidori, "Soft-photon corrections in multi-body meson decays," *Eur. Phys. J.* **C53** (2008) 567–571, arXiv:0709.2439 [hep-ph].

[104] M. Bordone, A. Greljo, G. Isidori, D. Marzocca, and A. Pattori, "Higgs Pseudo Observables and Radiative Corrections," *Eur. Phys. J.* **C75** no. 8, (2015) 385, arXiv:1507.02555 [hep-ph].

[105] N. Davidson, T. Przedzinski, and Z. Was, "PHOTOS interface in C++: Technical and Physics Documentation," *Comput. Phys. Commun.* **199** (2016) 86–101, arXiv:1011.0937 [hep-ph].

[106] M. Bartsch, M. Beylich, G. Buchalla, and D. N. Gao, "Precision Flavour Physics with $B \to K\nu\overline{\nu}$ and $B \to Kl^+l^-$," *JHEP* **11** (2009) 011, arXiv:0909.1512 [hep-ph].

[107] F. Kruger and L. M. Sehgal, "Lepton polarization in the decays b —¿ X(s) mu+ mu- and B —¿ X(s) tau+ tau-," *Phys. Lett.* **B380** (1996) 199–204, arXiv:hep-ph/9603237 [hep-ph].

[108] J. Lyon and R. Zwicky, "Resonances gone topsy turvy - the charm of QCD or new physics in $b \to s\ell^+\ell^-$?," arXiv:1406.0566 [hep-ph].

[109] M. Beneke, T. Feldmann, and D. Seidel, "Systematic approach to exclusive $B \to Vl^+l^-$, $V\gamma$ decays," *Nucl. Phys.* **B612** (2001) 25–58, arXiv:hep-ph/0106067 [hep-ph].

[110] M. Beneke, T. Feldmann, and D. Seidel, "Exclusive radiative and electroweak $b \to d$ and $b \to s$ penguin decays at NLO," *Eur. Phys. J.* **C41** (2005) 173–188, arXiv:hep-ph/0412400 [hep-ph].

[111] R. Alonso, B. Grinstein, and J. Martin Camalich, "$SU(2) \times U(1)$ gauge invariance and the shape of new physics in rare B decays," *Phys. Rev. Lett.* **113** (2014) 241802, arXiv:1407.7044 [hep-ph].

[112] S. Sahoo and R. Mohanta, "Lepton flavor violating B meson decays via a scalar leptoquark," *Phys. Rev.* **D93** no. 11, (2016) 114001, arXiv:1512.04657 [hep-ph].

[113] A. Carmona and F. Goertz, "Lepton Flavor and Nonuniversality from Minimal Composite Higgs Setups," *Phys. Rev. Lett.* **116** no. 25, (2016) 251801, arXiv:1510.07658 [hep-ph].

[114] G. Hiller and M. Schmaltz, "R_K and future $b \to s\ell\ell$ physics beyond the standard model opportunities," *Phys. Rev.* **D90** (2014) 054014, arXiv:1408.1627 [hep-ph].

[115] D. Ghosh, M. Nardecchia, and S. A. Renner, "Hint of Lepton Flavour Non-Universality in B Meson Decays," *JHEP* **12** (2014) 131, arXiv:1408.4097 [hep-ph].

[116] S. Biswas, D. Chowdhury, S. Han, and S. J. Lee, "Explaining the lepton non-universality at the LHCb and CMS within a unified framework," *JHEP* **02** (2015) 142, arXiv:1409.0882 [hep-ph].

[117] S. L. Glashow, D. Guadagnoli, and K. Lane, "Lepton Flavor Violation in B Decays?," *Phys. Rev. Lett.* **114** (2015) 091801, arXiv:1411.0565 [hep-ph].

[118] A. Crivellin, G. D'Ambrosio, and J. Heeck, "Explaining $h \to \mu^\pm\tau^\mp$, $B \to K^*\mu^+\mu^-$ and $B \to K\mu^+\mu^-/B \to Ke^+e^-$ in a two-Higgs-doublet model with gauged $L_\mu - L_\tau$," *Phys. Rev. Lett.* **114** (2015) 151801, arXiv:1501.00993 [hep-ph].

[119] D. Aristizabal Sierra, F. Staub, and A. Vicente, "Shedding light on the $b \to s$ anomalies with a dark sector," *Phys. Rev.* **D92** no. 1, (2015) 015001, arXiv:1503.06077 [hep-ph].

[120] A. Crivellin, L. Hofer, J. Matias, U. Nierste, S. Pokorski, and J. Rosiek, "Lepton-flavour violating B decays in generic Z' models," *Phys. Rev.* **D92** no. 5, (2015) 054013, arXiv:1504.07928 [hep-ph].

[121] A. Celis, J. Fuentes-Martin, M. Jung, and H. Serodio, "Family nonuniversal Z? models with protected flavor-changing interactions," *Phys. Rev.* **D92** no. 1, (2015) 015007, arXiv:1505.03079 [hep-ph].

[122] B. Gripaios, M. Nardecchia, and S. A. Renner, "Composite leptoquarks and anomalies in B-meson decays," *JHEP* **05** (2015) 006, arXiv:1412.1791 [hep-ph].

[123] D. Bečirević, S. Fajfer, and N. Košnik, "Lepton flavor nonuniversality in b?s?$^+$?$^-$ processes," *Phys. Rev.* **D92** no. 1, (2015) 014016, arXiv:1503.09024 [hep-ph].

[124] I. de Medeiros Varzielas and G. Hiller, "Clues for flavor from rare lepton and quark decays," *JHEP* **06** (2015) 072, arXiv:1503.01084 [hep-ph].

[125] R. Barbieri, G. Isidori, A. Pattori, and F. Senia, "Anomalies in B-decays and $U(2)$ flavour symmetry," *Eur. Phys. J.* **C76** no. 2, (2016) 67, arXiv:1512.01560 [hep-ph].

[126] A. Crivellin, J. Heeck, and P. Stoffer, "A perturbed lepton-specific two-Higgs-doublet model facing experimental hints for physics beyond the Standard Model," *Phys. Rev. Lett.* **116** no. 8, (2016) 081801, arXiv:1507.07567 [hep-ph].

[127] M. Bauer and M. Neubert, "Minimal Leptoquark Explanation for the $R_{D^{(*)}}$, R_K , and $(g-2)_g$ Anomalies," *Phys. Rev. Lett.* **116** no. 14, (2016) 141802, arXiv:1511.01900 [hep-ph].

[128] S. Fajfer and N. Košnik, "Vector leptoquark resolution of R_K and $R_{D^{(*)}}$ puzzles," *Phys. Lett.* **B755** (2016) 270–274, arXiv:1511.06024 [hep-ph].

[129] D. Guadagnoli and K. Lane, "Charged-Lepton Mixing and Lepton Flavor Violation," *Phys. Lett.* **B751** (2015) 54–58, arXiv:1507.01412 [hep-ph].

[130] S. Sahoo and R. Mohanta, "Study of the rare semileptonic decays $B_d^0 \to K^* l^+ l^-$ in scalar leptoquark model," *Phys. Rev.* **D93** no. 3, (2016) 034018, arXiv:1507.02070 [hep-ph].

[131] A. Falkowski, M. Nardecchia, and R. Ziegler, "Lepton Flavor Non-Universality in B-meson Decays from a U(2) Flavor Model," *JHEP* **11** (2015) 173, arXiv:1509.01249 [hep-ph].

[132] H. Päs and E. Schumacher, "Common origin of R_K and neutrino masses," *Phys. Rev.* **D92** no. 11, (2015) 114025, arXiv:1510.08757 [hep-ph].

[133] B. Bhattacharya, A. Datta, D. London, and S. Shivashankara, "Simultaneous Explanation of the R_K and $R(D^{(*)})$ Puzzles," *Phys. Lett.* **B742** (2015) 370–374, arXiv:1412.7164 [hep-ph].

[134] D. Buttazzo, A. Greljo, G. Isidori, and D. Marzocca, "Toward a coherent solution of diphoton and flavor anomalies," *JHEP* **08** (2016) 035, arXiv:1604.03940 [hep-ph].

[135] B. Capdevila, S. Descotes-Genon, J. Matias, and J. Virto, "Assessing lepton-flavour non-universality from $B \to K^* \ell\ell$ angular analyses," *JHEP* **10** (2016) 075, arXiv:1605.03156 [hep-ph].

[136] D. Das, C. Hati, G. Kumar, and N. Mahajan, "Towards a unified explanation of $R_{D^{(*)}}$, R_K and $(g-2)_\mu$ anomalies in a left-right model with leptoquarks," *Phys. Rev.* **D94** (2016) 055034, arXiv:1605.06313 [hep-ph].

[137] S. M. Boucenna, A. Celis, J. Fuentes-Martin, A. Vicente, and J. Virto, "Phenomenology of an $SU(2) \times SU(2) \times U(1)$ model with lepton-flavour non-universality," *JHEP* **12** (2016) 059, arXiv:1608.01349 [hep-ph].

[138] D. Becirevic, S. Fajfer, N. Košnik, and O. Sumensari, "Leptoquark model to explain the B-physics anomalies, R_K and R_D," *Phys. Rev.* **D94** no. 11, (2016) 115021, arXiv:1608.08501 [hep-ph].

[139] G. Hiller, D. Loose, and K. Schoenwald, "Leptoquark Flavor Patterns & B Decay Anomalies," *JHEP* **12** (2016) 027, arXiv:1609.08895 [hep-ph].

[140] B. Bhattacharya, A. Datta, J.-P. Guévin, D. London, and R. Watanabe, "Simultaneous Explanation of the R_K and $R_{D^{(*)}}$ Puzzles: a Model Analysis," *JHEP* **01** (2017) 015, arXiv:1609.09078 [hep-ph].

[141] R. Barbieri, D. Buttazzo, F. Sala, and D. M. Straub, "Flavour physics from an approximate $U(2)^3$ symmetry," *JHEP* **07** (2012) 181, arXiv:1203.4218 [hep-ph].

[142] R. Barbieri, C. W. Murphy, and F. Senia, "B-decay Anomalies in a Composite Leptoquark Model," *Eur. Phys. J.* **C77** no. 1, (2017) 8, arXiv:1611.04930 [hep-ph].

[143] D. A. Faroughy, A. Greljo, and J. F. Kamenik, "Confronting lepton flavor universality violation in B decays with high-p_T tau lepton searches at LHC," *Phys. Lett.* **B764** (2017) 126–134, arXiv:1609.07138 [hep-ph].

[144] F. Feruglio, P. Paradisi, and A. Pattori, "Revisiting Lepton Flavor Universality in B Decays," *Phys. Rev. Lett.* **118** no. 1, (2017) 011801, arXiv:1606.00524 [hep-ph].

[145] M. Freytsis, Z. Ligeti, and J. T. Ruderman, "Flavor models for $\overline{B} \to D^{(*)}\tau\overline{\nu}$," *Phys. Rev.* **D92** no. 5, (2015) 054018, arXiv:1506.08896 [hep-ph].

[146] **Particle Data Group** Collaboration, C. Patrignani *et al.*, "Review of Particle Physics," *Chin. Phys.* **C40** no. 10, (2016) 100001.

[147] A. Pich, "Precision Tau Physics," *Prog. Part. Nucl. Phys.* **75** (2014) 41–85, arXiv:1310.7922 [hep-ph].

[148] R. Barbieri, D. Buttazzo, F. Sala, and D. M. Straub, "Flavour physics and flavour symmetries after the first LHC phase," *JHEP* **05** (2014) 105, arXiv:1402.6677 [hep-ph].

[149] **BaBar** Collaboration, "Search for $B^+ \to K^+\tau^+\tau^-$ at the BaBar experiment," arXiv:1605.09637 [hep-ex].

[150] J. Brod, M. Gorbahn, and E. Stamou, "Two-Loop Electroweak Corrections for the $K \to \pi\nu\overline{\nu}$ Decays," *Phys. Rev.* **D83** (2011) 034030, arXiv:1009.0947 [hep-ph].

[151] P. Gelhausen, A. Khodjamirian, A. A. Pivovarov, and D. Rosenthal, "Decay constants of heavy-light vector mesons from QCD sum rules," *Phys. Rev.* **D88** (2013) 014015, arXiv:1305.5432 [hep-ph]. [Erratum: Phys. Rev.D91,099901(2015)].

[152] S. Alte, M. König, and M. Neubert, "Exclusive Weak Radiative Higgs Decays in the Standard Model and Beyond," *JHEP* **12** (2016) 037, arXiv:1609.06310 [hep-ph].

[153] M. Bordone, G. Isidori, and S. Trifinopoulos, "Semi-leptonic B-physics anomalies: a general EFT analysis within $U(2)^n$ flavor symmetry," arXiv:1702.07238 [hep-ph].

[154] A. Crivellin, D. Müller, and T. Ota, "Simultaneous Explanation of $R(D^{(*)})$ and $b \to s\mu^+\mu^-$: The Last Scalar Leptoquarks Standing," arXiv:1703.09226 [hep-ph].

[155] J. F. Kamenik, Y. Soreq, and J. Zupan, "Lepton flavor universality violation without new sources of quark flavor violation," arXiv:1704.06005 [hep-ph].

[156] G. Buchalla and A. J. Buras, "The rare decays $K^+ \to \pi^+ \nu\overline{\nu}$ and $K_L \to \mu^+\mu^-$ beyond leading logarithms," *Nucl. Phys.* **B412** (1994) 106–142, arXiv:hep-ph/9308272 [hep-ph].

[157] F. Mescia and C. Smith, "Improved estimates of rare K decay matrix-elements from Kl3 decays," *Phys. Rev.* **D76** (2007) 034017, arXiv:0705.2025 [hep-ph].

[158] G. Isidori, F. Mescia, and C. Smith, "Light-quark loops in K —¿ pi nu anti-nu," *Nucl. Phys.* **B718** (2005) 319–338, arXiv:hep-ph/0503107 [hep-ph].

[159] G. Buchalla and A. J. Buras, "The rare decays $K \to \pi\nu\overline{\nu}$, $B \to X\nu\overline{\nu}$ and $B \to l^+l^-$: An Update," *Nucl. Phys.* **B548** (1999) 309–327, arXiv:hep-ph/9901288 [hep-ph].

[160] A. J. Buras, M. Gorbahn, U. Haisch, and U. Nierste, "Charm quark contribution to K+ —¿ pi+ nu anti-nu at next-to-next-to-leading order," *JHEP* **11** (2006) 002, arXiv:hep-ph/0603079 [hep-ph]. [Erratum: JHEP11,167(2012)].

[161] A. J. Buras, D. Buttazzo, J. Girrbach-Noe, and R. Knegjens, "$K^+ \to \pi^+ \nu\overline{\nu}$ and $K_L \to \pi^0 \nu\overline{\nu}$ in the Standard Model: status and perspectives," *JHEP* **11** (2015) 033, arXiv:1503.02693 [hep-ph].

[162] **NA62** Collaboration, G. Ruggiero, "Status of the CERN NA62 Experiment," *J. Phys. Conf. Ser.* **800** no. 1, (2017) 012023.

[163] **KOTO** Collaboration, B. Beckford, "Search for the rare decay of $\mathrm{K}_L^0 \to \pi^0 \nu\overline{\nu}$ with the KOTO detector," *PoS* **ICHEP2016** (2017) 580.

[164] F. Feruglio, P. Paradisi, and A. Pattori, "On the Importance of Electroweak Corrections for B Anomalies," arXiv:1705.00929 [hep-ph].

[165] A. J. Buras, J. Girrbach-Noe, C. Niehoff, and D. M. Straub, "$B \to K^{(*)} \nu\overline{\nu}$ decays in the Standard Model and beyond," *JHEP* **02** (2015) 184, arXiv:1409.4557 [hep-ph].

[166] A. J. Buras and R. Fleischer, "Bounds on the unitarity triangle, sin 2 beta and $K \to$ neutrino anti-neutrino decays in models with minimal flavor violation," *Phys. Rev.* **D64** (2001) 115010, arXiv:hep-ph/0104238 [hep-ph].

[167] W. Altmannshofer, A. J. Buras, D. M. Straub, and M. Wick, "New strategies for New Physics search in $B \to K^* \nu\overline{\nu}$, $B \to K\nu\overline{\nu}$ and $B \to X_s \nu\overline{\nu}$ decays," *JHEP* **04** (2009) 022, arXiv:0902.0160 [hep-ph].

[168] L.-S. Geng, B. Grinstein, S. Jäger, J. Martin Camalich, X.-L. Ren, and R.-X. Shi, "Towards the discovery of new physics with lepton-universality ratios of $b \to s\ell\ell$ decays," arXiv:1704.05446 [hep-ph].

[169] **Belle II** Collaboration, A. Zupanc, "Belle ii prospects,". Talk at Instant Workshop on B meson anomalies, CERN, 2017.

[170] S. M. Boucenna, A. Celis, J. Fuentes-Martin, A. Vicente, and J. Virto, "Non-abelian gauge extensions for B-decay anomalies," *Phys. Lett.* **B760** (2016) 214–219, arXiv:1604.03088 [hep-ph].

[171] D. Bečirević, N. Košnik, O. Sumensari, and R. Zukanovich Funchal, "Palatable Leptoquark Scenarios for Lepton Flavor Violation in Exclusive $b \to s\ell_1\ell_2$ modes," *JHEP* **11** (2016) 035, arXiv:1608.07583 [hep-ph].

[172] Y. Cai, J. Gargalionis, M. A. Schmidt, and R. R. Volkas, "Reconsidering the One Leptoquark solution: flavor anomalies and neutrino mass," *JHEP* **10** (2017) 047, arXiv:1704.05849 [hep-ph].

[173] E. Megias, M. Quiros, and L. Salas, "Lepton-flavor universality violation in R_K and $R_{D^{(*)}}$ from warped space," *JHEP* **07** (2017) 102, arXiv:1703.06019 [hep-ph].

[174] D. Buttazzo, A. Greljo, G. Isidori, and D. Marzocca, "B-physics anomalies: a guide to combined explanations," *JHEP* **11** (2017) 044, arXiv:1706.07808 [hep-ph].

[175] N. Assad, B. Fornal, and B. Grinstein, "Baryon Number and Lepton Universality Violation in Leptoquark and Diquark Models," *Phys. Lett.* **B777** (2018) 324–331, arXiv:1708.06350 [hep-ph].

[176] L. Di Luzio, A. Greljo, and M. Nardecchia, "Gauge leptoquark as the origin of B-physics anomalies," *Phys. Rev.* **D96** no. 11, (2017) 115011, arXiv:1708.08450 [hep-ph].

[177] L. Calibbi, A. Crivellin, and T. Li, "A model of vector leptoquarks in view of the B-physics anomalies," arXiv:1709.00692 [hep-ph].

[178] J. C. Pati and A. Salam, "Lepton Number as the Fourth Color," *Phys. Rev.* **D10** (1974) 275–289. [Erratum: Phys. Rev.D11,703(1975)].

[179] G. Isidori, "Flavor physics and CP violation," in *Proceedings, 2012 European School of High-Energy Physics (ESHEP 2012): La Pommeraye, Anjou, France, June 06-19, 2012*, pp. 69–105. 2014. arXiv:1302.0661 [hep-ph]. http://inspirehep.net/record/1217584/files/arXiv:1302.0661.pdf.

[180] G. F. Giudice, G. Isidori, A. Salvio, and A. Strumia, "Softened Gravity and the Extension of the Standard Model up to Infinite Energy," *JHEP* **02** (2015) 137, arXiv:1412.2769 [hep-ph].

[181] B. Grzadkowski, M. Iskrzynski, M. Misiak, and J. Rosiek, "Dimension-Six Terms in the Standard Model Lagrangian," *JHEP* **10** (2010) 085, arXiv:1008.4884 [hep-ph].

[182] S. Jaiswal, S. Nandi, and S. K. Patra, "Extraction of $|V_{cb}|$ from $B \to D^{(*)}\ell\nu_\ell$ and the Standard Model predictions of $R(D^{(*)})$," *JHEP* **12** (2017) 060, arXiv:1707.09977 [hep-ph].

[183] E. E. Jenkins, A. V. Manohar, and M. Trott, "Renormalization Group Evolution of the Standard Model Dimension Six Operators II: Yukawa Dependence," *JHEP* **01** (2014) 035, arXiv:1310.4838 [hep-ph].

[184] L. Di Luzio and M. Nardecchia, "What is the scale of new physics behind the B-flavour anomalies?," *Eur. Phys. J.* **C77** no. 8, (2017) 536, arXiv:1706.01868 [hep-ph].

[185] **CMS** Collaboration, A. M. Sirunyan *et al.*, "Search for third-generation scalar leptoquarks and heavy right-handed neutrinos in final states with two tau leptons and two jets in proton-proton collisions at $\sqrt{s} = 13$ TeV," *JHEP* **07** (2017) 121, arXiv:1703.03995 [hep-ex].

[186] **ATLAS** Collaboration, M. Aaboud *et al.*, "Search for new phenomena in dijet events using 37 fb^{-1} of pp collision data collected at $\sqrt{s}$ =13 TeV with the ATLAS detector," *Phys. Rev.* **D96** no. 5, (2017) 052004, arXiv:1703.09127 [hep-ex].

[187] **ATLAS** Collaboration, M. Aaboud *et al.*, "Search for new high-mass phenomena in the dilepton final state using 36 fb$^{?1}$ of proton-proton collision data at $\sqrt{s} = 13$ TeV with the ATLAS detector," *JHEP* **10** (2017) 182, arXiv:1707.02424 [hep-ex].

[188] N. Craig, D. Green, and A. Katz, "(De)Constructing a Natural and Flavorful Supersymmetric Standard Model," *JHEP* **07** (2011) 045, arXiv:1103.3708 [hep-ph].

[189] G. Honecker, "Chiral supersymmetric models on an orientifold of Z(4) x Z(2) with intersecting D6-branes," *Nucl. Phys.* **B666** (2003) 175–196, arXiv:hep-th/0303015 [hep-th].

[190] N. Arkani-Hamed, A. G. Cohen, and H. Georgi, "Electroweak symmetry breaking from dimensional deconstruction," *Phys. Lett.* **B513** (2001) 232–240, arXiv:hep-ph/0105239 [hep-ph].

[191] H. E. Haber, "Spin formalism and applications to new physics searches," in *Spin structure in high-energy processes: Proceedings, 21st SLAC Summer Institute on Particle Physics, 26 Jul - 6 Aug 1993, Stanford, CA*, pp. 231–272. 1994. arXiv:hep-ph/9405376 [hep-ph].